EFFECTS OF ATTENUATION ON REFLECTIONS

A DISSERTATION
SUBMITTED TO THE DEPARTMENT OF GEOPHYSICS
AND THE COMMITTEE ON GRADUATE STUDIES
OF STANFORD UNIVERSITY
IN PARTIAL FULFILLMENT OF THE REQUIREMENTS
FOR THE DEGREE OF
DOCTOR OF PHILOSOPHY

By
Thierry Bourbié
April 1982

printed as Stanford Rock Physics Project Report No. 14

by permission of the author

ABSTRACT

A well-known effect of attenuation is the change in frequency content and amplitude of a pulse propagating through an attenuating medium. Another aspect of wave propagation in viscoelastic media is the presence of frequency dependent reflection coefficients. This phenomenon is studied here in three differents ways.

The first way is theoretical. Relative effects of different viscoelastic models of attenuation on reflections are studied, and it is shown that all of the models verify the same conclusions. Then a review of the theory of wave propagation in laterally homogeneous viscoelastic media emphasizing the role of the quality factor Q is presented. The possibility of a quality factor Q independent of frequency in two dimensions is examined in detail.

In the second part of this study, a new method of generating laterally homogeneous synthetic seismograms by using wave equation extrapolation is derived. It takes into account attenuation in the different media but is applicable only for layered media. The attenuation model used is the so-called constant-Q model. The results of this computer simulation show that the effect of attenuation contrast is noticeable only in cases of a large Q-contrast relative to the change of elastic properties. In those situations one can observe a relative increase in the amplitude of post-critical reflections and a decrease in the amplitude of the head-waves. No phase effects is observed except near the critical angles.

The third section deals with the experimental verification of this effect. The results prove that attenuation contrast does have an important effect on reflections when the acoustic impedances of the two considered media are very close. While it is a very common property in the upper crust of the earth, this condition of very low acoustic impedance contrast is difficult to simulate in the laboratory and results in a high degree of inaccuracy in the data. Nevertheless by using samples of polymer and silicon rubber we have shown that with low acoustic impedance contrast and high attenuation an increase in the amplitude of reflections due to Q-contrast is observable. We have also simulated the recorded experimental signals at different angles of incidence by using a model of attenuation for which the Q quality factor is independent of frequency. Finally we have shown that for a large angle of incidence ($\geq$ 20 - 30 degrees) the Q-contrast effect dies out when the elastic reflection coefficient is very low. We always used angles lower than the critical angle to avoid problems due to the singularity of this zone. Theoretically according to the results of Part II, when the critical angle is low, the effects of attenuation occur at post-critical reflection angles and are observable in head-wave amplitudes.

TABLE OF CONTENTS

LIST OF FIGURES

LIST OF TABLES

INTRODUCTION

It has been a frequent occurrence in the past decade that lithologic interpretations of seismic sections have varied greatly from actual subsurface lithologies: traditional methods in signal processing yield only geometrical views of the subsurface. This divergence between the aim of seismic exploration and the results obtained has necessitated the development of numerous interpretive techniques. For example, seismic stratigraphy is one of them: its approach is qualitative dealing mainly with shapes of seismic interfaces and frequency content of the recorded signals. Another example of these new techniques is Rock Physics. In fact it is in itself a new domain trying to develop and understand physical properties of rocks (velocities, attenuations, permeabilities, porosities, dielectric constants) and the effect of *in situ* conditions on these properties. Among these properties we focus our interest on seismic wave attenuation in rocks and its application to seismic exploration.

What we call attenuation is the absorption and irreversible conversion of wave energy into heat. It is an important effect and it greatly affects the characteristics of the recorded signals. For example, and because it is the most obvious fact to observe, one can look at a seismic section and see clearly that, as the wave propagates deeper and deeper in the subsurface, the recorded signal looses its high frequencies and its resolution with respect to the seismic layers. Indeed this loss of high frequencies is not the only effect of attenuation on waves propagating in lossy materials. These effects can be separated in two different sets. One involves all propagation effects (decrease in amplitude, broadening of the pulse, interferences). The other one, which is studied here in some detail, involves the fact that the reflections are occurring at interfaces between viscoelastic media. This situation implies an effect on the recorded signals which can be an indicator of the value of the attenuation contrast (and so can give an idea on the fluid content for example) between the two media involved in the reflection. It is important to realize that we are interested in what is called "intrinsic" attenuation which is a characteristic of a particular medium. Other types of "attenuation" do exist in seismic sections. They are a consequence of particular wave-paths such as intrabed multiples, scattering or such phenomena. The study of the interface attenuation effect we describe here is done using three different methods.

In Part I, we set up the equations necessary to understand this phenomenon. We use linear viscoelasticity theory which seems to be a good theory to represent attenuation in

rocks: it is justified by the strain amplitudes involved in seismic exploration and by the phenomena responsible for wave attenuation that is to say pore fluid related processes (squirt flow mechanism , etc)

In Part II, a technique of computer simulation is developed avoiding as much as possible any dispersion-like grid dispersion which one observes when using finite differences methods. The non-dispersion condition is important, because we are looking at tiny effects which may be masked by any dispersive computer technique. This technique allows us to introduce easily attenuation in our models.

Finally in Part III to see if our theory is applicable we describe the apparatus we built to simulate an earth-like situation for acoustic impedances and attenuations and to determine whether the effect of Q-contrast on reflections is observable in the laboratory.

We expect these results to show that even if it is difficult to measure attenuation *in situ*, this difficulty is compensated by the possibility of getting some insight into the lithology of the subsurface. For instance studying some side effects can give us an idea of the saturation, fluid content, etc of a given formation.

PART I

ATTENUATION ON REFLECTIONS :

A THEORETICAL STUDY

A - THE EFFECT OF ATTENUATION ON REFLECTION COEFFICIENTS : ONE-DIMENSIONAL CASE

INTRODUCTION

For plane waves, in elastic media, the reflection coefficient is a function of the densities and the velocities of the two media we are considering. For the one-dimensional case, at normal incidence, the reflection coefficient is given by the well-known formula:

$$R = \frac{\rho_2 C_2 - \rho_1 C_1}{\rho_2 C_2 + \rho_1 C_1} \qquad (1.1.1)$$

$\rho_i C_i$ being the acoustic impedance of medium i

This formula shows that if there is not contrast in acoustic impedance between the two media, there is no reflection coefficient and therefore no reflection.

In fact actual media are not perfectly elastic, and a better way of describing them is by using the concept of linear viscoelasticity. This concept implies a linear response of the material to an applied load and a time-dependent relationship between stress and strain.

This concept provides a good working hypothesis:

The linearity is implied, because in the earth we deal with very low amplitude stresses whenever we move one or two wave-lengths away from the source.

Recent work (for example Winkler and Nur,1982) have shown that, at the strain amplitudes concerned in seismic exploration ($<10^{-6}$), the attenuation phenomenon is not due to friction but to the fluid content of the considered media.

The purpose of this paper is to calculate the effect of different types of viscoelasticity models on reflection coefficients at normal incidence. We show that, even with no contrast in acoustic impedance, there is a reflection depending on the contrast in attenuation coefficients.

I-EFFECT OF ATTENUATION CONTRAST ON REFLECTION AMPLITUDES

The linear viscoelasticity hypothesis implies that the stress-strain relationship can be written:

$$\sigma(t) = m(t) * \varepsilon(t) \tag{1.1.2}$$

where $\sigma(t)$ is the stress and $\varepsilon(t)$ the strain.

Or in the Fourier domain:

$$\Sigma(\omega) = M(\omega)\, E(\omega) \tag{1.1.3}$$

In his thesis, Kjartansson (1979) studied some standard viscoelastic models. Figure 1-1 gives the schematic diagrams used to represent these models and the frequency dependence of the modulus $M(\omega)$ relating stress and strain in the Fourier domain. We generalize these models and calculate the frequency dependence of the quality factor Q and the implied effect on the reflection coefficient for each of them.

Table I-1 shows the results. In the column giving the reflection coefficient, we have only written the first order approximation which is valid for large Q ($Q \geq 10$).

We have compared every result to the results given by the constant Q model derived by Kjartansson (1979) (CQ model in the following text).

Appendix A shows how the results of Table I-1 are derived. Note that, for large Q ($Q \geq 10$), the effect of Q-contrast on the reflection coefficient is nearly independent of the viscoelastic model considered; therefore studying this effect will not help determine which model best represents the mechanism responsible for wave attenuation.

Due to the non-dependence of the reflection coefficient on the different viscoelastic models, we use the formulation derived with the constant-Q model. We get:

$$R = \frac{\dfrac{\rho' C_0'}{\rho C_0}\left[\dfrac{i\omega}{\omega_0}\right]^{\gamma'-\gamma} - 1}{\dfrac{\rho' C_0'}{\rho C_0}\left[\dfrac{i\omega}{\omega_0}\right]^{\gamma'-\gamma} + 1} \tag{1.1.4}$$

where C_0 and C_0' are the phase velocities at the reference frequency ω_0, ρ and ρ' the densities, and γ and γ' parameters related to the quality factors by the relation

$$\gamma = \frac{1}{\pi}\tan^{-1}\frac{1}{Q}$$

MODEL	MAXWELL	VOIGT	3-PARAMETER SOLID	3-PARAMETER FLUID
Spring-Dashpot Representation		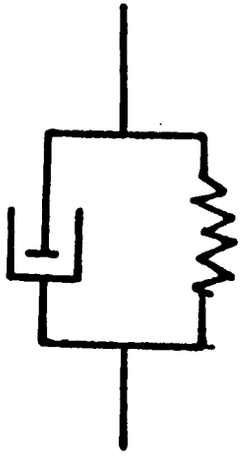	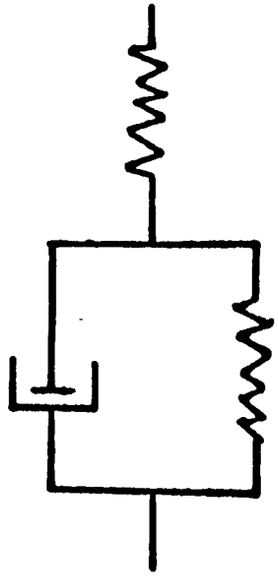	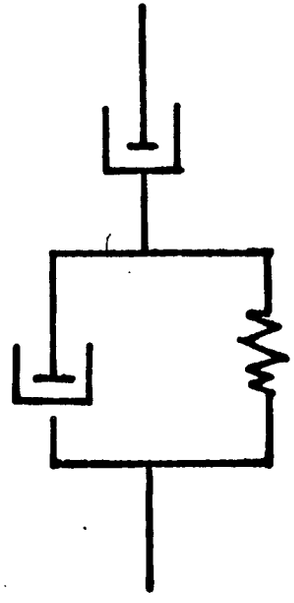
Modulus $M = M(\omega_1 = \frac{\omega}{\omega_o})$	$M_o = \frac{i\omega_1}{1 + i\omega_1}$	$M_o(1 + i\omega_1)$	$M_o \frac{1 + (1+\varepsilon)\, i\omega_1}{1 + \varepsilon + i\omega_1}$	$M_o \frac{i\omega_1 - \varepsilon\omega_1^2}{\varepsilon + i\omega_1}$

Fig.1-1 Schematic diagrams of four simple viscoelastic models.

TABLE I-1

Property / Model	Modulus $M(\omega_1 = \frac{\omega}{\omega_o})$	Q	Reflection Coefficient R [For Large Q (≥ 10)]
Constant Q	$M_o(i\omega_1)^{2\gamma}$	$\cot \pi\gamma$	$\frac{\rho' C_o' - \rho C_o}{\rho' C_o' + \rho C_o} + \frac{1}{2\pi}\left(\frac{1}{Q'} - \frac{1}{Q}\right) \operatorname{Log} \omega_1 + \frac{i}{4}\left(\frac{1}{Q'} - \frac{1}{Q}\right) \operatorname{sgn} \omega_1$
Generalized Maxwell Model	$M_o \frac{(i\omega_1)^{2\gamma}}{1 + (i\omega_1)^{2\gamma}}$	$\cot \pi\gamma + \frac{\omega_1^{2\gamma}}{\sin \pi\gamma}$	
Generalized Voigt Model	$M_o[1 + (i\omega_1)^{2\gamma}]$	$\cot \pi\gamma + \frac{\omega_1^{-2\gamma}}{\sin \pi\gamma}$	Identical for the 5 Models
Generalized 3-Parameter Solid Model	$M_o \frac{1 + (1+\varepsilon)(i\omega_1)^{2\gamma}}{1 + \varepsilon + (i\omega_1)^{2\gamma}}$	$\left(1 + \frac{2}{\varepsilon(\varepsilon+2)}\right) \cot \pi\gamma + \frac{1+\varepsilon}{\varepsilon(\varepsilon+2)} \frac{\omega_1^{2\gamma} + \omega_1^{-2\gamma}}{\sin \pi\gamma}$	
Generalized 3 Parameter Fluid Model	$M_o \frac{(i\omega_1)^{2\gamma} + \varepsilon(i\omega_1)^{4\gamma}}{\varepsilon + (i\omega_1)^{2\gamma}}$	$\frac{\frac{1}{\sin \pi\gamma}\left(\varepsilon \cos 2\pi\gamma + \frac{1}{\varepsilon}\right) + \cot \pi\gamma\left(\omega_1^{2\gamma} + \omega_1^{-2\gamma}\right)}{2\varepsilon \cos \pi\gamma + \omega_1^{2\gamma} + \omega_1^{-2\gamma}}$	

Q and Reflection coefficients for generalized Viscoelastic models. The viscoelastic models are obtained when $\gamma = 1/2$. All the results are given in function of $\omega_1 = \omega/\omega_o$, ω_o being a reference frequency.

By using the development derived in Appendices A and B this equation may be written:

$$R \approx \frac{\rho' C'_0 - \rho C_0}{\rho' C'_0 + \rho C_0} + \frac{1}{2\pi}\left(\frac{1}{Q'} - \frac{1}{Q}\right) Log\left|\frac{\omega}{\omega_0}\right| + \frac{i}{4}\left(\frac{1}{Q'} - \frac{1}{Q}\right) sgn(\omega) \qquad (1.1.5)$$

This approximation is valid even for very low Q (as small as 5).

This gives

$$|R| = \left[\left(R_0 + \frac{1}{2\pi} Log\left|\frac{\omega}{\omega_0}\right|\right)^2 + \frac{1}{16}\left(\frac{1}{Q'} - \frac{1}{Q}\right)^2\right]^{1/2} \qquad (1.1.6)$$

with $R_0 = \dfrac{\rho' C'_0 - \rho C_0}{\rho' C'_0 + \rho C_0}$

When R_0 is much bigger than $\left|\frac{1}{Q'} - \frac{1}{Q}\right|$ we can write:

$$|R| - |R_0| = \frac{1}{2\pi}\left|\frac{1}{Q'} - \frac{1}{Q}\right| Log\left|\frac{\omega}{\omega_0}\right| \qquad \text{if } |\omega| \neq |\omega_0| \qquad (1.1.7)$$

and

$$|R| - |R_0| = \frac{1}{32 R_0}\left(\frac{1}{Q'} - \frac{1}{Q}\right)^2 \qquad \text{if } |\omega| = |\omega_0| \qquad (1.1.8)$$

Figures 1-2 to 1-4 show the dependence of $|R| - |R_0|$ with respect to $\frac{\omega}{\omega_0}$, with ω_0 as the center frequency of the signal. In these three figures the values of Q given are in fact the values of $\left(\frac{1}{Q'} - \frac{1}{Q}\right)^{-1}$. When Q=0 this expression gives the value of Q'.

In Figure 1-2 there is no acoustic impedance contrast and so R_0=0.

In Figure 1-3 R_0=0.01. The results show that, for a typical seismic signal for which the spectrum width is about $\frac{\omega_N}{4}$(ω_N = Nyquist frequency) and the center frequency is $\frac{\omega_N}{3}$, we have an observable effect on the reflected amplitudes for Q around 70.

In Figure 1-4 R_0=0.1. In this case, to observe any effect, we need a Q of the order of 7 or smaller, which is unlikely in the earth.

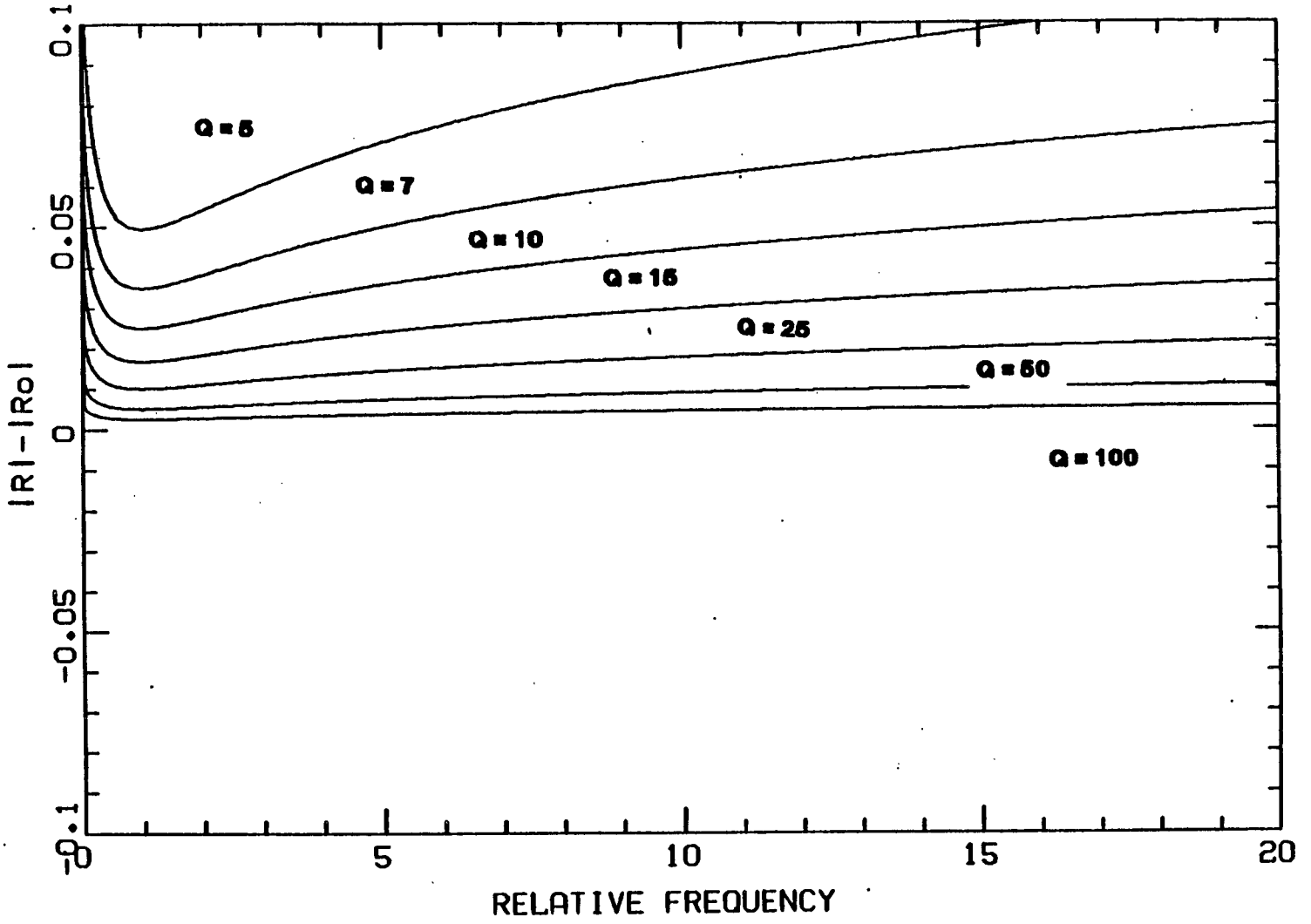

Fig.1-2 Additional effect of attenuation on the reflected amplitude. In this figure, the elastic reflection coefficient, Ro, is equal to 0. The different curves represent the amplitude effect of attenuation for different Q-contrasts. The given value of Q is equal to the inverse of (1/Q - 1/Q'). The relative frequency is $\frac{\omega}{\omega_0}$, ω_0 being the center frequency of the signal.

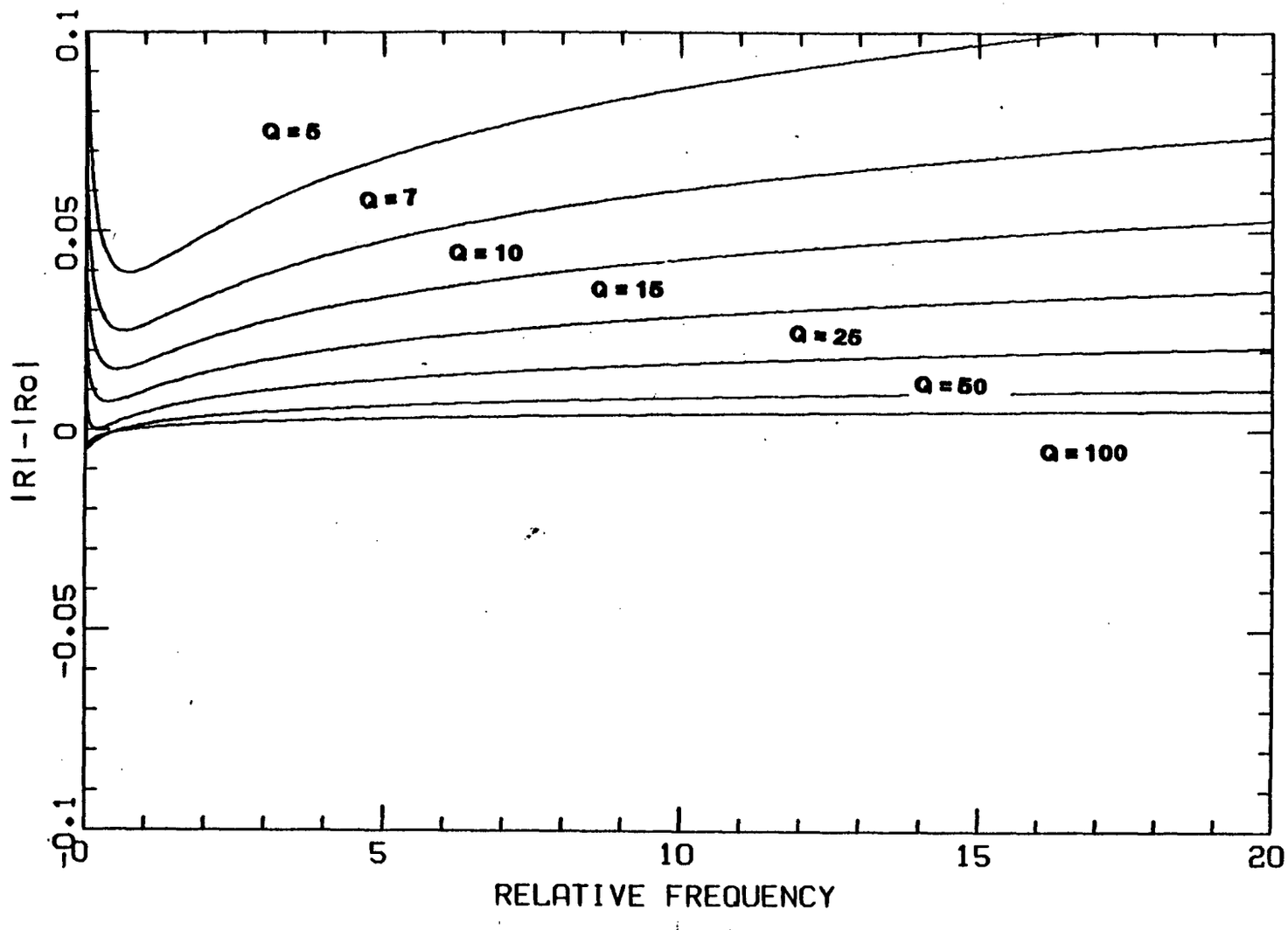

Fig.1-3 Additional effect of attenuation on the reflected amplitude. In this figure, the elastic reflection coefficient,Ro, is equal to 0.01. The different curves represent the amplitude effect of attenuation for different Q-contrasts. The given value of Q is equal to the inverse of (1/Q - 1/Q'). The relative frequency is $\frac{\omega}{\omega_0}$, ω_0 being the center frequency of the signal. In relative scale, each tick on the y-axis represent 100% of amplitude increase.

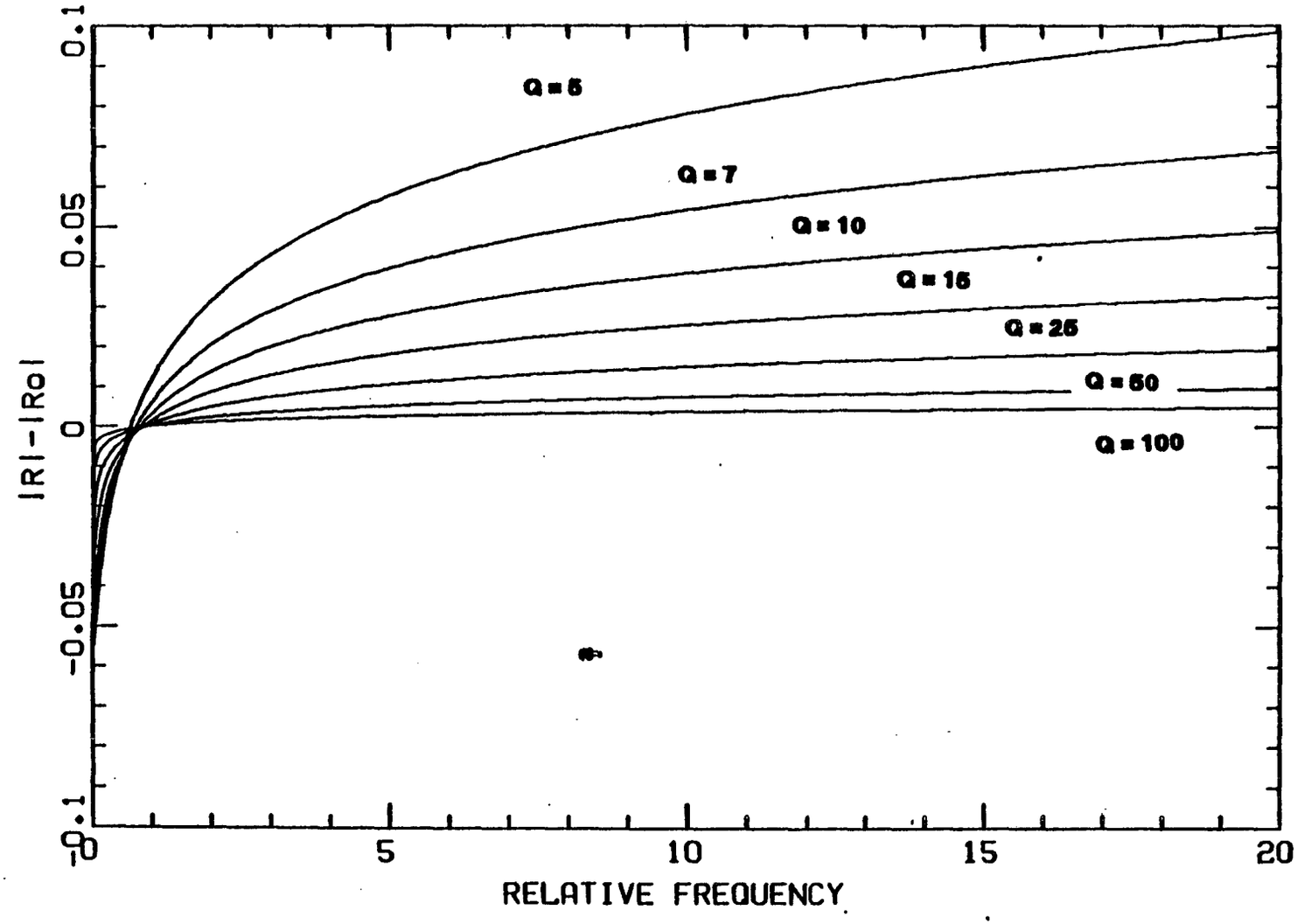

Fig.1-4 Additional effect of attenuation on the reflected amplitude. In this figure, the elastic reflection coefficient,Ro, is equal to 0.1. The different curves represent the amplitude effect of attenuation for different Q-contrasts. The given value of Q is equal to the inverse of (1/Q - 1/Q'). The relative frequency is $\frac{\omega}{\omega_0}$, ω_0 being the center frequency of the signal. In relative scale, each tick on the y-axis represent 10% of amplitude increase.

II-EFFECT OF ATTENUATION CONTRAST ON THE SHAPE OF THE TIME SIGNAL

Another interesting effect is that of the Q contrast on the shape of the signal. If the reflector is at a depth x and if the impulse response is $k(x,t)$ we have :

$$y(t) = s(t) * k(x,t) * r(t) * k(x,t) \tag{1.1.9}$$

with

$y(t)$ = recorded trace

$s(t)$ = signal

$r(t)$ = reflection coefficient which is a function of time when there is Q contrast.

We can write the Fourier Transform of the impulse response in the following form:

$$K(\omega) = e^{-\alpha x} e^{-i\omega\frac{x}{c}} \tag{1.1.10}$$

Then α and c are given by the model we are considering. In our case we still use the CQ model (Kjartansson,1979). With this model we have:

$$C = C_0 \left|\frac{\omega}{\omega_0}\right|^{\gamma} \tag{1.1.11}$$

with

$$C_0 = \frac{\left(\frac{M_0}{\rho}\right)^{1/2}}{\cos\left(\frac{\pi\gamma}{2}\right)} \tag{1.1.12}$$

$$\gamma = \frac{1}{\pi}\tan^{-1}\left(\frac{1}{Q}\right) \tag{1.1.13}$$

$$\alpha = \frac{\omega}{C}\tan\left(\frac{\pi\gamma}{2}\right) sgn(\omega) \tag{1.1.14}$$

The results for a Dirac source traveling in an attenuating medium are given in Figures 1-5, 1-6 and 1-7. The plots are time plots of the signal recorded.

In Figure 1-5 there is no impedance contrast, and we change the Q-contrast from trace to trace. The middle trace is the trace without Q-contrast. The change of sign for Q-contrast is equivalent to a change of phase on the signal.

In Figure 1-6 there is a slight impedance contrast and the effect of different Q-contrast on the pulse may be seen. This figure has the same scale as figure 1-5. As in the

previous figure one can see the pulse without the Q- contrast which corresponds to the well-known shape described by Kjartansson (1979) in his thesis.

In Figure 1-7 there is a bigger impedance contrast, and the effect of the Q-contrast is apparent only on the amplitudes. This figure has a different scale than the first two.

We shall show in Part III (Experimental part) the effect of the Q-contrast on a given signal.

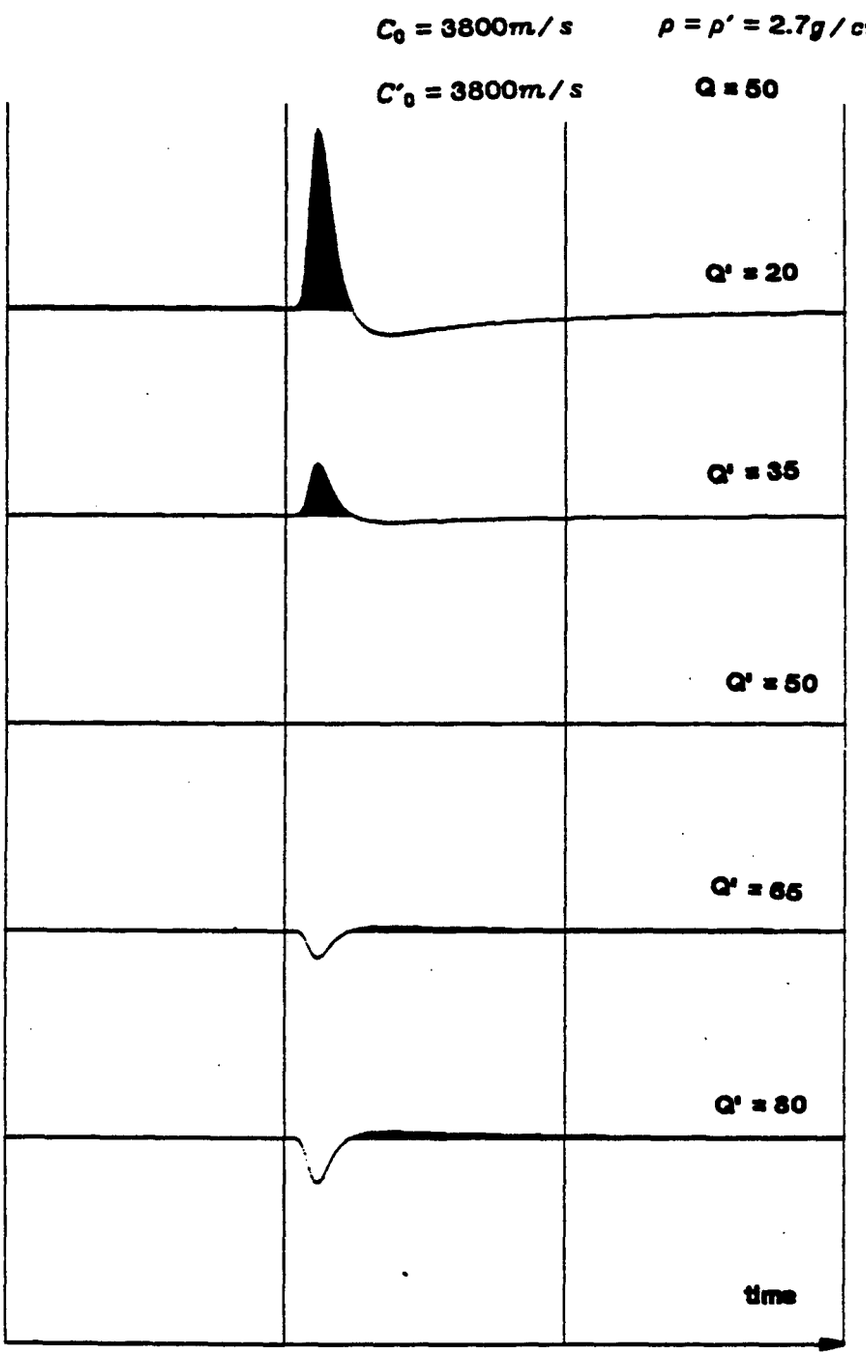

Fig.1-5 Effect of attenuation on a Dirac pulse (one dimensional case). The wave is traveling in a medium with a Q = 50 and is reflected at an viscoelastic interface, the second medium quality factor being variable (=Q'). There is absolutely no acoustic impedance contrast i.e Ro = 0. The third pulse is the pulse recorded when there is no Q-contrast effect on the reflection.

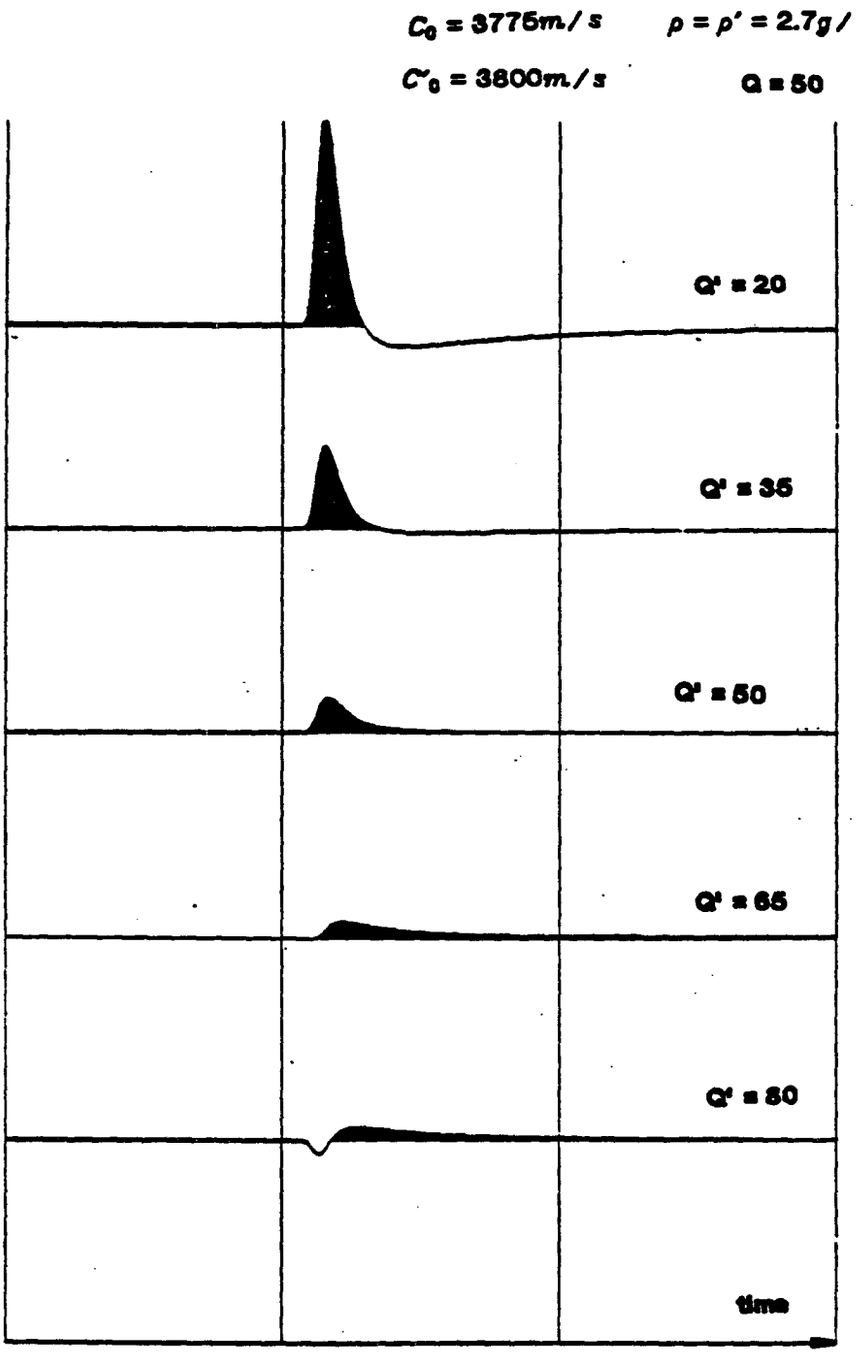

Fig.1-6 Effect of attenuation on a Dirac pulse (one dimensional case). The wave is traveling in a medium with a Q = 50 and is reflected at an viscoelastic interface, the second medium quality factor being variable (=Q'). There is a very small acoustic impedance contrast i.e Ro = 0.003. The third pulse is the pulse recorded when there is no Q-contrast effect on the reflection.

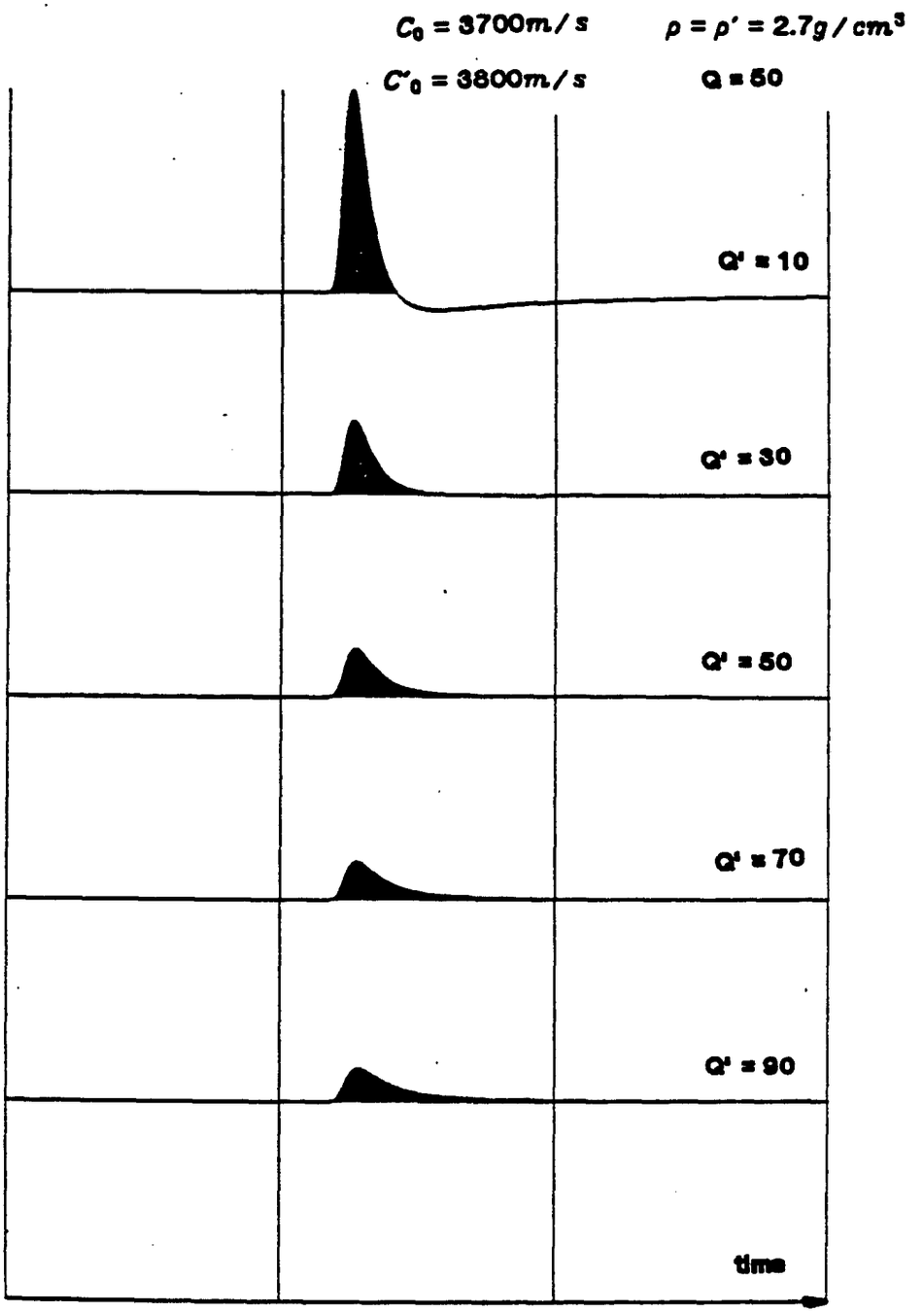

Fig.1-7 Effect of attenuation on a Dirac pulse (one dimensional case). The wave is traveling in a medium with a Q = 50 and is reflected at an viscoelastic interface , the second medium quality factor being variable (=Q'). There is a small acoustic impedance contrast i.e Ro = 0.013. The third pulse is the pulse recorded when there is no Q-contrast effect on the reflection.

APPENDIX A

Since the method of calculating Q and its effect on the reflection coefficient is similar for every viscoelastic model, we derive the results for only one of them, the generalized Maxwell model.

The relations we use are the following.

$$C^2(\omega) = \frac{M(\omega)}{\rho} \tag{1.1.16}$$

where $C(\omega)$ is the phase velocity and ρ the density.

$$\frac{1}{Q} = tan(\delta) \tag{1.1.16}$$

where δ is the phase angle between stress and strain which are related in the Fourier domain by the relation

$$\Sigma(\omega) = M(\omega)\, E(\omega) \tag{1.1.17}$$

We have also

$$R = \frac{\rho' C' - \rho C}{\rho' C' + \rho C} \tag{1.1.18}$$

where R is the reflection coefficient and (ρC) and $(\rho' C')$ the acoustic impedances of the two medias.

For the Maxwell model, we have

$$M(\omega) = M_0 \frac{(i\omega_1)^{2\gamma}}{1 + (i\omega_1)^{2\gamma}} \tag{1.1.19}$$

with

$$\omega_1 = \frac{\omega}{\omega_0} \tag{1.1.20}$$

As

$$(i\omega_1)^{2\gamma} = |\omega_1|^{2\gamma} e^{i\gamma\,\mathrm{sign}(\omega_1)} \tag{1.1.21}$$

we can write

$$M(\omega) = M_0 A(\omega_1) e^{i\phi(\omega_1)} \tag{1.1.22}$$

with

$$A(\omega_1) = \frac{|\omega_1|^{2\gamma}}{\left[1 + 2|\omega_1|^{2\gamma} x \cos(\pi\gamma) + |\omega_1|^{4\gamma}\right]^{1/2}} \tag{1.1.23}$$

and

$$\sigma(\omega_1) = \left[\gamma\pi - \tan^{-1}\left(\frac{|\omega_1|^{2\gamma}\sin(\pi\gamma)}{1 + |\omega_1|^{2\gamma}\cos(\pi\gamma)}\right)\right] sgn(\omega_1) \tag{1.1.24}$$

So using (1.1.15) we obtain

$$C(\omega) = C_0 A^{1/2}(\omega) e^{\frac{i\vartheta(\omega)}{2}} \tag{1.1.25}$$

with

$$C_0 = \left(\frac{M_0}{\rho}\right)^{1/2} \tag{1.1.26}$$

and using (1.1.16) and (1.1.17) we have

$$Q = \cot|\vartheta| \tag{1.1.27}$$

This gives

$$Q = \cot(\pi\gamma) + \frac{|\omega_1|^{2\gamma}}{\sin(\pi\gamma)} \tag{1.1.28}$$

To obtain R, we use (1.1.15) and (1.1.18) and a result, proved in Appendix B:

$$\frac{xy - 1}{xy + 1} \approx \frac{x - 1}{x + 1} + \frac{1}{2} Logy \tag{1.1.29}$$

So then we have

$$R = \frac{\frac{\rho' C'}{\rho C} - 1}{\frac{\rho' C'}{\rho C} + 1} \tag{1.1.30}$$

or

$$R = \frac{\frac{\rho' C'_0}{\rho C}\left[\frac{A'(\omega_1)}{A(\omega_1)}\right]^{1/2} e^{\frac{i}{2}(\vartheta' - \vartheta)} - 1}{\frac{\rho' C_0'}{\rho C_0}\left[\frac{A'(\omega_1)}{A(\omega_1)}\right]^{1/2} e^{\frac{i}{2}(\vartheta' - \vartheta)} + 1} \tag{1.1.31}$$

This can be written

$$R = \frac{\rho' C_0' - \rho C_0}{\rho' C_0' + \rho C_0} + \frac{1}{4} Log \frac{A'(\omega_1)}{A(\omega_1)} + \frac{i}{4}\left[\vartheta'(\omega_1) - \vartheta(\omega_1)\right] \tag{1.1.32}$$

with

$$\frac{A'(\omega_1)}{A(\omega_1)} = \left|\omega_1\right|^{\pi(\gamma'-\gamma)} \left[\frac{1 + 2\left|\omega_1\right|^{\pi\gamma}\cos(\pi\gamma) + \left|\omega_1\right|^{2\pi\gamma}}{1 + 2\left|\omega_1\right|^{\pi\gamma'}\cos(\pi\gamma') + \left|\omega_1\right|^{2\pi\gamma'}}\right]^{1/2} \tag{1.1.33}$$

and

$$\vartheta'(\omega_1) - \vartheta(\omega_1) = sgn(\omega)\left[\pi(\gamma'-\gamma) - \tan^{-1}\left(\frac{\left|\omega_1\right|^{\pi\gamma'}\sin\pi\gamma'}{1 + \left|\omega_1\right|^{\pi\gamma'}\omega\pi\gamma'}\right) + \tan^{-1}\left(\frac{\left|\omega_1\right|^{\pi\gamma}\sin\pi\gamma}{1 + \left|\omega_1\right|^{\pi\gamma}\omega\pi\gamma}\right)\right] \tag{1.1.34}$$

When Q and Q' are large (≥ 10) we can show that γ and γ' are small, and so we can develop the preceding expressions:

$$\frac{A'(\omega_1)}{A(\omega_1)} \approx \left|\omega_1\right|^{\pi(\gamma'-\gamma)} - \frac{1 + 2\gamma Log\left|\omega_1\right|}{1 + 2\gamma' Log\left|\omega_1\right|} \tag{1.1.35}$$

$$\vartheta'(\omega_1) - \vartheta(\omega_1) \approx \pi\, sgn(\omega)\,\frac{\gamma'-\gamma}{2} \tag{1.1.36}$$

So

$$R \approx \frac{\rho' C_0' - \rho C_0}{\rho' C_0' + \rho C_0} + \frac{1}{4}(\gamma'-\gamma) Log\left|\omega_1\right| + \frac{i}{8}\pi(sgn\,\omega)(\gamma'-\gamma) \tag{1.1.37}$$

We use the same type of approximations for Q and we obtain

$$Q = \frac{2}{\pi\gamma} \tag{1.1.38}$$

To compare with the constant Q model we must compare γ for different models but for the same medium, that is to say, the same Q.

We find that

$$Q_{(cq)} = \frac{1}{\pi\gamma_{(cq)}} \tag{1.1.39}$$

The subscript CQ means Constant Q Model. And

$$Q_{(M.W.)} = \frac{2}{\pi\gamma_{(M.W.)}} \tag{1.1.40}$$

The subscript M.W. indicates the Maxwell Model. So

$$\gamma_{(M.W.)} = 2\gamma_{(CQ)} \tag{1.1.41}$$

And so in terms of Q, $R_{(CQ)}$ and $R_{(M.W.)}$ have the same frequency dependence at a first order approximation:

$$R = R_0 + \frac{1}{2\pi}\left[\frac{1}{Q'} \quad \frac{-1}{Q}\right] Log\left|\omega_1\right| + \frac{i}{4}\left[\frac{1}{Q'} - \frac{1}{Q}\right] sgn(\omega_1) \tag{1.1.42}$$

APPENDIX B

We want to look at the accuracy of the following formula

$$\frac{xy-1}{xy+1} = \frac{x-1}{x+1} + \frac{1}{2}Logy \tag{1.1.43}$$

The power series expression of the inverse function of $\tanh^{-1}(r)$ is

$$\tanh^{-1}(r) = \frac{1}{2}Log\left(\frac{1+r}{1-r}\right) = r + \frac{r^3}{3} + \frac{r^5}{5} + \cdots \tag{1.1.44}$$

If we take

$$r = \frac{x-1}{x+1} \tag{1.1.45}$$

which is equivalent to

$$x = \frac{1+r}{1-r} \tag{1.1.45b}$$

Then we obtain

$$\tanh^{-1}\frac{(x-1)}{(x+1)} = \frac{x-1}{x+1} + \frac{1}{3}\left[\frac{x-1}{x+1}\right]^3 + \frac{1}{5}\left[\frac{x-1}{x+1}\right]^5 + \cdots \tag{1.1.46}$$

In the same way, we have :

$$\frac{1}{2}Logxy = \frac{xy-1}{xy+1} + \frac{1}{3}\left[\frac{xy-1}{xy+1}\right]^3 + \ldots\ldots = \frac{1}{2}Logx + \frac{1}{2}Logy \tag{1.1.47}$$

By combining (1.1.46) and (1.1.47), we obtain

$$\frac{xy-1}{xy+1} = \frac{x-1}{x+1} + \frac{1}{2}Logy + \frac{1}{3}\left[\frac{(x-1)^3}{(x+1)^3} - \frac{(xy-1)^3}{(xy+1)^3} + \cdots\right] \tag{1.1.48}$$

As we are looking at small effects, we can write

$$y = 1 + \varepsilon \tag{1.1.49}$$

with ε small

ε represents in our case the ratio $\left|\frac{\omega}{\omega_0}\right|^{r-r}$

Then

$$\left[\frac{xy-1}{xy+1}\right]^3 = \left[\frac{x-1+\varepsilon x}{x+1+\varepsilon x}\right]^3 = \left[1 + \frac{6\varepsilon x}{x^2-1} + \cdots\right] \tag{1.1.50}$$

And the error obtained in applying the approximate formula given by (1) becomes

$$\Delta = \frac{1}{3}\left[\frac{(x-1)^3}{(x+1)^3} - \frac{(xy-1)^3}{(xy+1)^3}\right] = 2\varepsilon x\frac{(x-1)^2}{(x+1)^4} \qquad (1.1.51)$$

It is interesting to give some values to what is the practical accuracy of this formula. If we take a huge value for a reflection coefficient that is to say:

$$r = \frac{x-1}{x+1} = 0.4 \qquad (1.1.52)$$

Then we get

$$\frac{|\Delta|}{r} = 0.17\varepsilon \qquad (1.1.53)$$

If now we take for ε a value of 10 % (which is very important too) we are getting

$$\frac{|\Delta|}{r} \approx 2\%$$

This is a good approximation.

A more reasonable, but still large, for r will be 0.1 . Then

$$\frac{|\Delta|}{r} = .05\varepsilon \qquad (1.1.54)$$

For ε we can take 5% and so we get

$$\frac{|\Delta|}{r} = .25\%$$

The formula is then very accurate.

REFERENCES

Kjartansson.E, Constant Q: Wave propagation and attenuation, J.Geophys.Res., 84, 4737-3748, 1979.

Kjartansson.E, Attenuation of seismic waves in rocks, Ph.D thesis, Stanford University, Stanford Calif., 1979.

Winkler.K, Nur.A, Seismic attenuation: Effects of pore fluids and frictional sliding, Geoph., 47, 1-15, 1982.

B - REFLECTION AND TRANSMISSION IN ATTENUATING MEDIA

INTRODUCTION

In this chapter we look at the reflection and transmission of plane waves in a laterally homogeneous attenuating space. To be more precise the space we work with is linear and viscoelastic. This hypothesis as an earth-model has already been justified in Part I-A.

We examine two cases:

1) solid-solid interface

2) liquid-solid interface

Our incident waves are either SV-waves or P-waves. The problem can be set up in exactly the same way for SH-waves and is simpler because there is no conversion from P to SV-waves or vice versa.

This paper is not innovative with respect to the material included but is an attempt to synthesize previous works and to define notations to be used subsequently (cf Part I-C " Constant-Q Model in Two-Dimensions ? ").

I- GENERAL THEORY OF VISCOELASTICITY

The linear viscoelasticity hypothesis can be expressed by a generalized Hooke's law relating the stresses σ to the strains ε.

$$\sigma_{ij}(t) = G_{ijkl}(t) * \dot{\varepsilon}_{kl}(t)$$

which is equivalent to

$$\sigma_{ij}(t) = C_{ijkl}(t) * \varepsilon_{kl}(t) \qquad (1.2.1)$$

where $C_{ijkl} = \dot{G}_{ijkl}$ In these equations, Einstein's notation is used (i.e summation on repeated indices). This notation will be employed throughout this thesis.

It is important to note that the matrix of "elasticity" is now time dependent. In the isotropic case the stress strain relation reduces to

$$\sigma_{ij}(t) = \delta_{ij}\left[K(t) - \frac{2\mu(t)}{3}\right] * \varepsilon_{kk}(t) + 2\mu(t) * \varepsilon_{ij}(t) \qquad (1.2.2)$$

with δ_{ij} = Kronecker symbol

$K(t)$ = Bulk Modulus

$\mu(t)$ = Shear Modulus

Here also the moduli are time-dependent. In the elastic case they may be written:

$$K(t)=K_0\delta(t) \qquad (1.2.3a)$$

$$\mu(t)=\mu_0\delta(t) \qquad (1.2.3b)$$

where $\delta(t)$ is the Dirac distribution.

The equations of motion are obtained by conservation of mass and linear momentum

$$\partial_j \sigma_{ij} + f_i = \rho \ddot{u}_i \qquad (1.2.4)$$

with f_i = body force per unit volume

and u_i = i^{th} component of the displacement

As we consider seismic waves, we use the approximation of infinitesimal strains. Strain amplitudes found in seismic exploration are very small: one or two wave-length from the source, the strain amplitude is of the order of 10^{-6} or smaller.

$$\varepsilon_{ij} = \frac{1}{2}(\partial_j u_i + \partial_i u_j) \qquad (1.2.5)$$

Combining equations (1.2.4) and (1.2.5) into (1.2.2) we obtain

$$\rho \ddot{u}_i = \delta_{ij}\left[K(t) - \frac{2\mu(t)}{3}\right] * \partial^2_{jk} u_k + \mu(t) * \partial^2_{jj} u_i + \mu(t) * \partial^2_{ij} u_j \qquad (1.2.6)$$

In this equation u is a function of time and spatial coordinates.

If we take a time dependent u of the form $e^{i\omega t}$, equation (1.2.6) can be written:

$$\rho \ddot{U}_i = \delta_{ij}\left[K(t) - \frac{2\mu(t)}{3}\right] * \left[\partial^2_{jk} U_k\, e^{i\omega t}\right] + \mu(t) * \left[\left[\partial^2_{jj} U_i + \partial^2_{ij} U_j\right] e^{i\omega t}\right] \qquad (1.2.7)$$

In this equation U is a function of spatial coordinates only.

This can be rewritten using the following relationship:

$$m(t)*\left[\partial^2_{jk} U_k \, e^{i\omega t}\right] = M(\omega)\, \partial^2_{jk} U_k \, e^{i\omega t} \tag{1.2.8}$$

This gives

$$-\rho\omega^2 U_i = \left[K(\omega) - \frac{2\mu(\omega)}{3}\right]\partial^2_{jk} U_k + \mu(\omega)\partial^2_{jj} U_i \tag{1.2.9}$$

We can rewrite this equation in terms of vectors instead of coordinates. We can also come back to a displacement function of time and spatial coordinates. This gives

$$\left[K(\omega) + \frac{\mu(\omega)}{3}\right]\vec{\nabla}\vartheta + \mu(\omega)\nabla^2\vec{u} = \rho\ddot{\vec{u}} \tag{1.2.10}$$

with ϑ = volumetric dilation = $\nabla\cdot\vec{u}$

This equation is the familiar form of the wave equation for elastic media. The only difference is that now we are dealing with frequency dependent moduli. To insure the causality of these moduli in the time domain they need to be complex in the frequency domain. We can now continue our theoretical development as for normal elasticity.

We can transform equation (1.2.14) by using the Helmholtz form for $\vec{u}$

$$\vec{u} = \vec{\nabla}\Phi + \vec{\nabla}\times\vec{\Psi} \tag{1.2.11}$$

with $\nabla\cdot\vec{\Psi} = 0$

Combining equation (1.2.11) into (1.2.10), we obtain the two well-known wave equations in elasticity theory

$$\nabla^2\Phi + k_p^2\Phi = 0 \tag{1.2.12a}$$

$$\nabla^2\vec{\Psi} + k_s^2\vec{\Psi} = 0 \tag{1.2.12b}$$

with $k_p = \dfrac{\omega}{\alpha}$

and $k_s = \dfrac{\omega}{\beta}$

in which

$$\alpha = \left[\frac{K + \frac{4}{3}\mu}{\rho}\right]^{1/2} \tag{1.2.13c}$$

and

$$\beta = \left[\frac{\mu}{\rho}\right]^{1/2} \tag{1.2.13d}$$

The general plane wave solution of equations of type (1.2.12) is

$$\Phi = \Phi_0 e^{i(\omega t - \vec{k}\cdot\vec{x})} \tag{1.2.14}$$

$\vec{k}$ is a complex vector and Φ_0 a complex constant

We can write

$$\vec{k} = \vec{P} - i\vec{\alpha} \tag{1.2.15}$$

with

$\vec{P}$ = propagation vector

$\vec{\alpha}$ = attenuation vector

And the solution to equation (1.2.14) becomes

$$\Phi = \Phi_0 e^{-\vec{\alpha}\cdot\vec{x}} e^{i(\omega t - \vec{P}\cdot\vec{x})} \tag{1.2.16}$$

Since we do not want the amplitude of the wave to increase in the direction of propagation, the angle γ between $\vec{A}$ and $\vec{P}$ must satisfy

$$0 \leq \gamma < \frac{\pi}{2}$$

The existence of this angle γ and its difference from 0 imply that the planes of constant phase and the planes of constant amplitude are not parallel. Figure 1-8 shows what happens to a plane wave front at a liquid-liquid interface if there is different attenuation in the two liquids.

The waves one usually work with are ones for which planes of constant phase are parallel to planes of constant amplitude, $\gamma = 0$. These waves are called homogeneous waves. When $\gamma \neq 0$, it is natural to call these new waves inhomogeneous waves.

Equations (1.2.15) and (1.2.16) give us

$$|\vec{k}| = \frac{\omega}{v} = k_v \tag{1.2.17}$$

where $v = \left(\frac{M}{\rho}\right)^{1/2}$

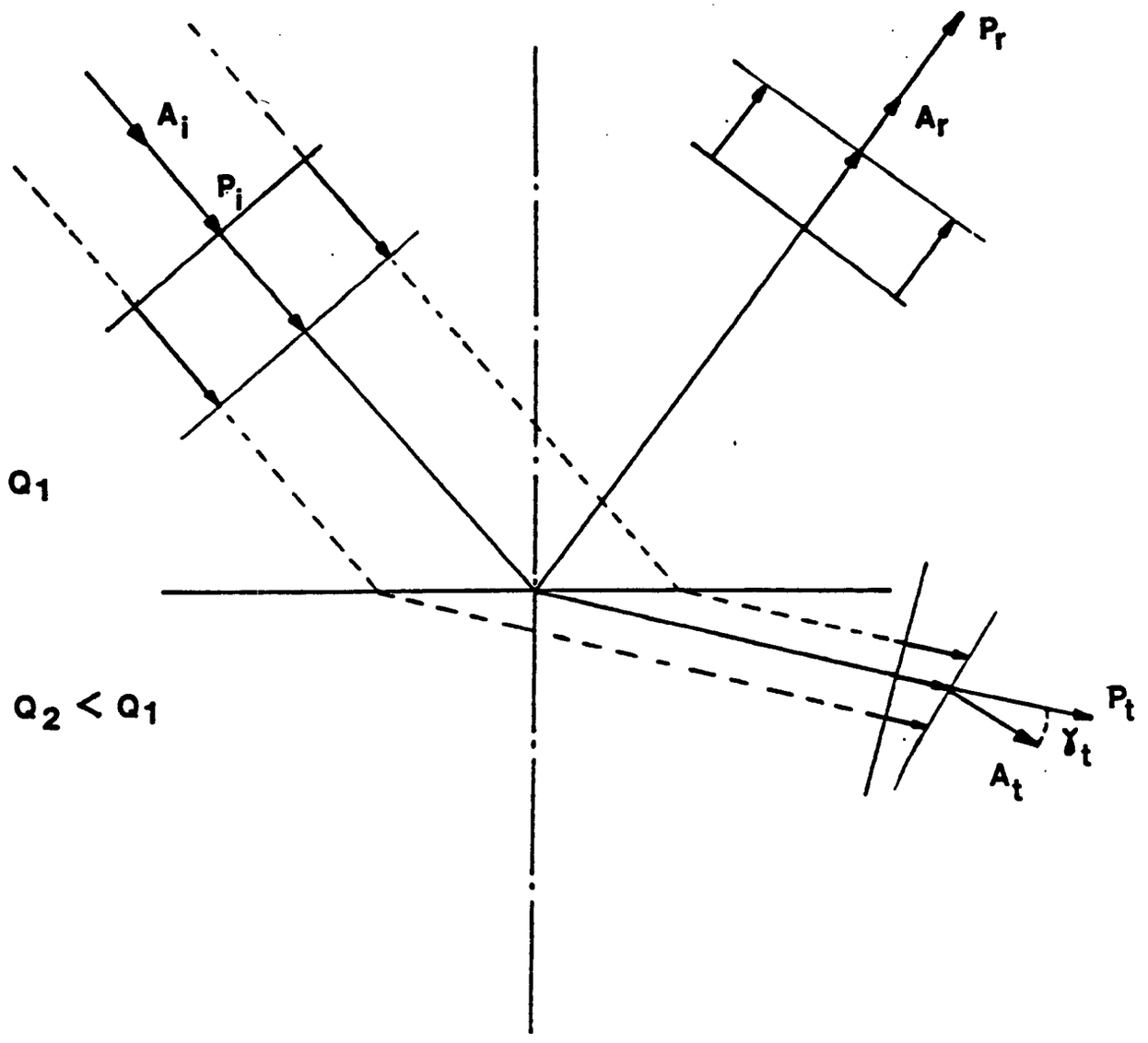

Fig.1-8 Reflection and transmission of a plane wave in a viscoelastic medium.The length of the arrows is proportional to the amplitude of the displacement. Letters A and P indicate respectively the attenuating and the propagating vectors.

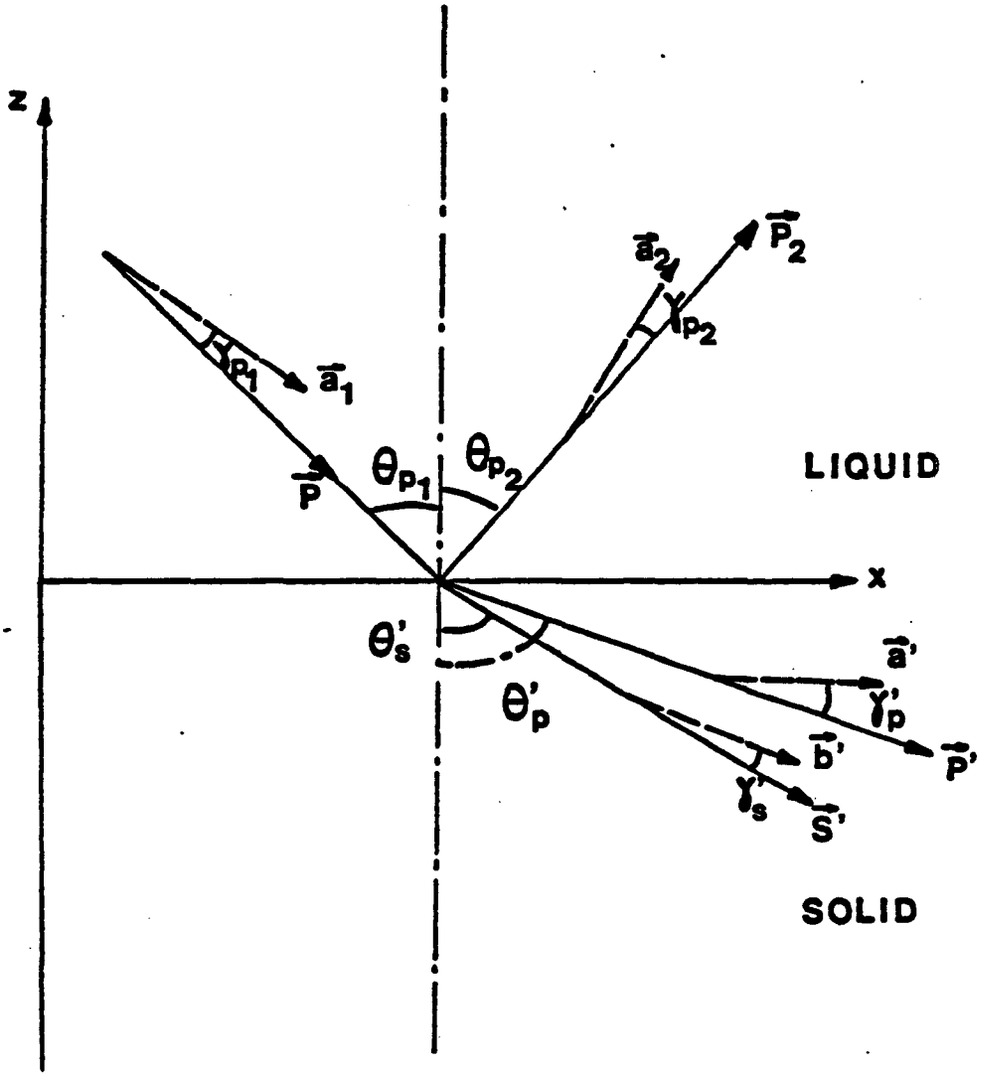

Fig.1-9 Reflection and transmission of a P-wave at a liquid-solid interface. The notations are the ones used in the text.

and where M is the elastic modulus:

for P-waves $\quad M = K + \frac{4\mu}{3}$

for S-waves $\quad M = \mu$

From (1.2.15) and (1.2.16) we also obtain :

$$|\vec{P}| = \left[\frac{1}{2}\left\{\mathrm{Re}k_v^2 + \left[(\mathrm{Re}k_v^2)^2 + \frac{(\mathrm{Im}k_v^2)^2}{\cos\gamma^2}\right]^{1/2}\right\}\right]^{1/2} \qquad (1.2.18a)$$

$$|\vec{a}| = \left[\frac{1}{2}\left\{-\mathrm{Re}k_v^2 + \left[(\mathrm{Re}k_v^2)^2 + \frac{(\mathrm{Im}k_v^2)^2}{\cos\gamma^2}\right]^{1/2}\right\}\right]^{1/2} \qquad (1.2.18b)$$

We can also calculate the phase velocity which is given by

$$\vec{V} = \omega\frac{\vec{P}}{|\vec{P}|^2} \qquad (1.2.19)$$

Following Borcherdt (1973), one can show, by using equations (1.2.18a) and (1.2.18b), that this velocity is greater for homogeneous waves than for inhomogeneous waves.

II. ENERGY EQUATION

We have seen that the displacement vector was $\vec{u}$. In fact the actual displacement vector is $\vec{u_R}$ and verifies the following equation derived from equation (1.2.10) .

$$\rho\ddot{\vec{u_R}} = (K_R + \frac{\mu_R}{3})\vec{\nabla}\vartheta_R + \mu_R\nabla^2\vec{u_R} + \frac{1}{\omega}\left\{(K_I + \frac{\mu_I}{3})\vec{\nabla}\dot{\vartheta}_R + \mu_I\nabla^2\dot{\vec{u_R}}\right\} \qquad (1.2.20)$$

In this equation and all the following ones the subscripts R and I indicates respectively the real and imaginary parts of the complex function involved.

To obtain an energy equation, we form the dot product with $\dot{\vec{u_R}}$ (Lindsay , 1960).

After transformation (Borcherdt , 1973) we obtain

$$\frac{\partial}{\partial t}\left\{\frac{\rho}{2}\dot{\vec{u_R}}^2 + \frac{1}{2}(K_R + \frac{\mu_R}{3})\vartheta_R^2 + \frac{1}{2}\mu_R\partial_j u_{Rk}.\partial_k u_{Rj}\right\}$$

$$+ \frac{1}{\omega}\left\{(K_I + \frac{\mu_I}{3})\dot{\vartheta}_R^2 + \mu_I\partial_j\dot{u}_{Rk}\dot{u}_{Rj}\right\} \qquad (1.2.21)$$

$$= \vec{\nabla}.\left\{(K_R + \frac{\mu_R}{3})\vartheta_R\dot{\vec{u_R}} + \frac{1}{\omega}(K_I + \frac{\mu_I}{3})\dot{\vartheta}_R\dot{\vec{u_R}}\right\} + \nabla\left\{\mu_R(\dot{\vec{u_R}}.\nabla\vec{u_R}) + \frac{1}{\omega}\mu_I(\dot{\vec{u_R}}.\nabla\dot{\vec{u_R}})\right\}$$

By integrating equation (1.2.21) over a volume V we obtain an equation of the form

$$\frac{\partial}{\partial t}\int_v E dv + \int_v D dv = -\int_s I.\vec{n}.d\vec{s} \qquad (1.2.22)$$

with : E= Kinetic and potential energy (in density).

D= Rate of energy dissipation per unit volume .

I= Energy flux per unit time .

Then, we can define the attenuation coefficient. This definition must be compatible with the one-dimension case. We apply the same definition as Borcherdt (1977) :

$$2\pi Q^{-1} = \frac{\textit{Loss in energy density per cycle of forced oscillation}}{\textit{Peak energy density stored during cycle}} \qquad (1.2.23)$$

By using equation (1.2.22) we can calculate this ratio. A complete development can be found in Borcherdt (1973). It gives

For P-SV waves

$$Q^{-1} = \frac{M_I + \mu_I \frac{M_I^2}{|M|^2}\tan^2\gamma}{M_R + \mu_R \frac{M_I^2}{|M|^2}\tan^2\gamma} \qquad (1.2.24)$$

The subscripts I , R are indicating the imaginary and real part respectively .

The variable M has a different expression for P and Sv waves:

For P-waves : $M = \lambda + 2\mu = K + \frac{4}{3}\mu$

For SV-waves : $M = \mu$

For SH-waves

$$Q^{-1} = \frac{2\mu_I}{\mu_R} \frac{\left[1 + \frac{\mu_I^2}{|\mu|^2}\tan\gamma^2\right]^{1/2}}{\left[1 + \left[1 + \frac{\mu_I^2}{|\mu|^2}\tan\gamma^2\right]^2\right]^{1/2}} \qquad (1.2.25)$$

These formulas are studied in more detail in the next chapter called, " Constant Q Model in Two-Dimensions " (Part I-C)

III. REFLECTION AND TRANSMISSION

Unlike the elastic case, four parameters are necessary to define completely each homogeneous wave:

1. The angle of propagation
2. The intensity of the propagation vector
3. The angle between the propagation vector and the attenuation vector
4. The intensity of the attenuation vector

These parameters are shown in a schematic way in Figure (1-9) for a liquid-liquid interface .

We are going to set up the equations that must be solved to get the transmission and reflection coefficients. In the following equations, the time dependence is omitted and understood to be $e^{i\omega t}$.

The equations are set in the case where the incident wave is a combination of P and SV-waves, and the solution to equation (1.2.10) is expressed as a function of potential solutions of equations (1.2.12a) and (1.2.12b) .

In all the following equations we have:

Subscript 1 indicating the incident waves

Subscript 2 indicating the reflected waves

Superscript ' indicating the transmitted waves

So the problem can be expressed in the following way:

$$\Phi = \Phi_1 + \Phi_2 = A_1 e^{-i(kx-dz)} + A_2 e^{-i(kx+dz)}$$

$$\Psi = \Psi_1 + \Psi_2 = B_1 e^{-i(kx-fz)} + B_2 e^{-i(kx+fz)}$$

$$\Phi' = A' e^{-i(k'x-d'z)}$$

$$\Psi' = B' e^{-i(k'x-f'z)} \qquad (1.2.26)$$

with

$$k^2 + d^2 = k_\alpha^2 = \frac{\omega^2}{\alpha^2} = \frac{\rho\omega^2}{K + \frac{4}{3}\mu}$$

$$k^2 + f^2 = k_\beta^2 = \frac{\omega^2}{\beta^2} = \frac{\rho\omega^2}{\mu}$$

$$k'^2 + d'^2 = k_\alpha'^2 = \frac{\omega^2}{\alpha'^2} = \frac{\rho\omega^2}{K' + \frac{4}{3}\mu'}$$

$$k'^2 + f'^2 = k_\beta'^2 = \frac{\omega^2}{\beta'^2} = \frac{\rho\omega^2}{\mu'} \qquad (1.2.27)$$

In all these equations the constants $(A_1, B_1, \cdots)$, the variables $(k, d, f, \cdots)$, the velocities $(\alpha, \ldots)$, the moduli $(K, \mu, \cdots)$ are complex valued quantities.

At the boundary, we have to express the continuity of stresses and displacements . Two cases must be considered :

1. SOLID-SOLID CASE

displacements $u_x = u_x'$

$u_z = u_z'$

stresses $\sigma_{xx} = \sigma_{xx}'$

$\sigma_{zz} = \sigma_{zz}'$

2. LIQUID-SOLID CASE

(The wave goes from a liquid to a solid .)

displacements $u_z = u_z'$

stresses $0 = \sigma_{xx}'$

$\sigma_{zz} = \sigma_{zz}'$

We emphasize the second case, and we take as the incident wave a homogeneous P-wave, a P-wave for which attenuation and propagation are parallel vectors.

The solid-solid case can be treated the same way . Figure (1-9) shows the notation we use. System (1.2.26) reduces to :

$$\Phi = A_1 e^{-i(kx - dz)} + A_2 e^{-i(kx + dz)}$$

$$\Psi = 0$$

$$\Phi' = A' e^{-i(k'x - d'z)}$$

$$\Psi' = B' e^{-i(k'x - f'z)} \qquad (1.2.28)$$

By definitions we have

$$\vec{P_1} = k_R\vec{x} - d_R\vec{z} = (k_R,0,-d_R) = (P_1\sin\vartheta_p,0,-P_1\cos\vartheta_p) \tag{1.2.29a}$$

$$\vec{a_1} = (-k_I,0,d_I) = (a_1\sin\vartheta_p,0,-a_1\cos\vartheta_p) \tag{1.2.29b}$$

$$\vec{P'} = (k'_R,0,-d'_R) = (P'\sin\vartheta'_p,0,-P'\cos\vartheta'_p) \tag{1.2.29c}$$

$$\vec{a'} = (-k'_I,0,-d'_I) = \left(a'\sin(\vartheta'_p-\gamma'_p),0,-a'\cos(\vartheta'_p-\gamma'_p)\right) \tag{1.2.29d}$$

and so on for the other vectors $\vec{P_2},\vec{a_2},\vec{S'},\vec{b'}$. The subscripts R and I stand for real and imaginary parts respectively . The letters $P_1,a_1,\ldots$ without arrows stand for the moduli $|\vec{P_1}|,|\vec{a_1}|,\ldots$

By using equations (1.2.18a) and (1.2.18b), we show that for an incident homogeneous wave we have:

$$P_1 = k_{aR} = \frac{\omega\sqrt{\rho}}{\left|K+\frac{4}{3}\mu\right|}\left[\frac{1}{2}\left(\left|K+\frac{4}{3}\mu\right| + K_R + \frac{4}{3}\mu_R\right)\right]^{1/2} \tag{1.2.30}$$

$$a_1 = -k_{aI} = \frac{\omega\sqrt{\rho}}{\left|K+\frac{4}{3}\mu\right|}\left[\frac{1}{2}\left(\left|K+\frac{4}{3}\mu\right| - K_R - \frac{4}{3}\mu_R\right)\right]^{1/2} \tag{1.2.31}$$

By using the boundary conditions we obtain :

$$k = k' \tag{1.2.32}$$

This relationship is important, because it is in fact a generalized Snell's law.

The boundary conditions also give us the following system:

$$\begin{aligned} &d(A_1 - A_2) = A'd' - B'k \\ &2d'kA' + B'(f'^2 - k^2) = 0 \\ &\rho\omega^2(A_1 + A_2) = \rho'\beta'^2\left[A'(f'^2 - k^2) - 2kf'B'\right] \end{aligned} \tag{1.2.33}$$

From these equations we can calculate the reflection coefficient which is given by the well-known formula (Ewing et al, 1957):

$$R = \frac{A_2}{A_1} = \frac{x-1}{x+1} \tag{1.2.34}$$

in which

$$x = \frac{\rho' \; d}{\rho \; d' \; k'_\beta{}^4} \left[(f'^2 - k^2)^2 + 4k^2 d' f' \right] \qquad (1.2.35)$$

These boundary conditions show that for reflected waves we have

$$\gamma_{P_1} = \gamma_{P_2} \qquad (1.2.36a)$$

$$\vartheta_{P_1} = \vartheta_{P_2} \qquad (1.2.36b)$$

and for transmitted waves , we obtain

$$\vartheta_p{}' = \tan^{-1} \left[\frac{\sqrt{2} k_R}{\left(\left| k_a{}'^2 - k^2 \right| + Real(k_a{}'^2 - k^2) \right)^{1/2}} \right] \qquad (1.2.37a)$$

$$\gamma_p{}' = \vartheta'_p - \tan^{-1} \left[\frac{\sqrt{2} k_I}{\left(\left| k_a{}'^2 - k^2 \right| - Real(k_a{}'^2 - k^2) \right)^{1/2}} \right] \qquad (1.2.37a)$$

and similar formulas for ϑ'_s and γ'_s .

The results are shown in Figures 1-10 to 1-14. In each figure we show the usual case (no attenuation) for comparison with the attenuating case .

REFERENCES

Borcherdt R.D., 1973, Energy and plane waves in linear viscoelastic media, J. Geophys. Res., 78, 2442-2463

Borcherdt R.D., 1977, Reflection and refraction of Type-II S-waves in elastic and anelastic medium, Bull. Seism. Soc. of Am., 67,43-67.

Cooper M.F. Jr., 1967, Reflection and transmission of oblique plane waves at a plane interface between viscoelastic media, J.Acoust. Soc. Am., 42, 1064-1069.

Ewing W.M., Jardetzky W.S., Press F., 1957, *Elastic Waves in Layered Media*, Mc Graw-Hill Book Co, New York.

Lindsay R.B., 1960, *Mechanical Radiation*, Mc Graw Hill, New-York.

Lockett F.J., 1962, The reflection and refraction of waves at an interface between viscoelastic media, J. Mech. Phys. Solids, 10, 53-64.

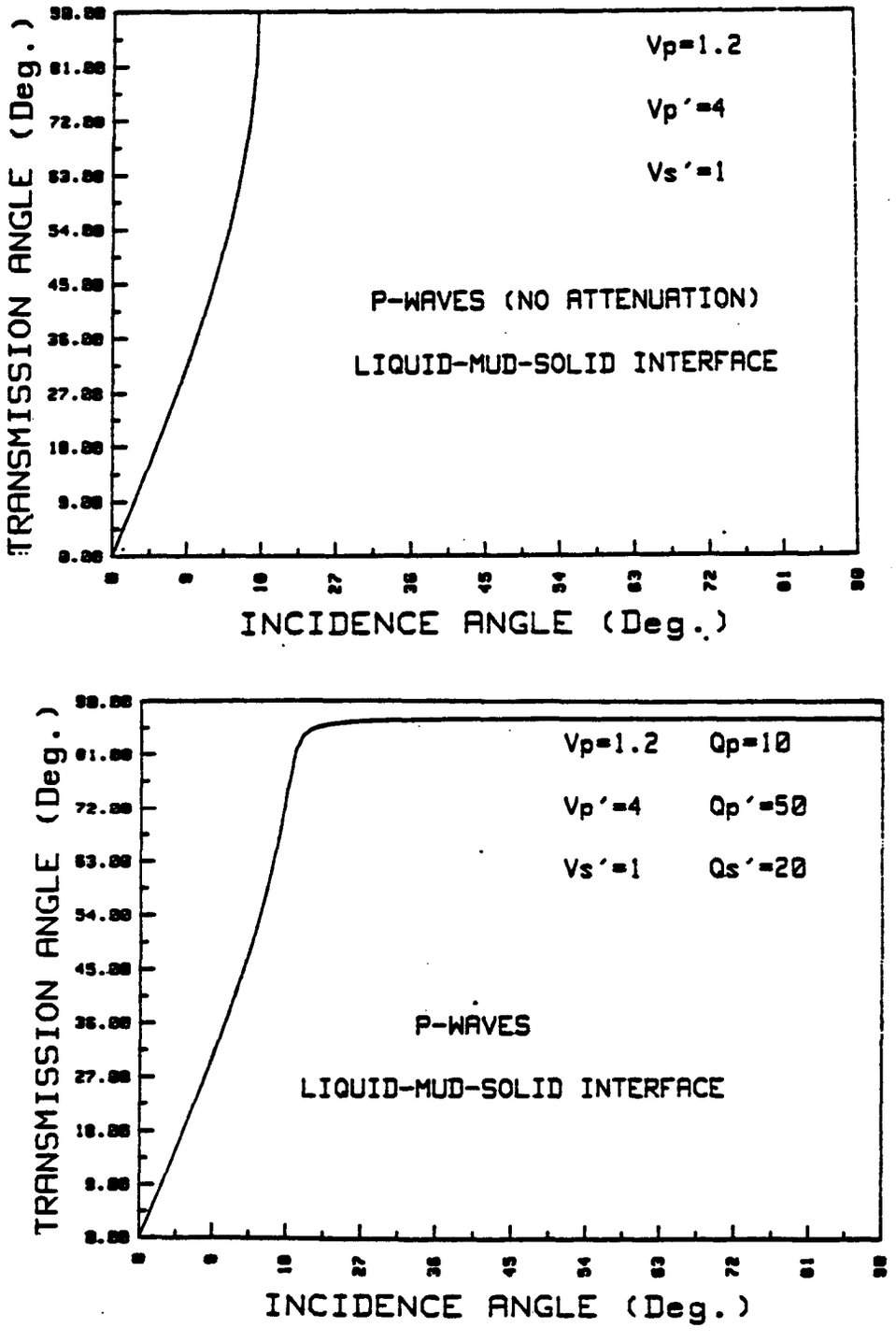

Fig.1-10 Effect of attenuation on P-transmission angle.In the top plot there is no attenuation.In the bottom one there is attenuation.

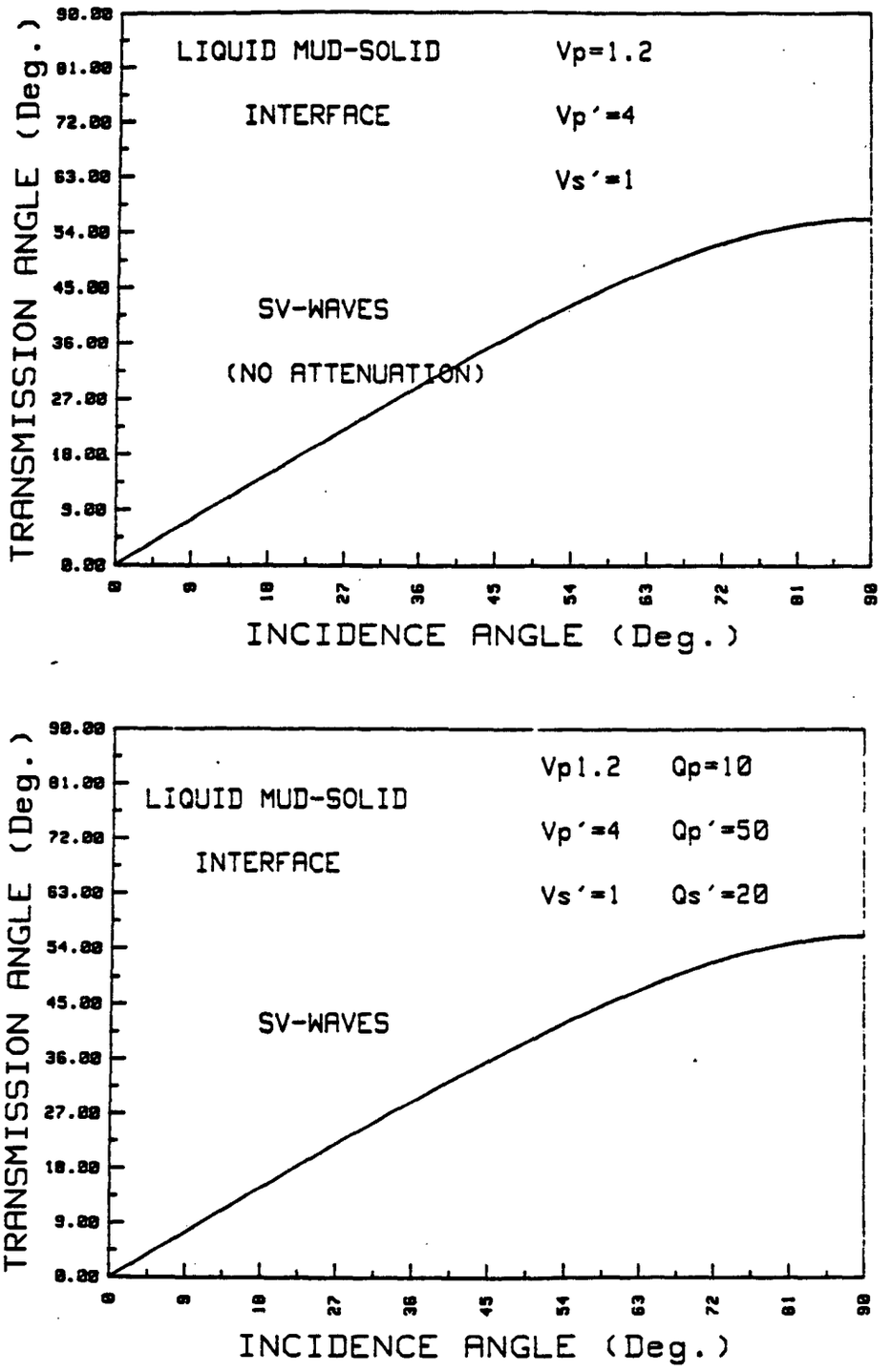

Fig.1-11 Effect of attenuation on SV-transmission angle.In the top plot there is no attenuation.In the bottom one there is attenuation.

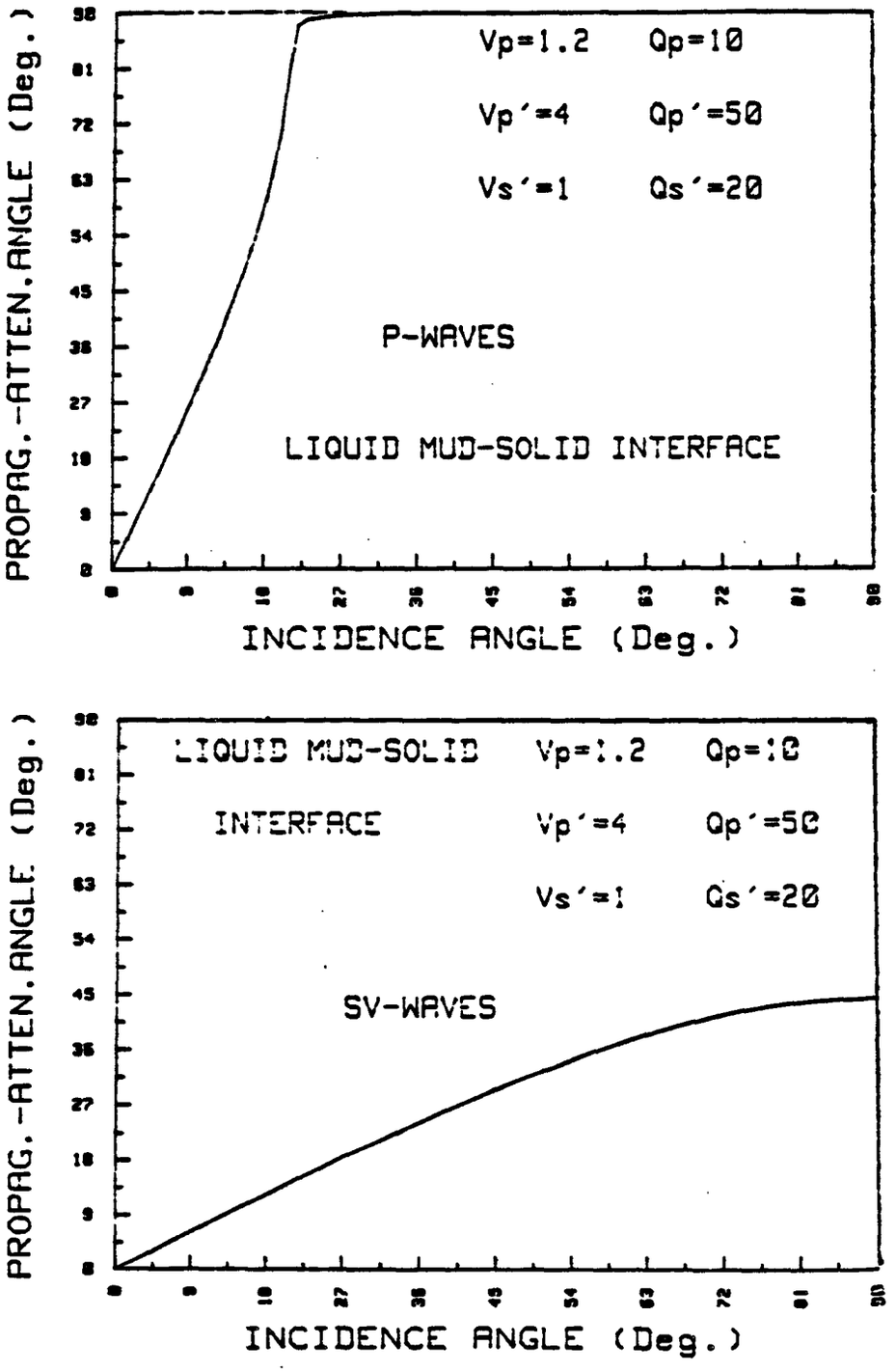

Fig.1-12 Effect of attenuation on Propagation-attenuation angle.It is the angle γ between the propagation vector and the attenuation one.In the top plot we are looking at the angle associated with P-wave . In the bottom we are looking at the angle associated with the S-wave .

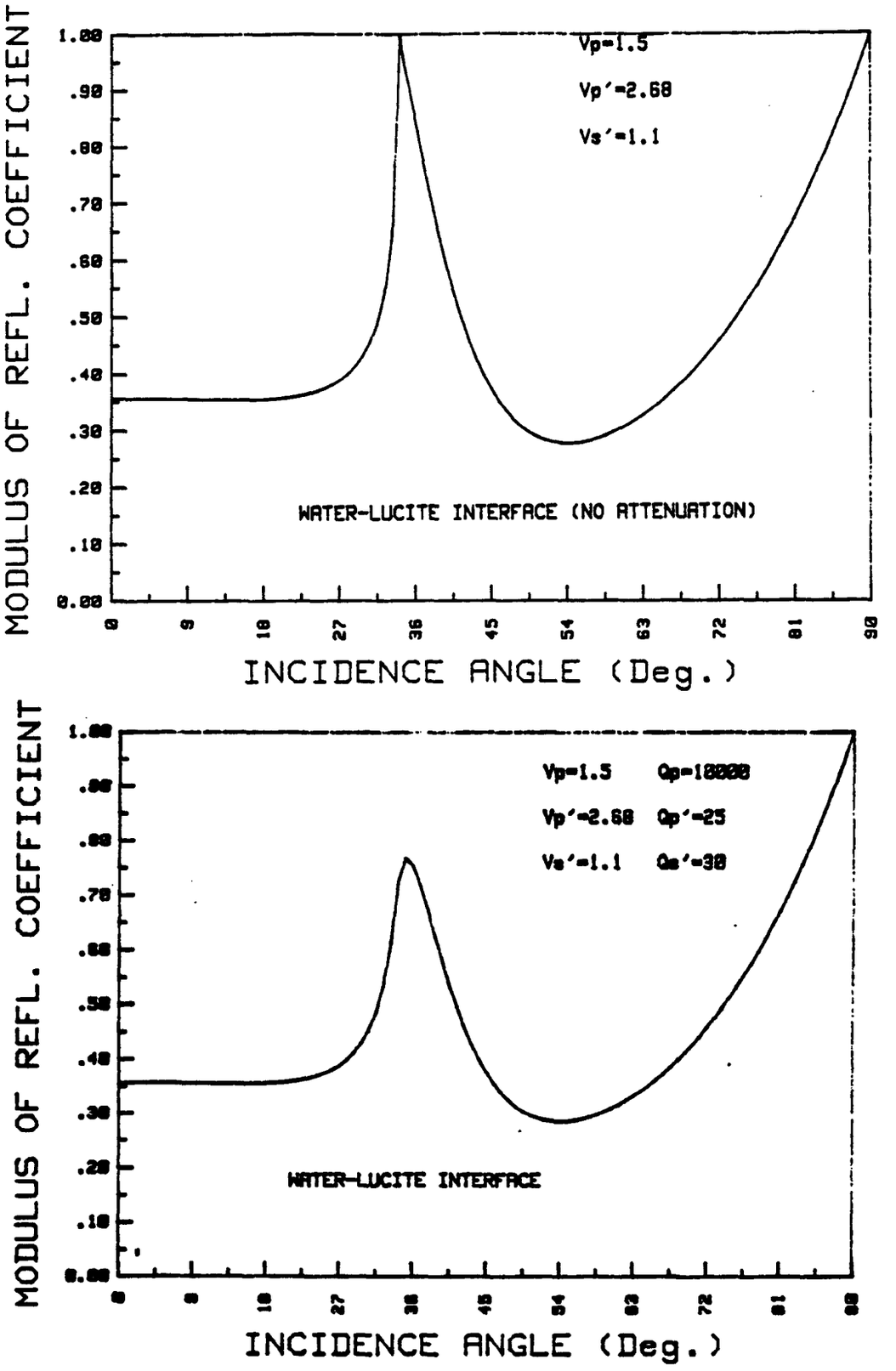

Fig.1-13 Modulus of reflection coefficient.

Top plot : No attenuation.

Bottom one : Attenuation.

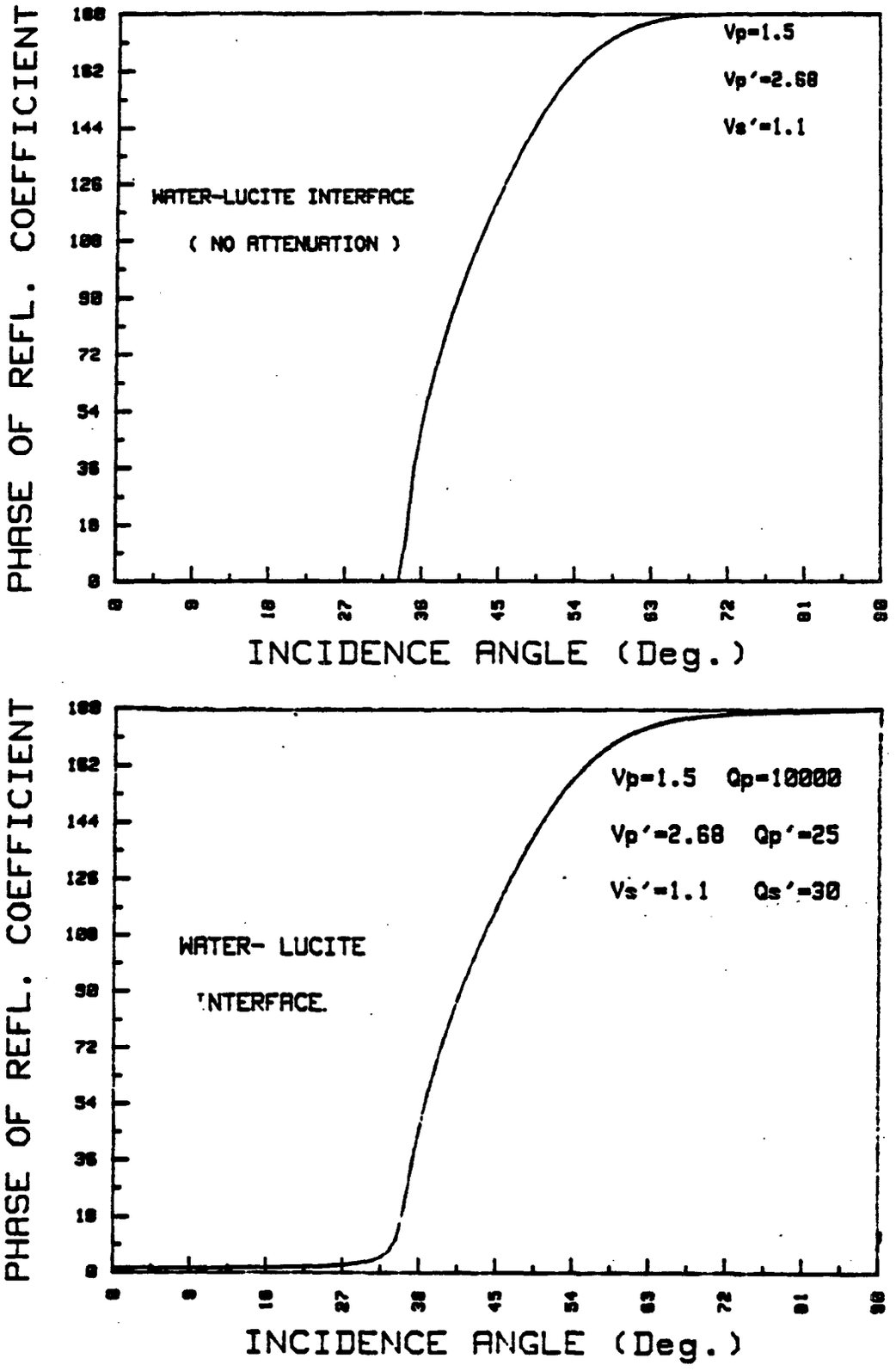

Fig.1-14 Phase of reflection coefficient.

Top plot : No attenuation.

Bottom one : Attenuation.

C - CONSTANT Q MODEL IN TWO DIMENSIONS ?

INTRODUCTION

Einar Kjartansson (1979) derived a rigorously constant-Q model for the one-dimensional case. Since in the previous chapter (Part I-B) we have derived the energy equation for wave propagation in viscoelastic media and the formulas for attenuation in a 2-D space, now we are going to study the possibility of deriving a rigorously constant Q (CQ) model in two dimensions and.

I. RECALLS

In the previous chapter (Part I-B "Reflection and transmission in linear viscoelastic media "), following Borcherdt (1977), we have defined the quality factor by the following ratio

$$2\pi Q^{-1} = \frac{Loss\ in\ energy\ per\ cycle\ of\ forced\ oscillations}{Peak\ energy\ density\ stored\ during\ the\ cycle}$$

This has given to us

$$Q_p^{-1} = \frac{(\lambda_I + 2\mu_I) + \mu_I \dfrac{(\lambda_I + 2\mu_I)^2}{|\lambda + 2\mu|^2}\tan^2\gamma_P}{(\lambda_R + 2\mu_R) + \mu_R \dfrac{(\lambda_I + 2\mu_I)^2}{|\lambda + 2\mu|^2}\tan^2\gamma_P} \qquad (1.3.1)$$

$$Q_{SV}^{-1} = \frac{\mu_I + \dfrac{\mu_I^3}{|\mu|^2}\tan^2\gamma_{SV}}{\mu_R + \dfrac{\mu_R\mu_I^2}{2|\mu|^2}\tan^2\gamma_{SV}} \qquad (1.3.2)$$

$$Q_{SH}^{-1} = \frac{2\mu_I}{\mu_R} \frac{\left[1 + \dfrac{\mu_I^2}{|\mu|^2}\tan^2\gamma_{SH}\right]^{1/2}}{1 + \left[1 + \dfrac{\mu_I^2}{|\mu|^2}\tan^2\gamma_{SH}\right]^{1/2}} \qquad (1.3.3)$$

The subscripts P,SH,SV indicate the type of wave we are looking at.

The subscripts R,I indicate the real and imaginary parts respectively.

The angles γ are the angles between the propagation and the attenuation vectors as defined previously.

In one dimension we have $\gamma_P = \gamma_S = \gamma_{SH} = 0$ and this gives the well-known formulas

$$Q_P^{-1} = \frac{\lambda_I + 2\mu_I}{\lambda_R + 2\mu_R} \tag{1.3.4}$$

$$Q_{SV}^{-1} = \frac{\mu_I}{\mu_R} = Q_{SH}^{-1} \tag{1.3.5}$$

Figures 1-15, 1-16 and 1-17 show $Q_P^{-1}, Q_{SV}^{-1}, Q_{SH}^{-1}$ as functions of the angles γ.

One can see that the effect is small even for the large attenuations that have been plotted. As a rule of thumb, one can say that the effect begins to be observable for $\gamma > 72°$.

We have seen in Part I-B that γ_P may reach values greater than 72° when the incidence angle gets close to the critical one. So we have to take into account this variation of Q as a function of γ to derive a rigorously constant-Q model. On another hand we must remember that the γ dependence is very small which implies that Q may be considered as nearly constant and equal to the 1-D value as soon when we stay under the critical angle.

We need to recall also the results derived by Einar Kjartansson (1979) for the constant Q model in one dimension.

The solution he gave is the following:

Q is a constant function of ω if the viscoelastic modulus corresponding to the considered wave is given by

$$M(\omega) = M_0 \left(\frac{i\omega}{\omega_0}\right)^{2\alpha} = M_0 \left|\frac{\omega}{\omega_0}\right|^{2\alpha} e^{i\pi\alpha\,\mathrm{sgn}(\omega)} \tag{1.3.6}$$

which gives for Q :

$$Q^{-1} = \tan(\pi\alpha) \tag{1.3.7}$$

ω_0 being a reference frequency and $M_0 = M(\omega_0)$

This result will be used in the next paragraph.

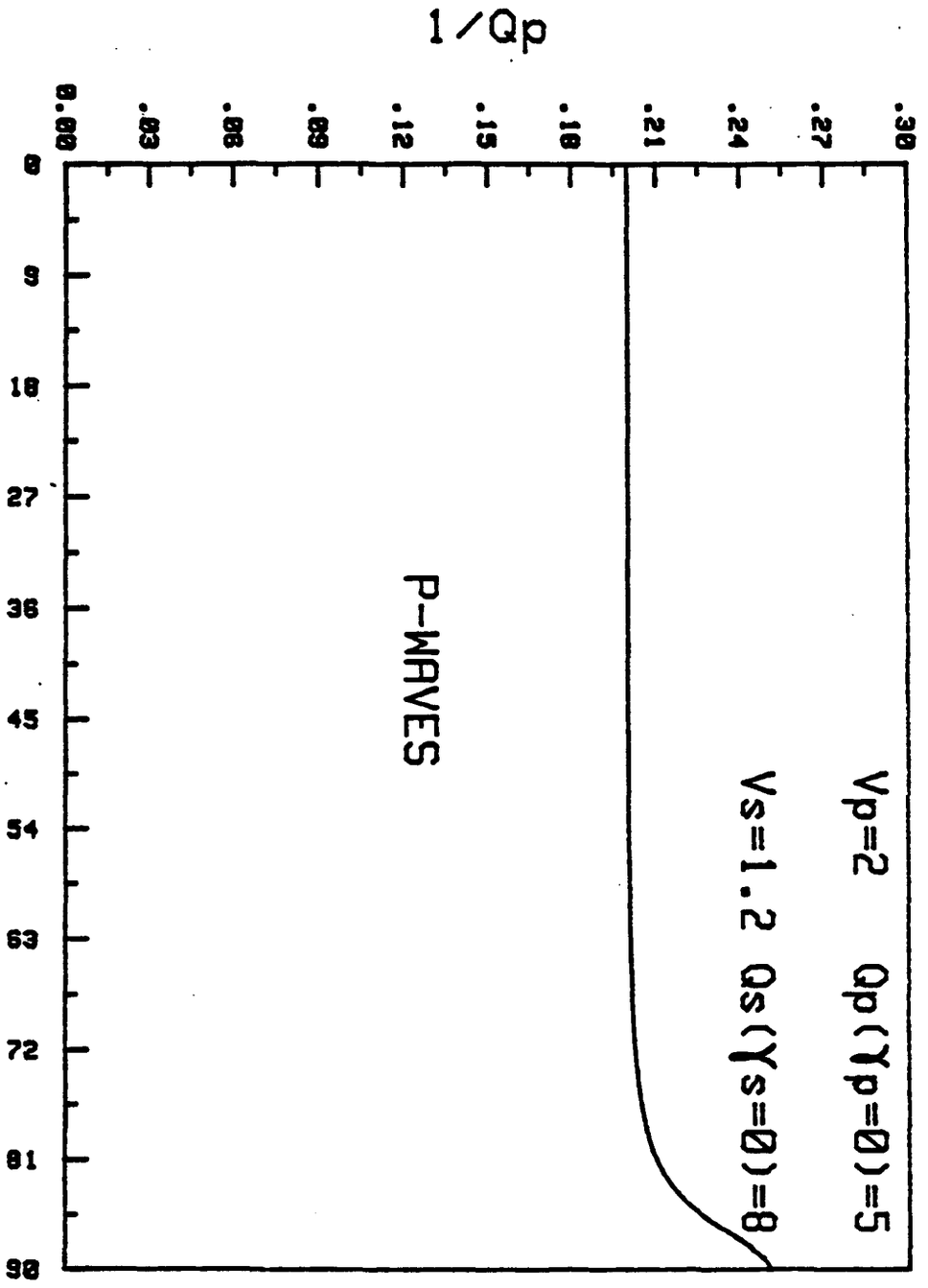

Fig.1-15 Q_P^{-1} **as a function of** γ_P **the propagation-attenuation angle.**

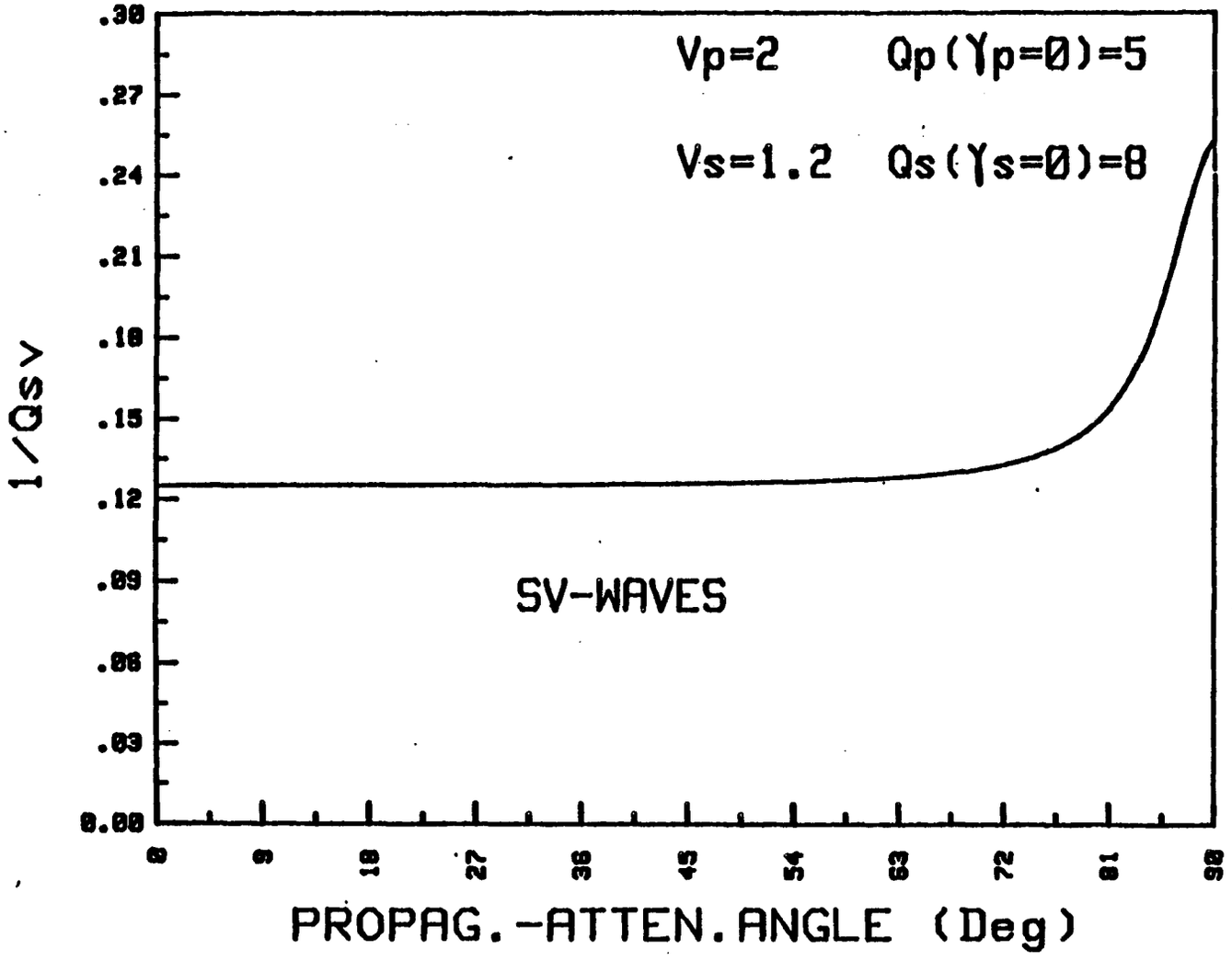

Fig.1-16 Q_{Sv}^{-1} as a function of γ_{Sv} the propagation-attenuation angle.

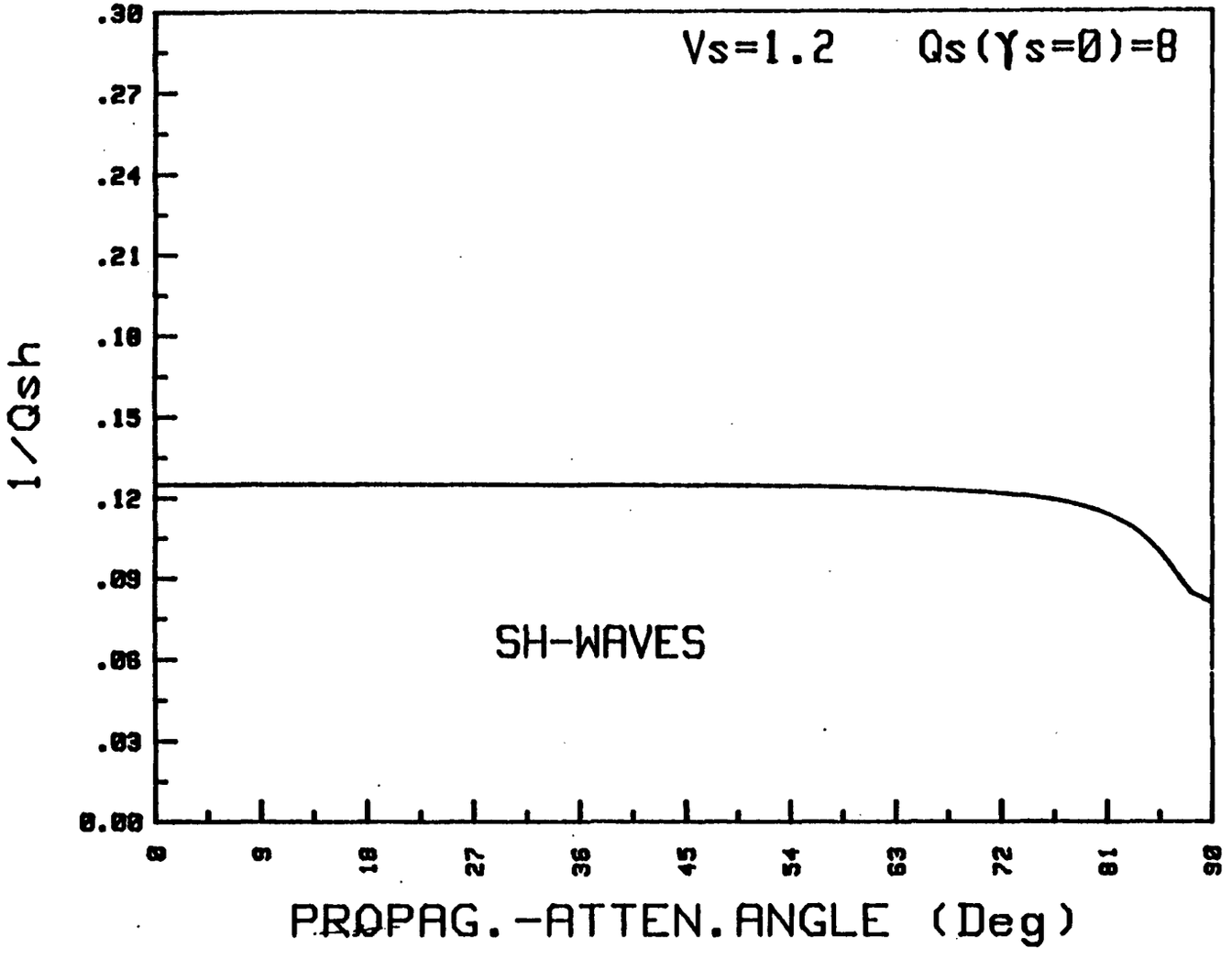

Fig.1-17 Q_{Sh}^{-1} as a function of γ_{Sh} the propagation-attenuation angle.

II.CONSTANT Q MODEL IN TWO DIMENSIONS

1. FIRST CASE - SH-WAVES

If we write $x = \frac{\mu_I}{\mu_R}$, using equation (1.3.3) we obtain:

$$Q_{SH}^{-1} = 2x \frac{\left[1 + \frac{x^2}{1+x^2}\tan^2\gamma_{SH}\right]^{1/2}}{1 + \left[1 + \frac{x^2}{1+x^2}\tan^2\gamma_{SH}\right]^{1/2}} \tag{1.3.8}$$

We look for Q_{SH}^{-1} independent of ω for every value of γ_{SH} . Since this is true for every value of ω , it will be true in particular for the value $\gamma_{SH} = 0$.

A necessary condition for Q_{SH}^{-1} independent of ω is to have $x = \frac{\mu_I}{\mu_R}$ independent of ω.

Having x independent of ω, insures that Q_{SH}^{-1} is independent of ω for all γ_{SH}.

So in two dimensions, we have a constant Q model for SH-waves if and only if $\frac{\mu_I}{\mu_R}$ is independent of ω . The solution is the one derived by Kjartansson:

$$\mu(\omega) = \mu_0 \left[\frac{i\omega}{\omega_0}\right]^{2\beta}$$

which implies that

$$x = \frac{\mu_I}{\mu_R} = \tan \pi\beta$$

and so gives

$$Q_{SH}^{-1} = 2\tan \pi\beta \frac{\left[1 + \sin^2\pi\beta\tan^2\gamma_{SH}\right]^{1/2}}{1 + \left[1 + \sin^2\pi\beta\tan^2\gamma_{SH}\right]^{1/2}} \tag{1.3.9}$$

which is in fact independent of ω.

2. SECOND CASE - SV-WAVES

If, as in the first case, we write $x = \frac{\mu_I}{\mu_R}$, using equation (1.3.2) we obtain

$$Q_{SV}^{-1} = x \frac{1 + \frac{x^2}{1+x^2}\tan^2\gamma_{SV}}{1 + \frac{x^2}{2(1+x^2)}\tan^2\gamma_{SV}} \tag{1.3.10}$$

As in the previous case, to have Q_{SV}^{-1} independent of ω for all values of the angle γ_{SV}, we must have x independent of ω. It is also, in this case, a necessary and sufficient condition.

So we have the following result

If

$$\mu(\omega) = \mu(\omega_0)\left[\frac{i\omega}{\omega_0}\right]^{2\beta}$$

Then we get

$$x = \frac{\mu_I}{\mu_R} = \tan \pi\beta$$

which gives

$$Q_{SV}^{-1} = \tan \pi\beta \frac{1 + \sin^2\pi\beta\tan^2\gamma_{SV}}{1 + \frac{\sin^2\pi\beta\tan^2\gamma_{SV}}{2}} \tag{1.3.11}$$

which is dependent of ω.

3. THIRD CASE - P-WAVES

Consider

$$x = \frac{M_I}{M_R} = \frac{\lambda_I + 2\mu_I}{\lambda_R + 2\mu_R}$$

In terms of x, equation (1.3.1) becomes

$$Q_P^{-1} = \frac{x + \frac{\mu_I}{\mu_R}\frac{\mu_R}{M_R}\frac{x^2}{1+x^2}\tan^2\gamma_P}{1 + \frac{1}{2}\frac{\mu_R}{M_R}\frac{x^2}{1+x^2}\tan^2\gamma_P} \tag{1.3.12}$$

As before for having Q_P^{-1} independent of ω for all value of γ_P, a necessary condition is obtained by putting γ_P to 0 in the previous equation. This implies that we must have

$$x = \frac{M_I}{M_R} \text{ independent of } \omega.$$

that is to say

$$M(\omega) = M_0\left[\frac{i\omega}{\omega_0}\right]^{2a} \tag{1.3.13}$$

Now we can take another particular case. When γ_P goes to $\frac{\pi}{2}$ equation (1.3.12) becomes

$$Q_P^{-1} = \frac{2\mu_I}{\mu_R}$$

So to have Q_P^{-1} independent of ω, another condition besides (1.3.13) is implied

$$\frac{\mu_I}{\mu_R} \text{ independent of } \omega .$$

which implies

$$\mu(\omega) = \mu_0 \left[\frac{i\omega}{\omega_0}\right]^{2\beta} \tag{1.3.14}$$

These two conditions are not enough to insure that Q_P^{-1} is independent of ω. If we plug (1.3.13) and (1.3.14) in equation (1.3.12) we get

$$Q_P^{-1} = 2\tan\pi\beta \frac{\tan\pi\alpha \cot\pi\beta + \frac{\mu_0}{M_0}\frac{\cos\pi\beta}{\cos\pi\alpha}\sin^2\pi\alpha\tan^2\gamma_P \left|\frac{\omega}{\omega_0}\right|^{2(\beta-\alpha)}}{2 + \frac{\mu_0}{M_0}\frac{\cos\pi\beta}{\cos\pi\alpha}\sin^2\pi\alpha\tan^2\gamma_P \left|\frac{\omega}{\omega_0}\right|^{2(\beta-\alpha)}} \tag{1.3.15}$$

Three different cases must be examined

3-a : $\alpha = \beta$

In this case we have

$$Q_P^{-1}(\gamma_P=0) = Q_{SV}^{-1}(\gamma_{SV}=0)$$

which added to the two conditions

$$M(\omega) = M_0 \left[\frac{i\omega}{\omega_0}\right]^{2\alpha}$$

with

$$M(\omega) = \lambda(\omega) + 2\mu(\omega)$$

and

$$\mu(\omega) = \mu_0 \left[\frac{i\omega}{\omega_0}\right]^{2\alpha}$$

assures that Q_P^{-1} is independent of ω and equal to

$$Q_P^{-1} = \tan\pi\alpha \frac{1 + \frac{\mu_0}{M_0}\sin^2\pi\alpha\tan^2\gamma_P}{1 + \frac{\mu_0}{2M_0}\sin^2\pi\alpha\tan^2\gamma_P} \qquad (1.3.16)$$

3-b : $\tan\pi\alpha \cot\pi\beta = 2$

Then Q_P^{-1} is dependent of ω and

$$Q_P^{-1} = 2\tan\pi\beta = \tan\pi\alpha$$

Even more than constant, Q_P^{-1} is independent of γ_P.

3-c : General case

In this case equation (1.3.15) can be written

$$\left|\frac{\omega}{\omega_0}\right|^{2(\beta-\alpha)} \frac{\mu_0}{M_0}\frac{\cos\pi\beta}{\cos\pi\alpha}\sin^2\pi\alpha\,\tan^2\gamma_P[Q_P^{-1} - 2\tan\pi\beta] + 2[Q_P^{-1} - \tan\pi\alpha] = 0 \qquad (1.3.17)$$

To verify this equation we must equate to zero the coefficient of $\left|\frac{\omega}{\omega_0}\right|^{2(\beta-\alpha)}$. Then by eliminating the two cases already studied, we are left with the system

$$\frac{\mu_0}{M_0}\frac{\cos\pi\beta}{\cos\pi\alpha}\sin^2\pi\alpha = 0$$

$$Q_P^{-1} = \tan\pi\alpha$$

This system has no interesting solutions. It shows that we have a constant Q_P model only in the following cases

- If we are in a liquid then $Q_P^{-1} = \tan\pi\alpha$, when $M(\omega) = M_0\left[\frac{i\omega}{\omega_0}\right]^{2\alpha}$

- If $\frac{M_I}{M_R} = 0$ which means that there is no dissipation for P-waves. This is a trivial solution:

$$Q_P^{-1} = 0$$

So for P-waves, one can see that we can derive a strict constant Q_P model in two dimensions in very particular cases. In general there is no such thing as a strictly constant-Q model in two dimensions for P-waves. Nevertheless, as already stated the dependence of Q on the angle γ is small and takes place only for angles approximatively equal or larger than the critical angle; therefore we can assume a nearly constant-Q model as soon as we define the viscoelastic moduli as functions of the type

$$M(\omega) = M_0 \left(\frac{i\omega}{\omega_0}\right)^{2a}$$

The results for all three types of waves are summarized in Table I-2.

TABLE I-2 Constant Q Models in 1 and 2 Dimensions

	Constant Q Model in 1 Dimension	Constant Q Model in 2 Dimensions
SH WAVES	$\mu(\omega) = \mu(\omega_o)(\frac{i\omega}{\omega_o})^{2\beta}$ $Q_{SH}^{-1} = \tan \pi\beta$	$\mu(\omega) = \mu(\omega_o)(\frac{i\omega}{\omega_o})^{2\beta}$ $Q_{SH}^{-1} = 2 \tan \pi\beta \frac{(1 + \sin^2 \pi\beta \tan^2 \gamma_{SH})^{1/2}}{1 + (1 + \sin^2 \pi\beta \tan^2 \gamma_{SH})^{1/2}}$
SV WAVES	$\mu(\omega) = \mu(\omega_o)(\frac{i\omega}{\omega_o})^{2\beta}$ $Q_{SV}^{-1} = \tan \pi\beta$	$\mu(\omega) = \mu(\omega_o)(\frac{i\omega}{\omega_o})^{2\beta}$ $Q_{SV}^{-1} = \tan \pi\beta \frac{1 + \sin^2\pi\beta \tan^2\gamma_{SV}}{1 + .5 \sin^2\pi\beta \tan^2\gamma_{SV}}$
P WAVES	$M(\omega) = M(\omega_o)(\frac{i\omega}{\omega_o})^{2\alpha}$ $Q_P^{-1} = \tan \pi\alpha$	1. $M(\omega) = M(\omega_o)(\frac{i\omega}{\omega_o})^{2\alpha}$ and Liquid Medium $Q_P^{-1} = \tan \pi\alpha$ 2. $M(\omega) = M(\omega_o)(\frac{i\omega}{\omega_o})^{2\alpha}$ and $\mu(\omega) = \mu(\omega_o)(\frac{i\omega}{\omega_o})^{2\alpha}$ $Q_P^{-1} = \tan \pi\alpha \frac{1 + \mu(\omega_o)/M(\omega_o) \sin^2\pi\alpha\tan^2\gamma_P}{1 + \mu(\omega_o)/2M(\omega_o) \sin^2 \pi\alpha \tan^2\gamma_P}$ 3. $M(\omega) = M(\omega_o)(\frac{i\omega}{\omega_o})^{2\alpha}$, $\mu(\omega) = \mu(\omega_o)(\frac{i\omega}{\omega_o})^{2\beta}$, $\tan \pi\alpha = 2\tan \pi\beta$ $Q_P^{-1} = \tan \pi\alpha$ 4. Trivial case $M_I/M_R = 0$ $Q_P^{-1} = 0$

PART II

SYNTHETIC SEISMOGRAMS

IN VISCOELASTIC MEDIA

A - EFFECT OF REFLECTION COEFFICIENTS ON SYNTHETIC SEISMOGRAMS

INTRODUCTION

Our aim in this paper is to derive the equations to be used in generating a 2-D synthetic seismogram by wavefield extrapolation with the wave equation. We work in the (ω,k_x) domain because it is straightforward to include attenuation effects by specifying complex frequency-dependent elastic moduli. We derive the appropriate Green's function and an expression for the reflection coefficient at a liquid-solid interface.

I. THEORY

1. Calculus of the Green's function for the wave equation.

Consider the wave equation when the driving force is a Dirac source at time $t = 0$ and at the point $(x=0,z=0)$. Its solution is the Green's function $G(x,z,t)$ and it is given by:

$$\left[\frac{\partial^2}{\partial x^2}+\frac{\partial^2}{\partial z^2}-\frac{1}{v^2}\frac{\partial^2}{\partial t^2}\right] G(x,z,t) = -2\pi\delta(x)\delta(z)\delta(t) \qquad (2.1.1)$$

Taking the triple Fourier Transform of equation (2.1.1) using the definitions

$$F(k_x,k_z,\omega) = \int\int\int f(x,z,t)\, e^{ik_x x + ik_z z - i\omega t}\, dx\, dz\, dt$$

$$f(x,z,t) = \frac{1}{(2\pi)^3}\int\int\int F(k_x,k_z,\omega)\, e^{-ik_x x - ik_z z + i\omega t}\, dk_x\, dk_z\, d\omega$$

we obtain

$$\left[k_x^2 + k_z^2 - \frac{\omega^2}{v^2}\right] G(k_x,k_z,\omega) = 2\pi$$

which gives for $G(k_x,k_z,\omega)$

$$G(k_x,k_z,\omega) = \frac{2\pi}{k_x^2 - (\frac{\omega^2}{v^2} - k_z^2)}$$

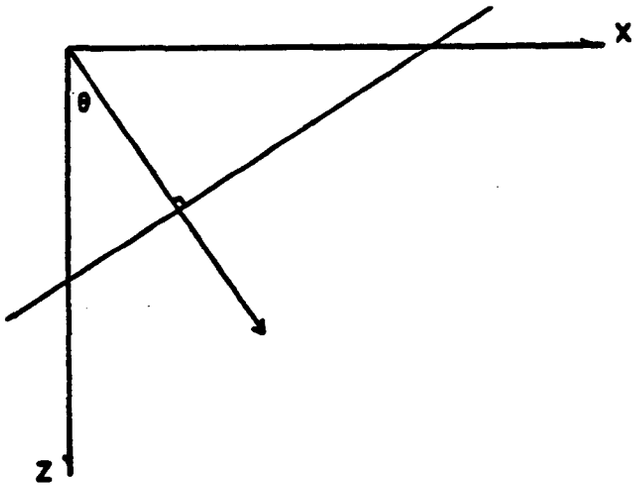

FIG. 2-1. Definition of ray parameter

By definition of the ray parameter p (see Figure 2-1), $p = \frac{k_x}{\omega} = \frac{\sin\vartheta}{v}$, we have $k_x = \frac{\omega}{v}\sin\vartheta$. Therefore

$$\frac{\omega^2}{v^2} - k_x^2 = \frac{\omega^2}{v^2}\cos^2\vartheta \geq 0$$

and

$$G(k_x,k_z,\omega) = \frac{2\pi}{\left[k_z - \left(\frac{\omega^2}{v^2} - k_x^2\right)^{1/2}\right]\left[k_z + \left(\frac{\omega^2}{v^2} - k_x^2\right)^{1/2}\right]}$$

This gives

$$G(k_x,\omega,z) = \int_{-\infty}^{+\infty} \frac{e^{-ik_z z}\,dk_z}{\left[k_z - \left(\frac{\omega^2}{v^2} - k_x^2\right)^{1/2}\right]\left[k_z + \left(\frac{\omega^2}{v^2} - k_x^2\right)^{1/2}\right]} \qquad (2.1.2)$$

Since we want a causal function for $G(k_x,\omega,z)$, we take the following contour of integration [Figure 2-2]. The poles must be slightly under the real axis due to causality.

Using Cauchy's integral formula in equation (2.1.2), we get

$$G(k_x,\omega,z) = 0 \qquad z < 0 \quad (2.1.3)$$

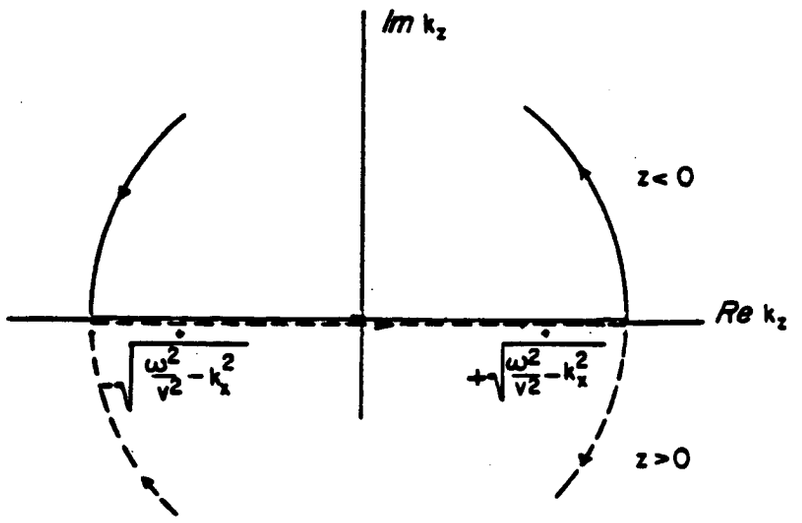

FIG. 2-2. Path of integration for the Green's function

$$G(k_x,\omega,z) = i\pi \left[\frac{e^{-i\left[\frac{\omega^2}{v^2}-k_x^2\right]^{1/2} z}}{\left[\frac{\omega^2}{v^2}-k_x^2\right]^{1/2}} - \frac{e^{i\left[\frac{\omega^2}{v^2}-k_x^2\right]^{1/2} z}}{\left[\frac{\omega^2}{v^2}-k_x^2\right]^{1/2}} \right] \qquad z > 0$$

This formula contains the upcoming and downgoing waves. It is necessary to separate them for every ω in order to write $G(k_x,\omega,z)$ as a function of $\frac{\omega}{v}\left[1-\left(\frac{k_x v}{\omega}\right)^2\right]^{1/2}$.

As we have

$$\left[\frac{\omega^2}{v^2}-k_x^2\right]^{1/2} = \frac{\omega}{v}\,\mathrm{sgn}\,\omega \left[1-\left(\frac{k_x v}{\omega}\right)^2\right]^{1/2}$$

we can rewrite $G(k_x,\omega,z)$ as

$$G(k_x,\omega,z) = i\pi \left[\frac{e^{-i\frac{\omega}{v}\mathrm{sgn}\,\omega\left[1-\left(\frac{vk_x}{\omega}\right)^2\right]^{1/2} z}}{\frac{\omega}{v}\mathrm{sgn}\,\omega\left[1-\left(\frac{vk_x}{\omega}\right)^2\right]^{1/2}} - \frac{e^{i\frac{\omega}{v}\mathrm{sgn}\,\omega\left[1-\left(\frac{vk_x}{\omega}\right)^2\right]^{1/2} z}}{\frac{\omega}{v}\mathrm{sgn}\,\omega\left[1-\left(\frac{vk_x}{\omega}\right)^2\right]^{1/2}} \right]$$

which gives

$$G(k_x,\omega,z) = i\pi \left[\frac{e^{-i\frac{\omega}{v}\left|1-\left(\frac{vk_x}{\omega}\right)^2\right|^{1/2} z}}{\frac{\omega}{v}\left|1-\left(\frac{vk_x}{\omega}\right)^2\right|^{1/2}} - \frac{e^{i\frac{\omega}{v}\left|1-\left(\frac{vk_x}{\omega}\right)^2\right|^{1/2} z}}{\frac{\omega}{v}\left|1-\left(\frac{vk_x}{\omega}\right)^2\right|^{1/2}} \right] \qquad \omega > 0$$

and

$$G(k_x,\omega,z) = G(k_x,-\omega,z) \tag{2.1.4}$$

(therefore $G(k_x,\omega,z)$ is an even function of ω).

The downgoing wave (DW) and the upcoming wave (UW) are represented by the following parts of the total Green's function,

$$DW: \qquad i\pi \frac{e^{-i\frac{\omega}{v}\left|1-\left(\frac{vk_x}{\omega}\right)^2\right|^{1/2} z}}{\frac{\omega}{v}\left|1-\left(\frac{vk_x}{\omega}\right)^2\right|^{1/2}}$$

$$UW: \qquad -i\pi \frac{e^{i\frac{\omega}{v}\left|1-\left(\frac{vk_x}{\omega}\right)^2\right|^{1/2} z}}{\frac{\omega}{v}\left|1-\left(\frac{vk_x}{\omega}\right)^2\right|^{1/2}}$$

Remark: We could have put the source at the point $(x=x_0,z=z_0,t=t_0)$ and the problem would not have been changed in principle. The Green's function solution of the full wave equation would have been

$$G(k_x,k_z,\omega) = 2\pi \frac{e^{ik_x x_0 + ik_z z_0 - i\omega t_0}}{k_x^2 - (\frac{\omega^2}{v^2} - k_z^2)}$$

and in the (ω,k_x,z) domain, the solution would have been

$$G(k_x,\omega,z) = 0 \qquad z < z_0$$

$$G(k_x,\omega,z) = i\pi \left[\frac{e^{-i\left[\frac{\omega^2}{v^2}-k_x^2\right]^{1/2}(z-z_0)}}{\left[\frac{\omega^2}{v^2}-k_x^2\right]^{1/2}} - \frac{e^{i\left[\frac{\omega^2}{v^2}-k_x^2\right]^{1/2}(z-z_0)}}{\left[\frac{\omega^2}{v^2}-k_x^2\right]^{1/2}} \right] e^{ik_x x_0 - i\omega t_0}$$

$$z > z_0$$

2. Synthetic seismogram for a liquid-solid interface.

We can model the effects of the reflection coefficient for a liquid-solid interface with the following experiment (Figure 2-3): put a source function $s(x,t)$ at the sea-surface, go to the sea-floor by using the Green's function derived previously, multiply by the reflectivity function and use wavefield extrapolation to the surface to get the synthetic seismogram. In our discussion we will consider the source function separately from the reflection coefficients.

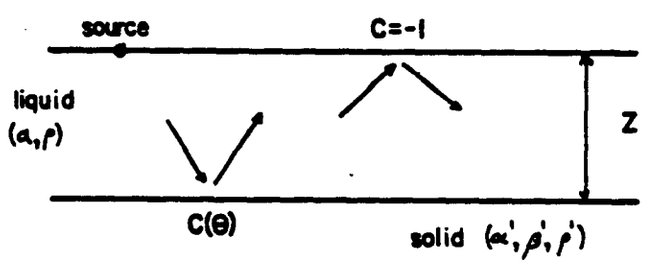

FIG. 2-3. Schematic view of the studied interface

Adding the source function, the right-hand side of equation (2.1.1) becomes

$$\left[\frac{\partial^2}{\partial x^2} + \frac{\partial^2}{\partial z^2} - \frac{1}{v^2}\frac{\partial^2}{\partial t^2}\right] G(x,z,t) = -2\pi\delta(x)\delta(z)\delta(t) ** s(x,t)$$

where ** denotes convolution in space and time.

The total Green's function becomes

$$G_{total}(k_x,\omega,z) = S(k_x,\omega)\, i\pi \left[\frac{e^{-ik_z z}}{k_z} - \frac{e^{ik_z z}}{k_z} \right]$$

where $S(k_x,\omega)$ is the two-dimensional Fourier transform of the source function, and $k_z = \frac{\omega}{v}\left[1 - \frac{v^2 k_x^2}{\omega^2}\right]^{1/2}$

The Green's function for the downgoing wave is

$$G_{DW}(k_x,\omega,z) = i\pi\, S(k_x,\omega)\, \frac{e^{-ik_z z}}{k_z}$$

To come back to the surface, we must multiply by the well-known extrapolation function, which is

$$e^{-ik_z z}$$

the total wavefield will be a superposition of primary and multiple reflections. Since we know that the reflection coefficient at the air-water interface is very close to −1, we can write the total wavefield as

$$\left[1 - \frac{1}{1 + C(k_x,\omega)\, \frac{e^{-2ik_z \Delta z}}{k_z}} \right] S(k_x,\omega) =$$

$$= S(k_x,\omega) \left[C(k_x,\omega)\, \frac{e^{-2ik_z \Delta z}}{k_z} - C^2(k_x,\omega)\, \frac{e^{-4ik_z \Delta z}}{k_z} + \cdots \right] \qquad (2.1.5)$$

This series comes from the fact that the first sea-floor multiple has traveled a distance $2\Delta z$ while the primary has traveled only Δz. Their amplitudes are, at each bounce, multiplied by the reflection coefficient $C(\vartheta(k_x,\omega))$, where $\sin\vartheta = \frac{vk_x}{\omega}$.

The synthetic seismogram is obtained by taking the inverse Fourier transform of equation (2.1.5),

$$f(x,t) =$$

$$\frac{i}{2(2\pi)^2} \int\int \left[C(k_x,\omega)\, \frac{e^{-2ik_z \Delta z}}{k_z} - C^2(k_x,\omega)\, \frac{e^{-4ik_z \Delta z}}{k_z} + \cdots \right] S(k_x,\omega)\, e^{-ik_z z + i\omega t}\, dk_x\, d\omega$$

where $k_z = \frac{\omega}{v}\left[1 - \left[\frac{vk_x}{\omega}\right]^2\right]^{1/2}$

3. Reflection coefficient.

For a *liquid–solid* interface, the reflection coefficient is given in many books and articles (see for example Ewing *et al*, 1957). We give an outline of the derivation of this formula. The notation is given in figure 2-4.

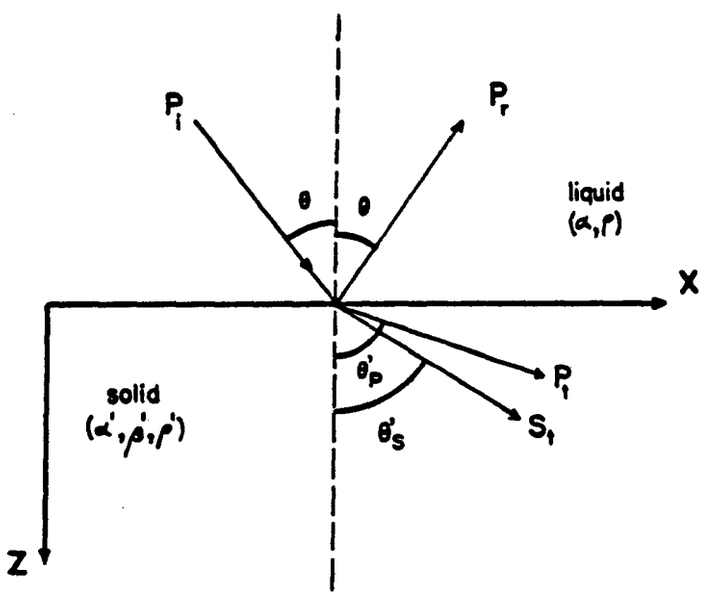

FIG. 2-4. Reflections and transmissions at a liquid-solid interface

In terms of P and S wave potentials we have for the incident, reflected and transmitted waves

$$\Phi_i = A_1 e^{ik_\alpha(x \sin\theta + z \cos\theta) - i\omega t}$$

$$\Phi_r = A_2 e^{ik_\alpha(x \sin\theta - z \cos\theta) - i\omega t}$$

and $\Phi = \Phi_i + \Phi_r, \quad \Psi = 0$

$$\Phi_t = A' e^{ik_{\alpha'}(x \sin\theta'_p + z \cos\theta'_p) - i\omega t}$$

$$\Psi_t = B' e^{ik_{\beta'}(x \sin\theta'_s + z \cos\theta'_s) - i\omega t}$$

and $\Phi' = \Phi_t$, $\Psi' = \Psi_t$.

$$k_\alpha = \frac{\omega}{\alpha} \quad k_{\alpha'} = \frac{\omega}{\alpha'} \quad k_{\beta'} = \frac{\omega}{\beta'}$$

Snell's law gives

$$\frac{\sin\vartheta}{\alpha} = \frac{\sin\vartheta'_p}{\alpha'} = \frac{\sin\vartheta'_s}{\beta'}$$

Continuity of stresses and displacements must be applied at the boundary, giving:

I) displacement: $u_z = u'_z$ or

$$\frac{\partial\Phi}{\partial z} = \frac{\partial\Phi'}{\partial z} + \frac{\partial\Psi'}{\partial x}$$

II) stresses: $\sigma'_{zz} = 0$, $\sigma_{zz} = \sigma'_{zz}$ or

$$2\frac{\partial^2\Phi'}{\partial x\,\partial z} - \frac{\partial^2\Psi'}{\partial z^2} + \frac{\partial^2\Psi'}{\partial x^2} = 0$$

$$\lambda\Delta\Phi + 2\mu\left(\frac{\partial^2\Phi}{\partial z^2} + \frac{\partial^2\Psi}{\partial x\,\partial z}\right) = \lambda'\Delta\Phi' + 2\mu'\left(\frac{\partial^2\Phi'}{\partial z^2} + \frac{\partial^2\Psi'}{\partial x\,\partial z}\right)$$

The reflection coefficient is obtained by solving the preceding system and this gives

$$C = \frac{\rho'\alpha'\cos\vartheta\left[(1-2\sin^2\vartheta'_s)^2 + \frac{4\beta'^3}{\alpha^2\alpha'}\sin^2\vartheta\cos\vartheta'_p\cos\vartheta'_s\right] - \rho\alpha\cos\vartheta'_p}{\rho'\alpha'\cos\vartheta\left[(1-2\sin^2\vartheta'_p)^2 + \frac{4\beta'^3}{\alpha^2\alpha'}\sin^2\vartheta\cos\vartheta'_p\cos\vartheta'_s\right] + \rho\alpha\cos\vartheta'_p} \tag{2.1.6}$$

or

$$C = \frac{A-B}{A+B}$$

where A and B can also be written:

$$A = \rho'\alpha'\cos\vartheta\left[(1-2\frac{\beta'^2}{\alpha^2}\sin^2\vartheta)^2 + \frac{4\beta'^3}{\alpha^2\alpha'}\sin^2\vartheta\left[1-\frac{\alpha'^2}{\alpha^2}\sin^2\vartheta\right]^{1/2}\left[1-\frac{\beta'^2}{\beta^2}\sin^2\vartheta\right]^{1/2}\right]$$

$$B = \rho\alpha\left[1-\frac{\alpha'^2}{\alpha^2}\sin^2\vartheta\right]^{1/2}$$

This formula is valid for the angle ϑ less than the smallest critical angle.

If $\alpha \geq \alpha'$, there is *no* critical angle and equation (2.1.3) holds everywhere.

If $\beta' \leq \alpha < \alpha'$, there is *one* critical angle defined by $\vartheta_c = \sin^{-1} \frac{\alpha}{\alpha'}$.

Formally, the mathematics can be derived in the same way for $\vartheta > \vartheta_c$. The difference is that $\cos\vartheta'_p$ is purely imaginary, implying that the transmitted P energy will be evanescent in the z direction. Since we do not want to increase the energy with propagation, we must have a *minus* sign in front of the square root. Therefore

$$\text{"}\cos\vartheta'_p\text{"} = i\left(\frac{\alpha'^2}{\alpha^2}\sin^2\vartheta - 1\right)^{1/2}$$

In this case the reflection coefficient is complex-valued, which means that there is a phase shift after critical angle. The expression for the reflection coefficient is thus given by

$$C(\vartheta) = \frac{D + i(E - F)}{D + i(E + F)} = C_1(\vartheta) + iC_2(\vartheta) \qquad (2.1.7)$$

where

$$C_1(\vartheta) = \frac{D^2 + E^2 - F^2}{D^2 + (E + F)^2}$$

$$C_2(\vartheta) = \frac{-2DF}{D^2 + (E + F)^2}$$

and

$$D = \rho'\alpha'\cos\vartheta\,(1 - 2\frac{\beta'^2}{\alpha^2}\sin^2\vartheta)^2$$

$$E = \left(\frac{\alpha'^2}{\alpha^2}\sin^2\vartheta - 1\right)^{1/2}\rho'\alpha'\cos\vartheta\,\frac{4\beta'^3}{\alpha^2\alpha'}\sin^2\vartheta\left(1 - \frac{\beta'^2}{\beta^2}\sin^2\vartheta\right)^{1/2}$$

$$F = \rho\alpha\left(\frac{\alpha'^2}{\alpha^2}\sin^2\vartheta - 1\right)^{1/2}$$

If $\alpha < \beta' < \alpha'$, we have two critical angles

$$\vartheta_{c_1} = \sin^{-1}\frac{\alpha}{\alpha'}$$

$$\vartheta_{c_2} = \sin^{-1}\frac{\alpha}{\beta'}$$

For $\vartheta < \vartheta_{c_1}$, equation (2.1.6) holds for the reflection coefficient.

For $\vartheta_{c_1} < \vartheta < \vartheta_{c_2}$, equation (2.1.7) holds for the reflection coefficient.

For $\vartheta > \vartheta_{c_2}$, we have to consider the *pseudo–S–transmission* angle defined like the one for P waves by

$$\text{"}\cos\vartheta'_s\text{"} = i\left[\frac{\beta'^2}{\alpha^2}\sin^2\vartheta - 1\right]^{1/2}$$

accordingly we obtain for $C(\vartheta)$

$$C(\vartheta) = \frac{G - iH}{G + iH} = E_1(\vartheta) + iE_2(\vartheta) \qquad (2.1.8)$$

where

$$E_1(\vartheta) = \frac{G^2 + H^2}{G^2 + H^2}$$

$$E_2(\vartheta) = \frac{-2HG}{G^2 + H^2}$$

and

$$G = \rho'\alpha'\cos\vartheta\left[\left[1 - 2\frac{\beta'^2}{\alpha^2}\sin^2\vartheta\right]^2 - \frac{4\beta'^3}{\alpha^2\alpha'}\sin^2\vartheta\left[\frac{\alpha'^2}{\alpha^2}\sin^2\vartheta - 1\right]^{1/2}\left[\frac{\beta'^2}{\beta^2}\sin^2\vartheta - 1\right]^{1/2}\right]$$

$$H = \rho\alpha\left[\frac{\alpha'^2}{\alpha^2}\sin^2\vartheta - 1\right]^{1/2}$$

4. Reflection coefficient in the (ω,k_x) plane

To define the reflection coefficient in the (ω,k_x) plane, we must give its value in the four quadrants. It is possible to do that utilizing the properties of the 2D-inverse Fourier transform of the reflection coefficient, that is $c(t,x)$. This function must be *real*, *symmetric* in x and *causal*.

First condition: *Reality*.

A general function of two variables can be written in terms of its even and odd parts as:

$$C(\omega,k_x) = \text{Re}\, E_{k_x}E_\omega + \text{Re}\, E_{k_x}O_\omega + \text{Re}\, O_{k_x}E_\omega + \text{Re}\, O_{k_x}O_\omega$$

$$+ i\,(\text{Im}\, E_{k_x}E_\omega + \text{Im}\, E_{k_x}O_\omega + \text{Im}\, O_{k_x}E_\omega + \text{Im}\, O_{k_x}O_\omega)$$

where Re refers to the *real* part and Im to the *imaginary* part, E_{k_x} refers to the *even* part

of k_z, O_ω refers to the *odd* part of ω, and so on.

Since the Fourier transform of a real-even function is real-even, and of a real-odd function is imaginary-odd, to guarantee $c(x,t)$ to be real, $C(\omega,k_z)$ must be of the form

$$C(\omega,k_z) = \text{Re } E_{k_z} E_\omega + \text{Re } O_{k_z} O_\omega + i\,(\text{Im } E_{k_z} O_\omega + \text{Im } O_{k_z} E_\omega)$$

Second condition: *Symmetry* in x.

The condition of symmetry in the x direction implies that $C(\omega,k_z) = C(\omega,-k_z)$, thus we are left with

$$C(\omega,k_z) = \text{Re } E_k E_\omega + i\,\text{Im } E_k O_\omega$$

if we call

$$C(|\omega|,|k_z|) = C_1(|\omega|,|k_z|) + i\,C_2(|\omega|,|k_z|)$$

then

$$C(\omega,k_z) = C_1(|\omega|,|k_z|) + i\,sgn\,\omega\,C_2(|\omega|,|k_z|)$$

Let us define now $C(|\omega|,|k_z|)$. We can use (2.1.6), (2.1.7) and (2.1.8) and replace $\sin\vartheta$ by $\frac{vk_z}{\omega}$. In fact it is better to write C as a function of $(-i\omega)$ to help inspection for causality later. (2.1.6), (2.1.7) and (2.1.8) become

$$C(|\omega|,|k_z|) = \frac{A^\circ - B^\circ}{A^\circ + B^\circ} = C_1(|\omega|,|k_z|) + i\,C_2(|\omega|,|k_z|) \qquad (2.1.9)$$

where

$$A^\circ = \rho'\alpha'\left[(-i\omega)^2 + \alpha^2 k_z^2\right]^{1/2}$$

$$\left\{\left[(-i\omega)^2 + 2\beta'^2 k_z^2\right]^2 - \frac{4\beta'^3 k_z^2}{\alpha'}\left[(-i\omega)^2 + \alpha'^2 k_z^2\right]^{1/2}\left[(-i\omega)^2 + \beta'^2 k_z^2\right]^{1/2}\right\}$$

$$B^\circ = \rho\alpha(-i\omega)^4\left[(-i\omega)^2 + \alpha'^2 k_z^2\right]^{1/2}$$

with

$$\left[(-i\omega)^2 + v^2 k_z^2\right]^{1/2} = \begin{cases} (-i\omega)\left[1 - \dfrac{v^2 k_z^2}{\omega^2}\right]^{1/2} & \text{for } 1 - \dfrac{v^2 k_z^2}{\omega^2} \geq 0 \\ \omega\left[\dfrac{v^2 k_z^2}{\omega^2} - 1\right]^{1/2} & \text{for } 1 - \dfrac{v^2 k_z^2}{\omega^2} < 0 \end{cases}$$

whence

$$C(\omega, k_z) = \frac{\mathrm{Re}\,(A^\circ - B^\circ) + i\, sgn\,\omega\, \mathrm{Im}\,(A^\circ - B^\circ)}{\mathrm{Re}\,(A^\circ + B^\circ) + i\, sgn\,\omega\, \mathrm{Im}\,(A^\circ + B^\circ)}$$

Third condition: *Causality*.

To verify causality of the reflection coefficient, we apply simplified Muir's rules for causal operators: (F.Muir's personal communication). Namely:

I) The sum of two causal operators is causal.

II) The product of two causal operators is causal.

III) The inverse of a causal operator is causal if it has a positive real part.

We know that $(-i\omega)$ is causal (F.Muir's personal communication).

Therefore $\left[(-i\omega)^2 + v^2 k_z^2\right]^{1/2}$ and $\left[(-i\omega)^2 + 2\beta'^2 k_z^2\right]^2$ are causal.

This implies that $A^\circ - B^\circ$ and $A^\circ + B^\circ$ are causal.

To check the causality of C we have to verify that

$$\mathrm{Re}\left[Den = A^\circ + B^\circ\right] \geq 0$$

To do that, it is important to write $-i\omega$ in the form $-i\omega + \varepsilon$, so that when we will look at the real part of Den it will be the true one and not the imaginary one. We will take the limit for $\varepsilon \to 0$ to determine the sign of the real part of Den.

We have to distinguish the three cases:

I) $\alpha \geq \alpha'$

For this case

$$Den = Den1\,(Den2 + Den3) + Den4$$

with

$$Den1 = \rho'\alpha'(-i\omega+\varepsilon)\left[1+\frac{\alpha^2 k_z^2}{(-i\omega+\varepsilon)^2}\right]^{1/2}$$

$$Den2 = \left[2\beta'^2 k_z^2 + (-i\omega+\varepsilon)^2\right]^2 \qquad (2.1.10)$$

$$Den3 = \frac{-4\beta'^3}{\alpha'}k_z^2(-i\omega+\varepsilon)^2\left[1+\frac{\alpha'^2 k_z^2}{(-i\omega+\varepsilon)^2}\right]^{1/2}\left[1+\frac{\beta'^2 k_z^2}{(-i\omega+\varepsilon)^2}\right]^{1/2}$$

$$Den4 = \rho\alpha(-i\omega+\varepsilon)^5\left[1+\frac{\alpha'^2 k_z^2}{(-i\omega+\varepsilon)^2}\right]^{1/2}$$

After calculus to the first order with respect to ε we find for Re Den

$$\rho'\alpha'\varepsilon\left[1-\frac{\alpha^2 k_z^2}{\omega^2}\right]^{1/2}\left[(2\beta'^2 k_z^2-\omega^2)^2+\frac{4\beta'^3}{\alpha'}k_z^2\omega^2\left[1-\frac{\alpha'^2 k_z^2}{\omega^2}\right]^{1/2}\left[1-\frac{\beta'^2 k_z^2}{\omega^2}\right]^{1/2}\right]$$

$$+\ \rho\alpha\varepsilon\omega^4\left[1-\frac{\alpha'^2 k_z^2}{\omega^2}\right]^{1/2}$$

which is obviously positive.

Therefore $C(\omega,k_z)$ is causal.

ii) $\beta' \le \alpha < \alpha'$

We have two different regions to inspect

1-if $\vartheta \le \vartheta_c = \sin^{-1}(\alpha/\alpha')$, then Den is the same as in (2.1.10) and the real part is positive.

2-if $\vartheta > \vartheta_c$, then for this case we can write also Den in the form

$$Den = Den1\,(Den2 + Den3) + Den4$$

but with

$$Den1 = \rho'\alpha'(-i\omega+\varepsilon)\left[1+\frac{\alpha^2 k_z^2}{(-i\omega+\varepsilon)^2}\right]^{1/2}$$

$$Den2 = \left[2\beta'^2 k_z^2 + (-i\omega+\varepsilon)^2\right]^2 \qquad (2.1.11)$$

$$Den3 = \frac{-4\,i\,\beta'^3}{\alpha'}k_z^2(-i\omega+\varepsilon)^2\left[-\frac{\alpha'^2 k_z^2}{(-i\omega+\varepsilon)^2}-1\right]^{1/2}\left[1+\frac{\beta'^2 k_z^2}{(-i\omega+\varepsilon)^2}\right]^{1/2}$$

$$Den4 = i\rho\alpha(-i\omega+\varepsilon)^3\left[-\frac{\alpha'^2k_z^2}{(-i\omega+\varepsilon)^2}-1\right]^{1/2}$$

After calculus to the first order with respect to ε, the real part of Den is given by

$$\rho'\alpha'\left[1-\frac{\alpha^2k_z^2}{\omega^2}\right]^{1/2}\frac{4\beta'^3}{\alpha'}k_z^2\omega^3\left[\frac{\alpha'^2k_z^2}{\omega^2}-1\right]^{1/2}\left[1-\frac{\beta'^2k_z^2}{\omega^2}\right]^{1/2}$$
$$+\ \rho\alpha\omega^3\left[\frac{\alpha'^2k_z^2}{\omega^2}-1\right]^{1/2}$$

which is positive and therefore $C(\omega,k_z)$ is causal.

iii) $\alpha < \beta' < \alpha'$

1-If $\vartheta \le \vartheta_{c_1} = \sin^{-1}(\alpha/\alpha')$, then Den is the same as in (10).

If $\vartheta_{c_1} < \vartheta \le \vartheta_{c_2} = \sin^{-1}(\alpha/\beta')$, then Den is the same as in (11).

2-If $\vartheta > \vartheta_{c_2}$, then for this case, if we write

$$Den = Den1\,(Den2 + Den3) + Den4$$

we have

$$Den1 = \rho'\alpha'(-i\omega+\varepsilon)\left[1+\frac{\alpha^2k_z^2}{(-i\omega+\varepsilon)^2}\right]^{1/2}$$

$$Den2 = \left[2\beta'^2k_z^2+(-i\omega+\varepsilon)^2\right]^2$$

$$Den3 = \frac{4\beta'^3}{\alpha'}k_z^2(-i\omega+\varepsilon)^2\left[-\frac{\alpha'^2k_z^2}{(-i\omega+\varepsilon)^2}-1\right]^{1/2}\left[-\frac{\beta'^2k_z^2}{(-i\omega+\varepsilon)^2}-1\right]^{1/2}$$

$$Den4 = i\rho\alpha(-i\omega+\varepsilon)^3\left[-\frac{\alpha'^2k_z^2}{(-i\omega+\varepsilon)^2}-1\right]^{1/2}$$

After calculus to the first order with respect to ε, we find for Re Den

$$\rho\alpha\omega^3\left[\frac{\alpha'^2k_z^2}{\omega^2}-1\right]^{1/2}$$

which is positive. Therefore $C(\omega,k_z)$ is causal.

REMARKS:

1.We have not examined what was happening in the evanescent region, the region for which we have

$$\left|\frac{\alpha k_z}{\omega}\right| > 1$$

We can still write Den in the form

$$Den = Den1\,(Den2 + Den3) + Den4$$

Now the same type of calculus as the previous ones will show that the real part of Den is not always positive which means that $C(\omega,k_z)$ is not causal. It can be expressed also by saying that the denominator of the reflection coefficient has poles. This is a well-known problem (see Ewing and al,1957,p107). It corresponds to waves propagating with a velocity less than that of compressional or shear waves in either medium, called Stoneley waves.

2. We have examined the causality of the reflection coefficient but not the one of the plane wave itself. In fact it is also a well-known problem that reflected plane waves are not causal for angles greater than critical due to the non-causality of the Hilbert transform (see Ewing and al,1957,p90-93).

In the next part we discuss the implementation of these equations.

II. RESULTS

We show the results obtained by using the theory described in the previous paragraph. to generate synthetic seismograms. We will discuss the problems that have occurred in our trials, and will give the solutions which have been employed.

1. Green's Function Problem.

We have seen that the Green's function for our problem was of the form

$$\frac{e^{-ik_z\Delta z}}{k_z}$$

If we do not take any further precautions and calculate the synthetic seismogram for the primary reflection given by

$$f(x,t) = \frac{i}{2(2\pi)^2}\int\int S(k_x,\omega)\; C(k_x,\omega)\,\frac{e^{-2ik_z\Delta z}}{k_z}\,e^{-ik_x x + i\omega t}\,dk_x\,d\omega$$

with

$S(k_x,\omega)$ = source term,

$C(k_x,\omega)$ = reflection coefficient,

$$k_z = \frac{\omega}{v}\left[1 - \left[\frac{vk_x}{\omega}\right]^2\right]^{1/2},$$

we obtain only noise.

This effect comes from the fact that k_z can become *null*, and the particular frequency when this occurs becomes dominant.

The technique used to get rid of these artifact is not to solve the exact inverse Fourier transform, but rather to use a modified version for which the Green's function is

$$\frac{e^{-ik_z\Delta z}}{k_z + \frac{\omega}{v}\varepsilon} \qquad (2.1.12)$$

with ε being a small constant parameter with respect to $\left[1 - \left[\frac{vk_x}{\omega}\right]^2\right]^{1/2}$. This form keeps the causality of the Green's function.

In fact, since $\left[1 - \left[\frac{vk_x}{\omega}\right]^2\right]^{1/2} = \cos\vartheta$, we cannot have $\varepsilon \ll \cos\vartheta$ for every ϑ. As ϑ is approaching 90^0, $\cos\vartheta$ approaches 0 and thus ε can become bigger than $\cos\vartheta$.

If ε is too small, it does not take off all the effects of k_z becoming *null* . If ε is small enough, it gives a very clean seismogram (*cf* Figure 2-6).

Figure (2-6) is the seismogram obtained for a reflection coefficient $C(k_x,\omega) = 1$ with the corrections applied also in the evanescent region.

2. Evanescent Region Problem.

We have defined in our preceding paper the reflection coefficient for $0 \le \sin\vartheta \le 1$. In the evanescent region one can consider "$\sin\vartheta$" > 1 . In this region, the plane wave theory we are using is no longer valid, and formally the only way to deal with it correctly is by using *conical waves* (Cagniard's waves).

The way we approach the solution is by calculating the *reflection coefficient* in the evanescent region using the equations valid in the propagating region. Now the only difference is that

$$\left[1 - \left[\frac{vk_x}{\omega}\right]^2\right]^{1/2} = i\left[\left[\frac{vk_x}{\omega}\right]^2 - 1\right]^{1/2}$$

and this will guarantee causality as for the propagating region.

On the other hand, the Green's function is becoming a real exponential and as we do not want to increase the energy of the wave as it propagates, we must take a decreasing exponenetial, that is

$$\frac{e^{-ik_z\Delta z}}{k_z}$$

where $k_z = \frac{|\omega|}{v}\left[\left(\frac{vk_x}{\omega}\right)^2 - 1\right]^{1/2}$.

The problem with taking a Green's function like the one above, is that it is no longer causal and therefore will give anticausal events. These anticausal events will be of importance only about the region $k_z = 0$, because everywhere else the decaying exponential becomes negligible.

There is also the problem presented in the first paragraph ($k_z \to 0$), and we will handle it using the same implementation, namely replacing the Green's function by

$$\frac{e^{-ik_z\Delta z}}{k_z + \frac{|\omega|}{v}\varepsilon}$$

The results are presented for a constant reflection coefficient in Figure (2-6). One can see that the anticausal events are insignificant at all at the clip values used for plotting.

3. Synthetic Seismogram

The parameters used for generating the synthetic seismogram (Figure 2-7) are the following:

First medium:

water

P-velocity $= \alpha = 1500\ m/s$

density $= \rho = 1$

Second medium:

solid

P-velocity $= \alpha' = 2300\ m/s$

S-velocity $= \beta' = 1200\ m/s$

density $= \rho' = 2$

The plots of the amplitude, phase, real-part and imaginary-part of the reflection coefficient are shown in Figures (2-8) and (2-9) respectively.

The values chosen for the P-velocity and the S-velocity in the second medium are such that there exists only one head wave, as can be seen on Figure (2-7).

We must also remark on Figure (2-7) the π phase shift after critical angle, which has been predicted on Figure (2-8).

ACKNOWLEDGMENTS

We wish to thank M. Yedlin for suggesting the source waveform function which is shown in Figure 2-5.

REFERENCES

Ewing W.M., W.S. Jardetzky, F. Press, 1957; Elastic Waves in Layered Media. McGraw-Hill Book Co, New York.

Morse P.M., H. Feshbach, 1953; Methods of Theoretical Physics. McGraw-Hill Book Co, New York.

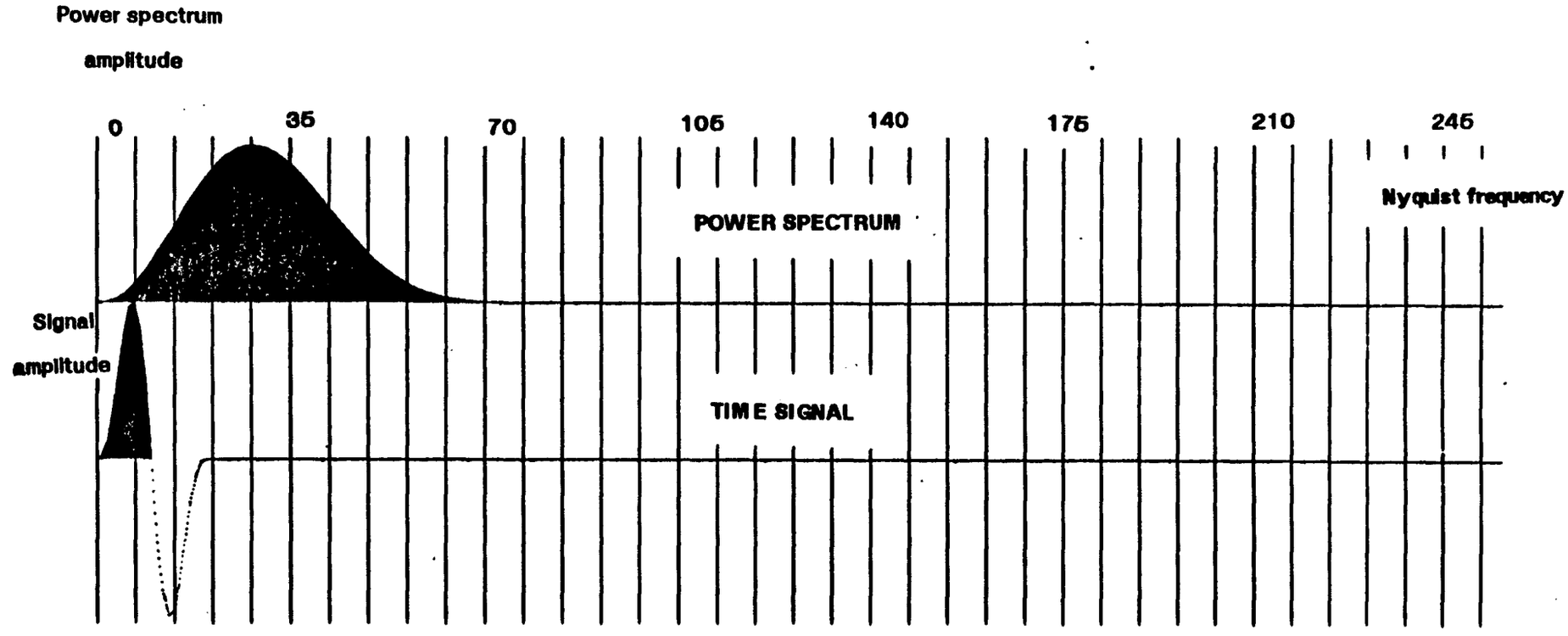

FIG. 2-5. Time signal and Power spectrum of the source employed in all the synthetic seismograms.

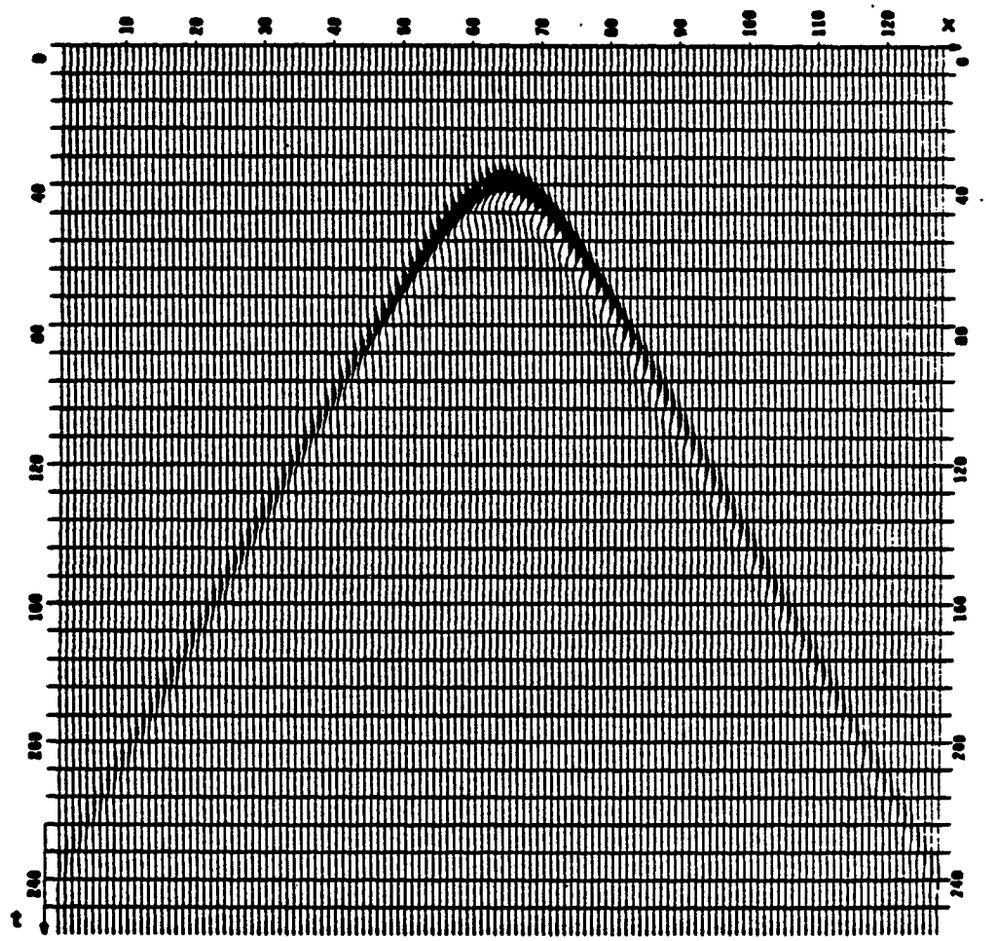

FIG. 2-6. In this figure $\varepsilon = 0.2$ which gives an accurate representation of angles up to 78.5^0. Here the reflection coefficient is 1 for all angles of incidence. The parameters used to generate this synthetic seismogram are: $dx = 86\,m$, $dt = 0.032\,s$, $nx = 128$, $nt = 256$, $nkx = 256$, $n\omega = 256$ and $\alpha = v_p = 1500\,m/s$. The density $\rho = 1$ in the first medium.

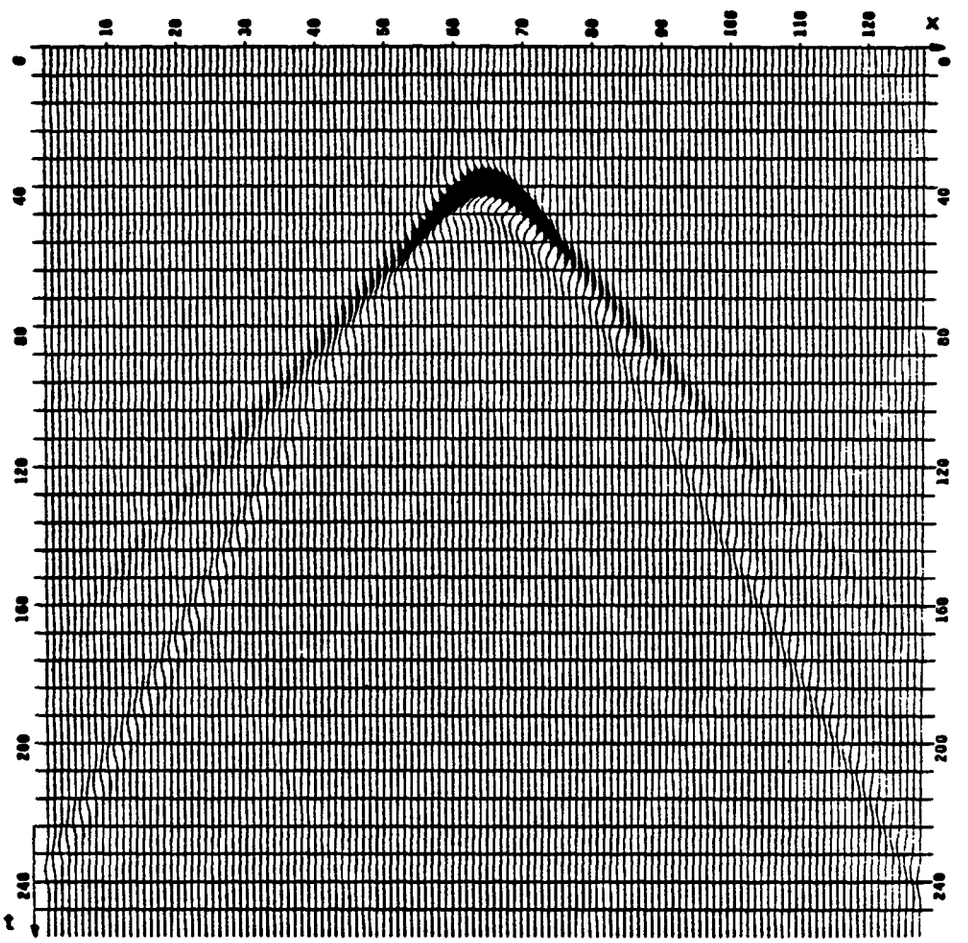

FIG. 2-7. In this figure $\varepsilon = 0.2$ as in figure (2-6). The reflection coefficient as a function of the angle of incidence is given in figures (2-8) and (2-9). The parameters used to generate this synthetic seismogram are the same as in figure (2-6) with velocities in the second medium $\alpha' = v_{p'} = 2500\ m/s$ $\beta' = v_{s'} = 1200\ m/s$. The density $\rho' = 2$. Note the prescence of the refracted wave, and the phase shift after critical angle.

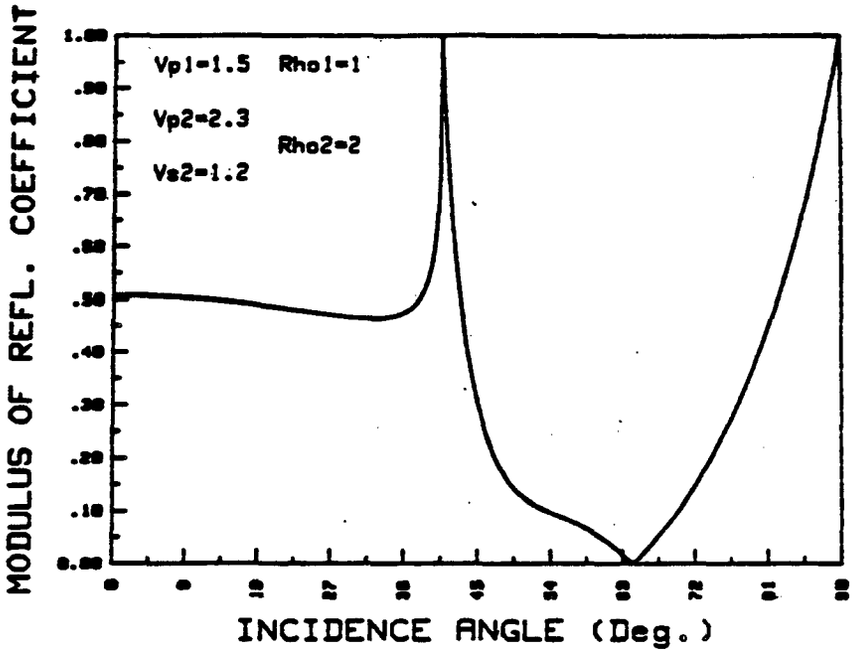

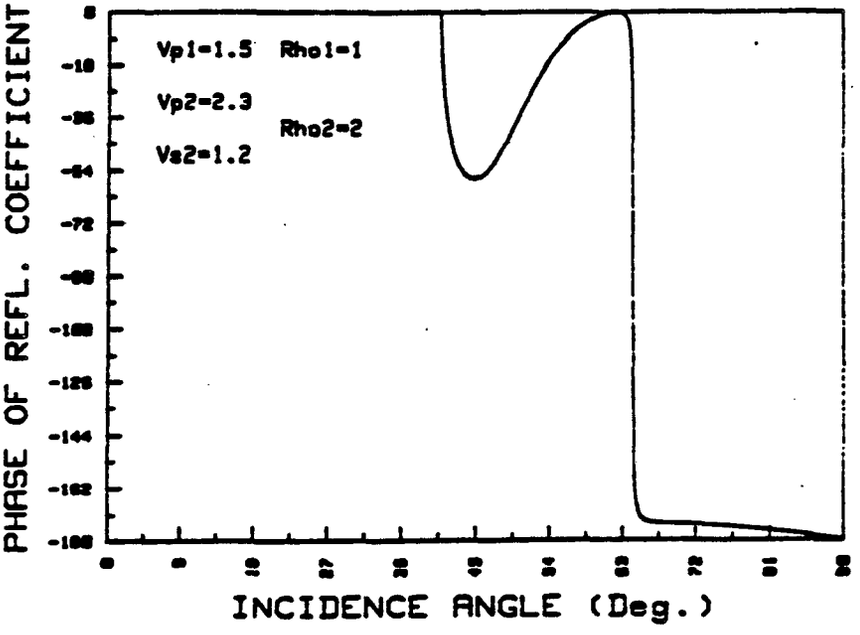

FIG. 2-8. Modulus and phase of the reflection coefficient used in Figure 2-7.

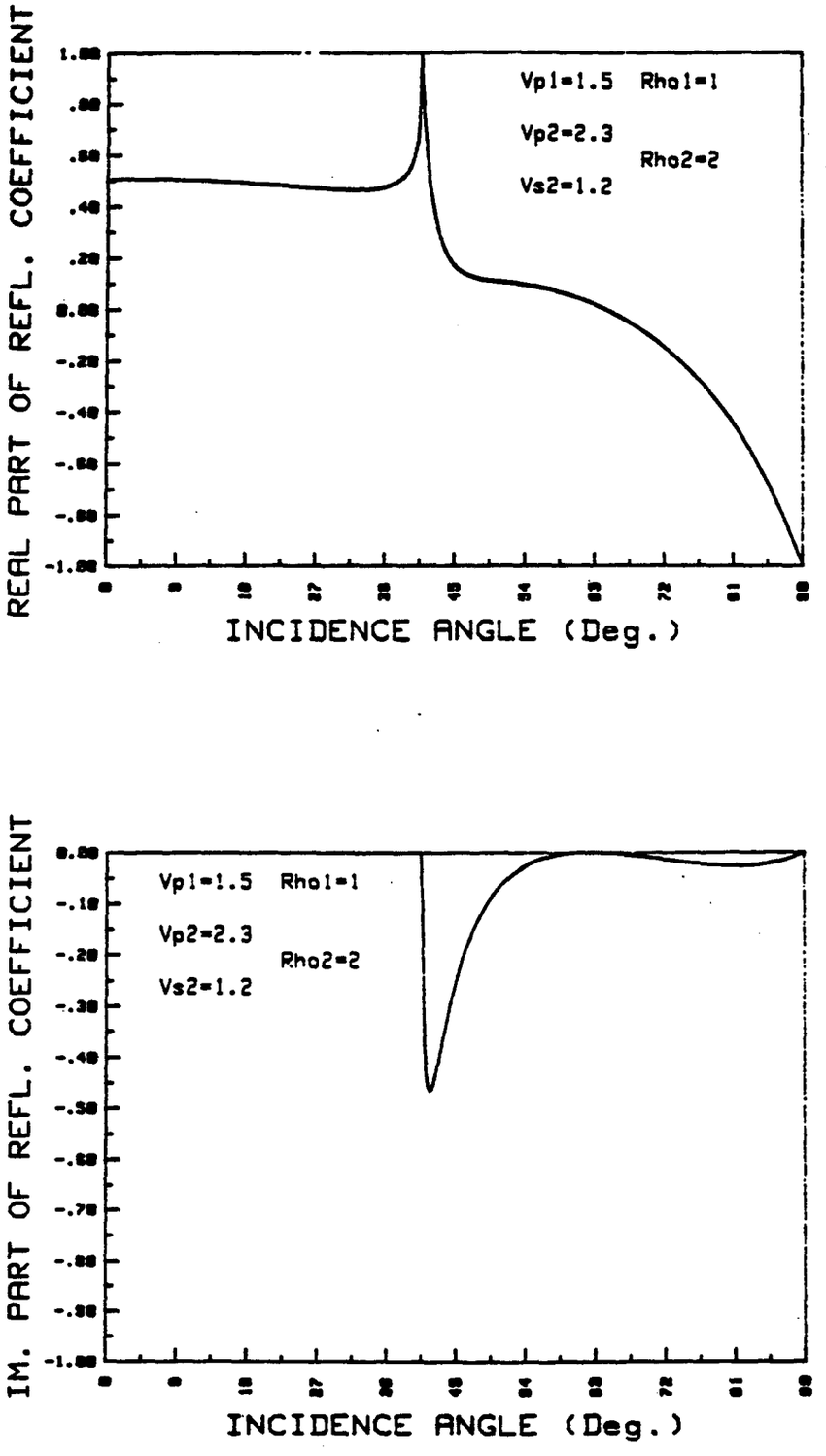

FIG. 2-9. Real and imaginary parts of the reflection coefficient used in Figure 2-7.

B-SYNTHETIC SEISMOGRAMS IN VISCOELASTIC MEDIA

INTRODUCTION

This article is the continuation of the previous paper (Effect of Reflection Coefficients on Synthetic Seismograms,Part II-A), where we discussed the computation of synthetic seismograms in an elastic medium, using an f-k domain wavefield extrapolation method. In this chapter we consider the case of waves propagating in a linear viscoelastic medium and the generation of the corresponding synthetic seismogram.No approximations are done,the restriction being that we need homogeneous layered media. Some papers have already been published on the same subject:

-some were dealing as a working space with the time domain either by using an asymptotic ray theory for SH-waves (Krebes.E.S and Hron.F 1980a,1980b) or by using an extended Haskell-Thompson matrix method (Silva.W 1976). or also by direct summation of plane waves components (Frasier C.W 1980).

-some were dealing as a working space with the f-k domain, like us. But they used an approximate matrix method (Kennett B.L.N (1979)).

Our goal is to model a marine seismogram and to study both the effect of P to S conversions and the effect of attenuation contrasts.

I. THEORY

1. Plane waves in a linear viscoelastic medium.

For the marine seismology case, the hypothesis of representing the medium by a linear viscoelastic model is completely justified. First, the phenomena we are studying are low amplitude in the far field (1 or 2 wavelengths from the source). Under this condition linearity of the stress-strain relationship becomes a good approximation. Second, at the strain amplitudes relevant to seismic exploration ($<10^{-6}$), attenuation phenomena are not friction phenomena but fluid phenomena (Winkler *et al*, 1979), which can be modeled by viscoelasticity theory.

In linear viscoelasticity the reciprocity principle is applicable (Borcherdt, 1977, or Part I-B). This allows us to write the elastodynamic equation for linear viscoelastic media by replacing, in the usual elastodynamic equation, the real elastic moduli with the complex frequency-dependent ones. This gives

$$\left[K(\omega) + \frac{\mu(\omega)}{3}\right] \nabla\vartheta + \mu(\omega)\, \nabla^2\mathbf{u} = \rho\ddot{\mathbf{u}} \qquad (2.2.1)$$

where $K(\omega)$ is the frequency-dependent complex bulk modulus, $\mu(\omega)$ is the frequency dependent shear modulus, $\vartheta = \nabla\cdot\mathbf{u}$ is the volumetric dilation, and $\mathbf{u} = \mathbf{u}(x,y,z,t)$ is the displacement vector.

Taking for the displacement u time-dependence of the form $e^{i\omega t}$, Equation (2.2.1) can be rewritten

$$\left[K(\omega) + \frac{\mu(\omega)}{3}\right] \nabla\vartheta + \mu(\omega)\, \nabla^2\mathbf{u} = -\rho\omega^2\mathbf{u} \qquad (2.2.1b)$$

In this equation $\mathbf{u} = \mathbf{u}(x,y,z)$.

This equation can be transformed using the Helmholtz form for the displacement u as function of potentials Φ and Ψ

$$\mathbf{u} = \nabla\Phi + \nabla\times\Psi \qquad (2.2.2)$$

$$\nabla\cdot\Psi = 0$$

then (2.2.1b) separates

$$\nabla^2 \begin{bmatrix} \Phi \\ \Psi \end{bmatrix} + \begin{bmatrix} k_\beta^2\Phi \\ k_\beta^2\Psi \end{bmatrix} = \begin{bmatrix} 0 \\ 0 \end{bmatrix} \qquad (2.2.3)$$

where

$$k_\beta^2 = \frac{\rho\omega^2}{K(\omega) + \frac{4}{3}\mu(\omega)}$$

$$k_\beta^2 = \frac{\rho\omega^2}{\mu(\omega)}$$

that are complex-valued quantities.

The general plane wave solution of equations of type (2.2.3) is

$$\Phi = \Phi_0\, e^{i(\omega t - \mathbf{K}\cdot\mathbf{r})} \qquad (2.2.4)$$

where K is a complex vector, and r is the position vector.

We can write K separating its real and imaginary parts:

$$K = P - iA \tag{2.2.5}$$

P will be called the propagating vector. A will be called the attenuating vector.

Rewriting equation (2.2.4) using these definitions we get

$$\Phi = \Phi_0 \, e^{-A \cdot r} e^{i(\omega t - Pr)} \tag{2.2.6}$$

In general, vectors P and A are not parallel, and the wave is said to be *inhomogeneous*. For the other case, where the angle between P and A is zero, $\gamma = (P,A) = 0$, the wave is said to be *homogeneous*.

From (2.2.3), (2.2.4) and (2.2.5) we also get

$$K \cdot K = |P|^2 - |A|^2 + 2i\,|A| \cdot |P| \cos\gamma = \frac{\rho\omega^2}{M} = \frac{\rho\omega^2}{|M|^2}[\, M_R - i\, M_I \,] \tag{2.2.7}$$

with

$M = M(\omega)$	complex modulus of the wave under consideration:
	$M = K + \frac{4}{3}\mu$ for a P wave
	$M = \mu$ for an S wave
M_R	Real part of M
M_I	Imaginary part of M
$\|M\|$	Modulus of M

In 2*D* (2.2.6) gives

$$\Phi = \Phi_0 \, e^{-(A_x x + A_z z)} \, e^{i\,[\,\omega t - (P_x x + P_z z)\,]}$$

so (2.2.7) can be written as

$$(P_x - iA_x)^2 + (P_z - iA_z)^2 = \frac{\rho\omega^2}{M} \tag{2.2.8a}$$

or

$$k^2 + k_z^2 = \frac{\rho\omega^2}{M} \tag{2.2.8b}$$

2. Green's function and Wavefield Extrapolators in linear viscoelastic medium

Since the reciprocity principle can be applied in the situation we are interested in, we use it to derive the operators we need to extrapolate the wavefield.

2a. Green's function for the acoustic wave equation

We have shown in Part II-A that for a Dirac source located at the origin and on the surface of an elastic liquid, the Green's function for the downgoing wave is given in the f-k domain by:

$$G_{D\nabla}(k_x,\omega,z) = i\pi \frac{e^{-ik_z z}}{k_z} \tag{2.2.9a}$$

with

$$k_z = \frac{\omega}{v}\left[1 - \left(\frac{vk_x}{\omega}\right)^2\right]^{1/2} \tag{2.2.9b}$$

The Fourier transform convention is

$$f(x,z,t) = \frac{1}{(2\pi)^3}\int\int\int F(k_x,k_z,\omega)\, e^{-ik_x x - ik_z z + i\omega t}\, dk_x\, dk_z\, d\omega$$

In this expression the ratio vk_x/ω is related to the angle of propagation of the wave ϑ by

$$\sin\vartheta = vk_x/\omega \tag{2.2.10}$$

The reciprocity principle gives us for a viscoelastic medium

$$G_{D\nabla}(k_x,\omega,z) = i\pi \frac{e^{-ik_z z}}{k_z} \tag{2.2.11a}$$

with

$$k_z = \frac{\omega}{v}\, p.v.\left[1 - \left(\frac{vk}{\omega}\right)^2\right]^{1/2} \tag{2.2.11b}$$

$p.v.$ meaning principal value of the square-root,
i.e. the square-root which has a positive real-part

v is a complex velocity given by $v^2 = \frac{M}{\rho}$, $v_R \geq 0$ (2.2.11c)

k is a complex number $k = k_x + i\,\mathrm{Im}(k) = P_x - iA_x$ (2.2.11d)

[cf. (2.2.8a), (2.2.8b)].

Note: To simplify notations, the fact that we are taking the principal value of every complex square-root will be understood in all following equations.

In our synthetic seismogram, the incident wave will be homogeneous. In this case, using (2.2.7), (2.2.11d) becomes

$$k = (|P| - i|A|)\sin\vartheta = \omega\sqrt{\rho/M}\sin\vartheta \qquad (2.2.12)$$

when ϑ is the angle defined in figure(2-10).

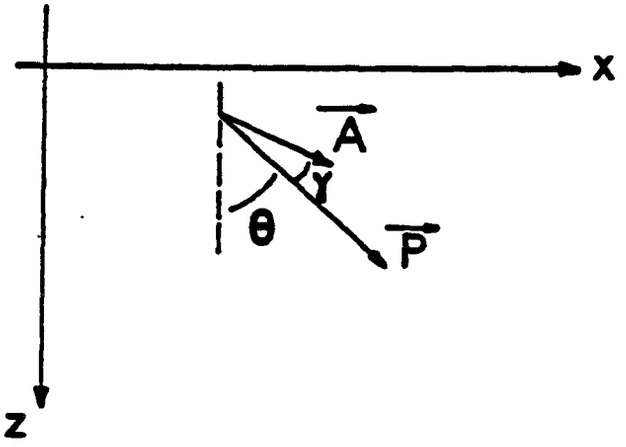

FIG. 2-10. Attenuation and propagation vectors

From figure(2-10), we can find an equivalent to (2.2.10),

$$\sin\vartheta = P_x/|P|$$

For an homogeneous wave, and by using (2.2.7) we obtain

$$\sin\vartheta = \frac{v_R^2 + v_I^2}{v_R}\frac{k_x}{\omega} \qquad (2.2.13)$$

with $v = \sqrt{M/\rho}$, or

$$v_R = \left[\frac{|M| + M_R}{2\rho}\right]^{1/2}$$

$$v_I = \left[\frac{|M| - M_R}{2\rho} \right]^{1/2}$$

2b. Wave field extrapolator for the acoustic wave equation

It is well known that in an elastic medium the wavefield extrapolator for the acoustic wave equation in the f-k domain is

$$\theta(\omega,k_x,z) = e^{-ik_z z}$$

This relation can be written for a viscoelastic medium, as done in paragraph 2.a, and so we have

$$\theta(\omega,k_x,z) = e^{-ik_z z}$$

with

$$k_z = \frac{\omega}{v}\left[1 - \left(\frac{vk}{\omega}\right)^2\right]^{1/2}$$

$$v = \sqrt{M/\rho}$$

$$k = k_x + i\,\mathrm{Im}k = \frac{\omega}{v}\sin\vartheta \text{ , or}$$

$$\sin\vartheta = \frac{v_R^2 + v_I^2}{v_R}\frac{k_x}{\omega} \text{ , for an homogeneous wave.}$$

Remark: Boundary conditions imply, as is shown in the next paragraph, a conservation of the x-coordinate of the wave vector K. This allows us to use equations obtained in the first medium for other media. In particular, in the case of an homogeneous incident wave, we apply equations (2.2.12) and (2.2.13) everywhere.

3. Reflections and Transmissions

In all the following equations, time dependence has been omitted, and it is understood to be of the form $e^{i\omega t}$.

Figure(2-11) shows the two media we are dealing with, and the notation employed. Only the propagation vector has been represented. All variables associated with the lower medium will be primed. In the first medium, subscript 1 refers to the amplitude of the incident wave, while subscript 2 refers to the reflected wave.

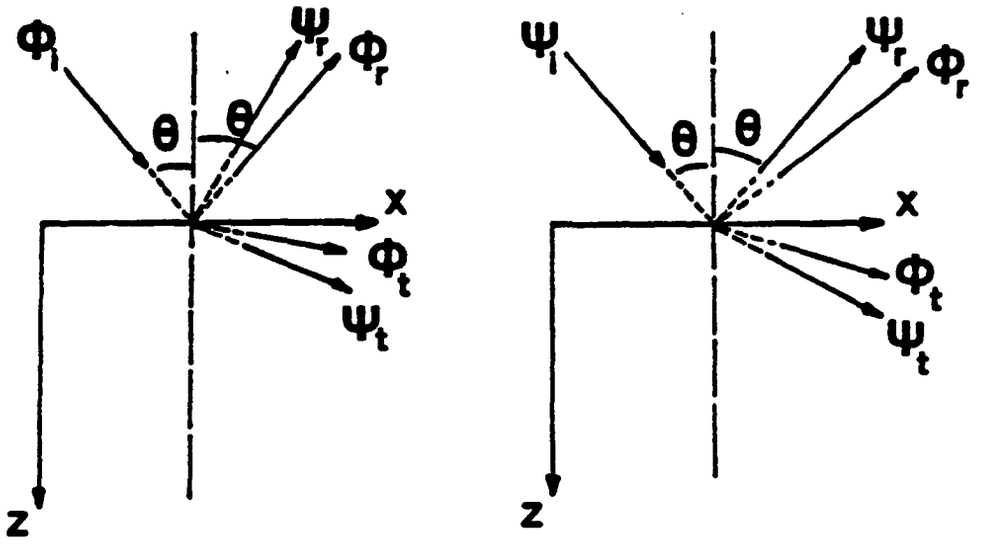

FIG. 2-11. Reflections and transmissions of potentials

In all the following derivations, we use potentials. As function of potentials, we have the following system of equations.

$$\Phi = \Phi_i + \Phi_r = A_1 e^{-i(kx + \alpha z)} + A_2 e^{-i(kx - \alpha z)}$$
$$\Psi = \Psi_i + \Psi_r = B_1 e^{-i(kx + \beta z)} + B_2 e^{-i(kx - \beta z)}$$
$$\Phi' = \Phi_t = A' e^{-i(k'x + \alpha' z)}$$
$$\Psi' = \Psi_t = B' e^{-i(k'x + \beta' z)}$$

with

$$k^2 + \alpha^2 = \frac{\rho\omega^2}{\lambda + 2\mu} \qquad \mathrm{Re}(\alpha) \geq 0$$
$$k^2 + \beta^2 = \frac{\rho\omega^2}{\mu} \qquad \mathrm{Re}(\beta) \geq 0$$
$$k'^2 + \alpha'^2 = \frac{\rho'\omega^2}{\lambda' + 2\mu'} \qquad \mathrm{Re}(\alpha') \geq 0$$
$$k'^2 + \beta'^2 = \frac{\rho'\omega^2}{\mu'} \qquad \mathrm{Re}(\beta') \geq 0$$

The displacements and stresses for the $2D$ case are given by:

Displacements:

$$u_x = \frac{\partial \Phi}{\partial x} - \frac{\partial \Psi}{\partial z}$$

$$u_z = \frac{\partial \Phi}{\partial z} + \frac{\partial \Psi}{\partial x}$$

Stresses:

$$\sigma_{zz} = \lambda \frac{\partial^2 \Phi}{\partial x^2} + (\lambda + 2\mu) \frac{\partial^2 \Phi}{\partial z^2} + 2\mu \frac{\partial^2 \Psi}{\partial x \partial z}$$

$$\sigma_{xz} = \mu \left[2 \frac{\partial^2 \Phi}{\partial x \partial z} - \frac{\partial^2 \Psi}{\partial z^2} + \frac{\partial^2 \Psi}{\partial x^2} \right]$$

Three cases are to be examined separately.

3a. Liquid-solid interface.

The incident wave is traveling in a liquid medium, this implies $\mu = 0$, $B_1 = B_2 = 0$. Continuity of displacements and stresses gives

$$\begin{aligned} u_z &= u'_z \\ 0 &= \sigma'_{xz} \\ \sigma_{zz} &= \sigma'_{zz} \end{aligned}$$

This implies $k = k'$, which can be considered as a generalized Snell's law.

$$\frac{A_2}{A_1} = R = \frac{\rho' d[(f'^2 - k^2)^2 + 4k^2 d' f'] - \rho d'(f'^2 + k^2)^2}{\rho' d[(f'^2 - k^2)^2 + 4k^2 d' f'] + \rho d'(f'^2 + k^2)^2}$$

$$\frac{A'}{A_1} = T_P = \frac{2\rho d(f'^4 - k^4)}{\rho' d[(f'^2 - k^2)^2 + 4k^2 d' f'] + \rho d'(f'^2 + k^2)^2}$$

$$\frac{B}{A_1} = T_S = \frac{4\rho d d' k(f'^2 + k^2)}{\rho' d[(f'^2 - k^2)^2 + 4k^2 d' f'] + \rho d'(f'^2 + k^2)^2}$$

3b. Solid–Liquid interface.

The incident wave is now traveling in a solid medium, and the transmitted wave is traveling in a liquid medium, therefore we have $\mu' = 0$, $B' = 0$. The continuity equations are now

$$\begin{aligned} u_z &= u'_z \\ \sigma_{zz} &= 0 \\ \sigma_{xz} &= \sigma'_{xz} \end{aligned}$$

This implies $k = k'$, as in case 3a. Now two incident waves are possible:

1. P-wave incident: $B_1 = 0$, we get

$$\frac{A_2}{A_1} = R_{PP} = \frac{\rho' d(f^2 + k^2)^2 + 4k^2 d d' f \rho - \rho d'(f^2 - k^2)^2}{\rho' d(f^2 + k^2)^2 + 4k^2 d d' f \rho + \rho d'(f^2 - k^2)^2}$$

$$\frac{B_2}{A_1} = R_{PS} = \frac{4k\rho d d'(f^2 - k^2)}{\rho' d(f^2 + k^2)^2 + 4k^2 d d' f \rho + \rho d'(f^2 - k^2)^2}$$

$$\frac{A'}{A_1} = T_{PP} = \frac{2\rho d(f^4 - k^4)}{\rho' d(f^2 + k^2)^2 + 4k^2 d d' f \rho + \rho d'(f^2 - k^2)^2}$$

2. S-wave incident: $A_1 = 0$, then we get

$$\frac{B_2}{B_1} = R_{SS} = \frac{4k^2 d d' f \rho - \rho d'(f^2 - k^2)^2 - \rho' d(f^2 + k^2)^2}{\rho' d(f^2 + k^2)^2 + \rho d'(f^2 - k^2)^2 + 4k^2 d d' f \rho}$$

$$\frac{A_2}{B_1} = R_{SP} = \frac{-4k d' f \rho(f^2 - k^2)}{\rho' d(f^2 + k^2)^2 + \rho d'(f^2 - k^2)^2 + 4k^2 d d' f \rho}$$

$$\frac{A'}{B_1} = T_{SP} = \frac{4k d f \rho(f^2 + k^2)}{\rho' d(f^2 + k^2)^2 + \rho d'(f^2 - k^2)^2 + 4k^2 d d' f \rho}$$

3c. Solid–Solid interface.

Two cases are possible: we can have either a P or an S incident wave. In both cases the equations of continuity are

$$\begin{aligned} u_z &= u'_z \\ u_x &= u'_x \\ \sigma_{zz} &= \sigma'_{zz} \\ \sigma_{xz} &= \sigma'_{xz} \end{aligned}$$

b1: P-wave incident: $B_1 = 0$, if we define

$$\begin{aligned} R_{PP} &= A_2/A_1 \\ R_{PS} &= B_2/A_1 \\ T_{PP} &= A'/A_1 \\ T_{PS} &= B'/A_1 \end{aligned}$$

They are solutions of the linear system

$$\mathbf{Ap} = \mathbf{b}$$

where

$$\mathbf{A} = \begin{bmatrix} k & f & -k & f' \\ -d & k & -d' & -k \\ -2kd\mu & -(f^2-k^2)\mu & -2kd'\mu' & (f'^2-k)\mu' \\ (f^2-k^2)\mu & -2kf\mu & -\mu'(f'^2-k^2) & -2kf'\mu' \end{bmatrix}$$

$$\mathbf{p} = \begin{bmatrix} R_{PP} \\ R_{PS} \\ T_{PP} \\ T_{PS} \end{bmatrix} \qquad \mathbf{b} = \begin{bmatrix} -k \\ -d \\ -2kd\mu \\ -\mu(f^2-k^2) \end{bmatrix}$$

b2: S-wave incident: $A_1 = 0$, the following definitions

$$\begin{aligned} R_{SP} &= A_2/B_1 \\ R_{SS} &= B_2/B_1 \\ T_{SP} &= A'/B_1 \\ T_{SS} &= B'/B_1 \end{aligned}$$

are solutions of the linear system

$$\mathbf{As} = \mathbf{c}$$

where

$$\mathbf{s} = \begin{bmatrix} R_{SP} \\ R_{SS} \\ T_{SP} \\ T_{SS} \end{bmatrix} \qquad \mathbf{c} = \begin{bmatrix} f \\ -k \\ \mu(f^2-k^2) \\ -2kf\mu \end{bmatrix}$$

Remark:

The calculus of the reflection or transmission coefficients in the (ω,k_x) domain does not depend on the Fourier transform convention taken. On the other hand the synthetic seismogram is given by the sum of expressions of the following type:

$$f(x,t) = \frac{i}{2(2\pi)^2}\int\int S(k_x,\omega)\, C(k_x,\omega)\,\frac{e^{-2ik_z\Delta z}}{k_z}\, e^{-ik_z z + i\omega t}\, dk_x\, d\omega$$

with

$S(k_x,\omega)$ = source term,

$C(k_x,\omega)$ = reflection coefficient

The result is real and so we have:

$$f(x,t) = \bar{f}(x,t) = \frac{i}{2(2\pi)^2}\int\int \bar{S}(k_x,\omega)\, \bar{C}(k_x,\omega)\,\frac{e^{2ik_z\Delta z}}{k_z}\, e^{ik_z z - i\omega t}\, dk_x\, d\omega$$

The synthetic seismogram can be calculated using the inverse Fourier transform convention. As the reflection coefficient is independent of the convention, while the Green's function and the source terms are dependent, we find that, if for one given convention the reflection coefficient used is $C(k_x,\omega)$ then for the opposite convention the right one to use is $\bar{C}(k_x,\omega)$.

4. Attenuation model

In previous chapters (Part I-A and Part I-C), it has been shown that the effect of attenuation on reflections is not, to a first order approximation, a function of the viscoelastic model chosen. In the same chapters it was also shown (following equations derived by Borcherdt, 1977) that the attenuation function in two dimensions is a slowly varying function of the angle γ between the attenuation and the propagation vectors. Under these conditions, we are confident of using a *constant $-Q$* model (Kjartansson, 1980) to represent viscoelastic behavior. This model will enable us to have the right order of variations modeled in the synthetic seismograms.

For review purposes, the constant-Q model is characterized by a frequency free representation of the quality factor Q, the model is the following:

The viscoelastic modulus is given by

$$M(\omega) = M_0\left[\frac{i\omega}{\omega_0}\right]^{2\gamma} = M_0\left|\frac{\omega}{\omega_0}\right|^{2\gamma} e^{i\pi\gamma\,\mathrm{sgn}\,\omega}$$

implying a phase velocity of

$$C_\varphi(\omega) = C_0\left|\frac{\omega}{\omega_0}\right|^{\gamma}$$

In all these, ω_0 is a reference frequency at which M_0 and C_0 have been measured. γ is given by

$$\gamma = \frac{1}{\pi}\tan^{-1}(1/Q)$$

5. Synthetic Seismogram

Our goal in this paper is to model a marine seismogram. For this purpose, we will assume a flat-layered earth model. Our experiment will be to put a source at the sea surface, as in Part II-A. To simplify the mathematical writing, we shall use a 3 layered earth. The generalization for more layers follows immediately.

The notations and the experimental setting are described in Figure(2-12).

Five primary waves are recorded at the sea-surface. They are the following, where the letters refer to the type of wave in each path: *PP*, *PPPP*, *PPSP*, *PSPP*, *PSSP*.

To find the expression for each of these waves in the f-k domain, we consider them as potentials, because potentials satisfy the acoustic wave equation, for which wave extrapolators are well known. On the other hand, if we were dealing with displacements, propagation would have to be done with the elastodynamic wave equation, for which we do not have wave extrapolators in the f-k domain. Thus we have:

PP:

$$i\pi R \frac{\exp[-i(2k_{zP_0}z_0)]}{k_{zP_0}} \cdot S(k_x,\omega)$$

PPPP:

$$i\pi T_P R_{12PP} T_{10PP} \frac{\exp[-i(2k_{zP_0}z_0 + 2k_{zP_1}z_1)]}{k_{zP_0}} \cdot S(k_x,\omega)$$

PSSP:

$$i\pi T_S R_{12SS} T_{10SP} \frac{\exp[-i(2k_{zP_0}z_0 + 2k_{zS_1}z_1)]}{k_{zP_0}} \cdot S(k_x,\omega)$$

PPSP:

$$i\pi T_P R_{12PS} T_{10SP} \frac{\exp[-i(2k_{zP_0}z_0 + k_{zP_1}z_1 + k_{zS_1}z_1)]}{k_{zP_0}} \cdot S(k_x,\omega)$$

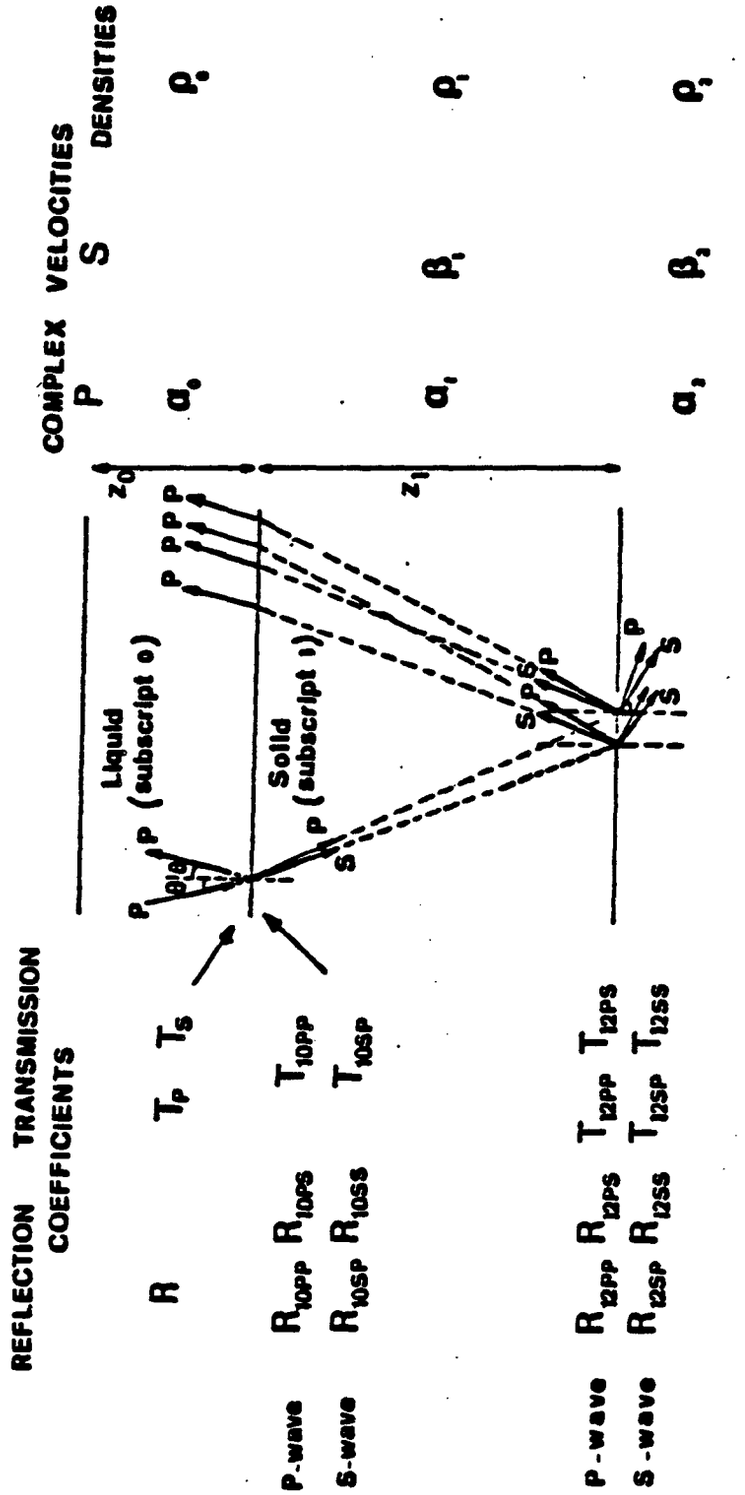
COMPLEX VELOCITIES
P
S
DENSITIES
α_0
β_0
ρ_0
α_1
β_1
ρ_1
α_2
β_2
ρ_2
z_0
z_1
Liquid (subscript 0)
Solid (subscript 1)
semi infinite solid (subscript 2)
REFLECTION TRANSMISSION COEFFICIENTS
R
T_P T_S
R_{10PP} R_{10PS}
R_{10SP} R_{10SS}
T_{10PP}
T_{10SP}
R_{12PP} R_{12PS}
R_{12SP} R_{12SS}
T_{12PP} T_{12PS}
T_{12SP} T_{12SS}
P-wave
S-wave
P-wave
S-wave

FIG. 2-12.

PSPP:

$$i\pi T_S R_{12SP} T_{10PP} \frac{\exp[-i(2k_{zP_0}z_0 + k_{zP_1}z_1 + k_{zS_1}z_1)]}{k_{zP_0}} \cdot S(k_x,\omega)$$

In these expressions

$$S(k_x,\omega) = 2D \text{ Fourier Transform of the source function}$$

$$k_{zP_0} = \frac{\omega}{\alpha_0}\left[1 - \left(\frac{\alpha_0 k}{\omega}\right)^2\right]^{1/2}$$

$$k_{zP_1} = \frac{\omega}{\alpha_1}\left[1 - \left(\frac{\alpha_1 k}{\omega}\right)^2\right]^{1/2}$$

$$k_{zS_1} = \frac{\omega}{\beta_1}\left[1 - \left(\frac{\beta_1 k}{\omega}\right)^2\right]^{1/2}$$

with $k = \frac{\omega}{\alpha_0}\sin\vartheta$, and $\sin\vartheta = \frac{\alpha_{0R}^2 + \alpha_{0I}^2}{\alpha_{0R}} \frac{k_x}{\omega}$

For primary waves, the synthetic seismogram in the f-k domain is the sum of the five upper expressions.

If we want to introduce multiple reflections or pegleg multiples, it is straightforward. Some examples are given in Figures (2-13a,b,c). The procedure can be generalized. The synthetic seismogram itself is obtained by taking an inverse $2D$ Fourier Transform of the expressions chosen in the f-k domain.

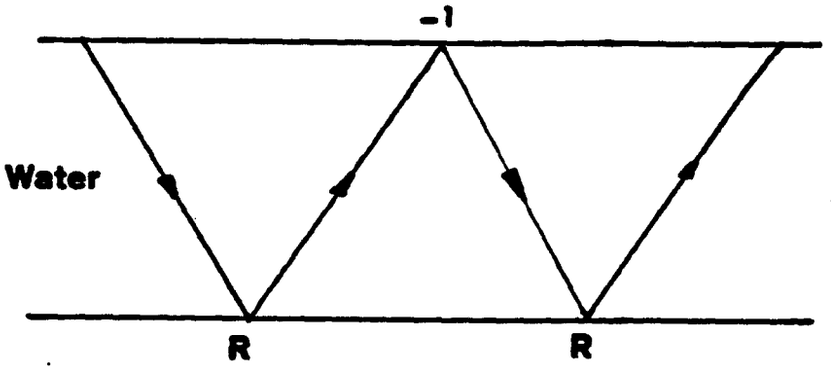

FIG. 2-13a. Water-Bottom multiple. Multiply the expression for *PP* by the factor: $-Re^{-2i\omega_z P_0 z_0}$

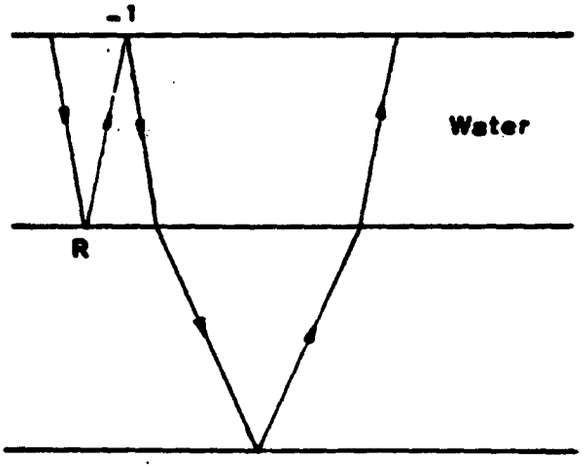

FIG. 2-13b. Peg-leg multiple. Multiply the expressions for *PP PPSPP PSPP PSSP* by the factor: $-Re^{-2i\omega_z P_0 z_0}$

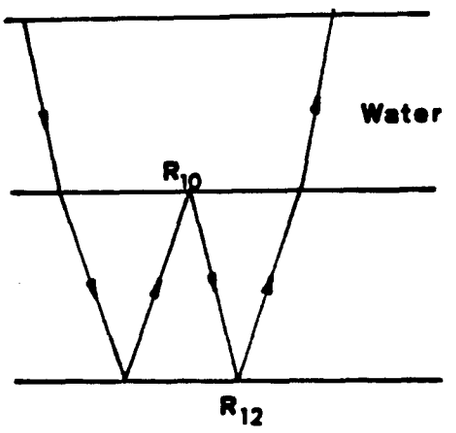

FIG. 2-13c. Intrabed multiples. If we take *PPPP* as the main wave, we can have as intrabed multiples:

path	computation
PP(PP)PP	$PPPP \cdot R_{12PP} R_{10PP}\, e^{-i(2k_{zP_1})z_1}$
PP(SP)PP	$PPPP \cdot R_{12PS} R_{10SP}\, e^{-i(2k_{zP_1} + k_{zS_1})z_1}$
PP(PS)PP	$PPPP \cdot R_{12SP} R_{10PS}\, e^{-i(2k_{zP_1} + k_{zS_1})z_1}$
PP(SS)PP	$PPPP \cdot R_{12SS} R_{10SS}\, e^{-i(2k_{zS_1})z_1}$

II. APPLICATION

The results presented in this paragraph are a direct application of the equations derived in the preceding one (*I. Theory*). Problems that have occurred in our trials are similar to those we had in our previous chapter (Part II-A), therefore we have solved them in the same manner. Different cases are presented in the following lines.

1. Liquid-Solid case: 1 Head wave.

Three different cases are presented here; velocities and densities remain the same for all of them. They are:

First medium: liquid (water)		
P-velocity	v_P	1500 m/s
Density	ρ	1 g/cm^3
Second medium: semi-infinite solid		
P-velocity	v'_P	2500 m/s
S-velocity	v'_S	1200 m/s
Density	ρ'	2 g/cm^3

Since $v'_S < v_P$, we get one critical angle and one head wave.

Since we are working in viscoelastic media, velocities are frequency dependent. The reference frequency at which they are taken is set for convenience at 1 Hz. This is a low frequency for our source wavelet spectrum.

The values taken for the quality factor Q are also at the 1 Hz reference frequency, they are:

a) Fig 2-14,2-15,2-18. *No attenuation, No Q contrast*:

First medium: liquid (water)		
P-quality factor	Q_P	10000
Second medium: semi-infinite solid		
P-quality factor	Q'_P	10000
S-quality factor	Q'_S	10000

b) Fig 2-14,2-16,2-18. *Q contrast*:

First medium: liquid (water)		
P-quality factor	Q_P	10000
Second medium: semi-infinite solid		

P-quality factor	Q'_P	14
S-quality factor	Q'_S	10

c) Fig 2-14,2-17,2-20. *High attenuation, No Q contrast*:

	First medium: liquid	
P-quality factor	Q_P	10
	Second medium: semi-infinite solid	
P-quality factor	Q'_P	10
S-quality factor	Q'_S	10

Comparing figures corresponding to each of these three cases, brings us to the following conclusions:

1. When there is no Q-contrast, the reflection coefficient is strictly equal to the elastic one if the model of attenuation used is the constant-Q model.

2. When there is no Q-contrast, (cases a and c), the wave velocities are different between elastic and viscoelastic cases. Higher frequencies than the reference frequency travel faster in a viscoelastic medium.

There is also the amplitude effect we were expecting: a low quality factor implies high attenuation.

A third type of effect can be observed: it is the modification of the frequency content between a wave traveling in an elastic medium and a wave traveling in a viscoelastic medium. Attenuation implies that we are loosing proportionally more high frequencies than low frequencies and so the signal we record is more spread out in a viscoelastic case than in an elastic one.

3. It is important also to consider the differences occurring between case a and b. Case a has nearly no attenuation ($Q_P = 10000$) and no Q-contrast, while case b has the same first medium attenuation as case a, with low Q in the second medium.

We observe that the effects of a Q-contrast appear mainly near critical angle, and that there is an increase of amplitude of post-critical reflections in the Q-contrast case with respect to the *No* Q-contrast one.

Another expected effect is that the amplitude of the head wave is smaller in the Q-contrast case, because the head-wave is traveling in the highly attenuating second medium.

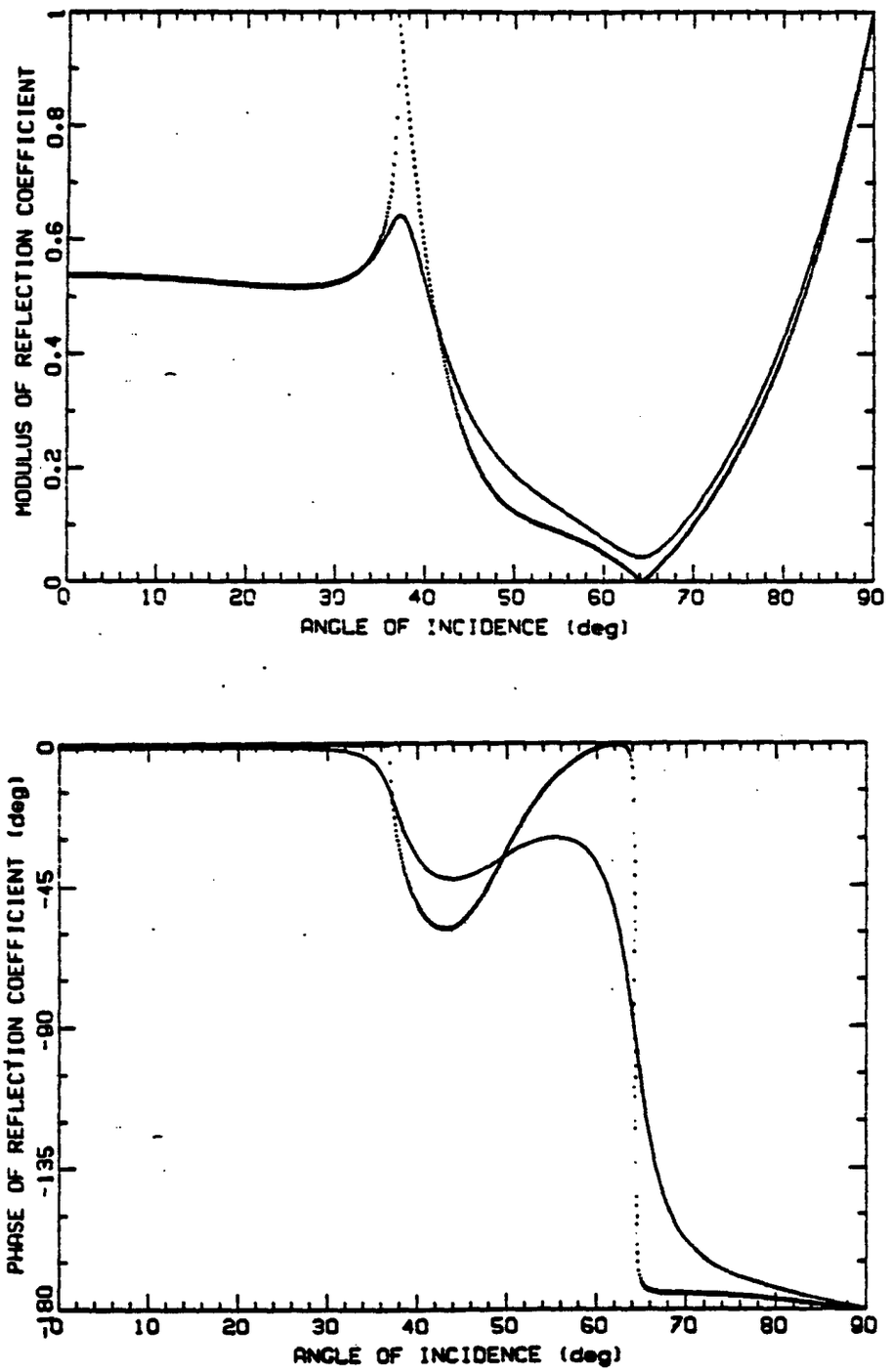

FIG. 2-14. 1-Head-wave case:
Modulus and phase of Reflection Coefficient. Comparison of elastic and viscoelastic reflection coefficients. The dotted lines represent the elastic reflection coefficient and the viscoelastic one when there is no Q-contrast.The solid line represent the viscoelstic one when there is Q-contrast. This is a frequency-dependent plot due to velocity dispersion in the second medium. The frequency chosen here is the reference frequency (1 Hz).

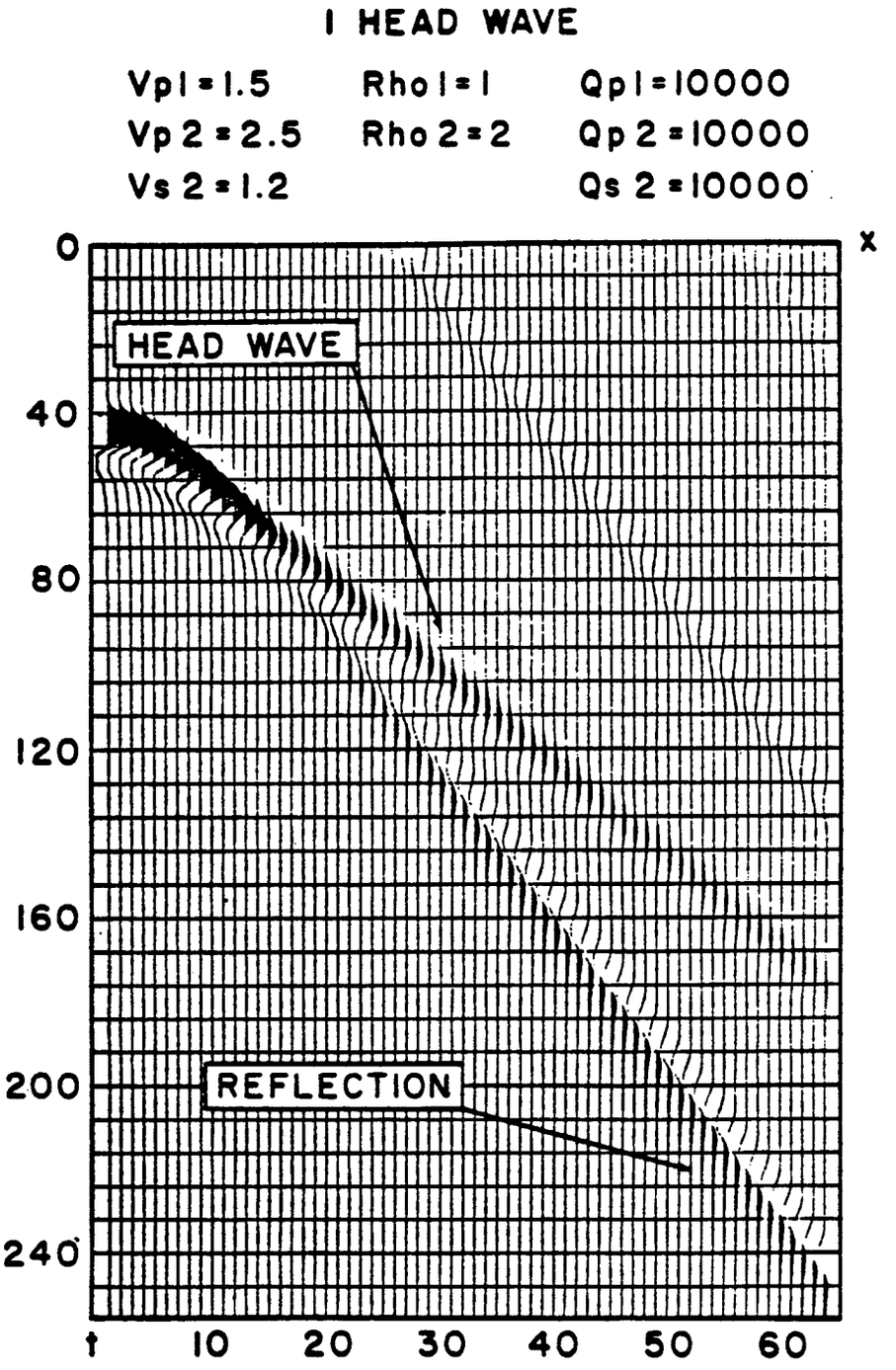

FIG. 2-15. 1-Head-wave case:
Synthetic seismogram. No attenuation included.
The parameters used to generate it are: dx = 86 m, dt = .032 s.

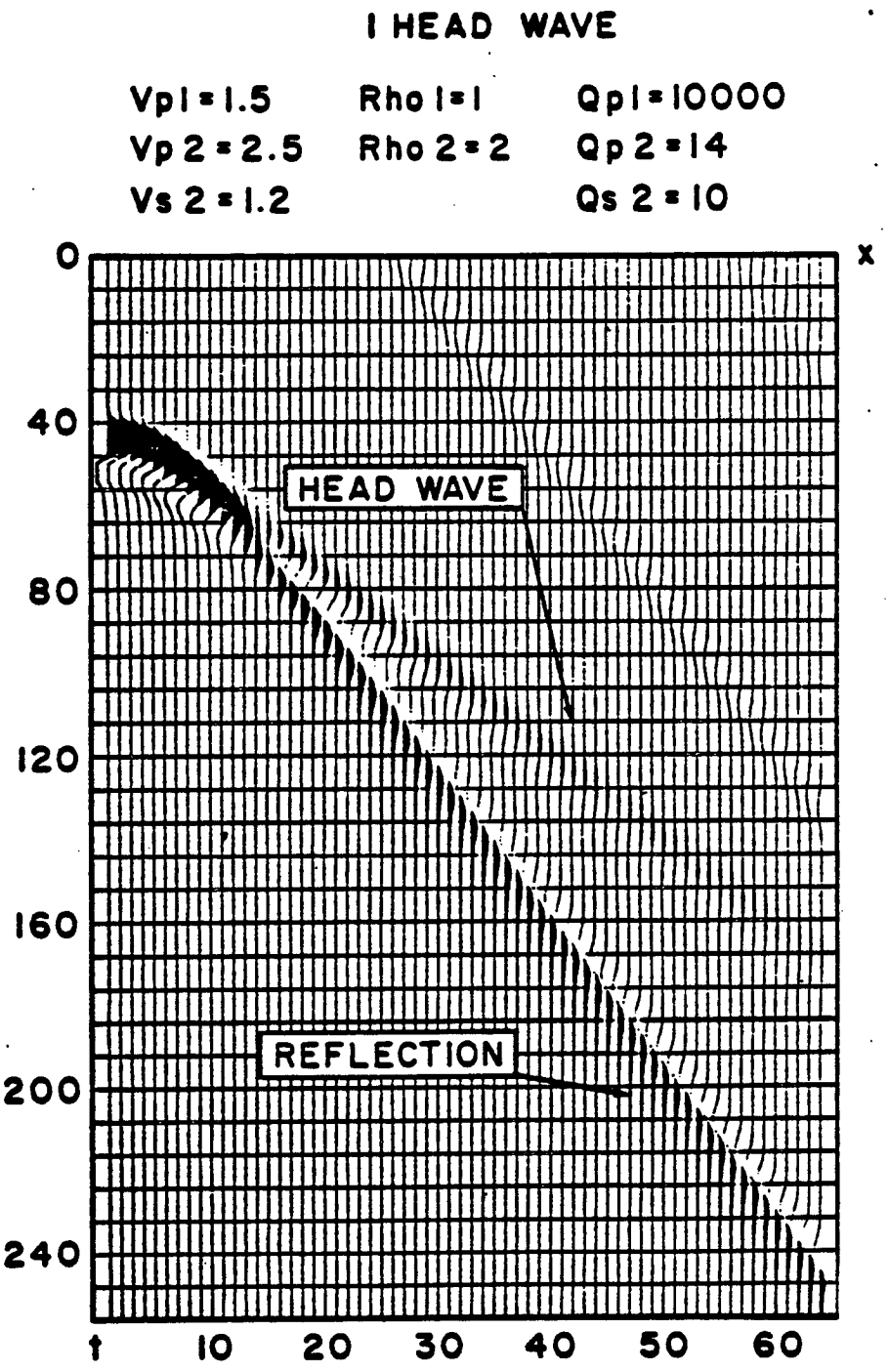

FIG. 2-16. 1-Head-wave case:
Synthetic seismogram. Attenuation and *Q*-contrast included.
Same clip value and parameters as in figure 2-15. Note the increase of amplitude of postcritical reflection and the decrease of amplitude of the head-wave with respect to figure 2-15. Note also the difference in arrival time for the head-wave.

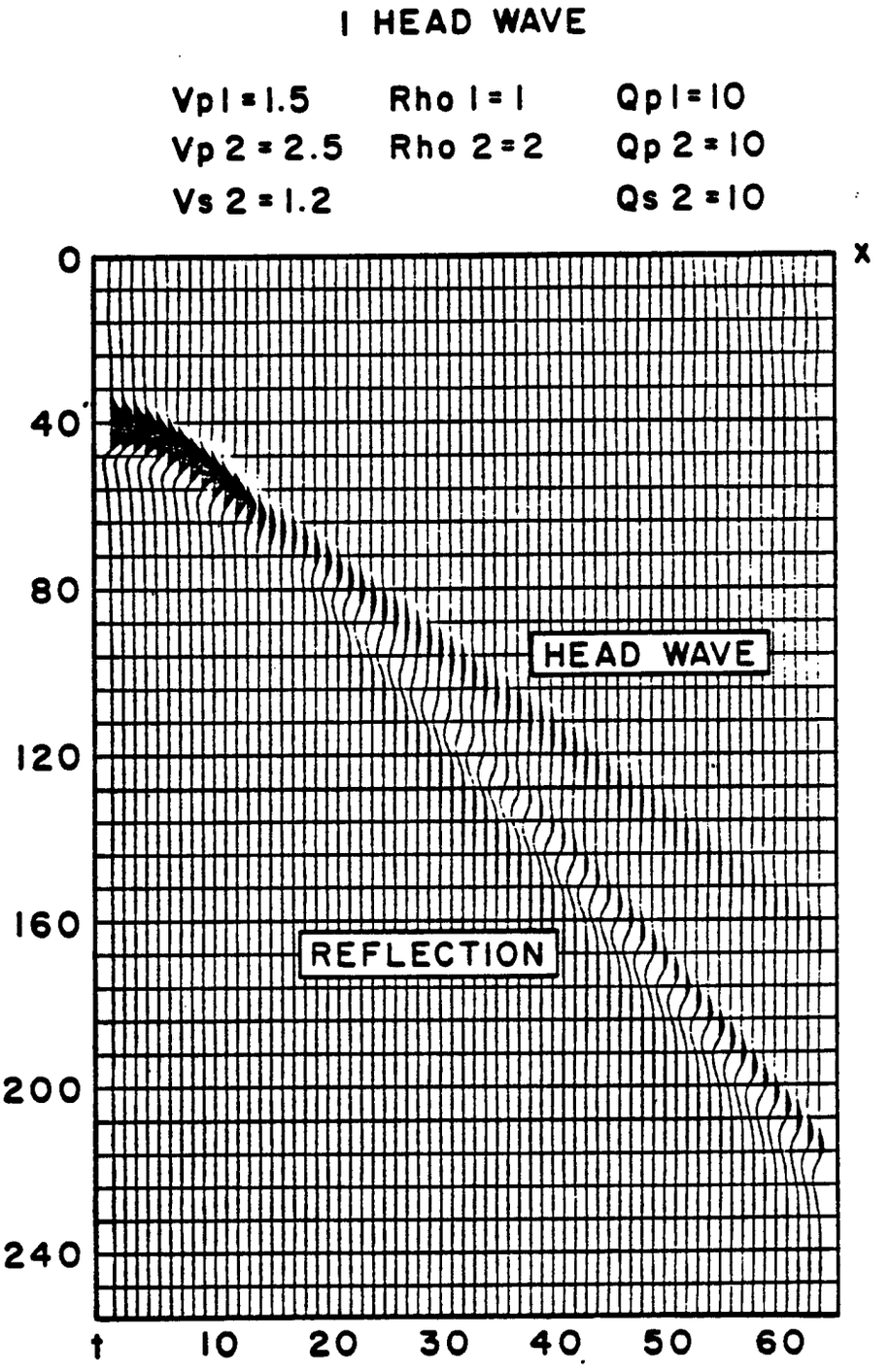

FIG. 2-17. 1-Head-wave case:
Synthetic seismogram. High attenuation and no *Q*-contrast.
Same clip value and parameters as in figure 2-15. Note the decrease of amplitude of the reflection and the decrease of amplitude of the head wave with respect to figure 2-15. Note also the differences in arrival times for the reflection and the head-wave.

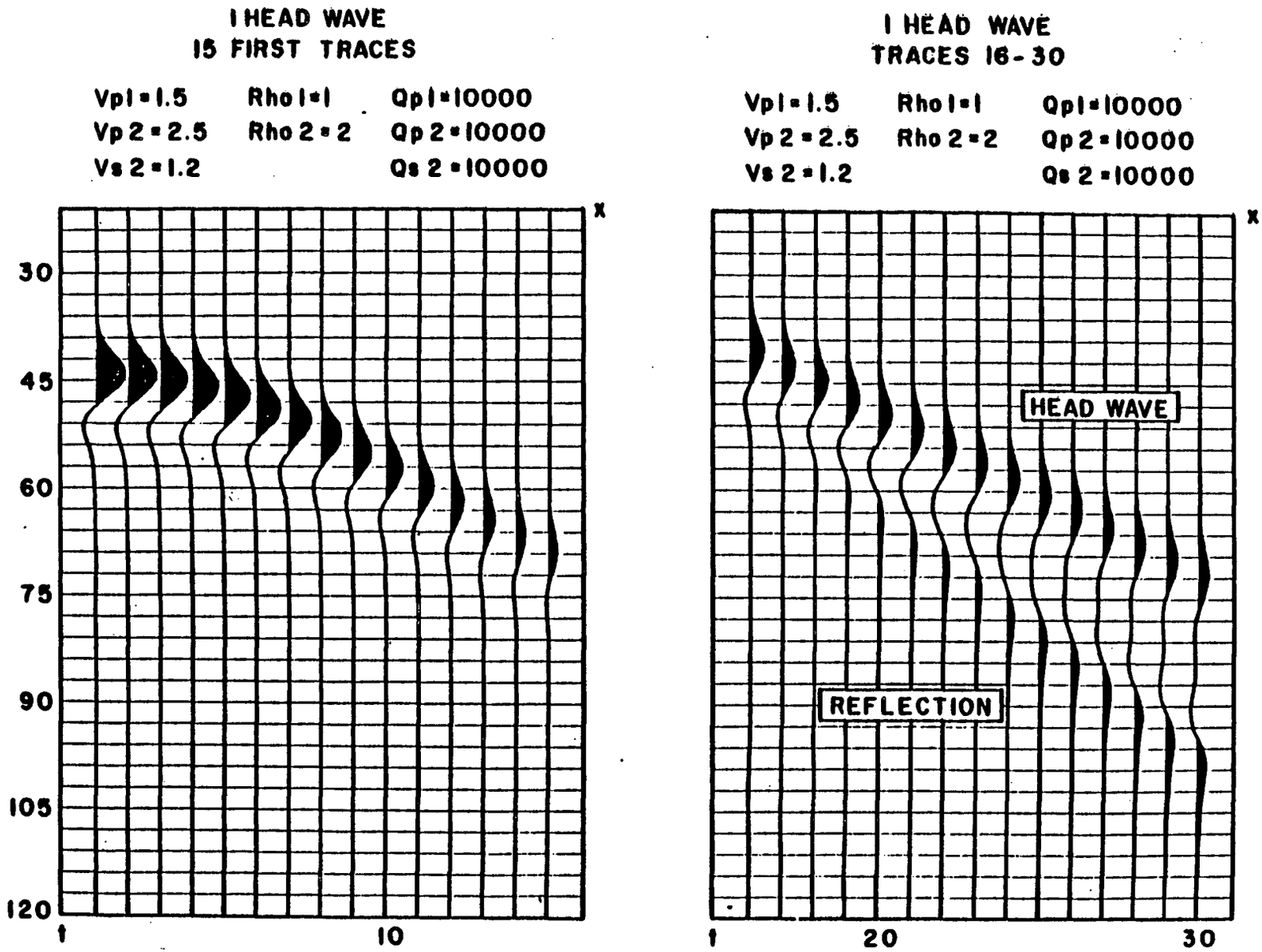

FIG. 2-18. 1-Head-wave case: No attenuation included. Window of figure 2-15. Left: traces 0-15. Right: traces 16-30. The figures are not clipped at the same value. These are the reference figures to compare with figures 2-19 and 2-20.

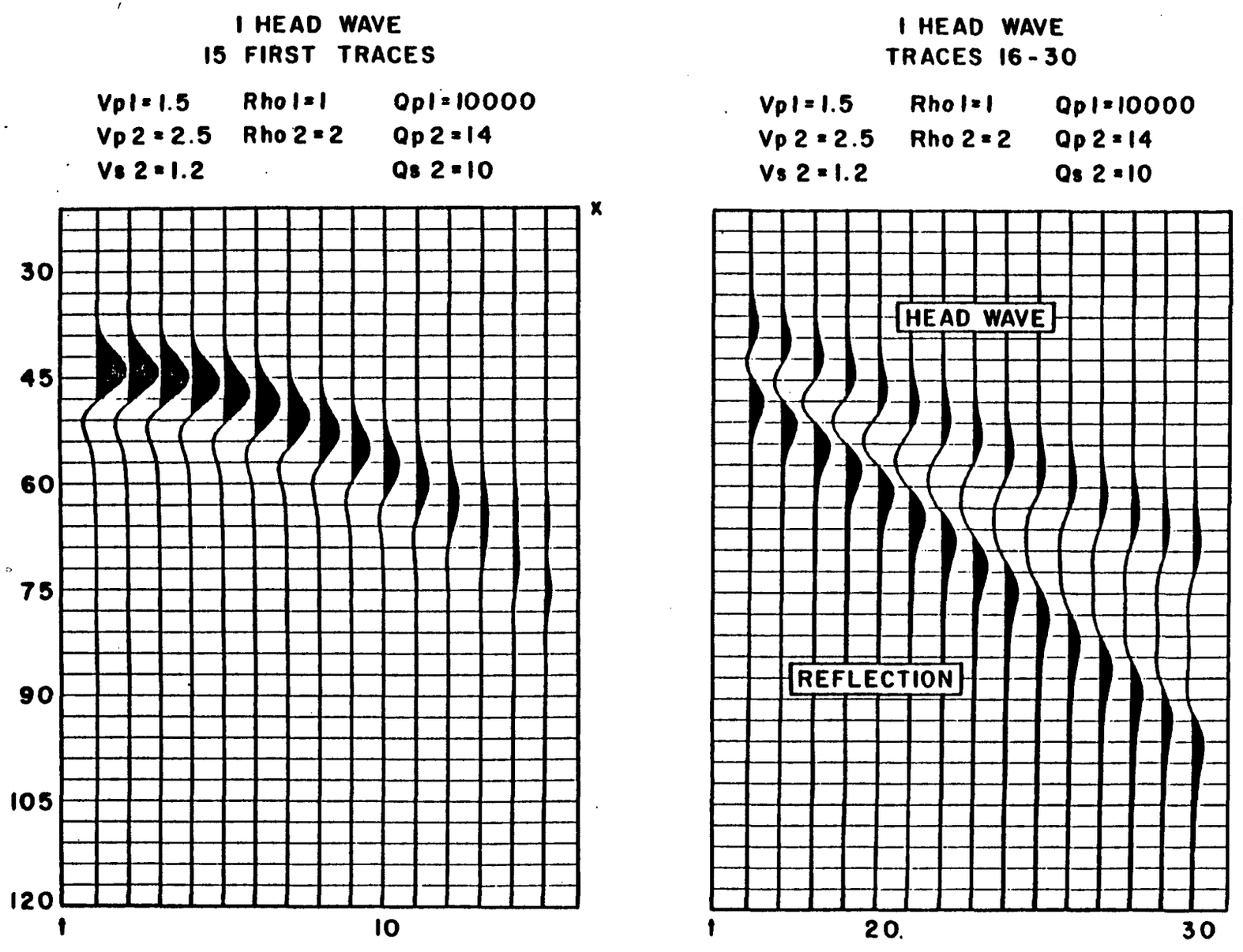

FIG. 2-19. 1-Head-wave case: Attenuation and Q-contrast included. Window of figure 2-16. Same traces and clip values as in figure 2-18. Remarks done in figure 2-16 are emphasized here.

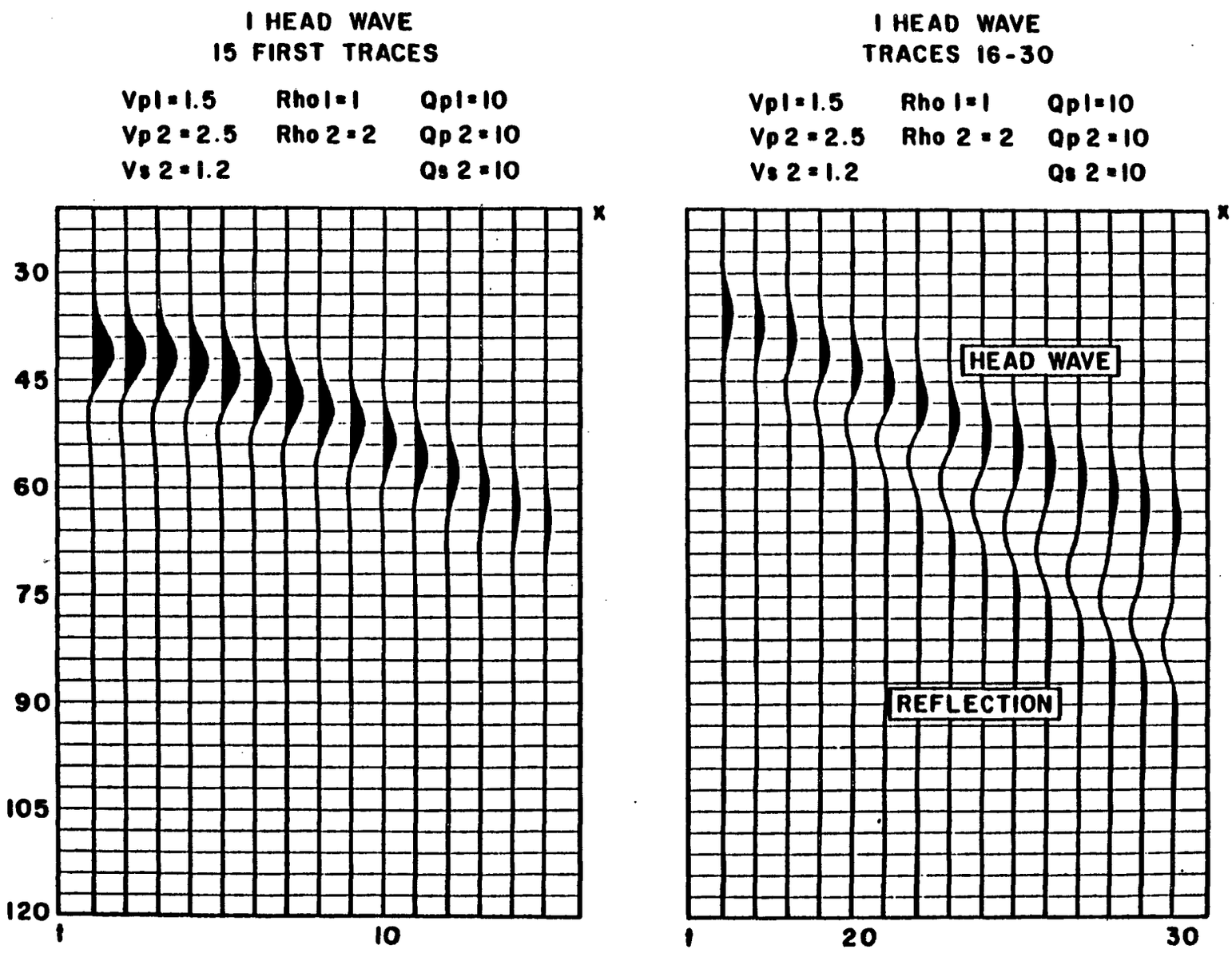

FIG. 2-20. 1-Head-wave case: High attenuation and no Q-contrast. Window of figure 2-17. Same traces and clip values as in figure 2-18. Remarks done in figure 2-17 are emphasized here.

2. Liquid-solid case: 2 Head waves.

Two different cases are presented here. For both of them velocities and densities are the same.

First medium: liquid (water)		
P-velocity	v_P	1500 m/s
Density	ρ	1 g/cm^3

Second medium: semi-infinite solid		
P-velocity	v'_P	3200 m/s
S-velocity	v'_S	1900 m/s
Density	ρ'	2.5 g/cm^3

As here $v'_S > v_P$, we have two critical angles and therefore two head waves.

The reference frequency is the same as in the one head-wave cases, ($w_0 = 1\ Hz$). For the quality factors, the values at this reference frequency are:

a) Fig 2-21,2-22. *No attenuation, No Q contrast*:

First medium: liquid (water)		
P-quality factor	Q_P	10000

Second medium: semi-infinite solid		
P-quality factor	Q'_P	10000
S-quality factor	Q'_S	10000

b) Fig 2-21,2-23. *Q contrast*:

First medium: liquid (water)		
P-quality factor	Q_P	10000

Second medium: semi-infinite solid		
P-quality factor	Q'_P	33
S-quality factor	Q'_S	20

Comparison of these two cases leads us to the same type of conclusions as in the one head-wave cases.

The amplitudes of the head waves which are propagating in attenuating media are smaller than the ones propagating in non-attenuating media. The frequency spectrum is also shifted to low frequencies.

For the reflections, there is a very slight effect near critical angle, but it seems that the acoustic impedance contrast is overwhelmingly high and masks the Q-contrast effect.

Besides that, we note that the amplitude of the PP head-wave is much weaker than the PS one. This forces us to overclip the plots, emphasizing wrap-around.

In Figure(2-22), the wrap-around energy is higher than in Figure(2-23), because it was padded with less zeros. The higher amplitude PP head-wave did not need so much padding.

The small amplitude of the PP head-wave with respect to the PS one is well known in well-logging data concerning measurements of velocities and quality factors.

It seems possible that this type of synthetic could be used to infer S-quality factors from actual borehole data, knowing the P-quality factor.

3. Solid-solid case:

As previously two different cases are going to be presented.For both of them velocities and densities are the same, that is:

First medium: liquid (water)		
P-velocity	v_p	1500 m/s
Density	ρ	1 g/cm^3
Second medium: solid		
P-velocity	v'_p	2500 m/s
S-velocity	v'_s	1200 m/s
Density	ρ'	2 g/cm^3
Third medium: semi-infinite solid		
P-velocity	v''_p	3000 m/s
S-velocity	v''_s	1400 m/s
Density	ρ''	2.5 g/cm^3

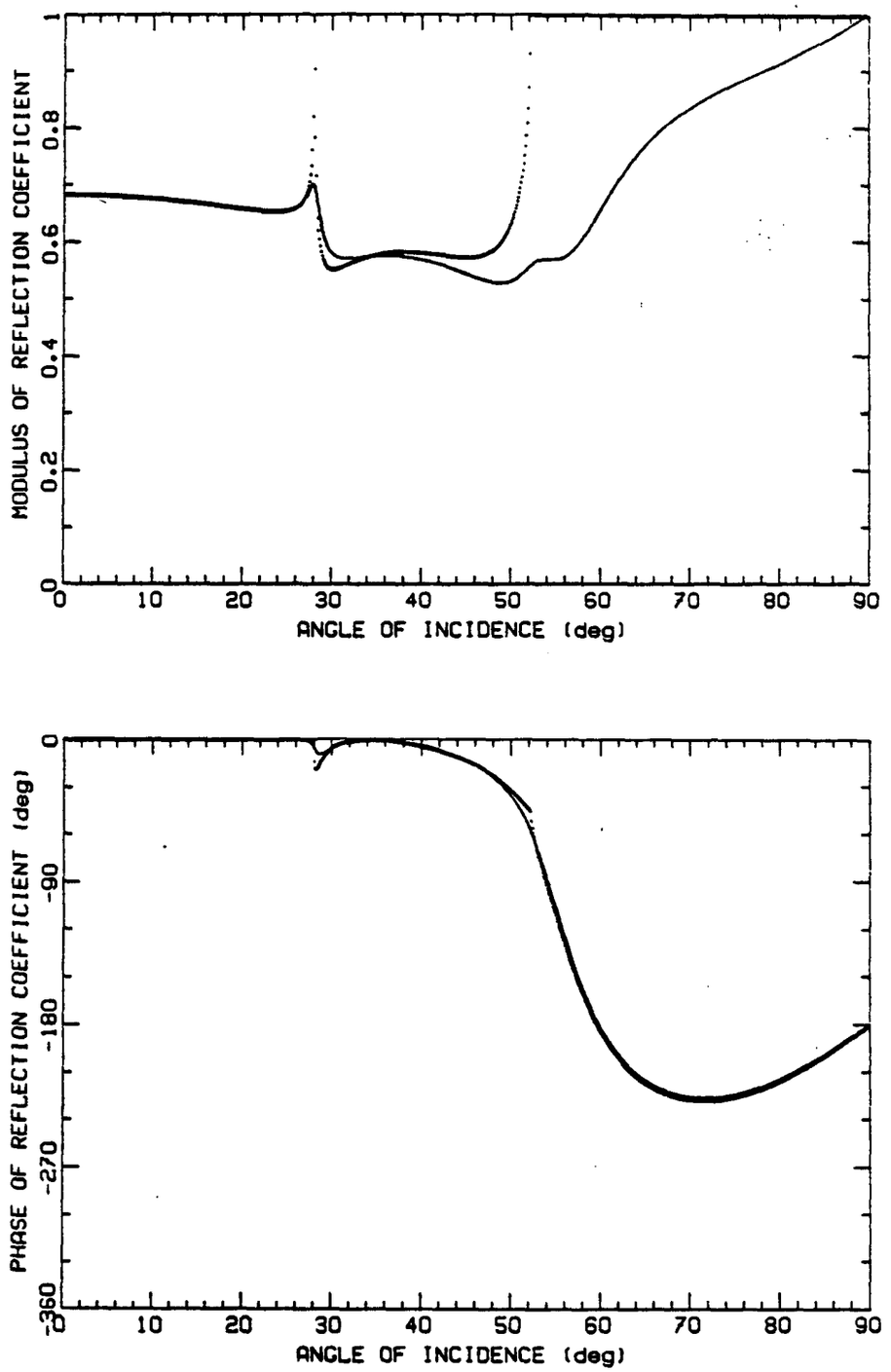

FIG. 2-21. 2-Head-waves case:
Modulus and phase of Reflection Coefficient. Comparison of elastic and viscoelastic reflection coefficients. The dotted lines represent the elastic reflection coefficient. The solid line represent the viscoelstic one when there is Q-contrast. This is a frequency-dependent plot due to velocity dispersion in the second medium. The frequency chosen here is the reference frequency (1 Hz).

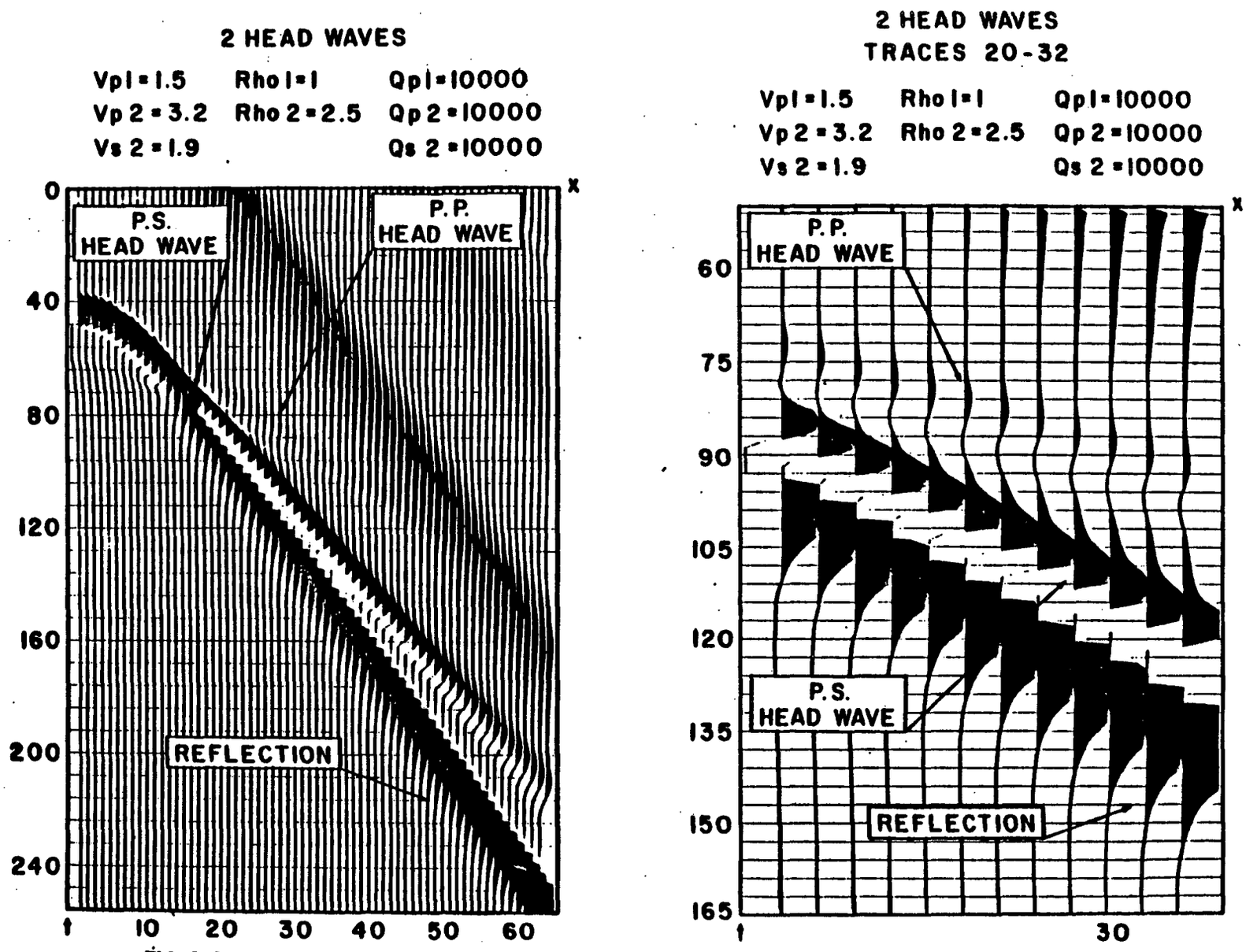

FIG. 2-22. 2-Head-waves case:
Synthetic seismogram. No attenuation included. The parameters used to generate it are the same as in figure 2-15. Left: Full seismogram. Right: Window, traces 21-32. These are reference figures for figure 2-23. Note the small amplitude of the *PP* head-wave with respect to the *PS* one.

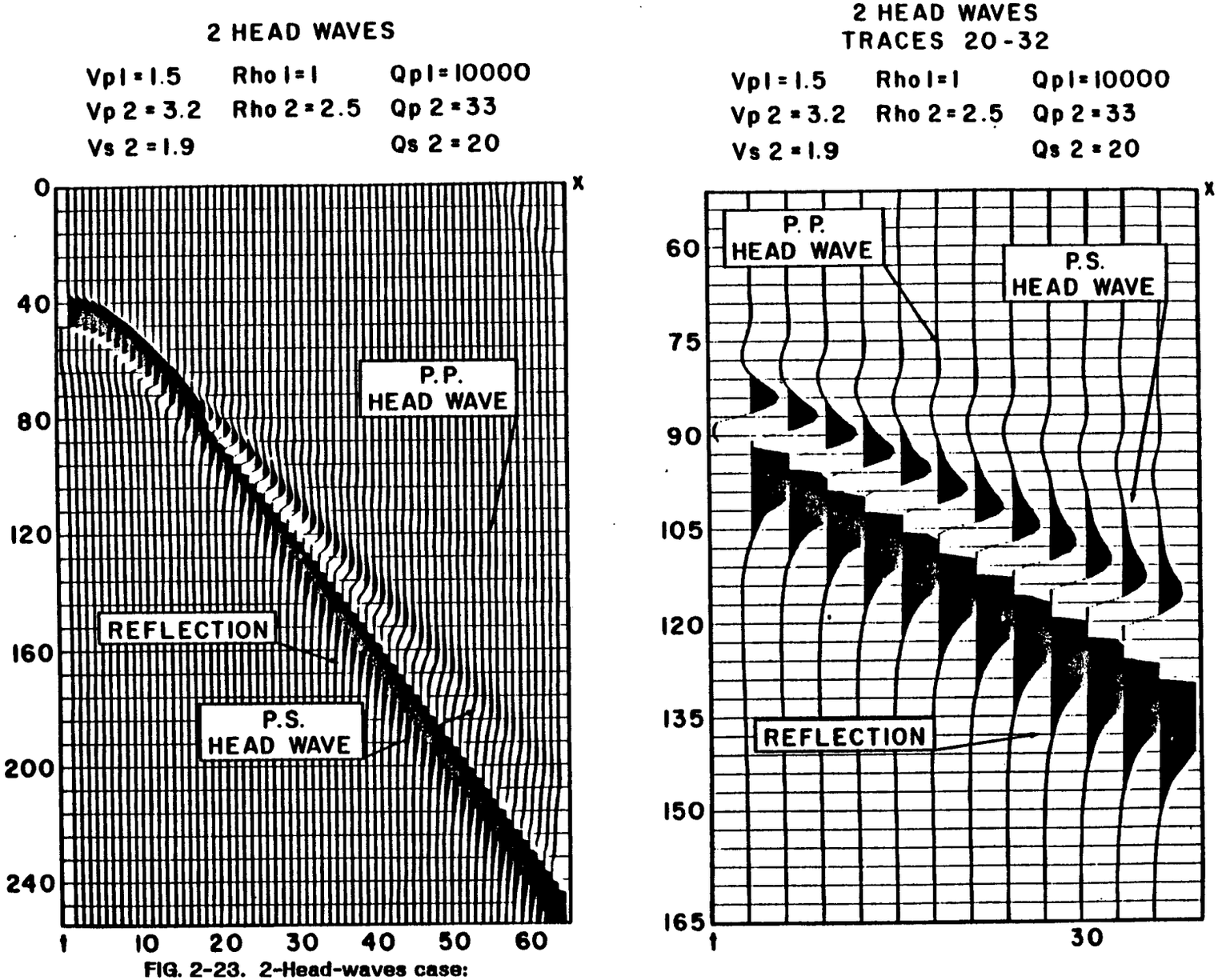

FIG. 2-23. 2-Head-waves case:
Synthetic seismogram. Attenuation and *Q*-contrast included. The parameters used to generate it are the same as in figure 2-15. Left: Full seismogram. Right: Window, traces 21-32. These figures were padded with more zeroes than figure 2-22. Note the smaller amplitude of both head-waves with respect to the previous case. Note also the differences in travel-times for both head-waves.

We also need the thicknesses of the two first layers. The third one is infinite. They are:

Liquid medium	$z_1 = 750\ m$
First Solid medium	$z_2 = 500\ m$

The reflection and transmission coefficients at each interface are given in Figures 2-24 to 2-31. In Figures 2-28 to 2-31, the reflection coefficient without attenuation is represented by a dotted line while the one with attenuation contrast is represented by a solid line. The reference frequency is the same as in the 1 head-wave cases, ($\omega_0 = 1\ Hz$). For the quality factors, the values at this reference frequency are:

a) Fig 2-32,2-34,2-36,2-37. *No attenuation, No Q contrast*:

First medium: liquid (water)		
P-quality factor	Q_P	10000
Second medium: solid		
P-quality factor	Q'_P	10000
S-quality factor	Q'_S	10000
Third medium: semi-infinite solid		
P-quality factor	Q''_P	10000
S-quality factor	Q''_S	10000

a) Fig 2-33,2-35,2-36,2-37. *Q contrast*:

First medium: liquid (water)		
P-quality factor	Q_P	10000
Second medium: solid		
P-quality factor	Q'_P	10000
S-quality factor	Q'_S	10000
Third medium: semi-infinite solid		

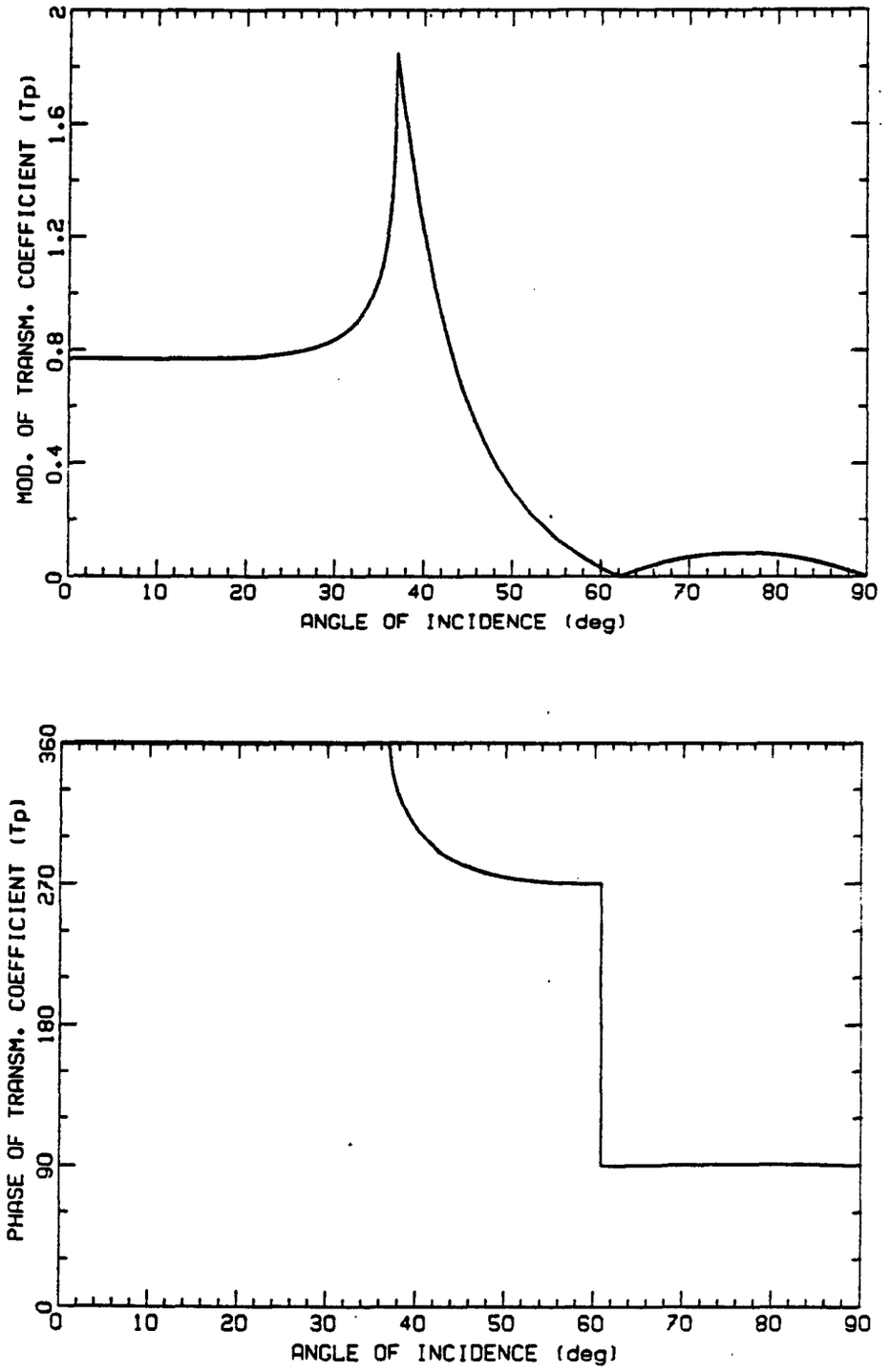

Fig.2-24. Liquid-solid : P-transmission coefficient . No attenuation .

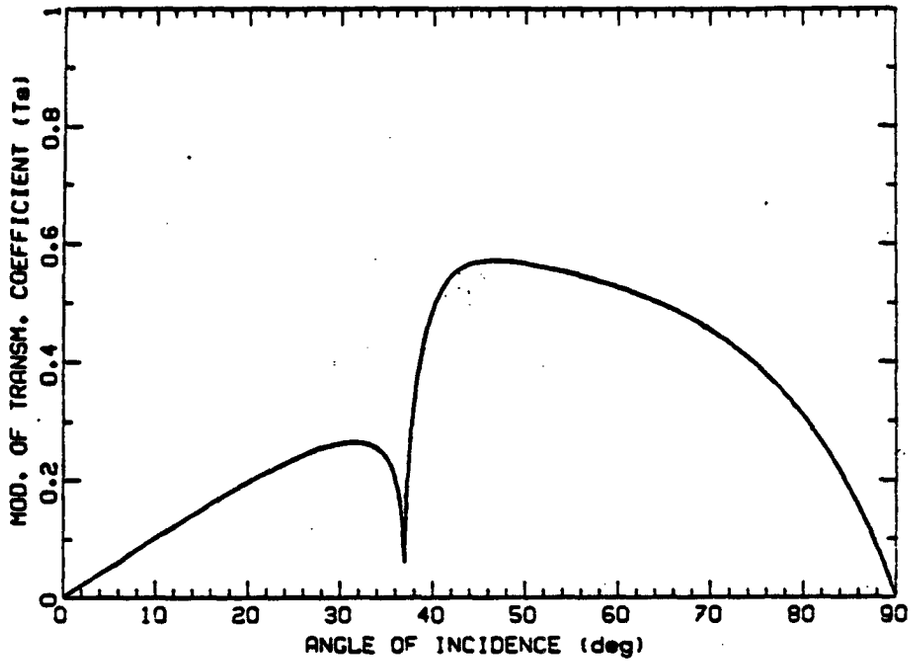

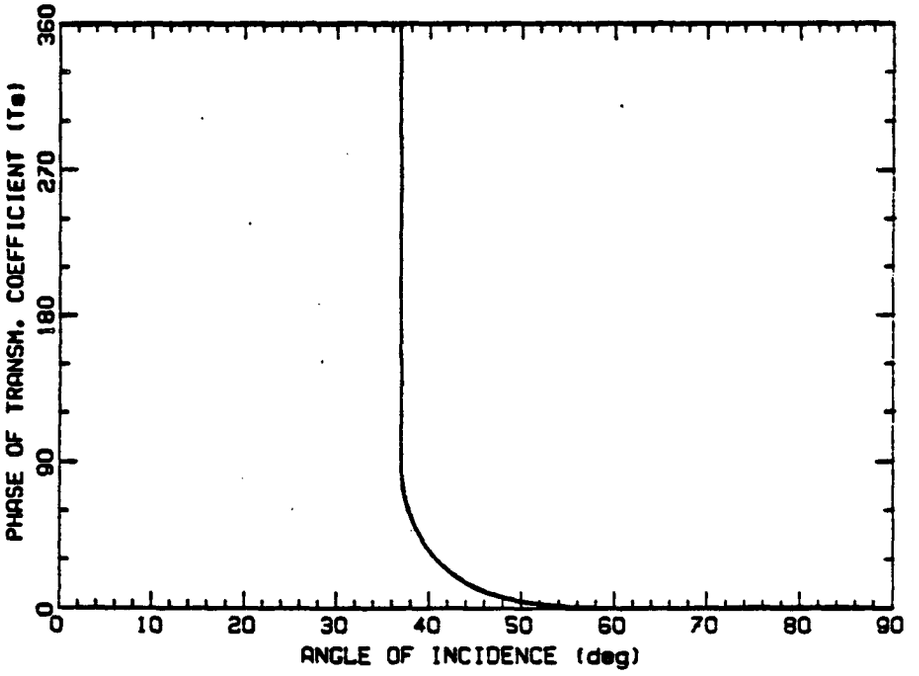

Fig.2-25. Liquid-solid : S-transmission coefficient . No attenuation .

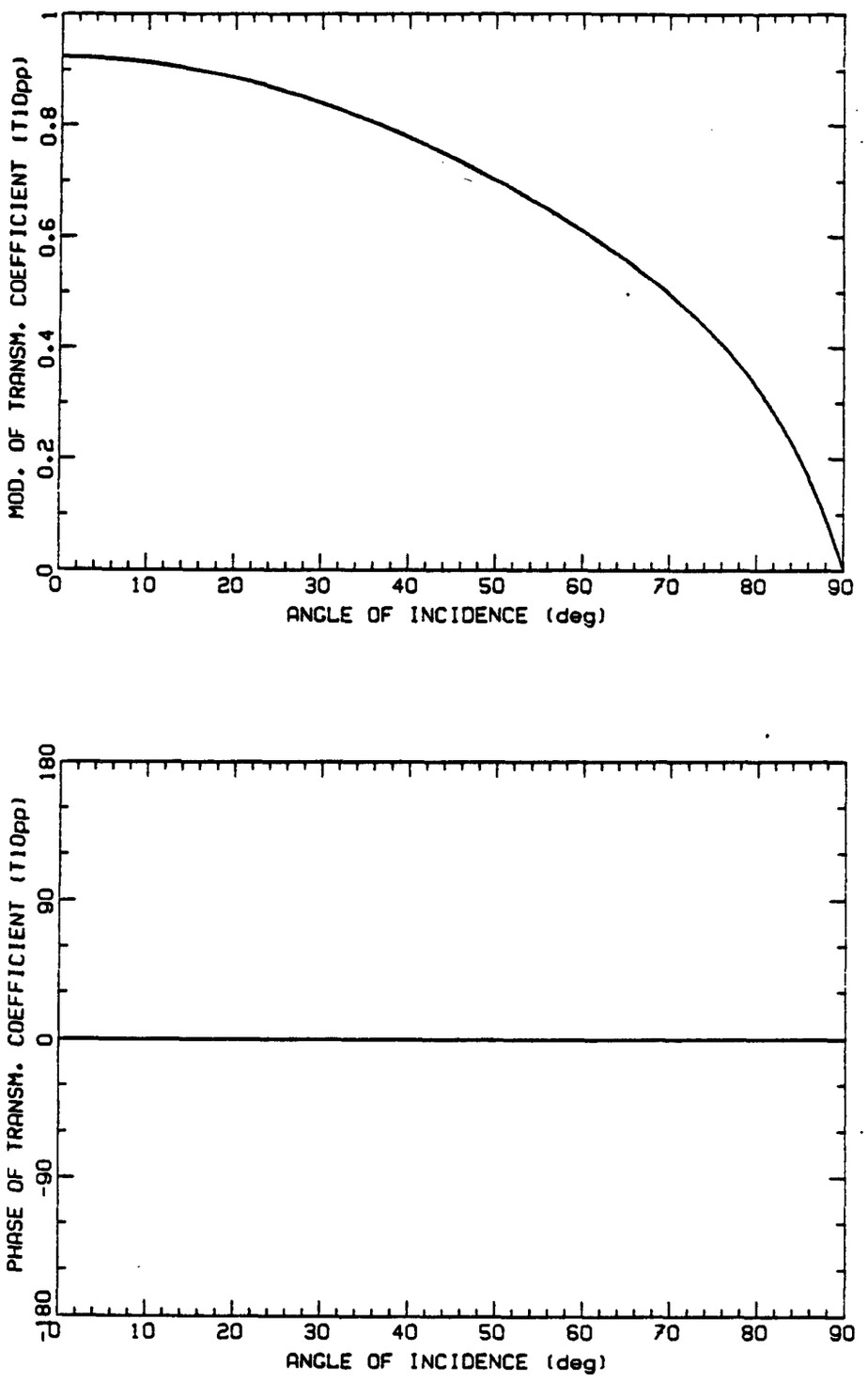

Fig.2-26. Solid-liquid : Transmission coefficient for a P-wave incident. No attenuation.

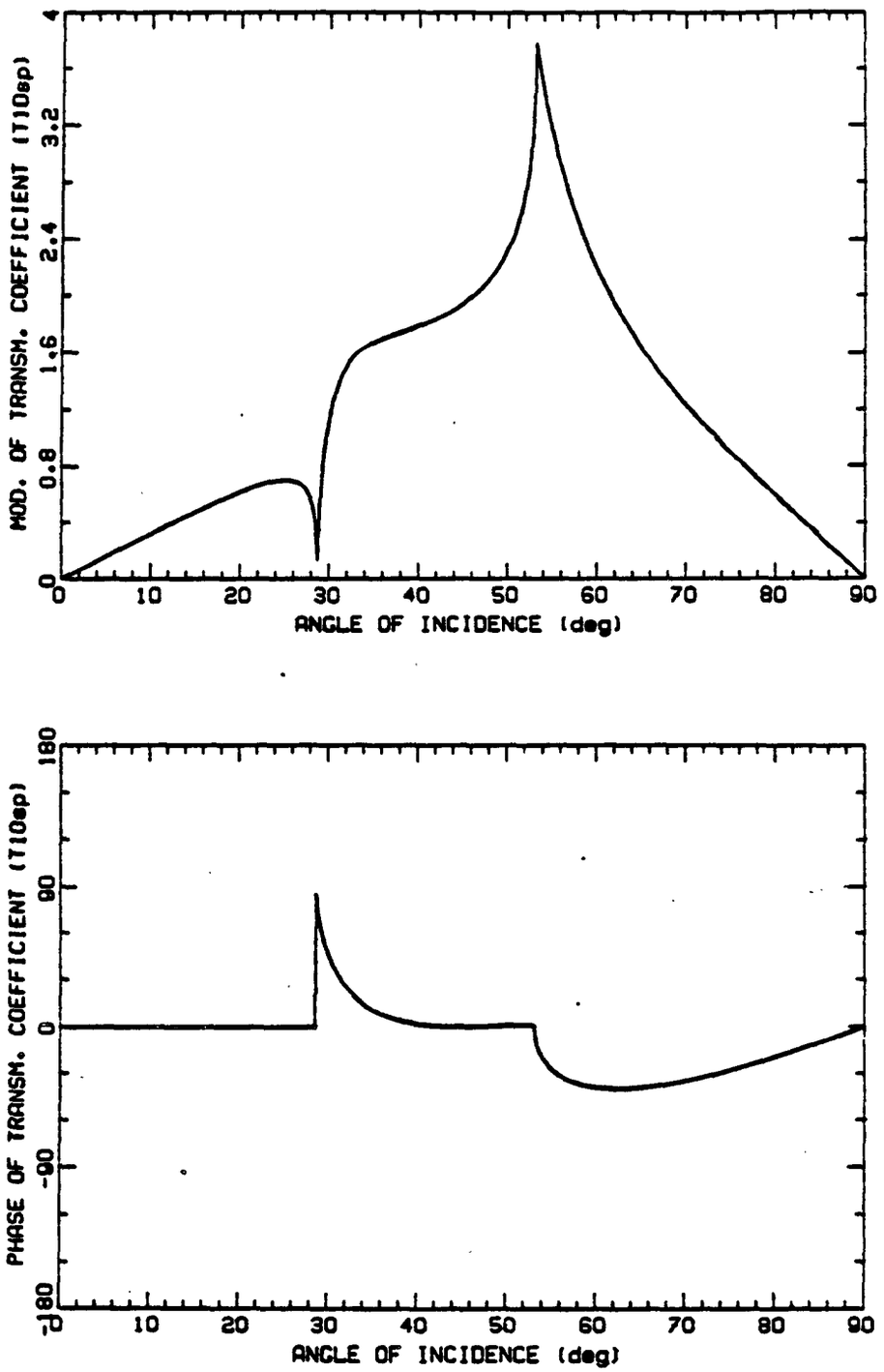

Fig.2-27. Solid-liquid : Tranemission coefficient for a S-wave incident. No attenuation.

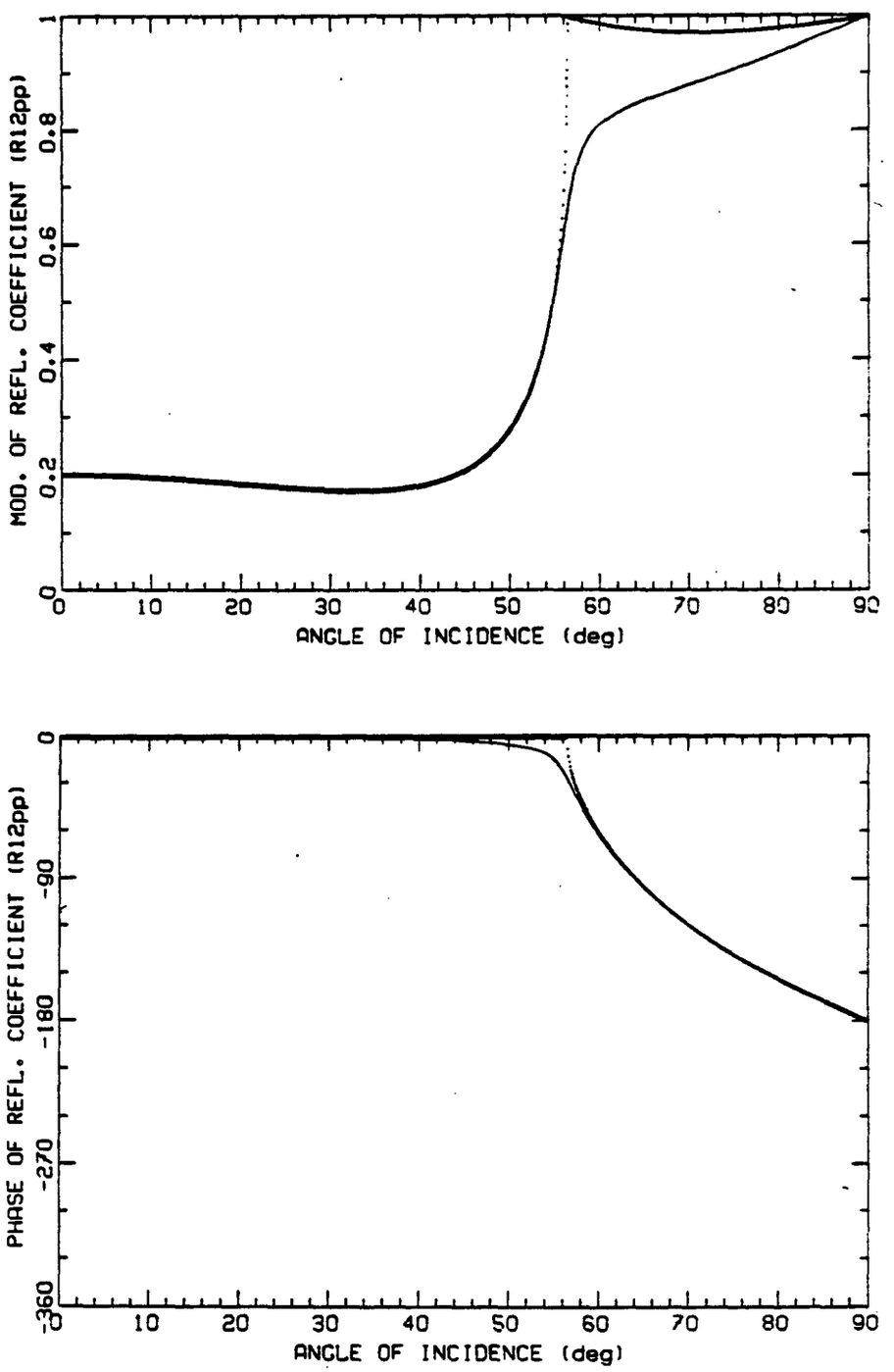

Fig.2-28. Solid-solid : P-reflection coefficient for a P-wave incident. The doted line is the elastic reflection coefficient.The solid one is the viscoelastic one.

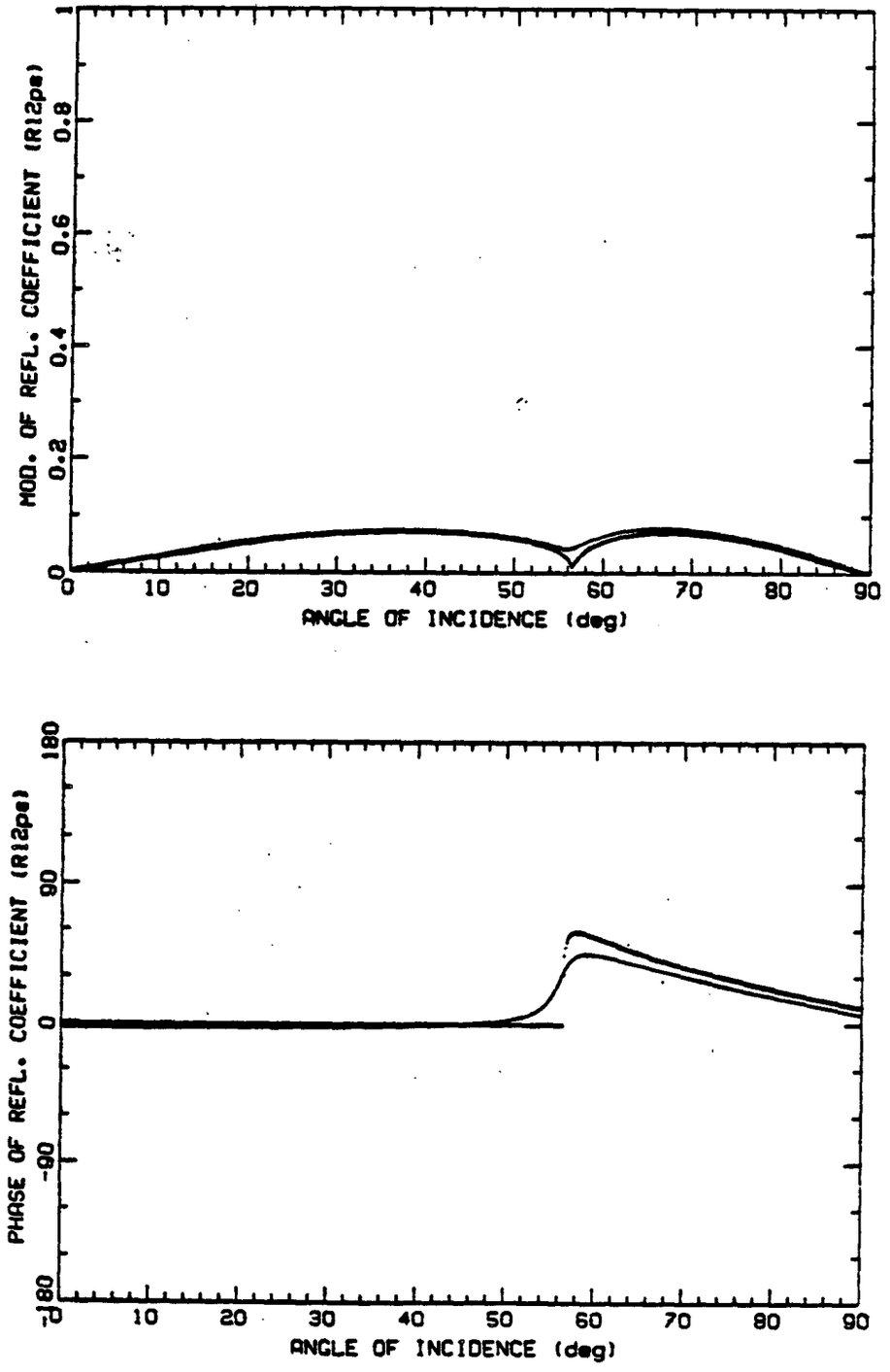

Fig.2-29. Solid-solid : S-reflection coefficient for a P-wave incident. The doted line is the elastic reflection coefficient.The solid one is the viscoelastic one.

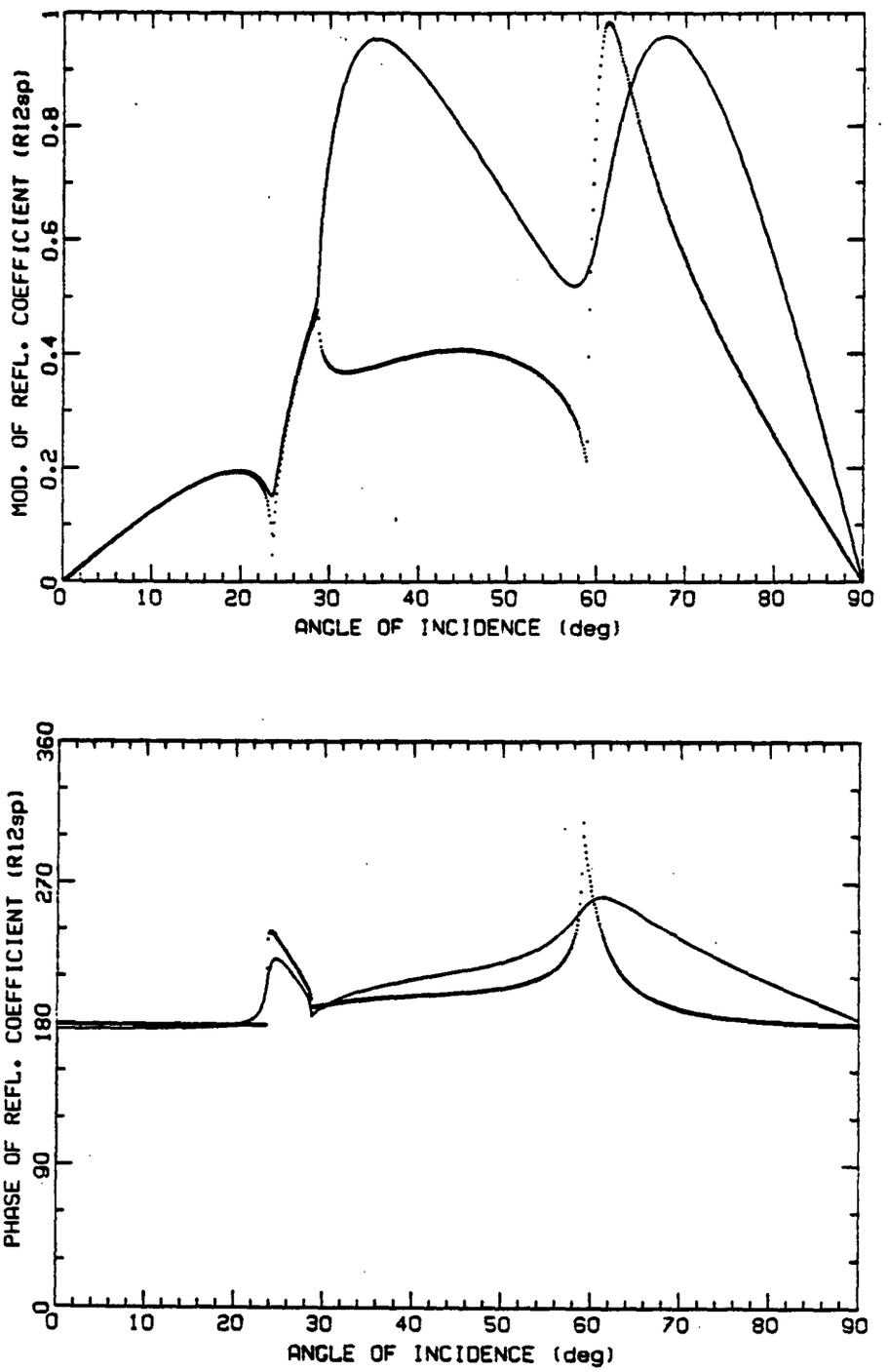

Fig.2-30. Solid-solid : P-reflection coefficient for a S-wave incident. The doted line is the elastic reflection coefficient.The solid one is the viscoelastic one.

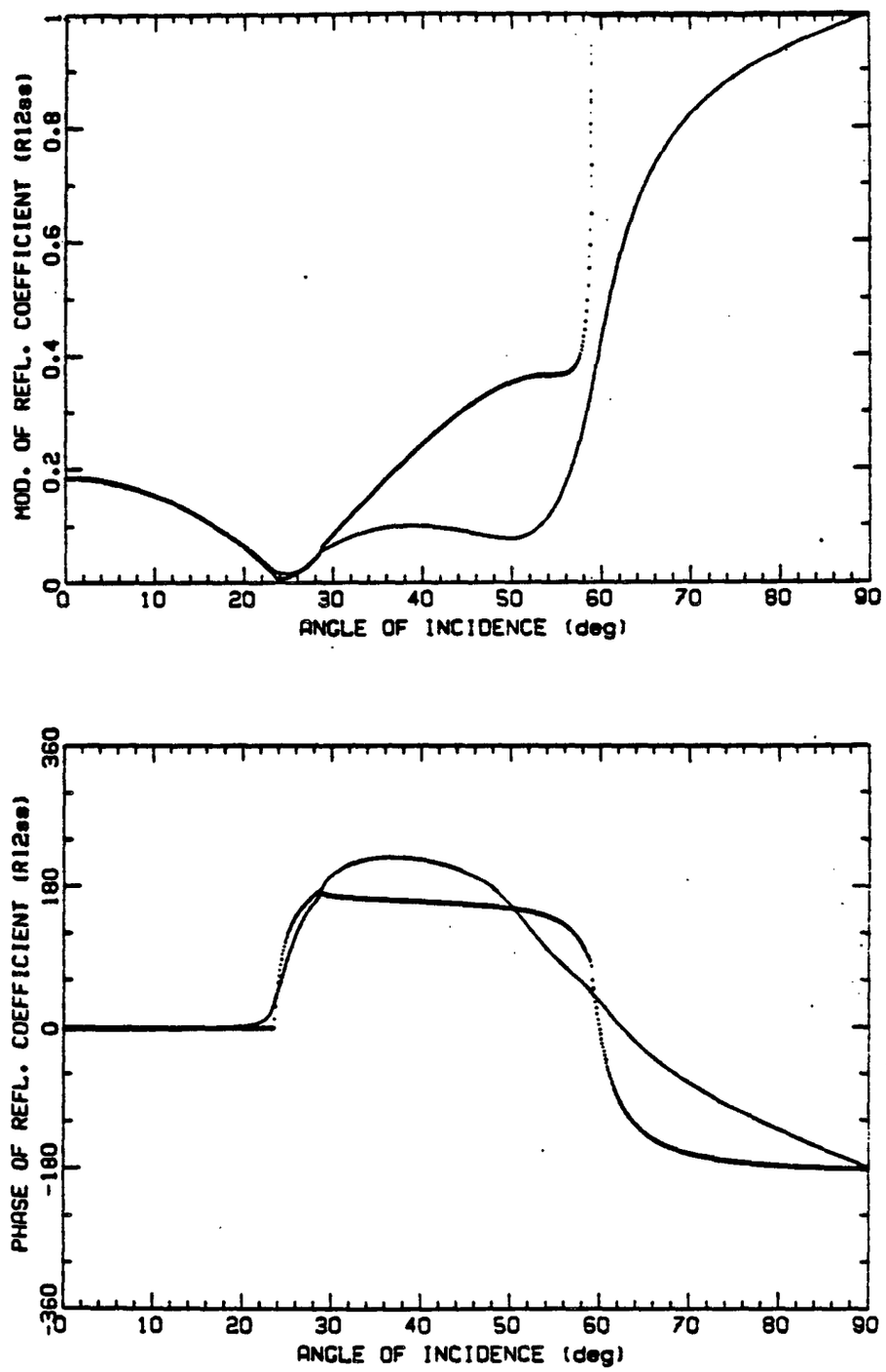

Fig.2-31. Solid-solid : S-reflection coefficient for a S-wave incident. The doted line is the elastic reflection coefficient.The solid one is the viscoelastic one.

P-quality factor	Q''_P	33
S-quality factor	Q''_S	20

In all the preceding figures we do not consider multiple reflections of any kind. Therefore primary signals do appear more clearly. The study of these figures lead us to the following conclusions.

1. When we look at converted waves, we see that their maximum amplitude is at least one third the non converted one. We also see that the waves labeled PPSP and PSPP (see notations in Figure 2-12) are of opposite polarities and so more or less cancel each other when added together (see Figures 2-36, 2-37). Therefore the only observable converted wave is the wave PSSP (Figures 2-33,2-35).

2. Basically the same type of conclusions as in cases 1 and 2 can be made when comparing figures with attenuation and figures without but the amplitude effects on head waves propagating in attenuating media seem smaller than in the previous cases. We also observe a phase effect on reflections around critical angle. The frequency spectrum is also shifted to low frequencies. The smaller effect of attenuation than previously is explained by the fact that we are having attenuation only in medium 3 and so that most of the wave-paths are purely elastic media wave-paths.

3. There are many different kinds of head-waves predicted by theory (Červeny and Ravindra 1971). Their paths are indicated schematically in the diagram below. The dotted line corresponds to a S-path. The solid one represents a P-path.

PPPP one head wave : PP(p3)PP

PPSP one head wave : PP(p3)SP

PSPP two head waves : PS(s3)PP

PS(p3)PP

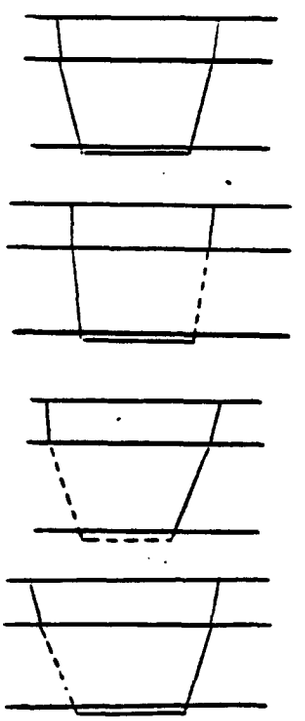

PSSP four head waves : PS(s3)SP

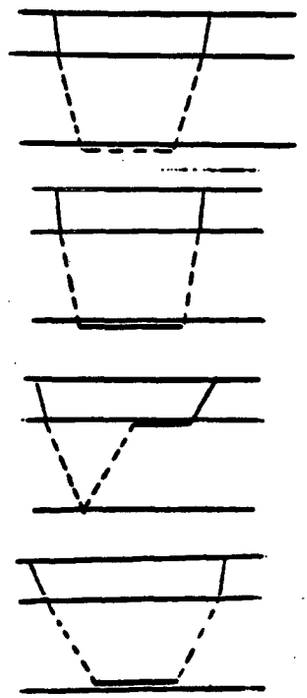

PS(p3)SP

PSS(p2)P

PS(p2)SP

All of these head-waves are present in the synthetic seismograms (see for example Figures 2-36,2-37) except in the case of the PSSP wave where it seems that, as in case 2 (liquid-solid with two Head-waves), all the energy has gone into the head wave PS(s3)SP making impossible the observation in our plots of any other head wave.

III. CONCLUSIONS

First it is important to emphasize the principal qualities and draw-backs of the method employed in this chapter to generate synthetic seismograms. Working in the f-k domain has made very easy the introduction of attenuation and the results obtained do not show any dispersion due to the method in itself. Head-waves of different types have been generated as well as reflected waves. The handling of the evanescent energy is not perfect and can give some anti-causal events if precautions are not taken. We have also to be careful that our Fourier transform convention agrees with the signs of our reflection and transmission coefficients so that all the waves generated are causal. The handling of non-layered media or of surface waves is not possible with this technique.

The different synthetic seismograms we have created show that, if we look at the effect of attenuation contrast on recorded signals, this phenomenon is important if all the following conditions are verified:

-low quality factors.

-high attenuation contrast.

-low acoustic impedance contrast.

When the acoustic impedance contrast gives reflection coefficients on the order of 0.1, the effect of attenuation contrast appears mainly on post critical reflections and refractions. It is a small effect (30-40% of the overall amplitude) in the cases we have presented earlier (Figures 2-15, 2-16 for example) where the elastic reflection coefficient at normal incidence was of the order of 0.5. It is important to note that this effect appear only on post-critical arrivals which correspond to particularly small reflection coefficients. In part III, we examine what happens in situations where the elastic reflection coefficient at normal incidence is smaller than <0.1 . We show that the absolute amplitude of the elastic reflection coefficient is a very important factor to decide whether or not the Q-contrast effect is observable.

ACKNOWLEDGMENTS

We thank M. Yedlin for suggesting the source waveform function (see Fig.2-5).

REFERENCES

Borcherdt, R.D., 1977, Reflection and Refraction of type-II S waves in elastic and anelastic medium, Bull.Seis.Soc. of Am., 67, 43-67.

Červeny V.,Ravindra R., 1971, *Theory of seimic head waves*, Univ. of Toronto Press, Toronto.

Ewing W.M., W.S. Jardetzky, F. Press, 1957, *Elastic Waves in Layered Media*, McGraw-Hill Book Co, New York.

Kennett B.L.N, 1979, Theoretical reflection seismograms for elastic media, Geoph.Prosp., 27, 301-321.

Kjartansson, E., 1979, Constant-Q, Wave propagation and attenuation, J.Geophys.Res, 84, 3737-3748.

Krebes E.S, Hron F, 1980, Ray-synthetic seismograms for SH waves in anelastic media Bull.Seis.Soc.Am., 70, 29-46

Krebes E.S, Hron F, 1980, Synthetic seismograms for SH waves in a layered anelastic medium by asymptotic ray theory, Bull.Seis.Soc.Am., 70, 2005-2020

Morse P.M., H. Feshbach, 1953, Methods of Theoretical Physics. McGraw-Hill Book Co, New York.

Pilant W.L., 1979, *Elastic waves in the earth*, Elsevier, The Netherlands.

Silva W, 1976, Body waves in a layered anelastic solid, Bull.Seis.Soc.Am., 5, 1539-1554.

Winkler K., 1979, The effects of pore fluids and frictional sliding on seismic attenuation, Stanford Rock Physics Project, 6.

Winkler K., A. Nur and M. Gladwin, 1979, Friction and seismic attenuation in rocks, Nature, 277, 525-531.

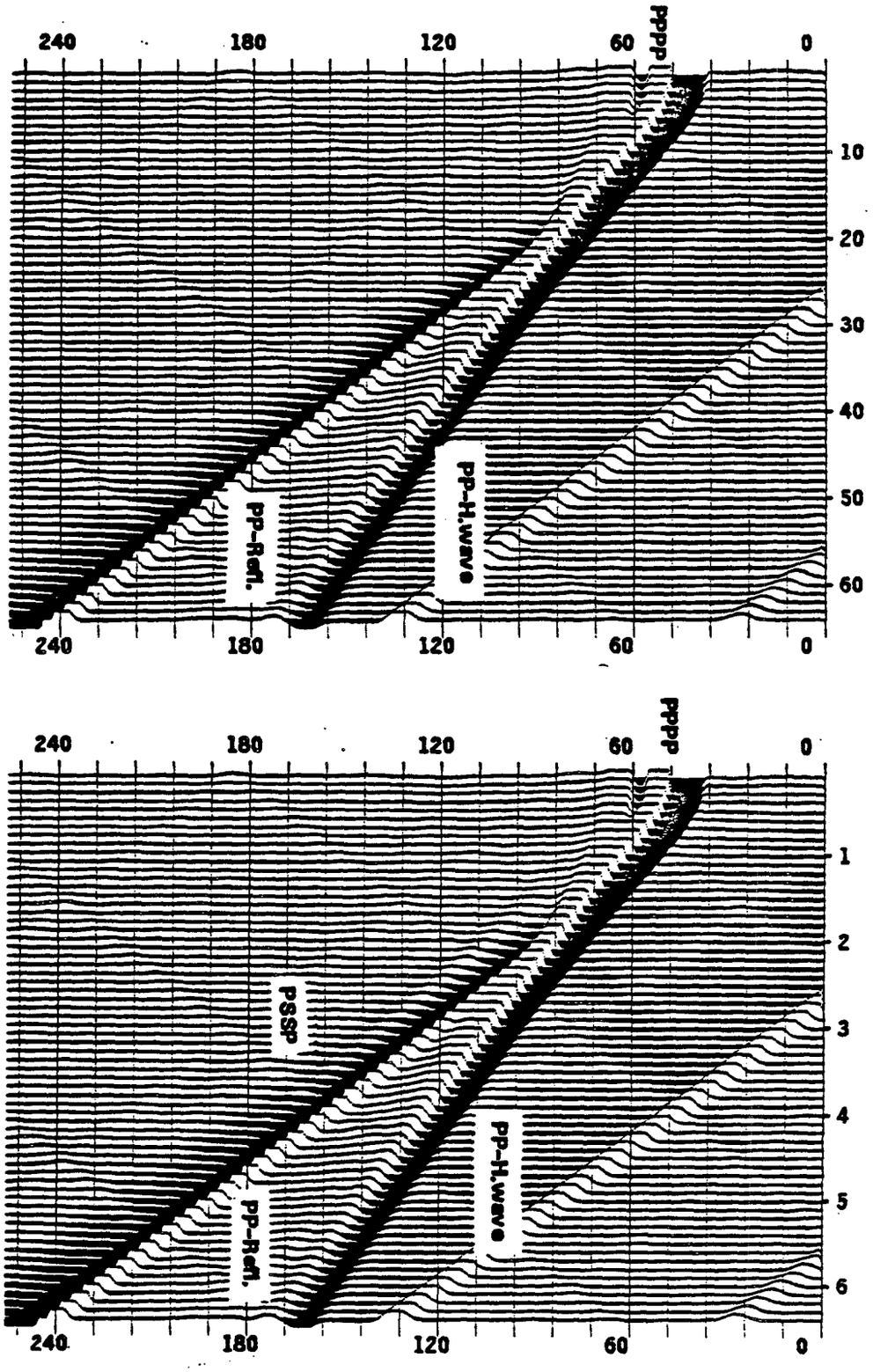

Fig.2-32 Synthetic seismogram. No attenuation included.

Left: Waves labeled PP and PPPP. Right: Waves PP, PPPP, PSPP, PPSP, PSSP.

The parameters used to generate it are the same as in Figure 2-15. Velocities are :

V_P= 1600 m/s , V_{P2}= 2500 m/s , V_{S2}= 1200 m/s , V_{P3}= 3000 m/s , V_{S3}= 1400 m/s .

Densities are : ρ = 1 g/cm^3 , ρ_2 = 2 g/cm^3 , ρ_3 = 2.5 g/cm^3 .

Quality factors are infinite.

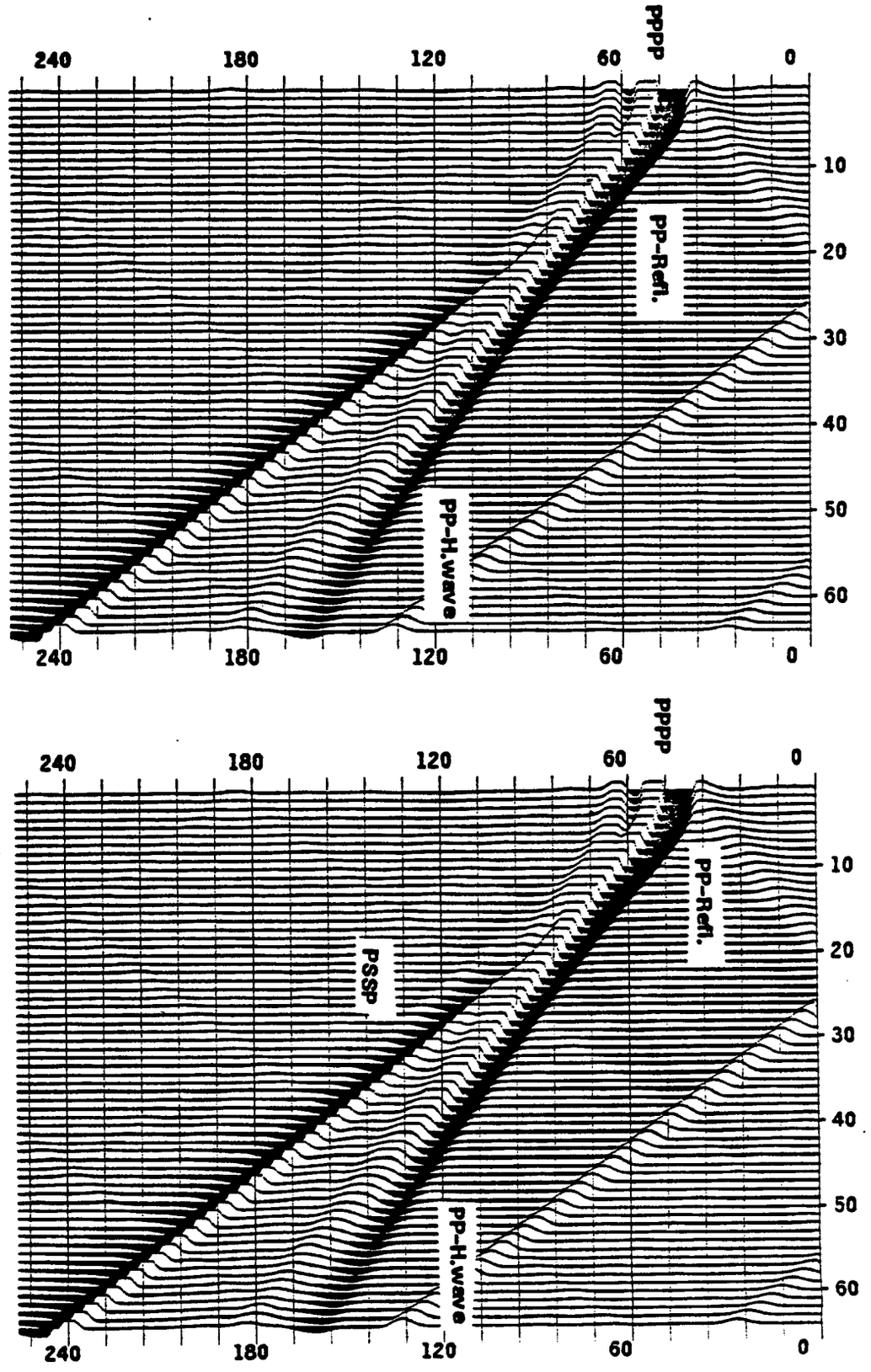

Fig.2-33 Synthetic seismogram. Attenuation included in medium 3.

Left: Waves labeled PP and PPPP. Right: Waves PP, PPPP, PSPP, PPSP, PSSP.

The parameters used to generate it are the same as in Figure 2-15. Velocities are :

V_P= 1500 m/s , V_{P2}= 2500 m/s , V_{S2}= 1200 m/s , V_{P3}= 3000 m/s , V_{S3}= 1400 m/s .

Densities are : ρ = 1 g/cm^3 , ρ_2 = 2 g/cm^3 , ρ_3 = 2.5 g/cm^3 .

Quality factors are infinite for the two first media and for the third one equal to:

Q_{P3} = 33 , Q_{S3} = 20 .

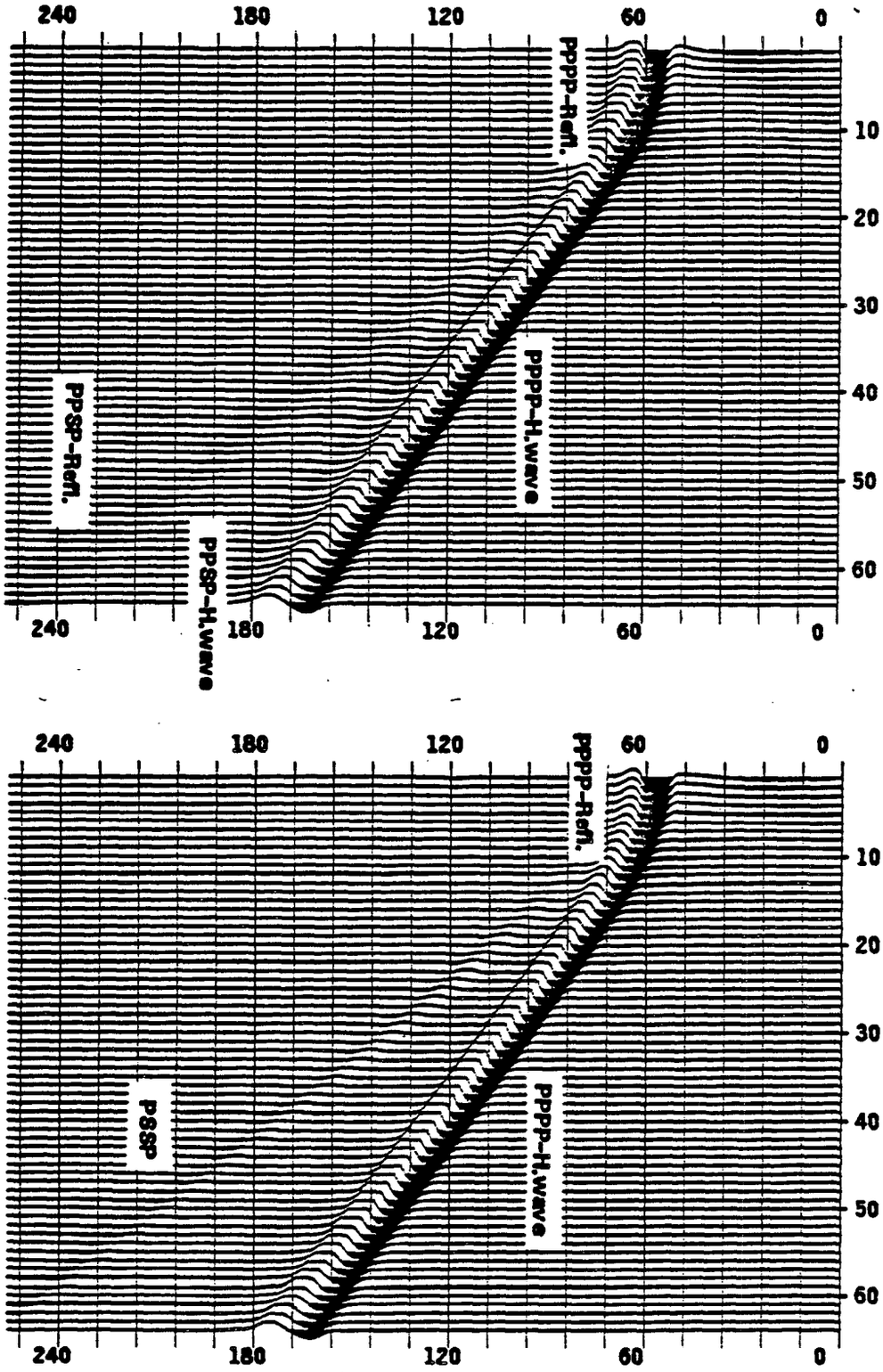

Fig.2-34 Synthetic seismogram. No attenuation included.

Left: Wave PPPP, PPSP. Right: Waves PPPP, PPSP, PSPP, PSSP.

The parameters used to generate it are the same as in Figure 2-15. Velocities are :

V_P = 1500 m/s , V_{P2} = 2500 m/s , V_{S2} = 1200 m/s , V_{P3} = 3000 m/s , V_{S3} = 1400 m/s .

Densities are : $\rho = 1\ g/cm^3$, $\rho_2 = 2\ g/cm^3$, $\rho_3 = 2.5\ g/cm^3$.

Quality factors are infinite.

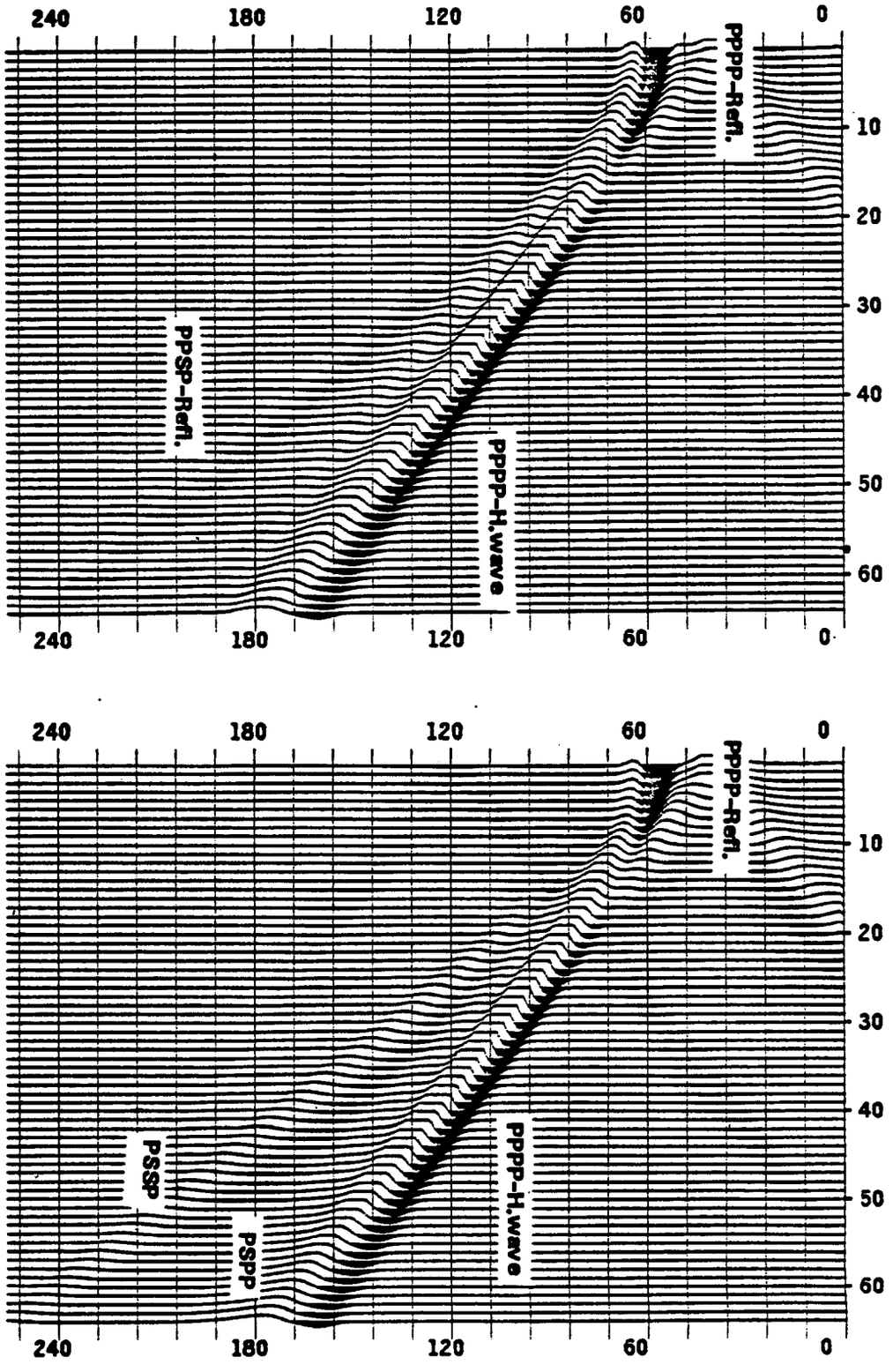

Fig.2-35 Synthetic seismogram. Attenuation included in medium 3.

Left: Wave PPPP, PPSP. Right: Waves PPPP, PPSP, PSPP, PSSP.

The parameters used to generate it are the same as in Figure 2-16. Velocities are :

V_P= 1600 m/s , V_{P2}= 2500 m/s , V_{S2}= 1200 m/s , V_{P3}= 3000 m/s , V_{S3}= 1400 m/s .

Densities are : ρ = 1 g/cm^3 , ρ_2 = 2 g/cm^3 , ρ_3 = 2.5 g/cm^3 .

Quality factors are infinite for the two first media and for the third one equal to:

Q_{P3} = 33 , Q_{S3} = 20 .

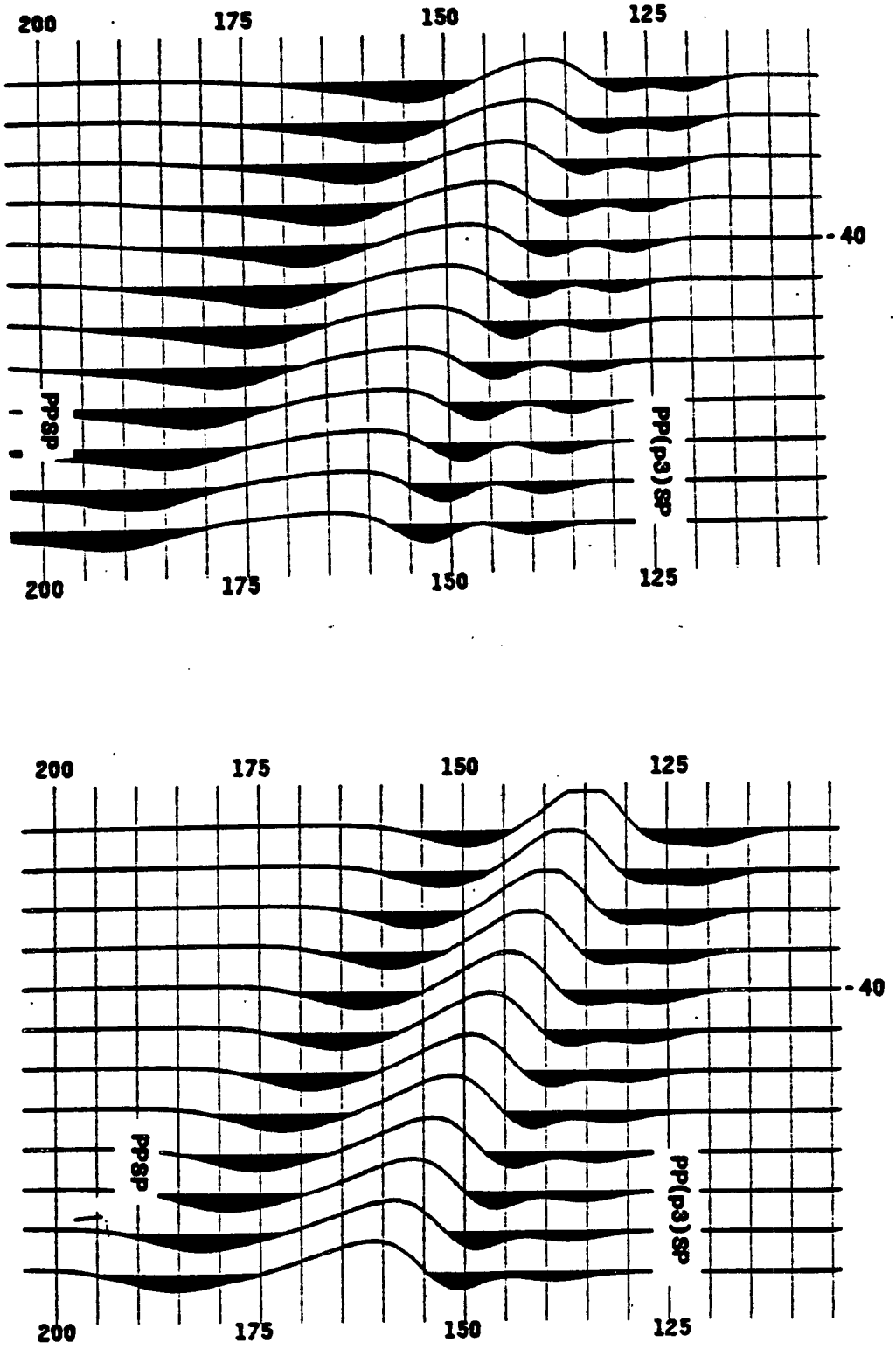

Fig.2-36 Synthetic Seismogram.

Traces 35-46 . Wave PPSP.

Left: No attenuation Right: Attenuation in medium 3

The values of velocities, densities and quality factors are given previous figures.

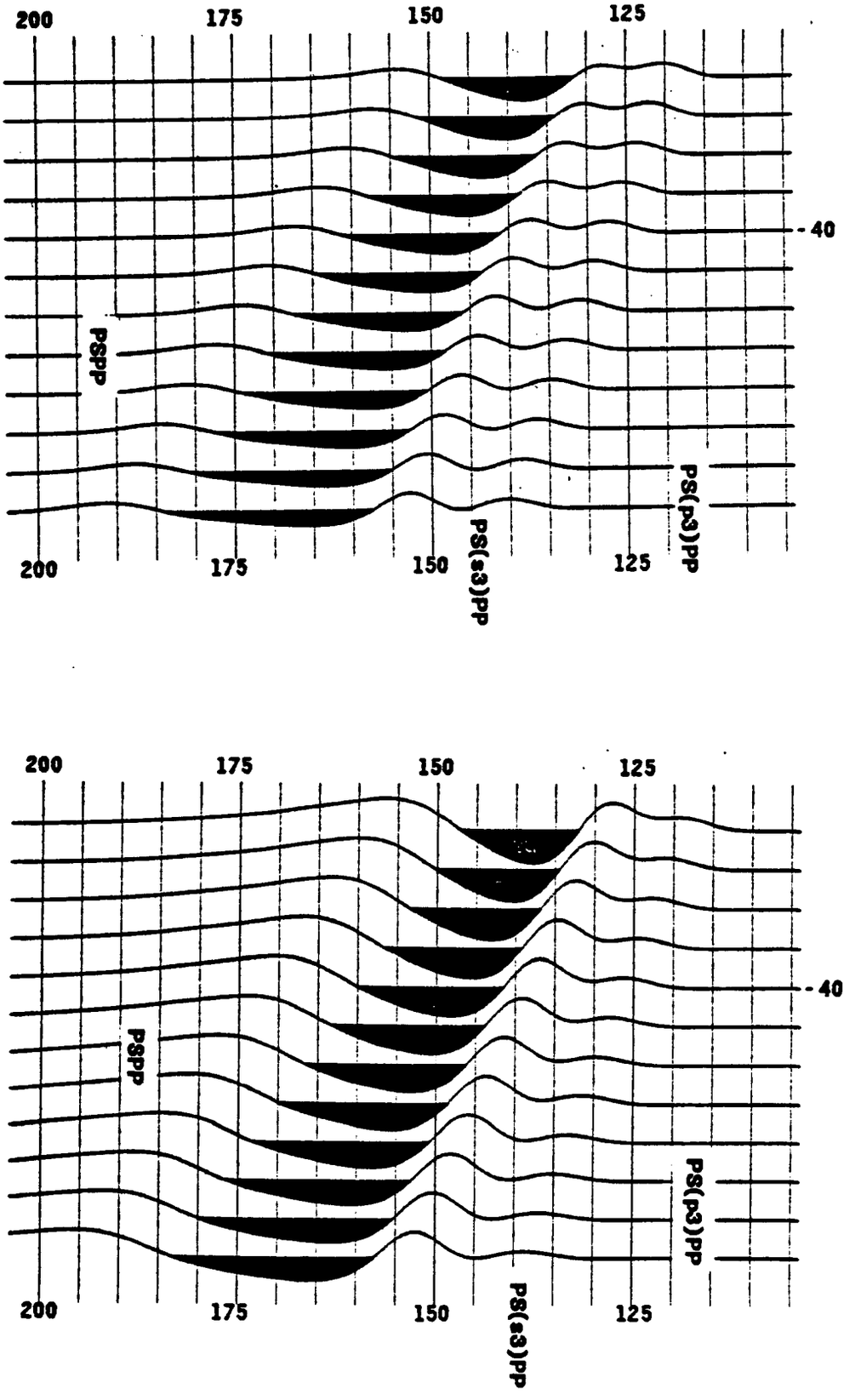

Fig.2-37 Synthetic Seismogram.

Traces 35-46 . Wave PSPP.

Left: No attenuation Right: Attenuation in medium 3

The values of velocities, densities and quality factors are given previous figures.

Note the opposite polarities between Figures 2-36 and 2-37.

PART III

EFFECTS OF ATTENUATION ON REFLECTIONS :

EXPERIMENTAL RESULTS

EFFECTS OF ATTENUATION ON REFLECTIONS : EXPERIMENTAL TEST

INTRODUCTION

As shown in previous publications [Kolsky (1956), Kjartansson (1979)] and also in Part I, the intrinsic attenuation of a given body has two different effects on propagating waves.

The more well-known effect is truly a propagating one: when a wave propagates in an attenuating medium, besides a geometrical spreading, there is a decrease in amplitude and a broadening of the pulse with propagation, because high frequencies are more attenuated than low frequencies.

The second effect is somewhat more complicated. We need two attenuating media in contact to observe it. Everyone is well aware that a reflection or a transmission between two elastic media is a function of the angle of incidence and of the acoustic impedance contrast between the two media. In the case of attenuating media, there is a third parameter to take into account, the Q-contrast between the two media. This Q-contrast increases or decreases (depending on its sign) the reflection coefficient which would be expected if the two media were elastic.

In the following experiment, we study the second effect and try to determine in which cases its importance is significant in seismic exploration.

I-PRINCIPLE OF THE EXPERIMENT

As stated in the introduction, we are interested in showing the effect of Q-contrast on reflection coefficients. This is a second order effect with respect to the acoustic impedance contrast except when this contrast is very small. Then it can become a large part of the reflection [cf Part I-A].

The experiment was conducted in a liquid medium for two main reasons:

- our reflected signal is not " contaminated " by S-waves reflections.
- the coupling between the two studied media is reliable and reproducible.

Borcherdt (1977), Kjartansson (1979), and Brennan and Smylie (1981) have shown that at a given angle for linear viscoelastic media the recorded reflected signal can be

expressed by the following formula:

$$y(t) = s(t) * r(t) \tag{3.1.1}$$

where

$s(t)$ = time signal for a wave having travelled twice the distance from the source to the interface.

$r(t)$ = reflection coefficient at the interface at the given angle of incidence.

$y(t)$ = recorded reflected signal.

In the case of "non-attenuating" media --the concept of non-attenuation being defined by the accuracy of the measurements, in our case, a medium with a Q greater than 100 is certainly elastic-- the reflection coefficient is no longer a time function but a Dirac in time. We have

$$r(t) = r_0\, \delta(t) \tag{3.1.2}$$

And so $y(t)$ becomes

$$y_0(t) = r_0\, s(t) \tag{3.1.3}$$

For this type of medium, using elasticity theory, we can calculate the theoretical reflection coefficient. Then, we can compare this result with the experimental value and look at the discrepancy between the two values. This discrepancy gives us an idea of the accuracy of the experimental set-up.

Then we consider attenuating media for which $r(t)$ is truly a time function. If we Fourier-transform (3.1.1) and (3.1.3), we obtain:

$$Y(\omega) = S(\omega)\, R(\omega) \tag{3.1.4}$$

$$Y_0(\omega) = S(\omega)\, r_0 \tag{3.1.5}$$

In $S(\omega)$ or $s(t)$ all geometrical effects (geometrical spreading, scattering, experimental losses, travelling attenuation in the first medium) are included. No matter what medium the wave is reflected by the same first medium, the same travelling path and the same geometry for the second medium are used.

By looking at the difference between $Y(\omega)$ and $Y_0(\omega)$, we are really observing the difference between $R(\omega)$ and r_0. Indeed, for an attenuating medium, we can always express $R(\omega)$ as

$$R(\omega) = r_1 + \Delta R(\omega) \qquad (3.1.6)$$

where

r_1 = Theoretical reflection coefficient if the medium were elastic.

$\Delta R(\omega)$ = Frequency dependent correction due to the presence of attenuation.

Therefore we can already say that there should be an effect, not only on the amplitude, but also on the shape of the signal or of the spectrum. Nevertheless, this shape effect is much more difficult to observe than the amplitude one. The spectrum of the emitted pulse [see Fig.3-3] is rather peaked. This peaked shape and the fact that $R(\omega)$ is only slightly frequency dependent imply that the shape effect is going to be negligible in most cases. On another hand, the importance of the amplitude effect depends greatly on the acoustic impedance contrast.

II-EXPERIMENTAL APPARATUS

The experimental apparatus is presented schematically in Fig.3-1. It consists mainly of two transducers and a sample holder allowing us to adjust the sample position and the angle of incidence of the beam.

The system is mounted on a plexiglas table, the upper surface of which is considered as the "horizontal". The sample is mounted on a device which allows two orthogonal displacements. The sample is leveled so that its upper surface is exactly at table level. This is done by using three different screws allowing us to orient the tray on which the sample and the sample holder are bolted. Before being mounted, samples are carefully ground so that their two faces are smooth and parallel.

Each transducer is set in a transducer-holder which is bolted to a rigid Γ-shape arm. These arms are then mounted on a pivot to the table so that the pivot point is exactly at the surface of the table. This insures that the beam is really focused on the sample's upper surface. A three-dimensional adjustment of the position of the transducer can be done by using screws located on the top of the transducer-holder (Fig.3-1).

Transducer and sample are adjusted so that their surfaces are parallel and their centers are on a same vertical line for normal incidence. For non-zero incidence angles, the adjustment is done so that both transducers are set-up at normal incidence; the angle is carefully adjusted afterwards. This insures the same orientation for the emitted beam and

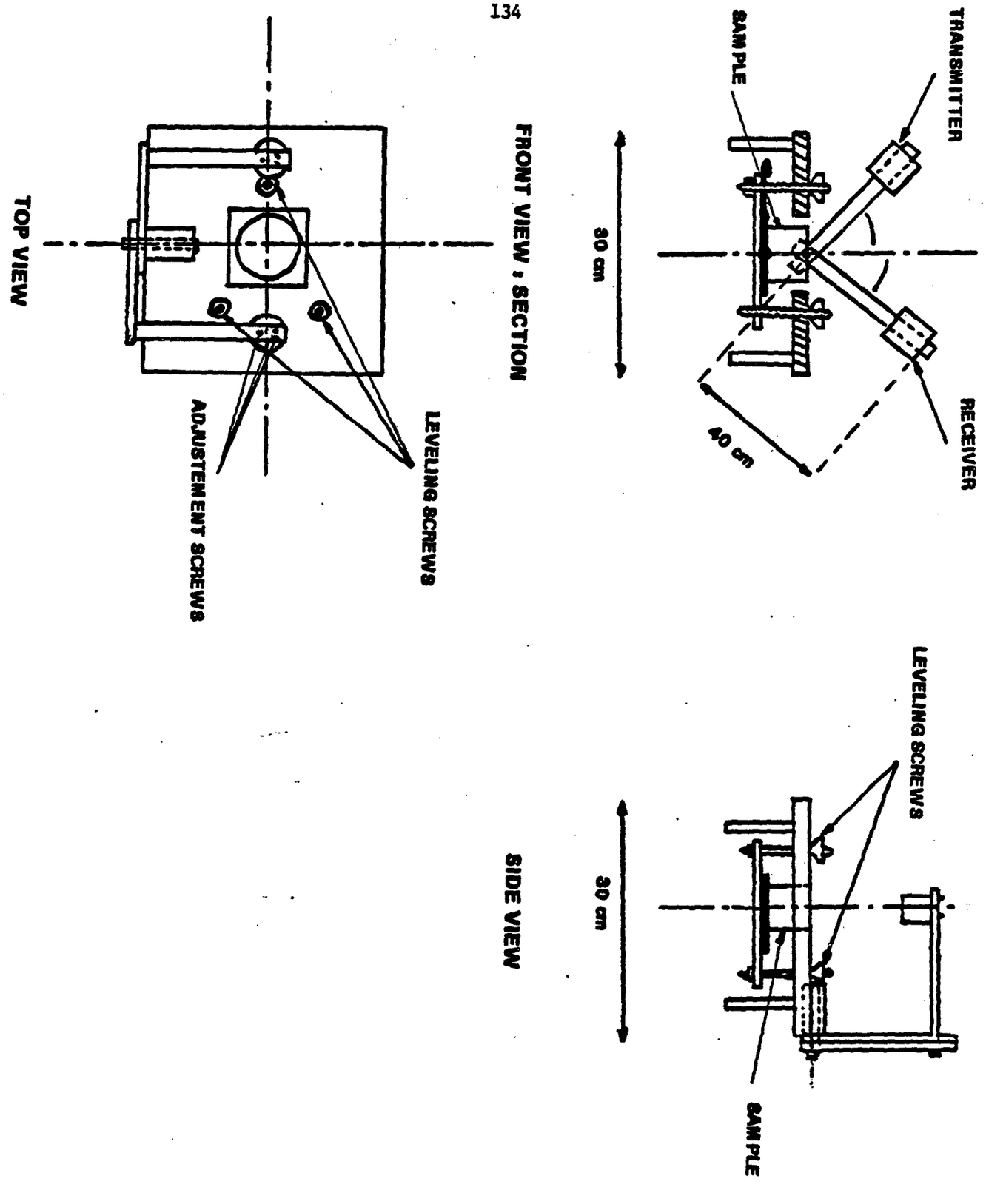

Fig.3-1 Schematic views of the apparatus

the received one.

The overall system is put in a water tank. Due to size limitations, angles greater than 40^0 are not used.

Then the whole apparatus is connected to several electronic devices, as described in Fig.3-2.

The transducers are connected to a pulse monitoring box [Panametrics Model 5052 PR] which allows us to use the same transducer for transmitting and receiving at normal incidence. The only problem is that absolute amplitudes and pulse shapes are different when we go from normal to non-normal incidence due to the different settings.

As soon as the signal is received, it is sent to a digital scope [Nicolet Model 204] and to a trigger delay [Tektronix TM 506]. The Nicolet allows to record the signal on floppy disks. The time sampling is 50 ns, and we have 4096 points recorded.

The scope is interfaced with a small computer [Hewlett-Packard 9845A] which allows us to Fourier-transform and to analyze the spectrum of the recorded signal.

The transducers are immersion Panametrics transducers [Model A 301S]. Their center frequency is 500 khz. Figures 3-3 and 3-4 show their different characteristics (Time signal, Power spectrum, Focusing of the Energy). It is important to note that the pulse used in our experiment is close to signals recorded in the field. An example of real data is given in figure 3-3b. These data come from a survey done by Amoco along the East coast of Canada (Flemish Cap) and the source used is an airgun. We see that the band-width is about the same as the one of our experimental signal that is to say two octaves.

III-SAMPLES

1-THE SAMPLES

Attenuating and non-attenuating media were used.

1a-Non-attenuating samples

For the non-attenuating media we used the following solids:

Stainless-steel

Brass

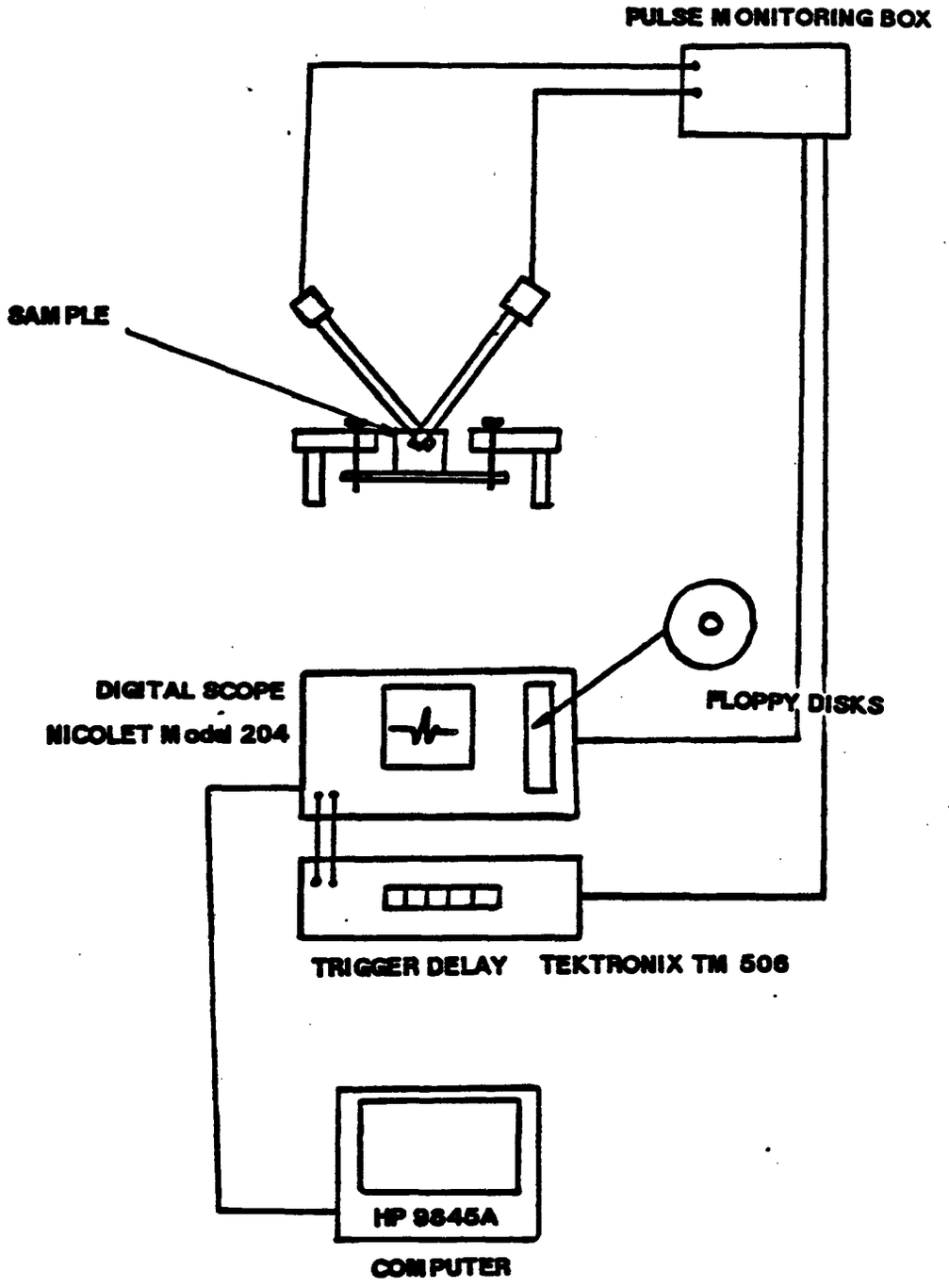

Fig.3-2 The electronic set-up

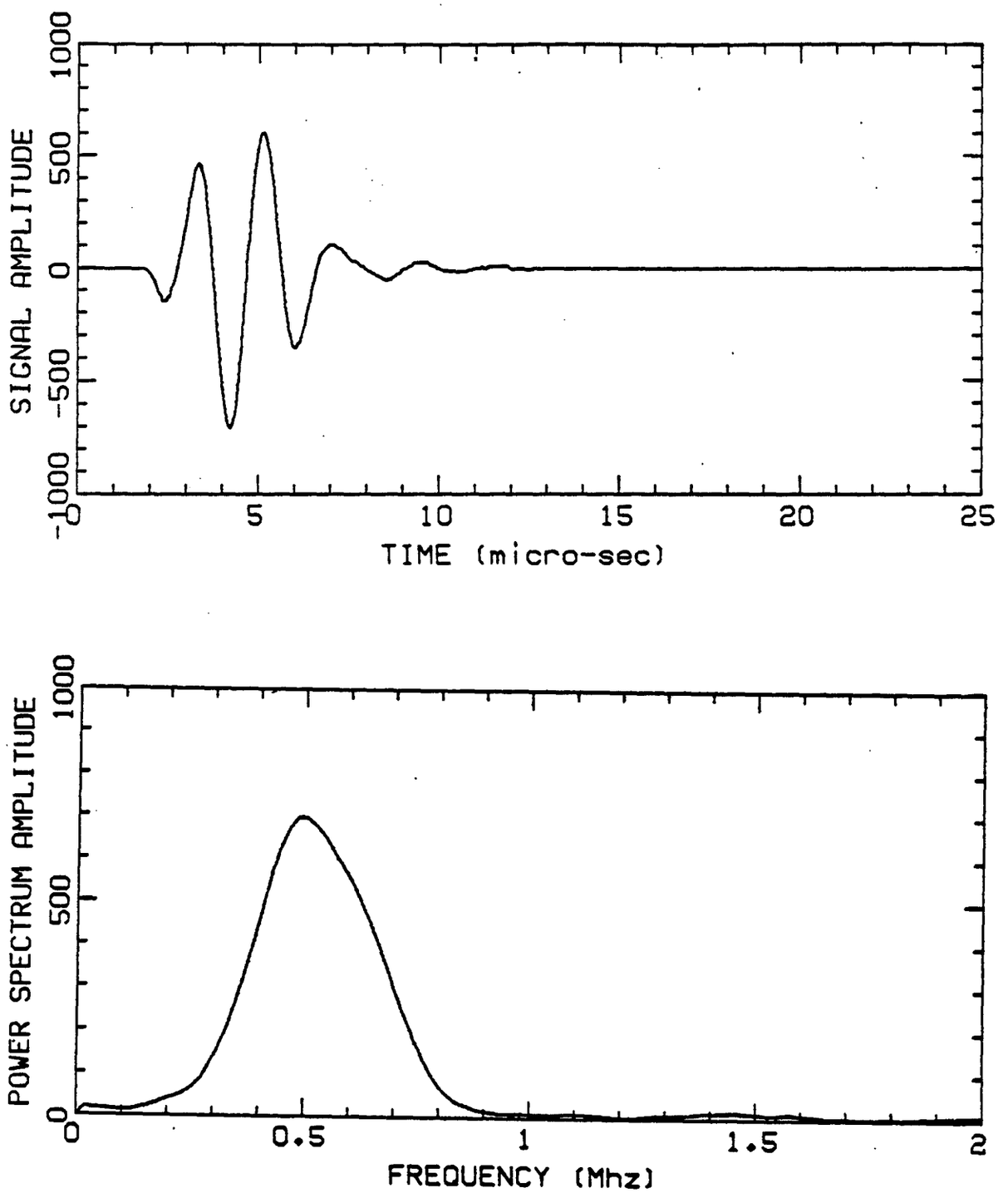

Fig.3-3 Time signal and Power spectrum of the transducers.

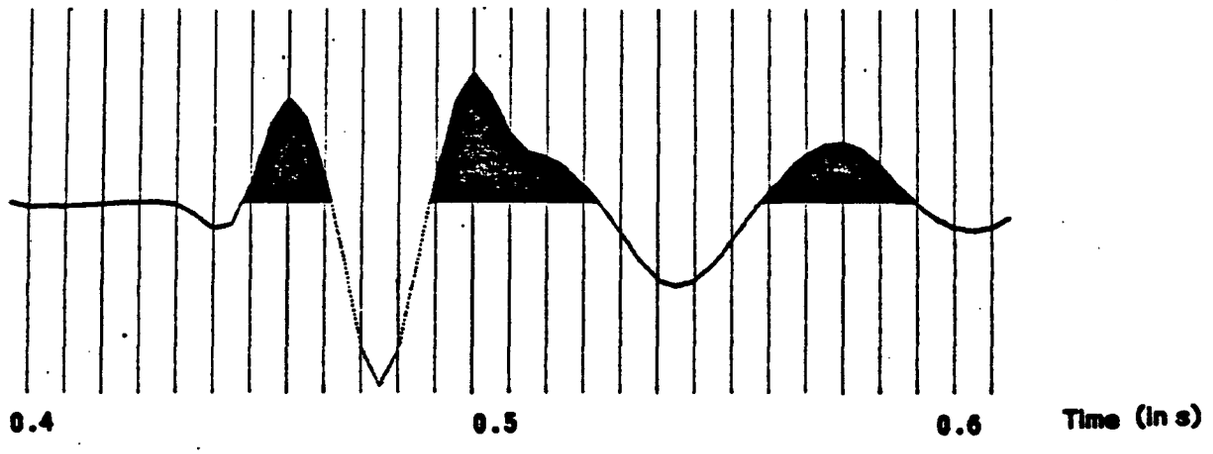

TIME SIGNAL

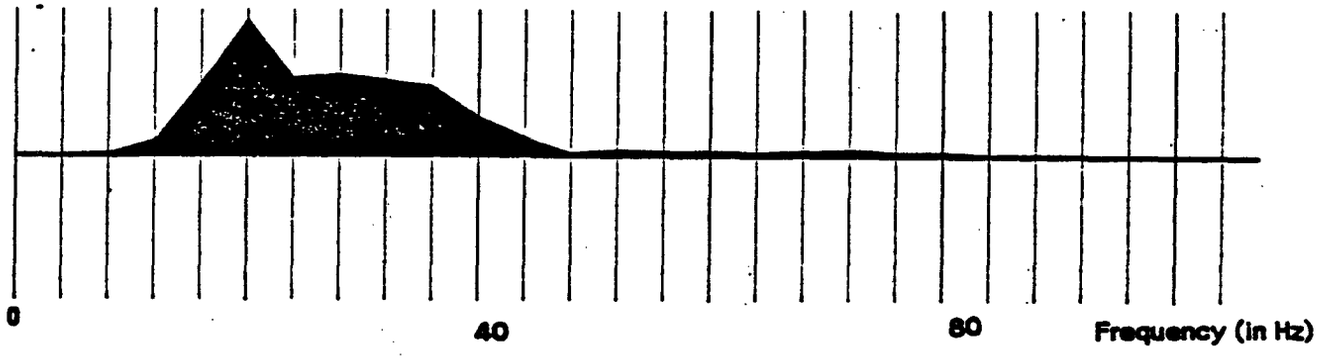

POWER SPECTRUM

Fig.3-3b Real data : Time signal and power spectrum.

These data are Amoco Flemish Cap data (East coast of Canada). The source is an air-gun. The sampling rate is 4ms.

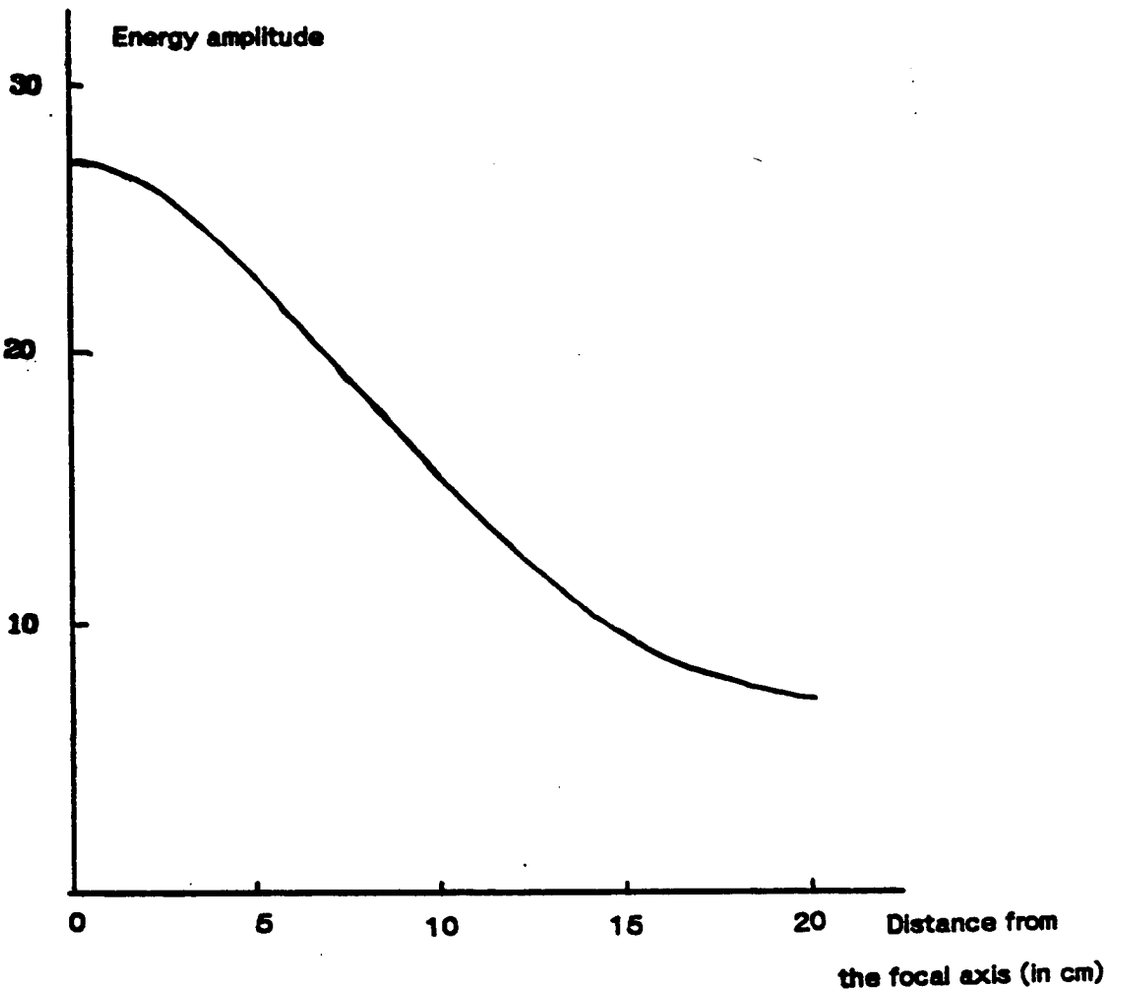

Fig.3-4 Energy radiated by the transducers at the focal distance (=7.5 cm). The x-axis represent the distance from the focal axis. The y-axis represent the amplitude of the energy radiated. The pattern of radiation is nearly independent of the distance from the transducer going from 3 cm to 30 cm.

Aluminium

Glass

To obtain a broad enough range of reflection coefficients at normal incidence we used a different set-up than the one already described. It allowed us to deal with reflections from Liquid-Liquid interfaces. We used

Water-Air interface

Water-Kerosene interface

The transducer was set-up in water in a horizontal position. As the interface between the two liquids or between the gas and the liquid was horizontal by definition, the transducer was parallel to the interface by construction. The signal was recorded at normal incidence using the same transducer for emitting and receiving the pulse.

1b-Attenuating samples

For the attenuating samples, different solids were used:

A-Lucite:

Lucite is a well-known plastic and its characteristics at the frequency we used can be found in the literature [Hartmann(1972,1974)]. In addition, Thomas Plona, from Schlumberger, had the kindness to compare these values to the ones he has measured. Lucite was used as a reference sample to test our measurements techniques.

B-Epoxies:

The samples are adjustable hardness epoxies and made in the laboratory. By changing the ratio between the two components of the epoxy, one is able to obtain very soft solids for which there is an important attenuation.

C-Silicon rubber:

We used this type of industrial rubber because its acoustic impedance is very close to the one of water and its attenuation is high.

D-Polymers:

Professor Knauss, from the Department of Material Sciences at Caltech, has had the kindness to send some of the polymers he has been working with. These are laboratory made samples, and they are highly attenuating. Their acoustic impedance is also close to the one of water.

For all these samples (B,C,D), our purpose was to simulate as much as possible the conditions found in the earth for lossy interfaces, that is to say:

-Low acoustic impedance contrast

-Relatively high attenuation

On another hand we wanted to obtain an experimental scattering due to grain size close to the one found within the earth. The ratio (wave-length / grain size) involved in this scattering is of the order of 10^{-4} or 10^{-5}. This value implies that the experimental wave-length must be smaller than a micron which is equivalent to the grain size of clay particles. Therefore it seems impossible to use any actual rock samples in our experiment: with rocks other than clay the grain size is too large and with clay the water contact is impossible to maintain without ruining the sample. A second reason is that whatever rock is considered, the acoustic impedance contrast with water - even with most of liquids - will be too big to show any attenuation effect on reflections.

2-SAMPLE PREPARATION, SIZES AND ROUGHNESSES

All the samples, except the rubber for which the raw surface was used, were surface ground so that the two faces were smooth and parallel.

Two types of experiments were conducted to find the optimum sample size and the dependence of the recorded reflections on the surface roughness.

For the size dependence, we have used aluminium and lucite samples of different sizes and shapes ranging from squares of 40cm length to cylinders of 5cm diameter. In this range we did not noticed any difference in the recorded reflected signal for angles from 0 to 35 degrees. During these tests the distance between the source and the sample was 20cm. The source radiation pattern of the source (Fig.3-4) shows how focused the emitted energy is and makes understandable how insignificant shapes and sizes are.

Since the center frequency of our emitted signal is 500 khz, the wave-lengths involved are of the order of one cm. We tried different kinds of surface roughnesses by using different grades of "sand" paper. Within a reasonable grain size for the "sand" paper (100-400 grit), we did not see any scattering effect showing that the surface quality is not a critical factor.

3-CHARACTERISTICS OF THE SAMPLES

Table III-1 gives all the characteristics used in our experiment:

Samples	Density ρ (g/cm^3)	P. Velocity Vp m/Sec	S. Velocity Vs m/Sec	P. Quality Factor Qp	Elastic Reflection Coefficient R	$\frac{\Delta\rho}{\rho}$	$\frac{\Delta Vp}{Vp}$	$\frac{\Delta Qp}{Qp}$	Theoretical Precision $\Delta R/R$	Experimental Accuracy
Stainless Steel	7.875	5746	3168	∞	0.936	$5\cdot10^{-4}$	$6\cdot10^{-3}$		.1%	1%
Brass	8.430	4308	2069	∞	0.921	$5\cdot10^{-4}$	$4\cdot10^{-3}$		.1%	1%
Aluminium	2.695	6344	3096	∞	0.840	$5\cdot10^{-4}$	$6\cdot10^{-3}$		.2%	1%
Glass	2.225	5166	2907	∞	0.771	$5\cdot10^{-4}$	$5\cdot10^{-3}$		.2%	1%
"Kerosene"	0.7725	1276		∞	-0.202	$5\cdot10^{-4}$	$2\cdot10^{-3}$		.8%	1%
Lucite	1.1895	2649	1315	45	0.359	$5\cdot10^{-4}$	$3\cdot10^{-3}$	.10	.5%	1%
Epoxy	1.0365	1993	705	18	0.163	$5\cdot10^{-4}$	$3\cdot10^{-3}$	.05	1.3%	1%
Polymer	1.0300	1636	613	15	0.063	$5\cdot10^{-4}$	$2\cdot10^{-3}$	.05	2.5%	1%
Silicon Rubber	1.505	995	341	50	0.004	$5\cdot10^{-4}$	$2\cdot10^{-3}$	.1	32%	1%

TABLE III-1

Physical characteristics of the different samples.

The theoretical precision is calculated from the formula giving R and by using the measurements' precision for the densities and the velocities. By experimental accuracy we mean the accuracy of the experimental set-up.

P-velocity = V_p

S-velocity = V_s

Density = ρ

P-wave quality factor = Q_p

S-wave quality factor = Q_s

Q_s is assumed to be equal to Q_p. This assumption is not a crucial one for the following reasons:

-the studied effect of attenuation is second order.

-the S-wave attenuation effect takes place only at non-normal incidence.

-this value will be used only in computer simulation. In this type of work the differential effect between P- and S-wave attenuations is a third order effect.

The liquid was water with bleach at room temperature, its density was 0.997 g/cm^3, and its P-wave velocity was 1489 m/s. Its P-quality factor could be considered infinite ($Q_p \approx 10000$).

4-MEASUREMENTS TECHNIQUES

4-a Density Measurements

We used Archimedes' principle to measure the volume of our samples. The accuracy of this measurement is strongly dependent on the precision of the scale used. In our case, weights were given to 10^{-2} g implying a relative accuracy on the density of the order of $5\ 10^{-4}$.

4-b Velocity Measurements

The velocity was measured with the sample set-up for the reflectivity measurements at normal incidence. The travel time we used was the one taken by the wave to travel inside the sample. With our apparatus we got a relative accuracy on velocities of $2\ 10^{-3}$ to $6\ 10^{-3}$ (see Table III-1). The S-velocity measurements were made with Panametrics S-transducers Model V151 which have a center frequency of 500 khz like the P-transducers.

4-c Attenuation Measurements

The spectral ratio technique which we used to measure attenuation has been described by Toksöz et al (1978). The reference sample we chose was aluminium. To verify the accuracy of the technique we used brass and lucite. The results are shown in Figures 3-5 and 3-6. They agree very well with the values we

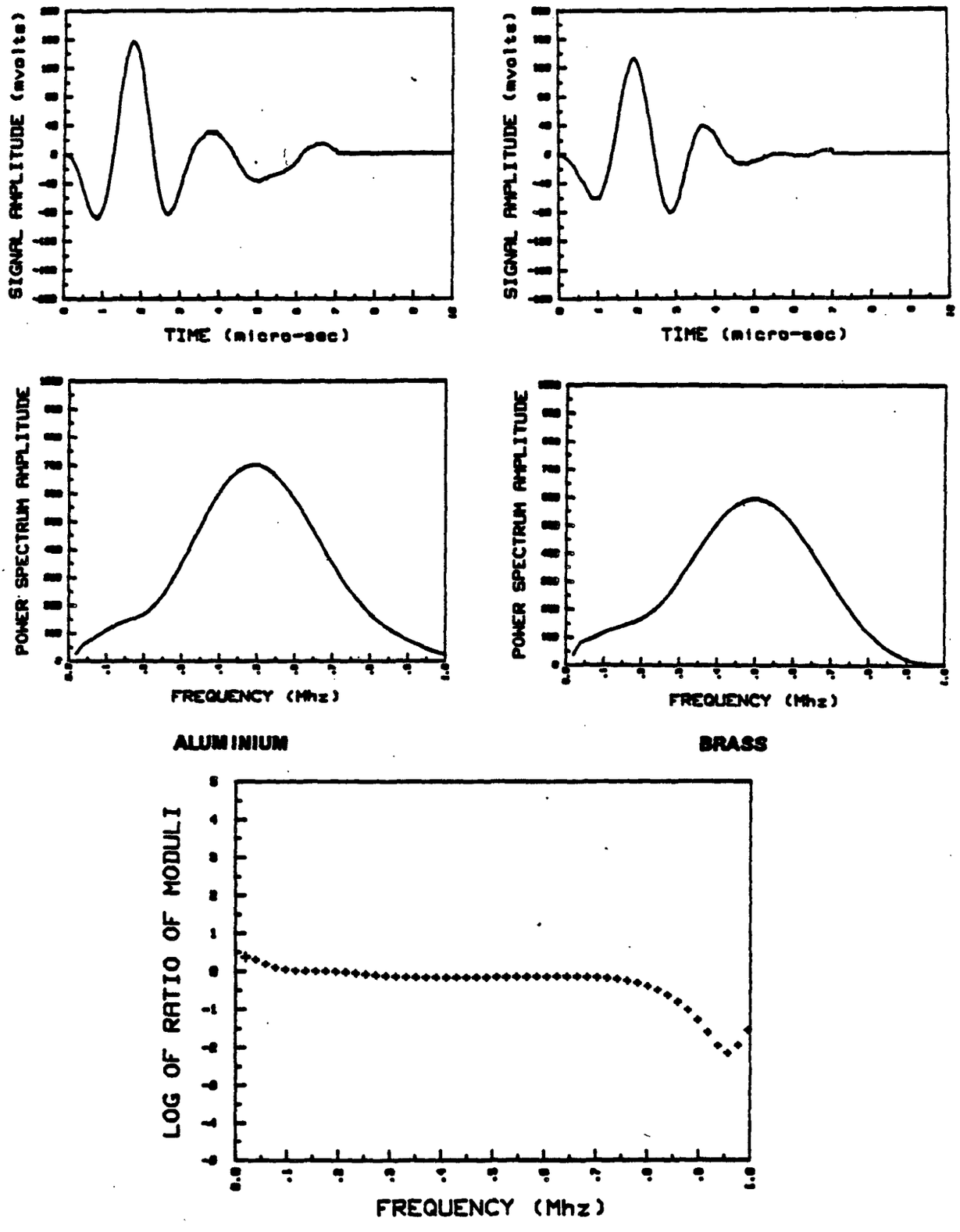

Fig.3-6 Aluminium and Brass samples:Signals,power spectra and their ratio

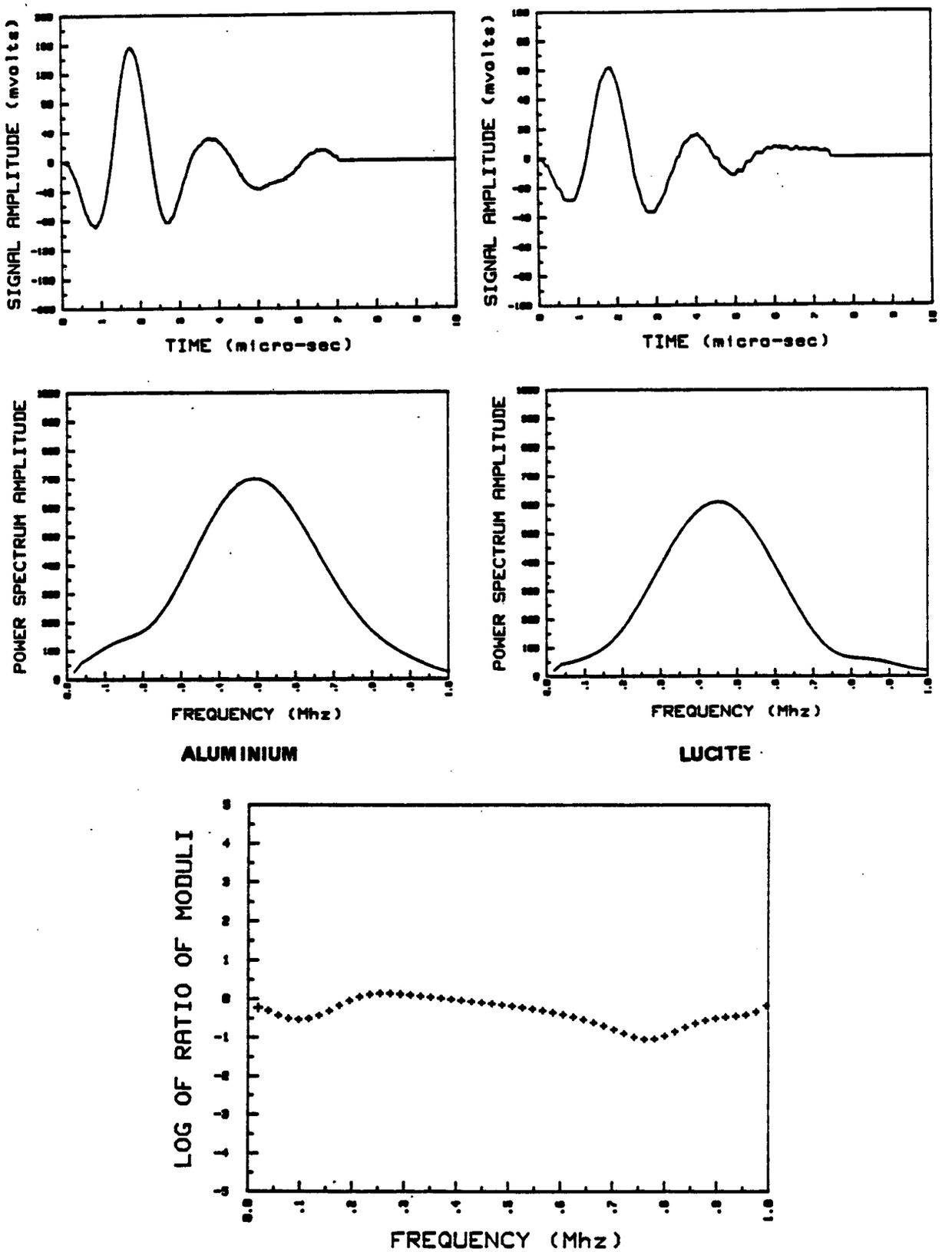

Fig.3-6 Aluminium and Lucite samples: Signals, power spectra and their ratio

found in the literature which are:

-brass : Q_p infinite for our measurement accuracy.

-lucite : Q_p =50 and Q_s =50 (T.Plona personal communication). The technique used to obtain these reference values is a resonant bar technique like the one described by K.Winkler(1979).

The relative accuracy of the spectral ratio type of measurement can be estimated to 5%-10%.

It is interesting to note that our measurement of Q is only based on the center part of the frequency spectrum (Fig.3-5 and 3-6). In fact the other parts are "falsified" because we windowed the signal using a square box before it was completely dampened. This method could be very questionable. That is why we tried applying windows of different lengths to the signal. The signal we used was the one obtained from the air-water interface; it is a very clean signal which is not contaminated by any other arrivals. The noise level is also very low. It is shown at the top of Figure 3-7. The windowing results are shown in Figures 3-7,3-7b,3-7c. Figure 3-7c shows the same results as Figure 3-7b but with normalized amplitudes. From these tests we can draw the following conclusions :

- For windows taking into account at least two and a half wave-lengths there does not seem to be any distorsion.

- For a two wave-length window the result is very acceptable especially if we take into account only the center part of the spectrum. The main discrepancy is around the dc component.

- For smaller windows --one and half and one wave-length-- the result of any spectral ratio is modified by applying this type of filter.

We must not forget that this result is valid only for this signal and cannot be generalized without precautions. For most of the samples for which we have measured Q_p , we used two and a half wave-lengths; Therefore we are confident about the results.

In Figure 3-7d we show that an exceedingly wide window can be troublesome! Indeed, both of the power spectra in this figure came from the same recording, a signal obtained from a silicon rubber-water interface. It is a very low energy signal; thus some noise which in all other cases was negligible now appears at the end of the signal itself explaining why when the window used is too wide (3 wave-lengths), the power spectrum is contaminated. On the other hand as seen

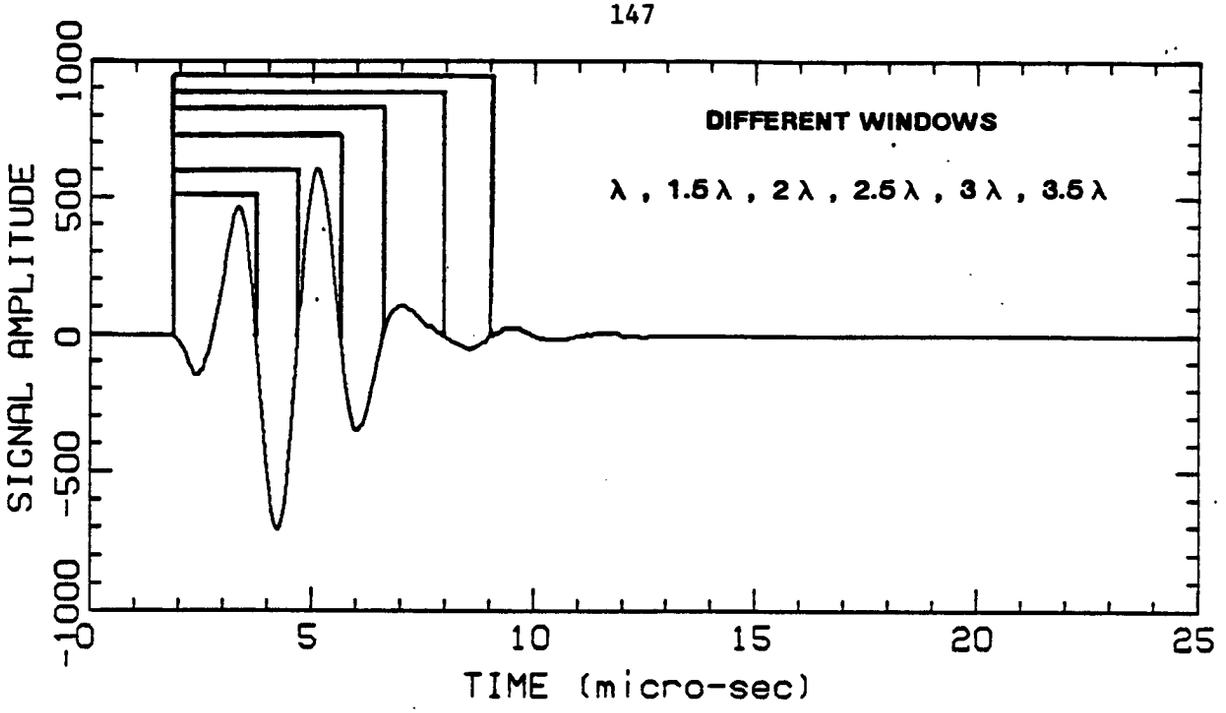

Time signal

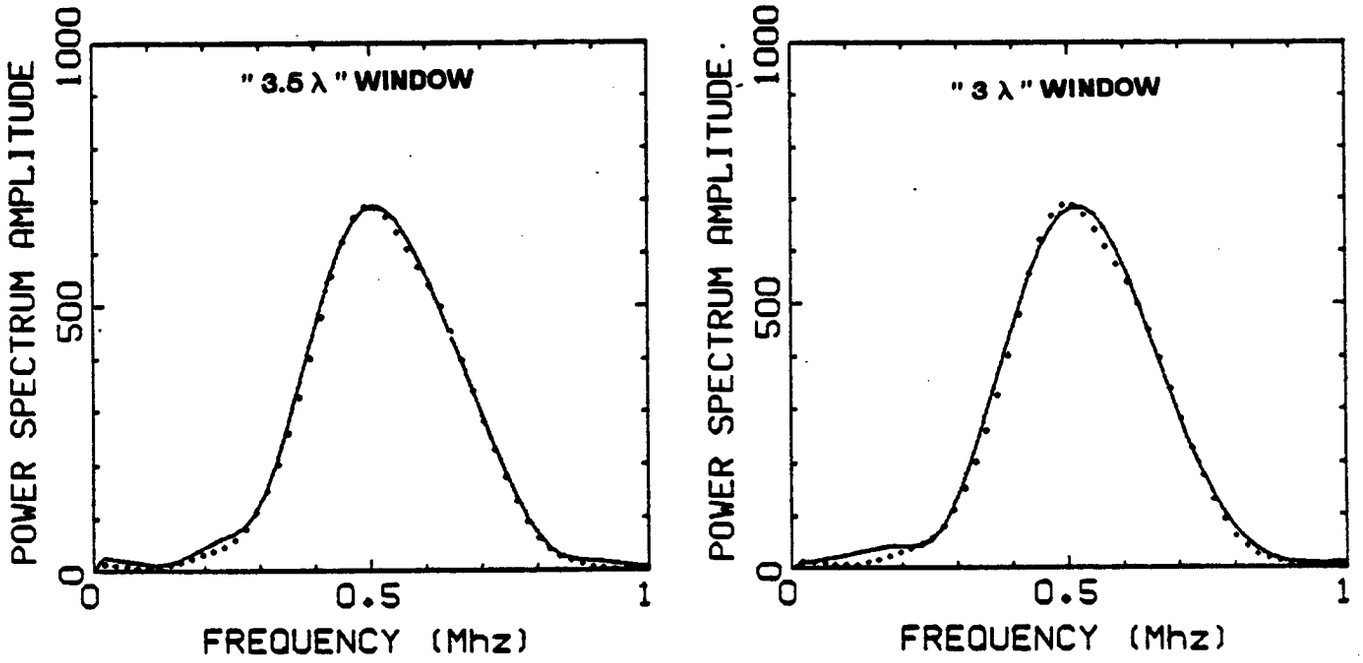

Fig.3-7 Effects of different sizes of time-windows on the power spectrum

The dots represent the full power spectrum

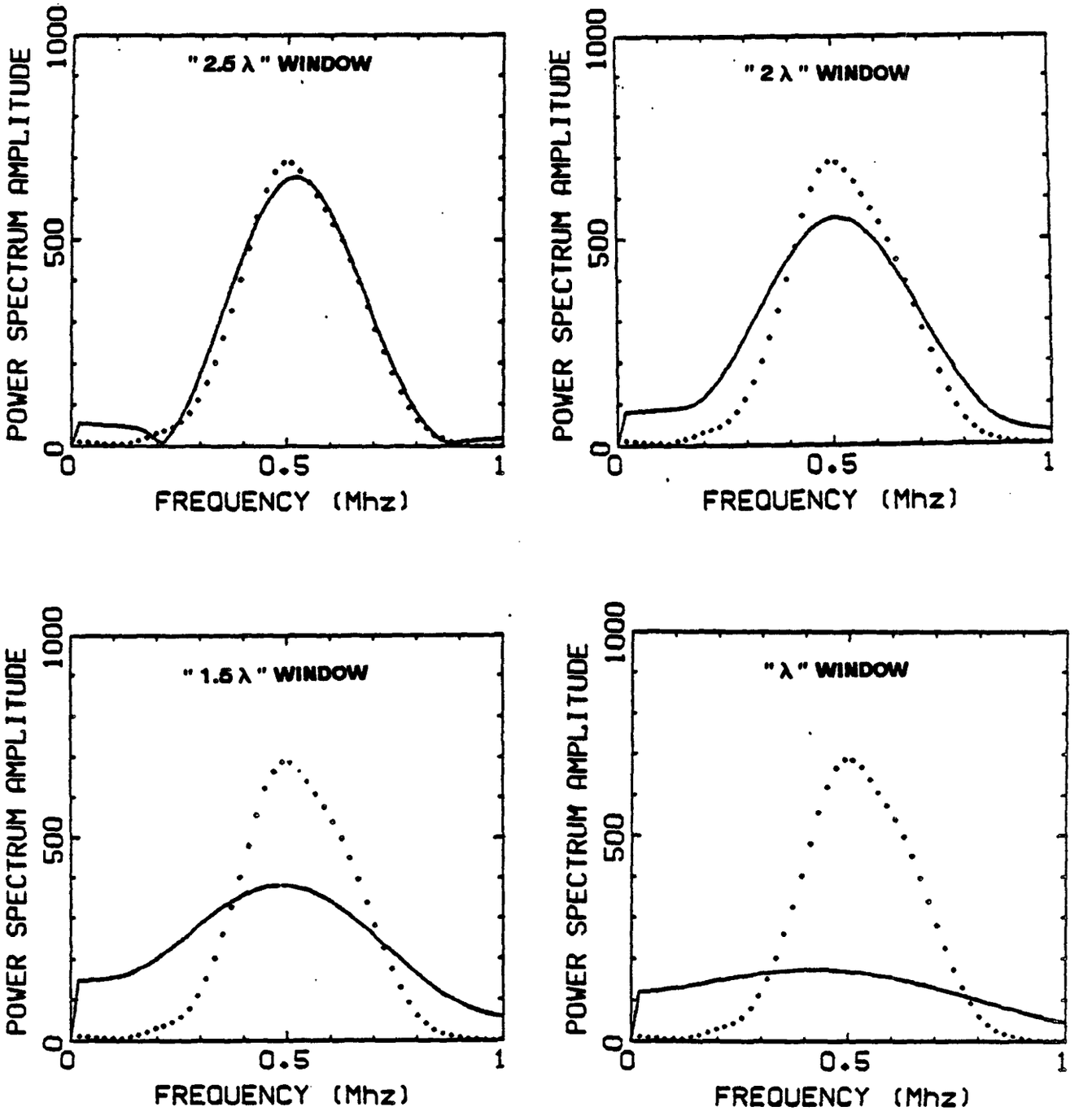

Fig.3-7b Effects of different sizes of time-windows on the power spectrum

The dots represent the full power spectrum.

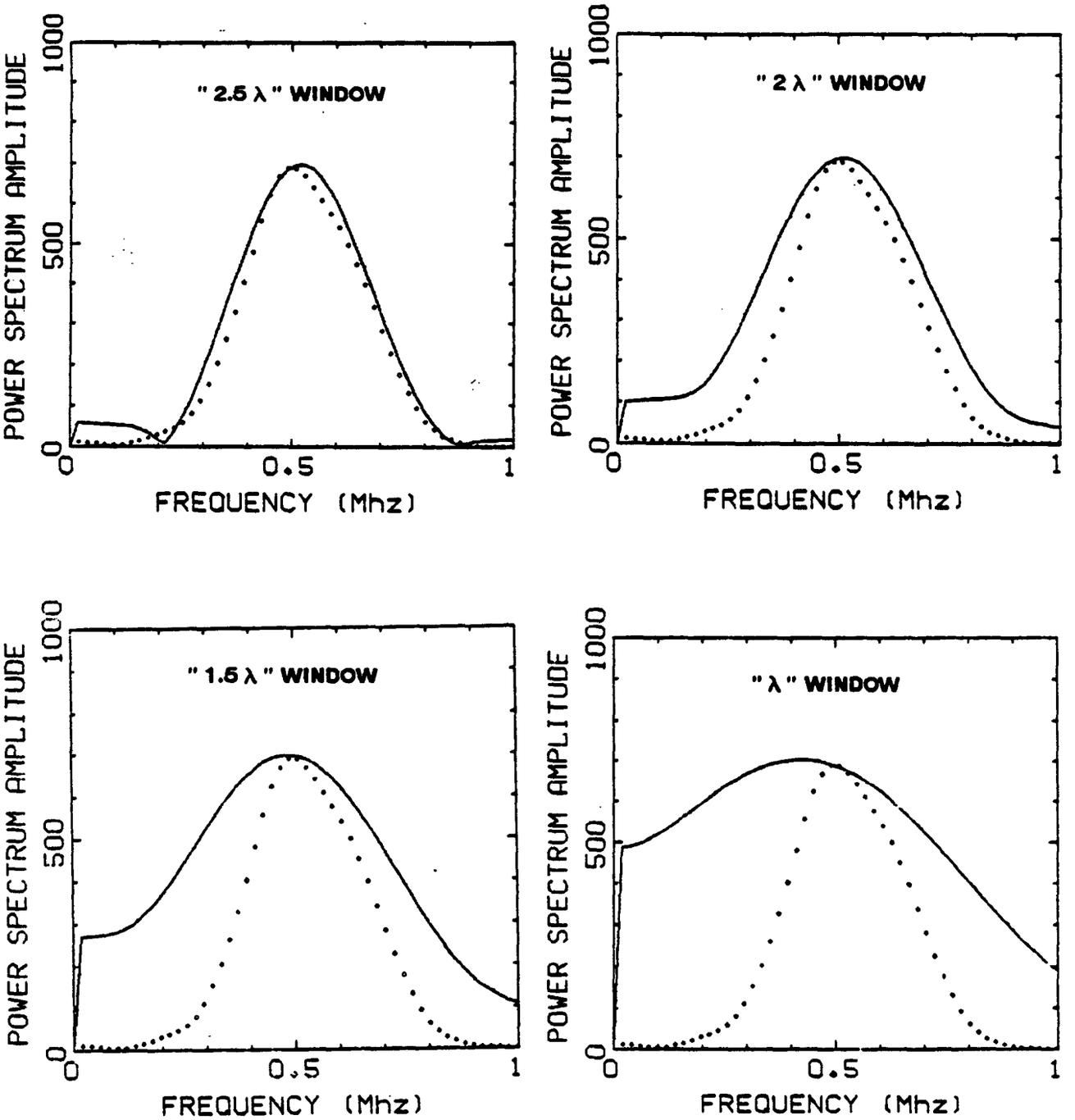

Fig.3-7c Effects of different sizes of time-windows on the power spectrum

Normalized Amplitudes

The dots represent the full power spectrum

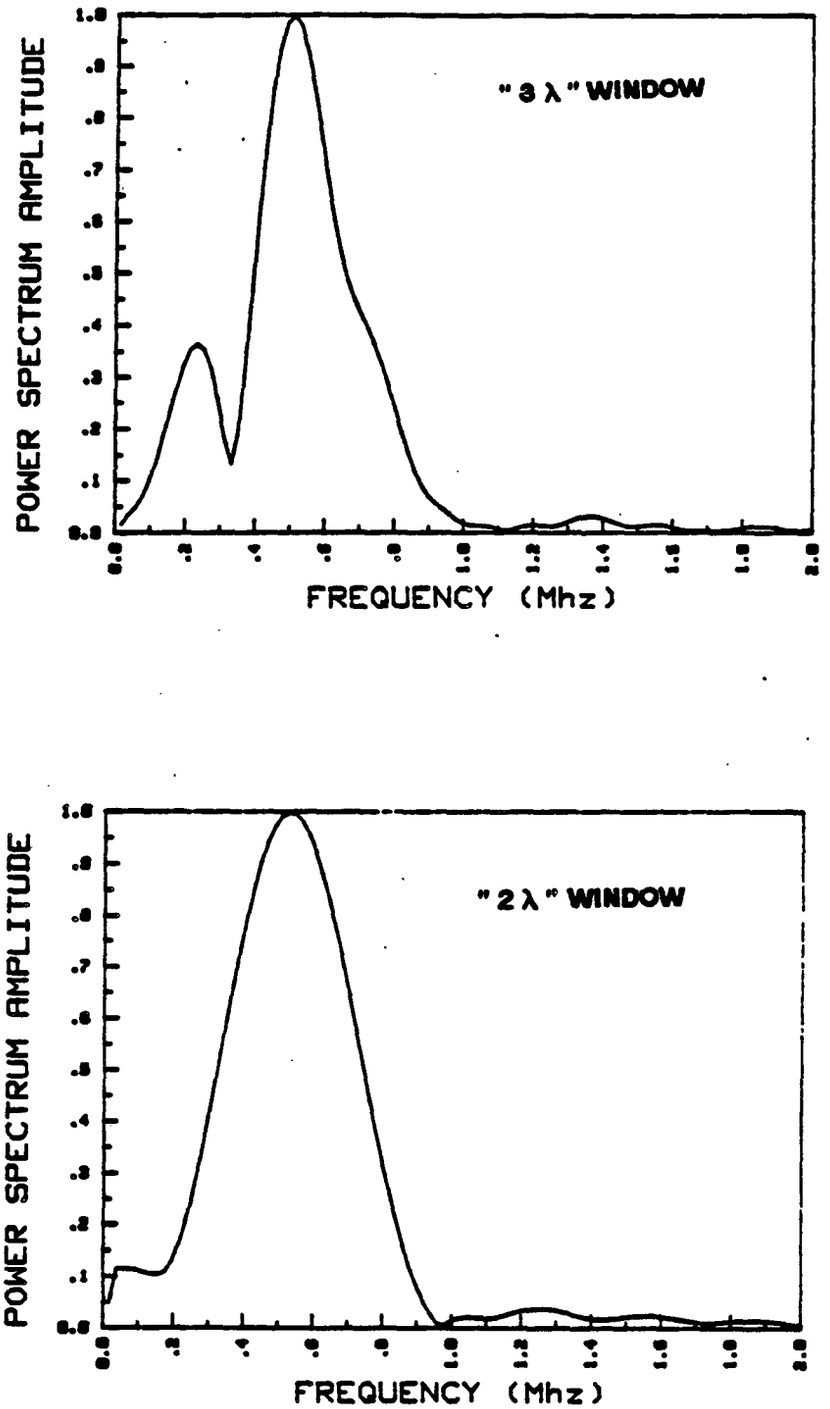

Fig.3-7d Effect of two different sizes windows on a Silicon rubber-Water signal

previously if the window is smaller (2 wave-lengths) the center part of the spectrum is well preserved but there is a large dc component. These results show that we must be very careful in windowing the data to get their power spectrum.

4-d Reflection coefficient calculation and accuracy

It is important to realize that the precision of the calculated theoretical value of the reflection coefficient diminishes greatly with its absolute value. This huge dependence is a well-known property of the homographic function $\frac{1-x}{1+x}$ when x is close to 1. Therefore in an earth-like case (reflection coefficient < 10^{-2}), our measurements become less and less precise. However, for very low acoustic impedance contrasts (polymer, silicon rubber), the attenuation effect is sufficient to show up even with the error bar we must attribute to the theoretical value of the reflection coefficient. The different values are found in Table III-1.

IV- REFLECTION RESULTS

1-NORMAL INCIDENCE

To work at normal incidence we used the same transducer to emit and receive the signal, a configuration which is possible using the pulse monitoring box already described.

For the liquid samples, we used the slightly different set-up mentioned in Paragraph III.

To obtain the experimental reflection coefficient, we worked in the frequency domain and, then, calculated the area of the power spectrum. We could have used the maximum amplitude of the signal or of the power spectrum, but we chose to use the area of the power spectrum to average all the little fluctuations of the signal due to the digitization and the ambient noise. The area was calculated by the method of trapeziums. We also tried to see if the "reflection coefficient" result obtained by zeroing the parts of the spectrum where the amplitude was too small to be reliable (<10% of the maximum amplitude, that could be considered mostly due to noise) was the same as the one obtained with the full spectrum: we did not find any noticeable difference. In consequence, we always used the whole area of the power spectrum.

For non-attenuating media we must use equation (3.1.5):

$$Y_0(\omega) = S(\omega)\, r_0 \tag{3.1.5}$$

which, if we take the power spectrum of the two sides, gives:

$$\left|Y_0(\omega)\right| = \left|S(\omega)\right| \left|r_0\right| \tag{3.1.5b}$$

This equation can be integrated :

$$\int_0^\infty \left|Y_0(\omega)\right| d\omega = \left|r_0\right| \int_0^\infty \left|S(\omega)\right| d\omega \tag{3.1.7}$$

or in the discrete domain

$$\sum_{i=0}^{i=\infty} \left|Y_0(\omega_i)\right| = \left|r_0\right| \left[\sum_{i=0}^{i=\infty} \left|S(\omega_i)\right|\right] \tag{3.1.8}$$

Since for air-water interface we know that $\left|r_0\right| = 1$, equation (3.1.8) can be rewritten in the form:

$$\left|r_0\right| = \frac{\sum_{i=0}^{i=\infty} \left|Y_0(\omega_i)\right|}{\sum_{i=0}^{i=\infty} \left|Y_0(\omega_i^{AW})\right|} \tag{3.1.9}$$

the superscript AW meaning that the values of Y_0 are the ones obtained in the air-water case.

For non-attenuating media at normal incidence, the theoretical reflection coefficient is given by:

$$\left|r_0\right| = \left|\frac{\rho_1 V_1 - \rho_2 V_2}{\rho_1 V_1 + \rho_2 V_2}\right| \tag{3.1.10}$$

So if we plot $\sum_{i=0}^{i=N} \left|Y_0(\omega_i)\right|$ as a function of $\left|r_0\right|$, we should get a straight line going through the origin. The results are shown in Figure 3-8 and Table III-2. The values found are within 1% of the theoretical ones, proving the accuracy of the experimental set-up.

For attenuating media it is completely different. The starting equation is:

$$Y(\omega) = S(\omega)\, R(\omega) \tag{3.1.4}$$

which can be rewritten in terms of power spectra

$$\left|Y(\omega)\right| = \left|S(\omega)\right| \left|R(\omega)\right| \tag{3.1.4b}$$

This equation can be integrated like equation (3.1.5), giving:

$$\int_0^{\infty} \left|Y(\omega)\right| d\omega = \int_0^{\infty} \left|S(\omega)\right| \left|R(\omega)\right| d\omega \tag{3.1.11}$$

We can always decompose $\left|R(\omega)\right|$ into an acoustic impedance part and a Q-contrast part [see Part I-A].

$$\left|R(\omega)\right| = \left|r_0\right| + \Delta R(\omega) \tag{3.1.12}$$

We can then rewrite equation (3.1.11)

$$\int_0^{\infty} \left|Y(\omega)\right| d\omega = \left|r_0\right| \int_0^{\infty} \left|S(\omega)\right| d\omega + \int_0^{\infty} \left|S(\omega)\right| \Delta R(\omega) d\omega \tag{3.1.13}$$

or

$$\left|r_0\right| + \Delta r_0 = \frac{\int_0^{\infty} \left|Y(\omega)\right| d\omega}{\int_0^{\infty} \left|S(\omega)\right| d\omega} \tag{3.1.14}$$

In the discrete domain and using the air-water values, we obtain:

$$\left|r_0\right| + \Delta r_0 = \frac{\sum_{i=0}^{i=\infty} \left|Y(\omega_i)\right|}{\sum_{i=0}^{i=\infty} \left|Y_0(\omega_i^{AW})\right|} \tag{3.1.15}$$

Now if we plot $\sum_{i=0}^{i=N} \left|Y(\omega_i)\right|$ as a function of $\left|r_0\right|$, the points will not fit the straight line going through the origin determined from the non-attenuating data. The results are shown in Figure 3-8. The actual values are given in Table III-2.

It is important also to realize that the area of the power spectrum is not exactly proportional to the modulus of the reflection coefficient $|R(\omega)|$: it is $|r_0| + \Delta r_0(\omega)$. This remark is important only for the cases where there is a very low acoustic impedance contrast and a very high attenuation. In all other cases $\Delta R(\omega)$ will be small enough compared with $|r_0|$ to be considered as independent of frequency which allows us to write equation (3.1.13):

$$\int_0^{\infty} \left|Y(\omega)\right| d\omega = \left|r_0\right| \int_0^{\infty} \left|S(\omega)\right| d\omega + \Delta R \int_0^{\infty} \left|S(\omega)\right| d\omega \tag{3.1.16}$$

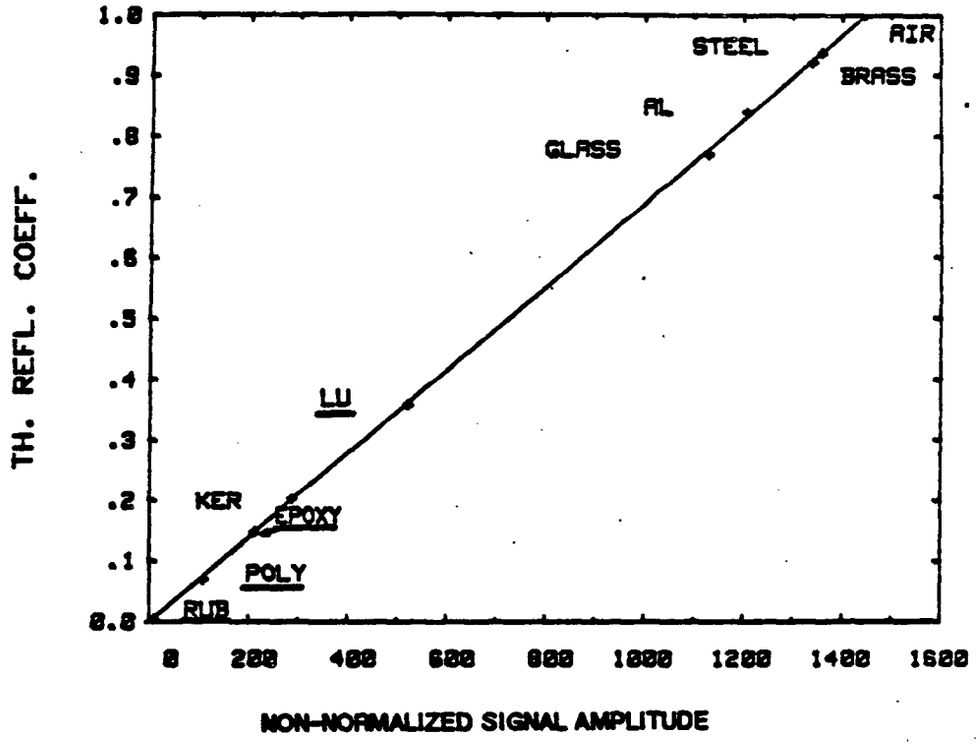

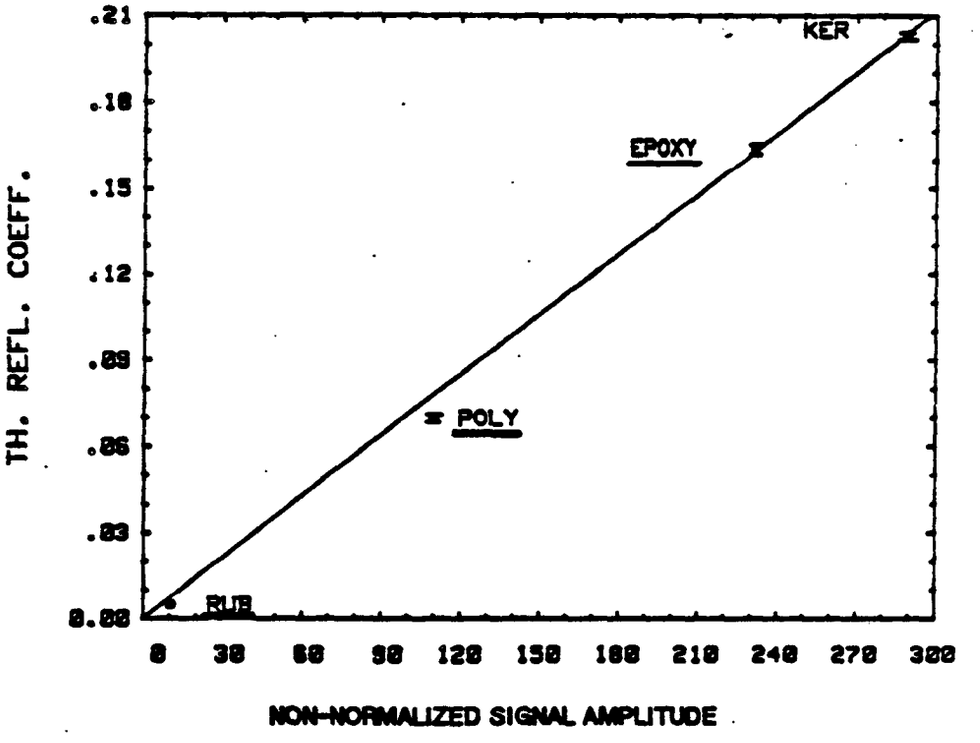

Fig.3-8. Reflected signal amplitude as a function of the theoretical elastic reflection coefficient. Normal incidence.

The underlined names represent the data obtained for attenuating samples.

which gives immediately

$$\Delta R \approx \Delta r_0$$

Table III-2 shows the discrepancy between the theoretical elastic reflected energy and the experimental one. The principal conclusions that can be drawn out of this Table are the following:

-for non-attenuating media the values of this discrepancy are within 1%, while the measurements' precision is even smaller.

-for attenuating media the values of this discrepancy vary greatly and can be as large as 80% for silicon rubber. On another hand the measurements' precision decreases with decreasing acoustic impedance contrast and reaches a value of 32% for silicon rubber.

The bottom plot in Figure 3-8 is a blow-up of the top one:it is an attempt to show that polymer and silicon rubber do not fit on the straight line which passes through the origin. Even with this expanded scale this misfit is not clear; therefore we have shown the same results in another way (Figure 3-9). This plot proves that when the elastic reflection coefficient is greater than 0.1 (whatever the attenuation), its effect is completely masked by the acoustic impedance (see, for example the epoxy sample for which Q is 18). Figure 3-9 also shows that the attenuation effect increases with decreasing acoustic impedance contrast but that, experimentally, this effect competes with the measurements' precision effect already mentioned.

Now if we look more particularly at the three attenuating samples (epoxy, polymer, silicon rubber), the first two having an attenuation of about the same value ($Q_p \approx 15$) and the last one a smaller value ($Q_p = 50$), while the elastic reflection coefficients range from 0.164 to 0.004, we note the following facts:

- For the epoxy sample with a reflection coefficient of 0.164, there is no observed effect on the amplitude of the reflection.

- In the case of the polymer (R=0.07) the effect is small in relative value but observable.

- Finally for the silicon rubber (R=0.004) the relative increase of reflection is on the order of 80%, but as we have already mentioned the error bar is now 32%!

For the shape of signals there is no noticeable difference for all the samples. For the silicon rubber, one can have an impression of slight distorsion with respect to all the other signals (see Figure 3-10). This "distorsion" will be examined in more detail in Paragraph V when we use computer simulation.

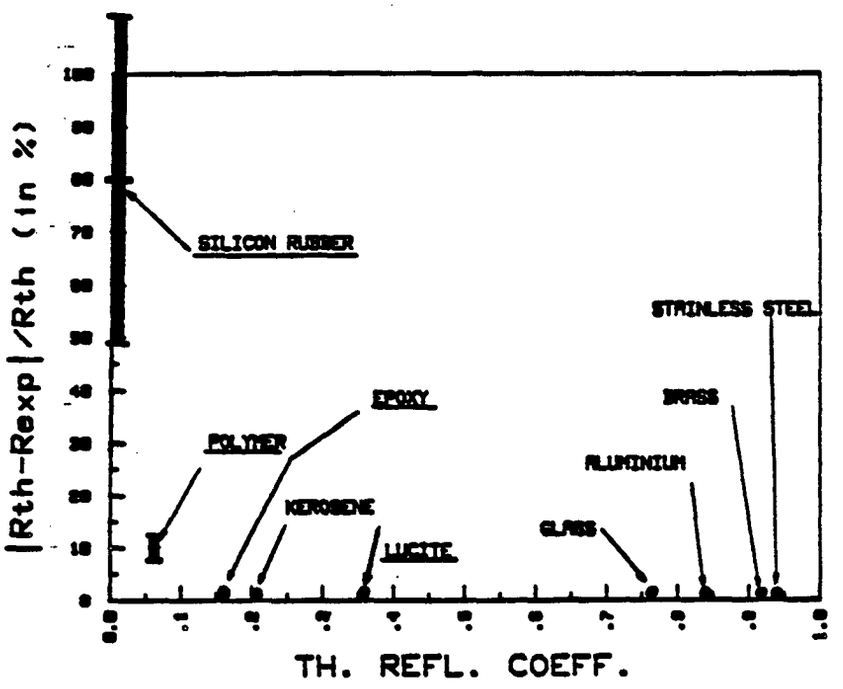

Fig.3-9. Discrepancy between theoretical elastic reflection coefficient and experimental one. The underlined names represent the data obtained for attenuating samples.

Samples	E_{th}	$\frac{\Delta E_{th}}{E_{th}}$	E_{exp}	$\frac{\lvert E_{th} - E_{exp} \rvert}{E_{th}}$
Stainless Steel	1353	.1%	1359	.5%
Brass	1332	.1%	1340	.6%
Aluminium	1215	.2%	1205	.8%
Glass	1115	.2%	1130	1.3%
Kerosene	292	.8%	289	1.0%
Lucite	519	.5%	522	.6%
Epoxy	236	1.3%	237	.4%
Polymer	91	2.5%	100	10%
Silicon Rubber	5.5	32%	10	80%

Table III-2: Values of theoretical and Experimental Reflected Energy

E_{th} = Theoretical Reflected Energy (Elastic)

E_{exp} = Experimental Reflected Energy

$\frac{\Delta E_{th}}{E_{th}}$ = Relative Precision on E_{th} due to measurements' accuracy

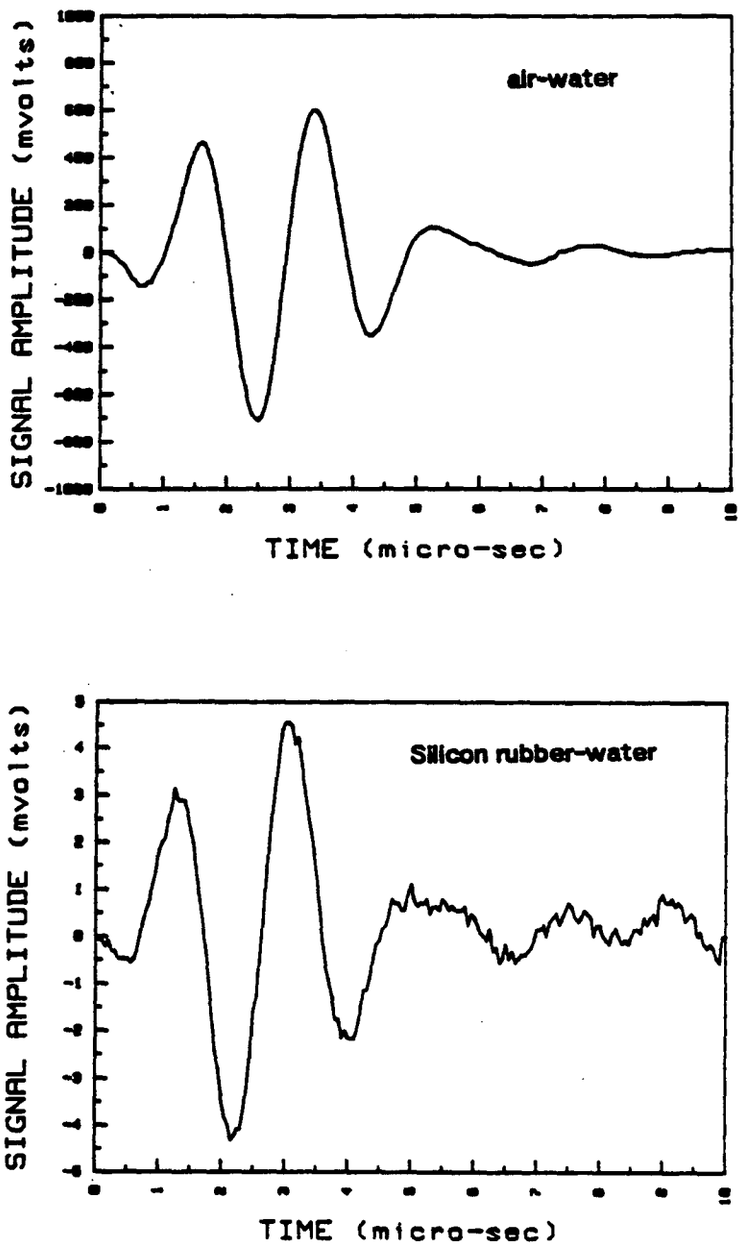

Fig.3-10 Reflected signals at normal incidence.

Top: air-water

Bottom : Silicon rubber-water

2-NON-NORMAL INCIDENCE

At non-normal incidence we monitored the pulse differently than at normal incidence. So, as we have already said, it is impossible to compare the results with the ones obtained at normal incidence. Nevertheless, we know that for non-attenuating samples our system is very accurate (1%). We can always set a new reference with this pulse monitoring by using a well-known sample with a high reflection coefficient. We used stainless steel at an incidence angle of $\vartheta = 7^0$. By a simple multiplication we obtained the "experimental" reflected energy for a reflection coefficient of amplitude 1 and compared other data to this reference using theoretical elastic values.

Due to sample size problems and space limitation in the tank we did not exceed angles of 35^0. Even to go to angles of 35^0 we needed to employ larger samples than the usual ones (7.5 cm diameter instead of 5 cm). Other problems must be pointed out. If we went to angles close to critical angles, the following phenomena need to be considered:

-The reflection coefficient is largely a function of frequency for spherical waves at angles close to critical even in the absence of any attenuation [Červeny et al (1977)], because ray theory is not applicable in the vicinity of the critical ray; the wave front can no longer be described by geometrical optics. Therefore the shape of the amplitude curve depends not only on the elastic characteristics of the different media but also on the thicknesses and dips of the interfaces and on the focal depth. Figure 3-11 shows an example, reprinted by permission from Červeny et al, of this phenomenon for the Moho interface.

-At angles beyond the critical angle, the head wave interferes with the reflected signal itself. Then it becomes nearly impossible to know if the observed effect is due to attenuation or to any interference pattern. It may even be difficult to decide where the breaking point of the signal is. This problem is shown, for example, in Figure 3-12 (bottom right signal).

The angle dependence of reflection coefficients is shown for the following samples:

Aluminium

Lucite

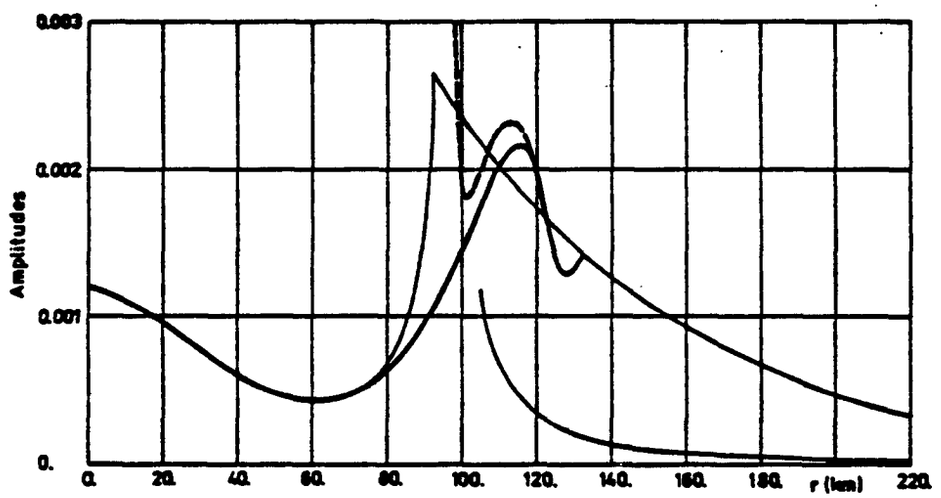

Fig. 7.4 Amplitude-distance curves of the wave reflected from the Mohorovičić discontinuity and of the corresponding head wave in the medium shown in Fig. 3.4, frequency $f = 4$ Hz. Thin lines- computed by standard ray theory, dashed line- interference of a reflected and a head wave, computed by the standard ray theory, heavy line- computed by modified methods

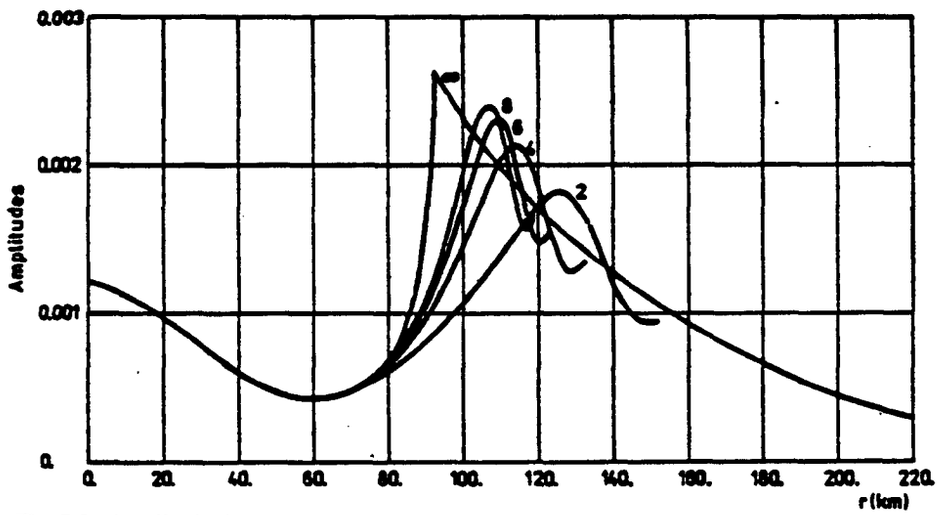

Fig. 7.5 Amplitude-distance curves of the wave reflected from the Moho discontinuity in the critical region, in the model of medium shown in Fig. 3.4. Computed by modified methods, for frequencies $f = 2$ Hz, 4 Hz, 6 Hz and 8 Hz

Fig.3-11 Reprint from V.Cerveny and al : Ray Method in Seismology (Prague 1977)

Polymer

Silicon rubber

The first sample is the only non attenuating one. We do not show the behavior of the epoxy sample, because the attenuation effect is hidden behind the acoustic impedance effect, as in the normal incidence case.

The theoretical modulus of the reflection coefficient is plotted against the experimental one in Figures 3-12 to 3-15. We have also plotted the time signals for the different angles at which measurements were taken. In a third part of the plot we show the theoretical phase of the reflection coefficient. The values of densities, velocities and attenuations used to generate these plots are given in Table III-1.

Various observations are made:

-For aluminium and lucite the agreement between the experimental and the theoretical moduli of the reflection coefficients is very good. Nevertheless certain points are far from the theoretical curve. First, it was impossible to observe the peaks of moduli which were found theoretically, as explained by Červeny et al (see also Figure 3-11). Second, for aluminium at $\vartheta = 30^0$ the experimental point is completely out of the theoretical curve, because the signal we observed is composed of the reflected signal and the P-S head-wave. Since this head-wave is out of phase with the reflected one, we have a considerable decrease in apparent amplitude. This decrease is also supported by the fact that if we look at the signal recorded at $\vartheta = 35^0$ this head-wave appears as a precursor of opposite polarity to the reflected one. It is interesting to note that we did not see any P-P head-wave precursor after we passed the first critical angle. This absence is explained by looking at signals recorded in bore-holes, where the P-P head wave is very low amplitude with respect even to the P-S one: a ratio of 1 to 10 in amplitudes is not at all unusual and so the P-P head-wave is too low amplitude to be noticed in our experiment.

-For polymer there is not much to say except that the experimental points do not seem to fit well either on the elastic or on the viscoelastic curves. This disparity may be due to the fact that the integration of the power spectrum is not equivalent to the modulus of the reflection coefficient, as already shown in Paragraph IV-1. The viscoelastic reflection coefficient has been calculated for the reference frequency. Finally we can note that, theoretically and experimentally, the attenuation effect seems to disappear

ALUMINIUM

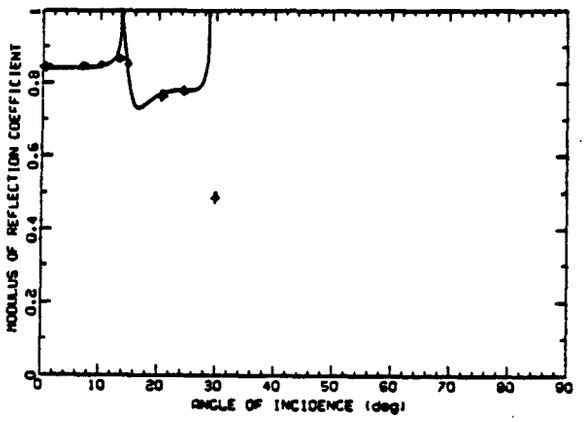

Theoretical Modulus

Experimental points = Crosses

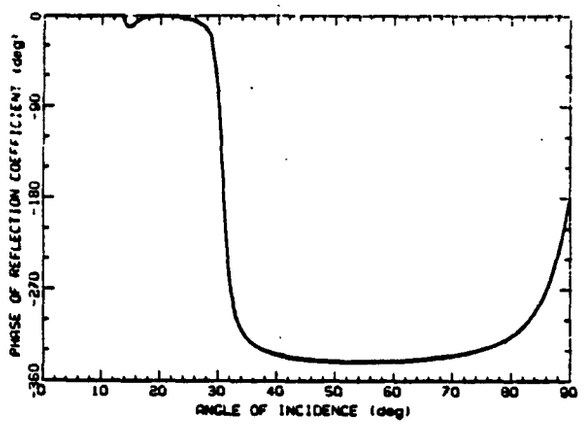

Theoretical Phase

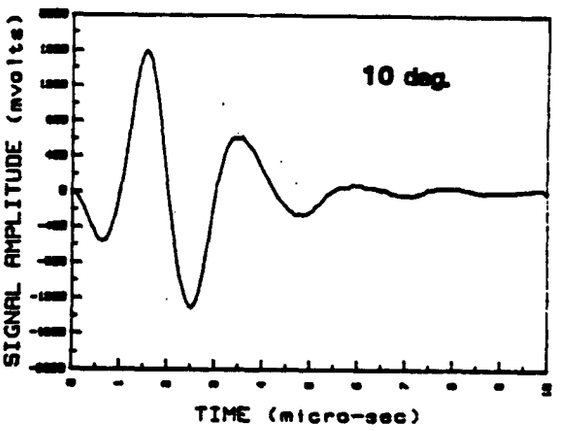

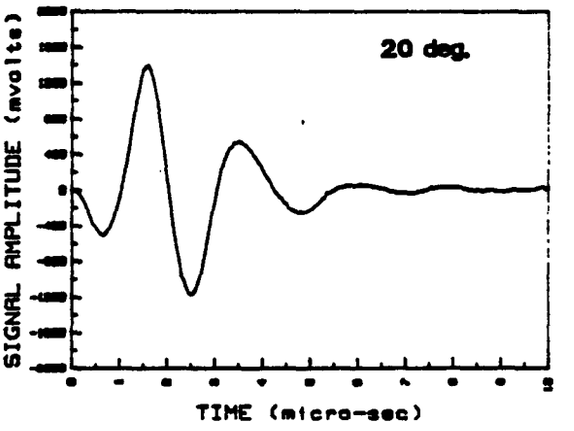

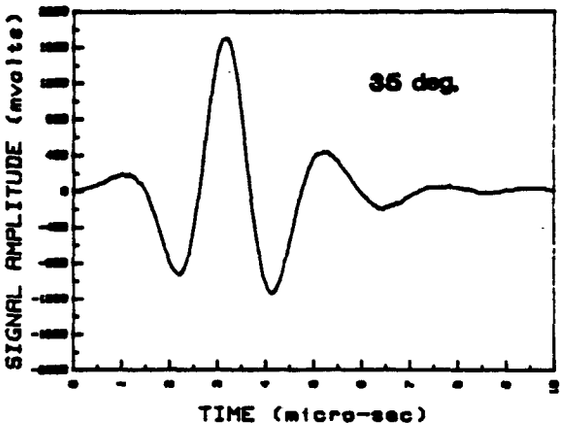

Experimental Signals

Fig.3-12 Aluminium

Right : Signals obtained for different angles

Left : Theoretical and experimental Reflection coefficient

LUCITE

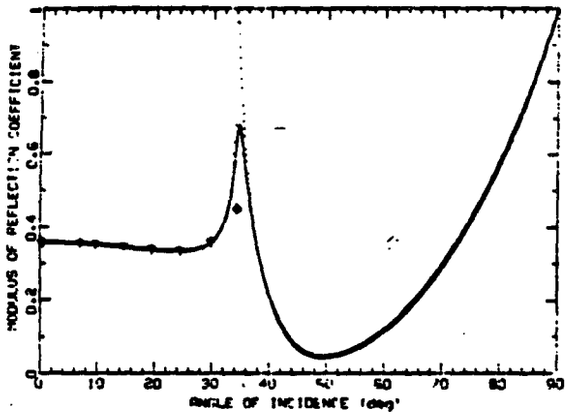

Theoretical Modulus

Experimental points = Crosses

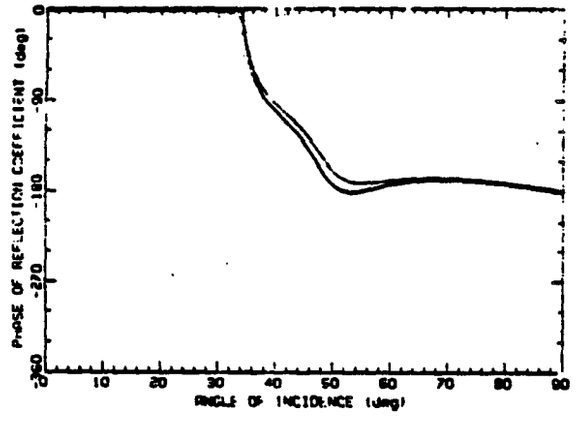

Theoretical Phase

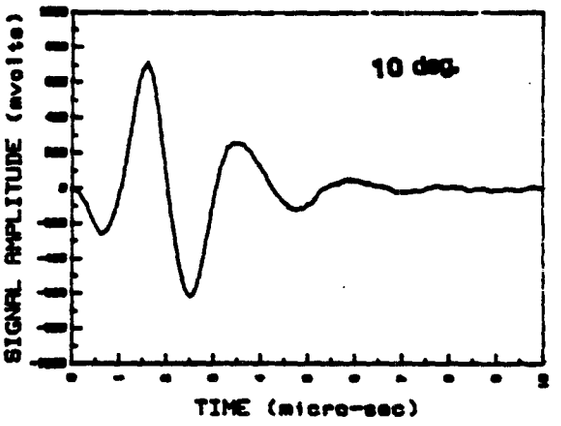

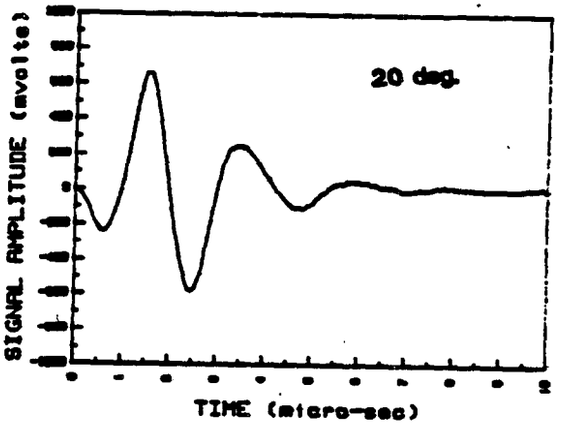

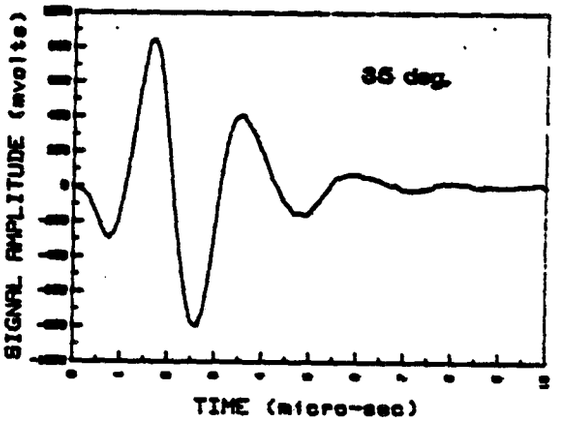

Experimental Signals

Fig.3-13 Lucite

Right : Signals obtained for different angles

Left : Theoretical and experimental Reflection coefficient

The dotted lines represent the reflection coefficient if there was no attenuation

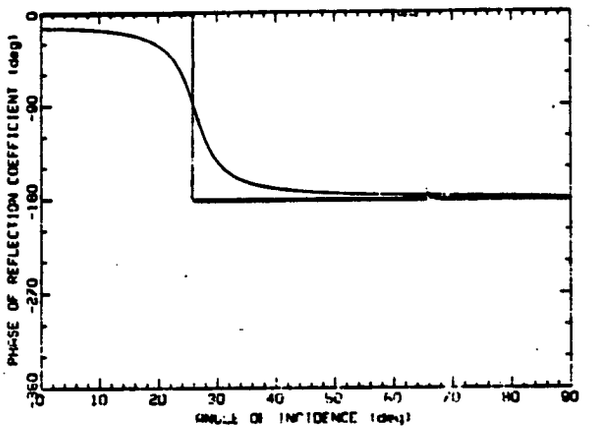

Theoretical Phase

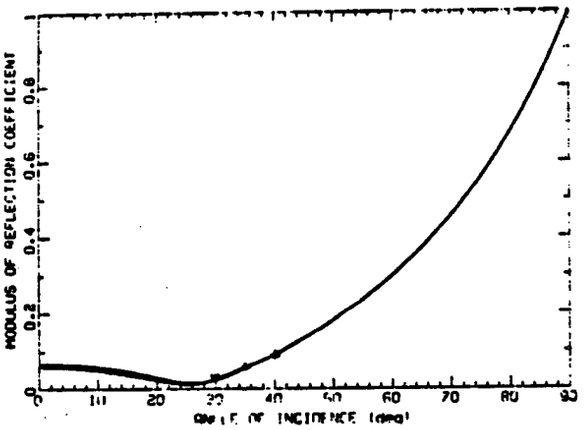

Theoretical Modulus

Experimental points = Crosses

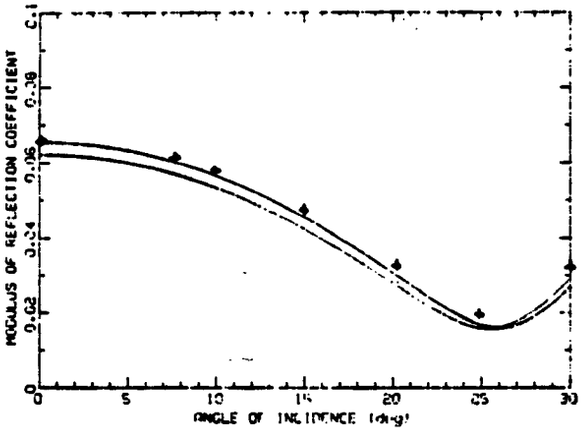

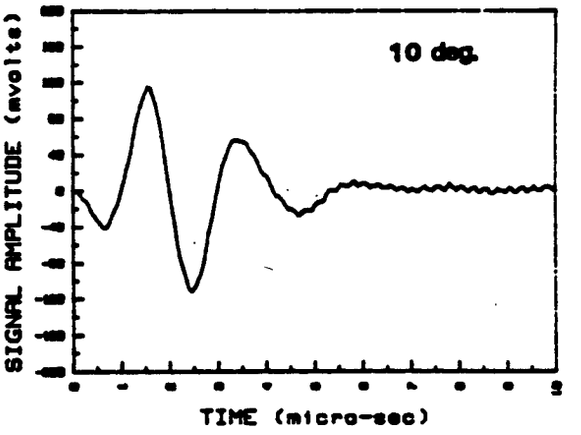

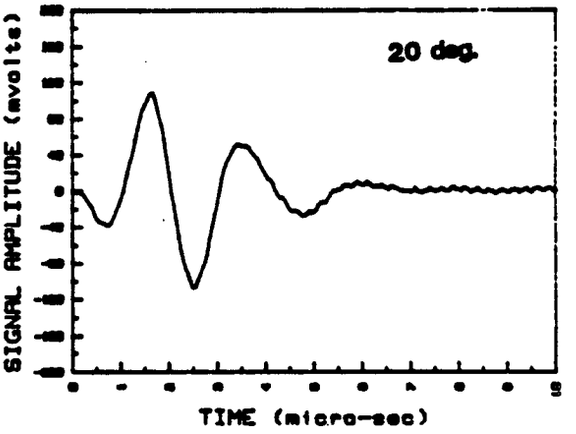

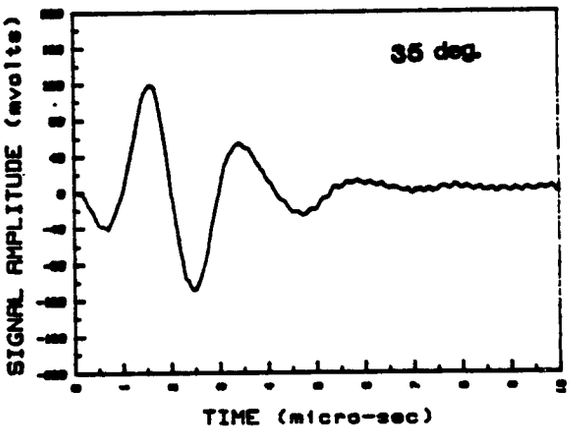

Experimental Signals

Fig.3-14 Polymer

Right : Signals obtained for different angles

Left : Theoretical and experimental Reflection coefficient

The dotted lines represent the reflection coefficient if there was no attenuation

as soon as we get to angles larger than 20^0–30^0. This disappearance does not surprise us because we have already seen that for high values of elastic reflections (>.1) the attenuation effect is completely masked.

-For silicon rubber we observe the same result as for the polymer: experimental points do not fit on either the elastic or the viscoelastic curves but this misfit is less pronounced. This result is probably due to the accuracy of the different measured values and not to the attenuation which is not big enough to create the effect mentioned for the polymer sample. The theoretical effect of attenuation is now tremendously big and it doubles the expected reflection modulus. Again we observe that for large incidence angles ($\geq 20^0$), there is no attenuation effect due to a large reflection coefficient. The theoretical phase information is interesting because it seems to explain qualitatively the slight change of shape from the usual signal we observed for silicon rubber (see Figure 3-10). This problem will be examined in more detail in Paragraph V with computer simulation.

In general there is no observable phase information in the recorded signals. The reason is that we are staying beyond critical angles to avoid the problems already described and so that the phases are pretty much constant and equal to zero. There is one exception and it is silicon rubber for which there is an observable phase change of 180^0 which corresponds to the expected value (see Figure 3-15 and 3-22, 3-23). On another hand, the recorded signal is not minimum phase and needs an unwrapping before being used. This unwrapping has been done and showed a monotonically increasing function.

V-COMPUTER SIMULATION AND COMPARISON WITH THE DATA

1-NORMAL INCIDENCE

We want to simulate on the computer the reflection of a wave at an interface. We know that we have equation (3.1.1):

$$y(t) = s(t) * r(t) \qquad (3.1.1)$$

Experimentally we can easily extract $s(t)$: at normal incidence it is the signal we have recorded for the air-water interface. To generate $y(t)$, we need $r(t)$. Equation (3.1.1) can be written in the frequency domain and it gives equation (3.1.4)

SILICON RUBBER

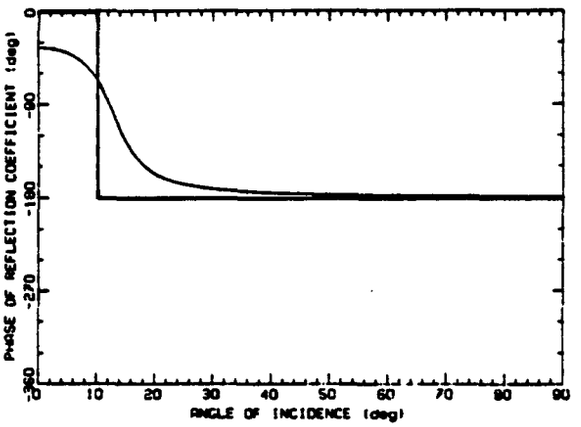

Theoretical Phase

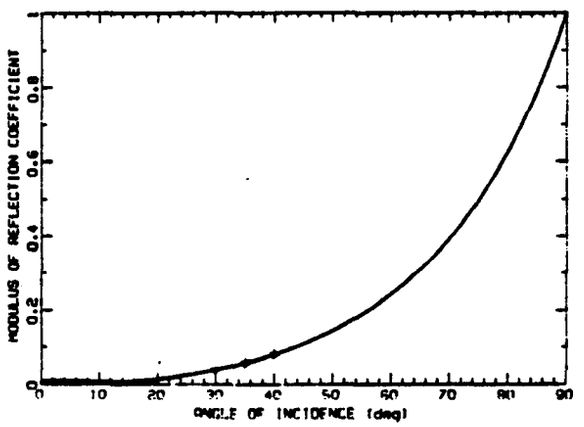

Theoretical Modulus

Experimental points = Crosses

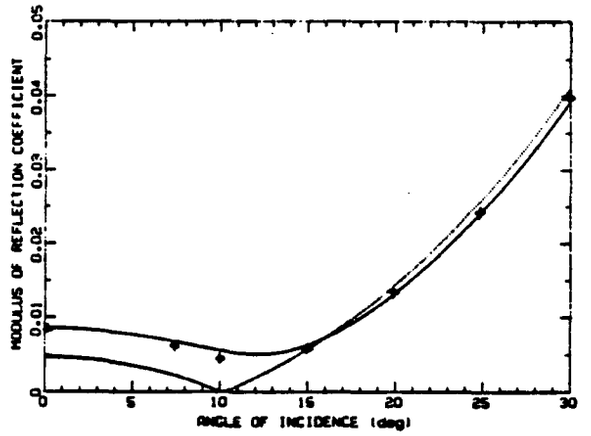

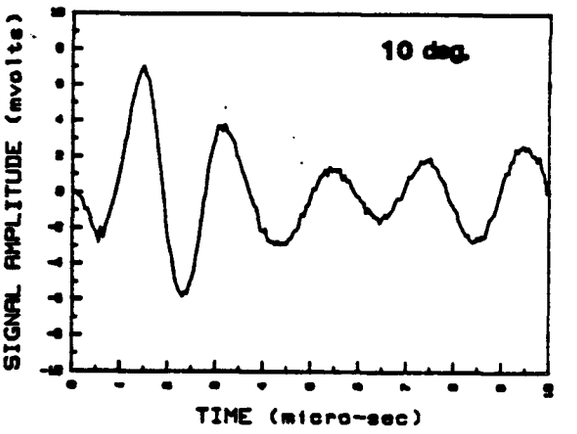

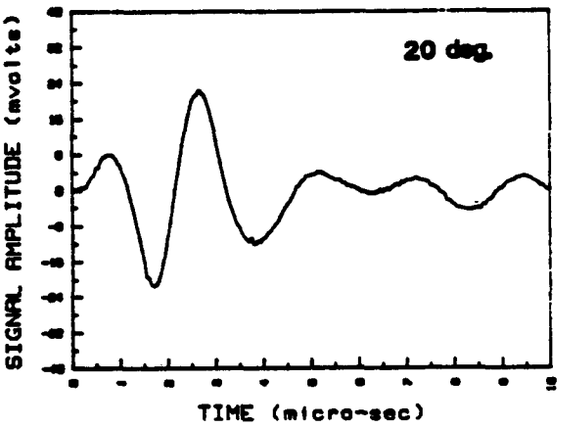

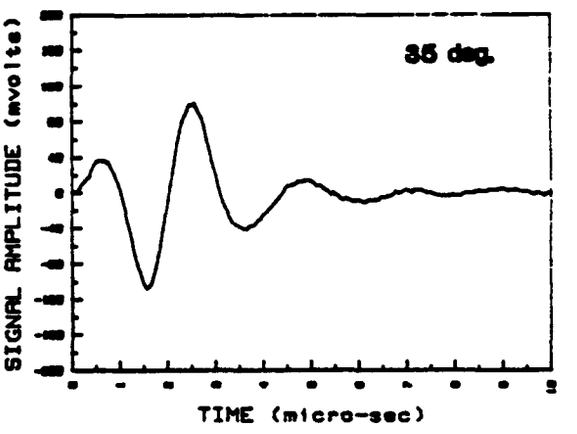

Experimental Signals

Fig.3-15 Silicon rubber

Right : Signals obtained for different angles

Left : Theoretical and experimental Reflection coefficient

The dotted lines represent the reflection coefficient if there was no attenuation

$$Y(\omega) = S(\omega)\, R(\omega) \tag{3.1.4}$$

One can determined $R(\omega)$ theoretically. To do that we need a model of attenuation. In Part I-A, it is shown that whatever viscoelastic model we use, the effect is the same on the reflection coefficient. This is easily understood if we consider it as a second order effect. Therefore the result does not depend on third order effects like diffrent type of frequency dependence for the quality factor Q. Therefore we use the constant-Q model derived by Kjartansson (1979). With this model, at normal incidence, $R(\omega)$ can be written:

$$R(\omega) = \frac{\rho_1 C_1 - \rho_2 C_2}{\rho_1 C_1 + \rho_2 C_2} \tag{3.1.17}$$

with

$$C_1 = C_{01} \left[\frac{i\omega}{\omega_0}\right]^{\gamma_1}$$

$$C_2 = C_{02} \left[\frac{i\omega}{\omega_0}\right]^{\gamma_2}$$

where

C_{01} and C_{02} are the phase velocities taken at the reference frequency ω_0.

and γ_1 , γ_2 are defined in terms of Q_1 and Q_2 by:

$$\frac{1}{Q} = \tan(\pi\gamma)$$

We know [Claerbout and Kjartansson(1979)] that the reflection coefficient at normal incidence is a causal function.

So the process to use for computer simulation is now clear:

- $s(t)$ and so $S(\omega)$ are given by the experiment for the air-water interface.
- $r(t)$ is calculated in the Fourier domain using equation (3.1.17).
- $Y(\omega)$ is obtained by equation (3.1.4).
- $y(t)$ is calculated by inverse Fourier transforming equation (3.1.4).

We have not specified if the medium was lossy or not. Non-lossy materials will be a particular case of lossy ones for which γ is equal to 0.

The results of the simulation are shown in Figures 3-16 to 3-18 for the three lossy materials epoxy, polymer, silicon rubber.

The agreement is good, showing that we could not expect to see any attenuation effect on the epoxy sample.

For the polymer the results show the slight observed increase in amplitude (10%).

For the silicon rubber the results are more interesting because the attenuation effect is bigger. We see a very good agreement in the shapes and in the amplitudes between the simulated and the experimental signal. The values used for the computer simulation are the ones listed in Table III-1.

In Figures 3-19 to 3-21 we show the expected theoretical effect for different Q-contrasts and elastic reflection coefficient on our signal. This is shown both in time and spectrum domains. We can make the following conclusions:

There is no attenuation effect on the power spectrum no matter the elastic reflection coefficient is.

The effects on the time signal are mainly amplitude effects increasing with decreasing values of Q except, may be, at very low Q (i.e 10).

As already shown by the experiment, the lower the elastic reflection the higher the attenuation effect. Figure 3-21b give schematically the amplitude of the effect we should observe on reflected energies at a viscoelastic interface. Different iso-amplitude contour lines are drawn as a function of the elastic reflection coefficient and the quality factor. We also consider typical earth situations and their approximate location on the plot: the expression geothermal granites stand for granites in geothermal areas and values for saturated sandstones are taken to represent "typical" bright spots. The Q values, for tight gas sands, have been extrapolated from low pressure measurements. The values of the elastic reflection coefficients are there to give an idea of typical earth reflections but are not actual measured values.

2-NON-NORMAL INCIDENCE

At non-normal incidence, for a given angle, we also have a one-dimensional problem which can be expressed by a modified equation (3.1.1):

EPOXY

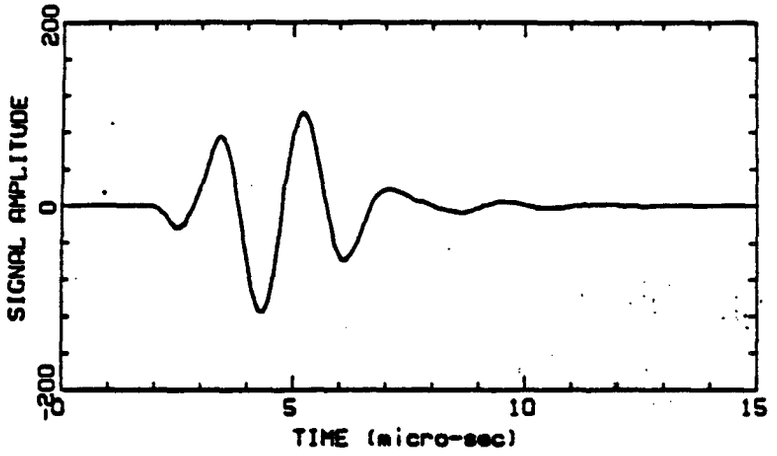

Theoretical Signal if NO Attenuation

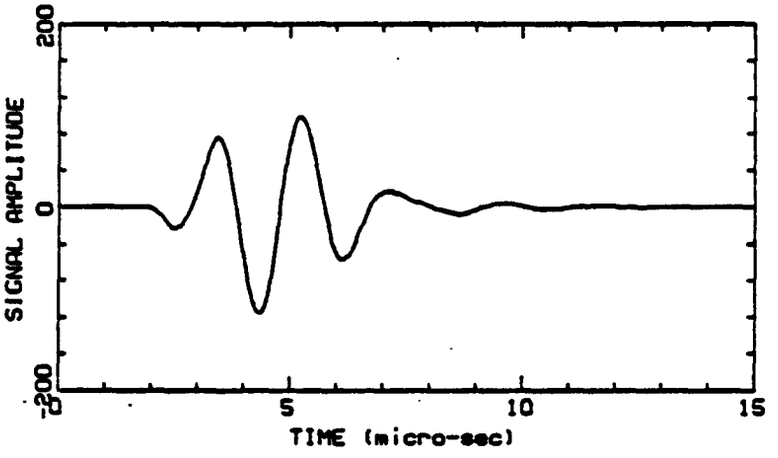

Theoretical signal, Measured Attenuation included

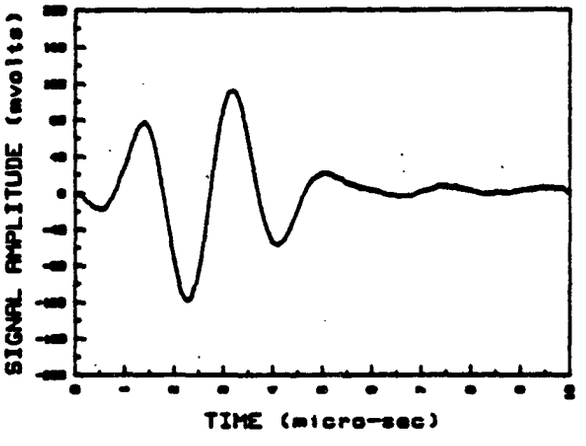

Experimental Signal

Fig.3-16 Epoxy : Comparison of simulated and experimental signals at normal incidence

POLYMER

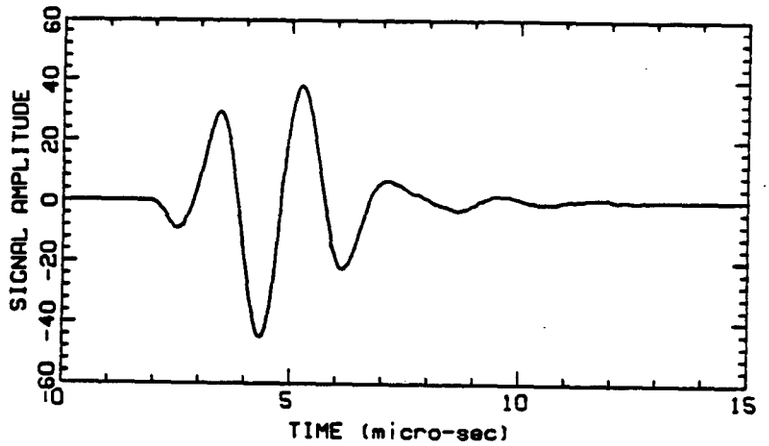

Theoretical Signal if NO Attenuation

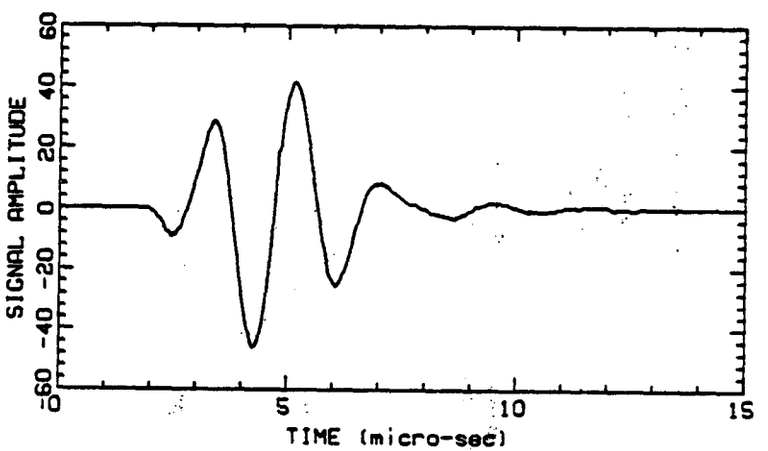

Theoretical signal, Measured Attenuation included

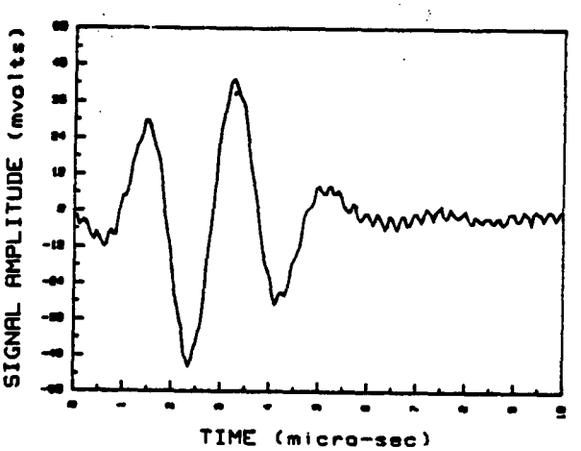

Experimental Signal

Fig.3-17 Polymer : Comparison of simulated and experimental signals at normal incidence

SILICON RUBBER

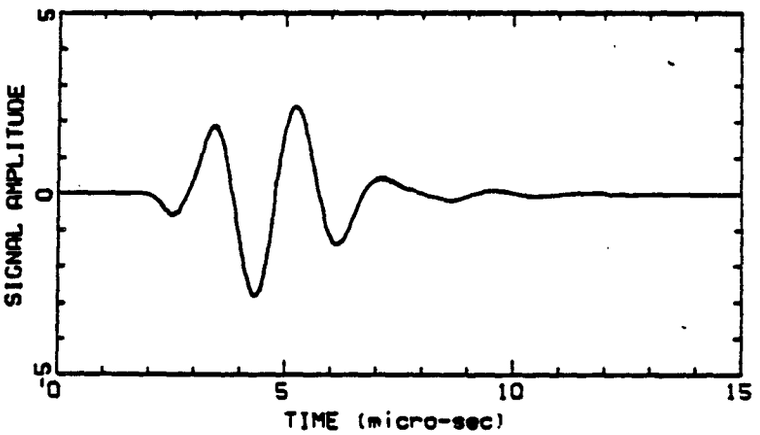

Theoretical Signal if NO Attenuation

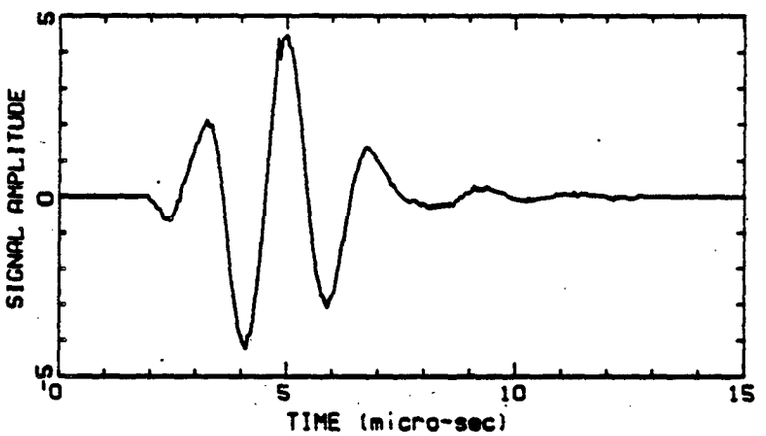

Theoretical signal, Measured Attenuation included

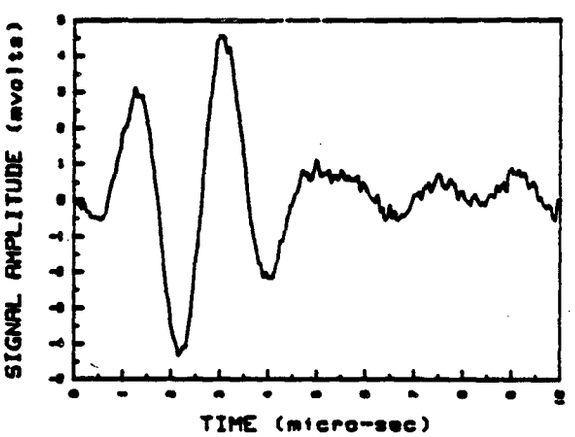

Experimental Signal

Fig.3-18 Silicon Rubber : Comparison of simulated and experimental signals at normal incidence

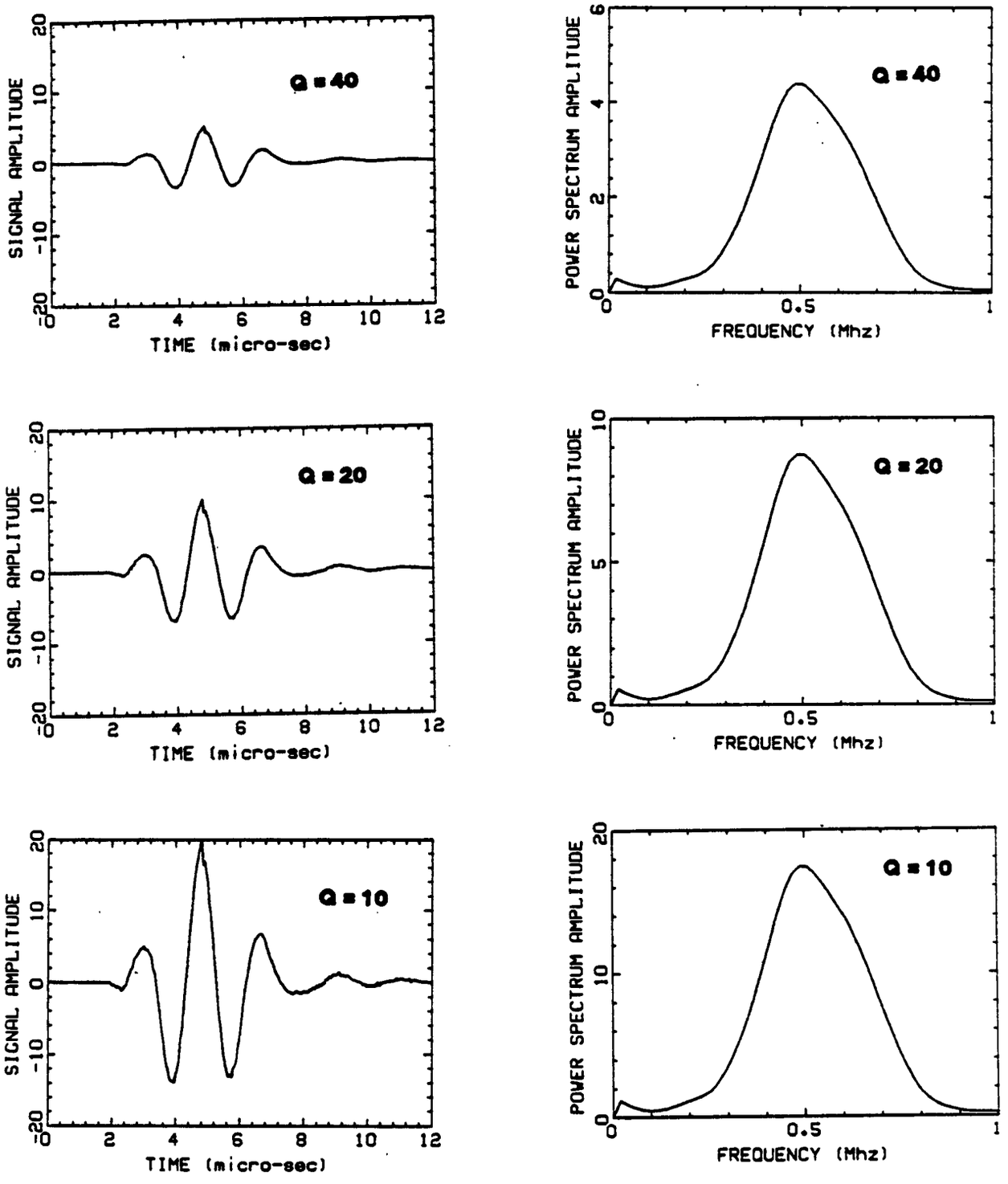

Time signals **Power spectra**

Fig.3-19 Effect of attenuation on reflections - Simulated signals

No attenuation in the first medium

No acoustic impedance contrast

Normal incidence

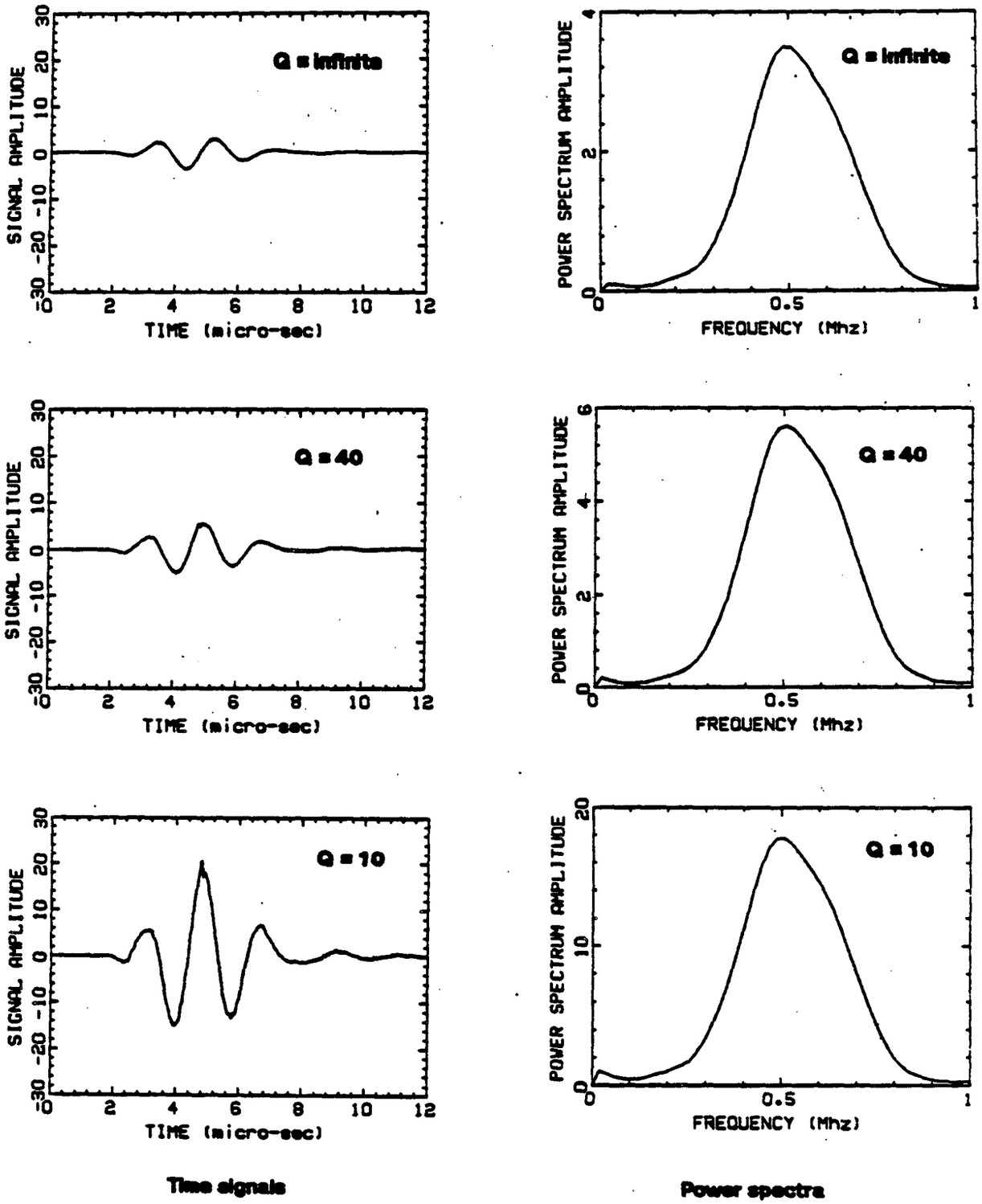

Fig.3-20 Effect of attenuation on reflections - Simulated signals

No attenuation in the first medium

Elastic Reflection coefficient = 0.005

Normal incidence

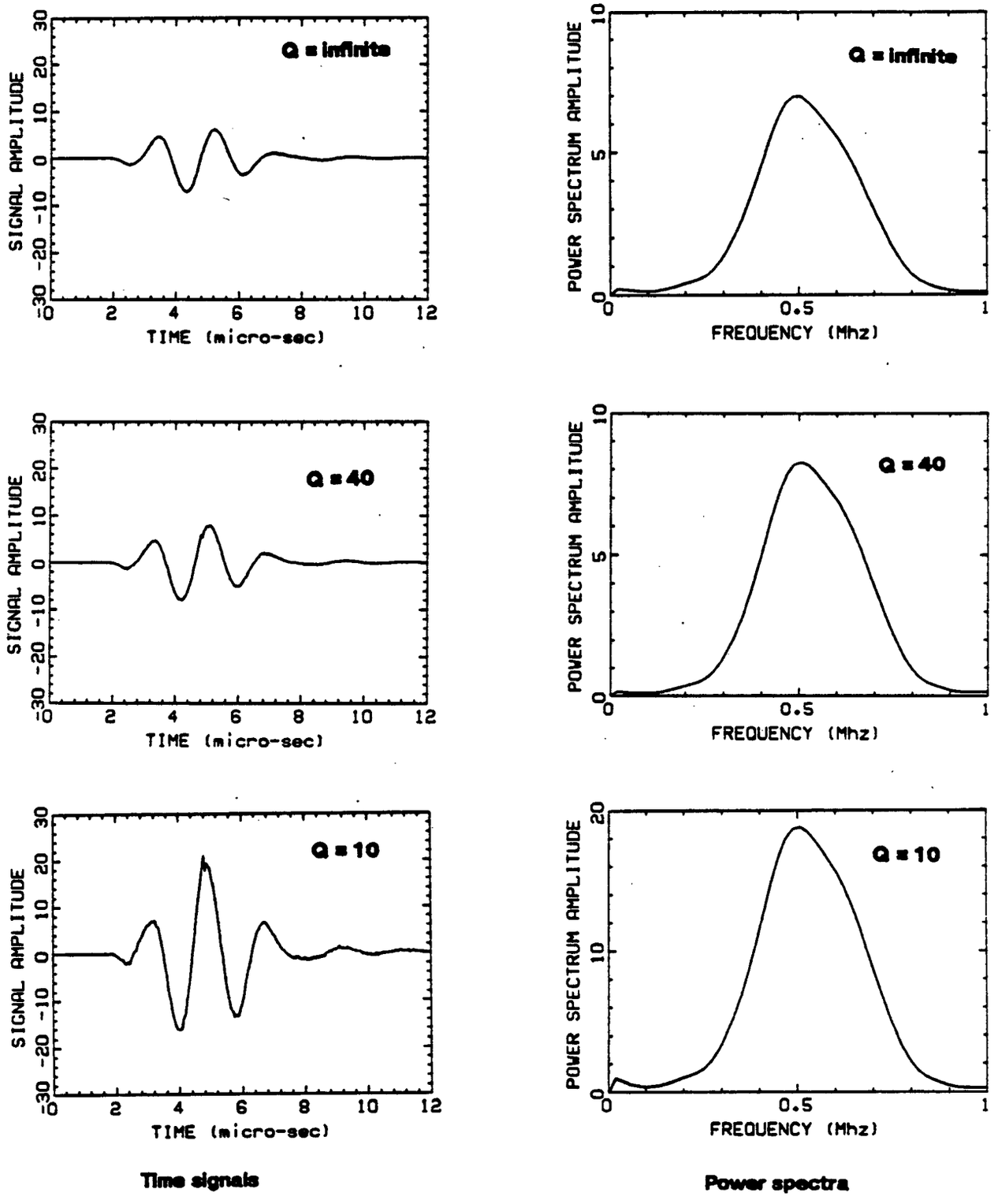

Fig.3-21 Effect of attenuation on reflections - Simulated signals

No attenuation in the first medium

Elastic Reflection coefficient = 0.01

Normal incidence

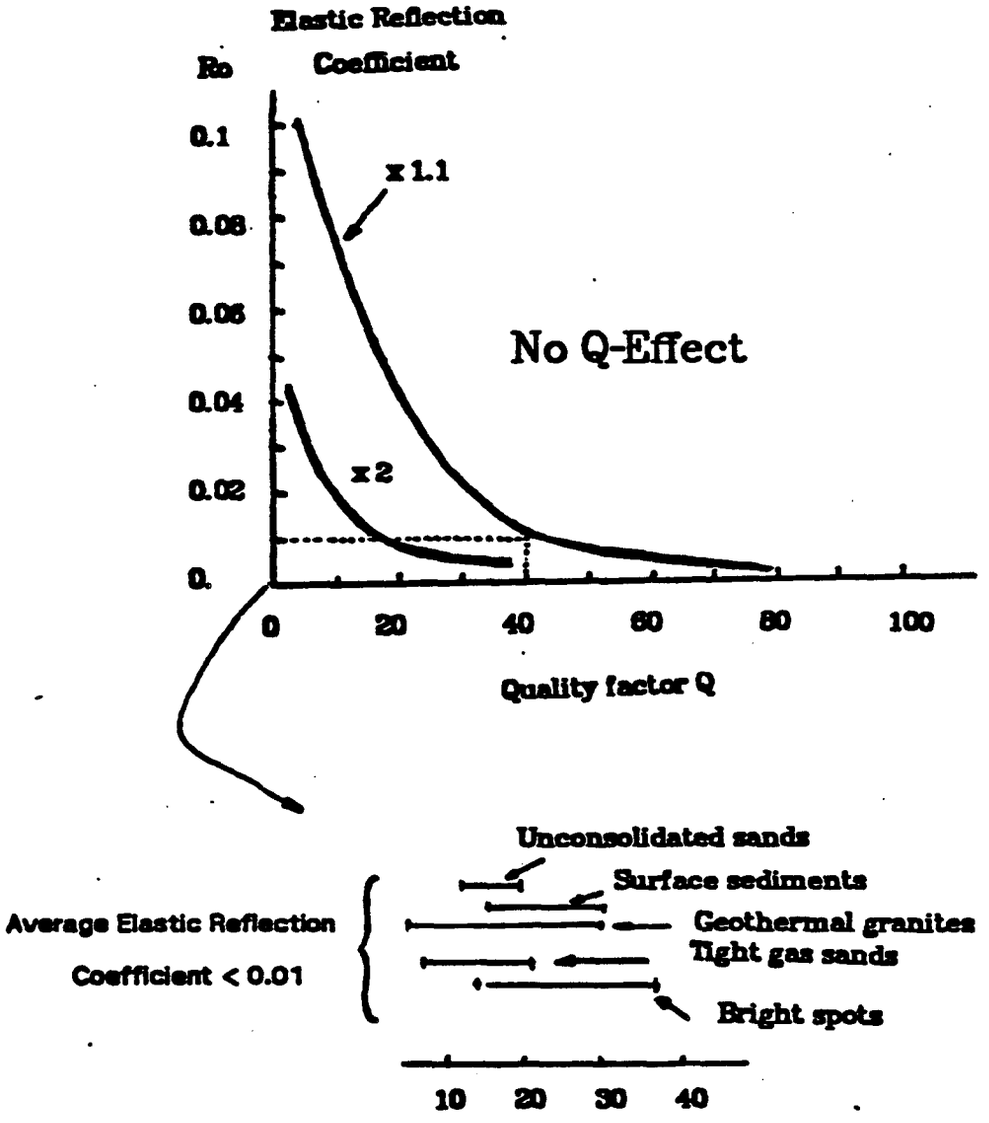

FIG. 3-21b. Schematic diagram showing zones with attenuation effect on the amplitude of the reflected wave. The multiplicative factors 1.1 and 2 indicate the relative increase in reflected amplitude when there is attenuation. The plotted value of Q is the one of the most attenuating medium constituting the interface. The second Q value is then considered to be infinite compare to the plotted one.

$$y(t) = s(t) * r_\vartheta(t) \tag{3.1.18}$$

or in the frequency domain

$$Y(\omega) = S(\omega)\, R_\vartheta(\omega) \tag{3.1.19}$$

In these equations ϑ represent the angle of incidence.

In the frequency domain, the general 2-D reflection coefficient is a function of ω the frequency and of k_x the horizontal wave number; therefore we have:

$$sin(\vartheta) = \frac{vk_x}{\omega} \tag{3.1.20}$$

we also know that in the elastic case the reflection coefficient is only a function of the ratio $\frac{k_x}{\omega}$, that is to say $sin(\vartheta)$ in the attenuating case, supposing an homogeneous medium, we can write

$$R(\omega,k_x) = R(\omega,\vartheta) = R_\vartheta(\omega)$$

The theoretical expression of $R(\omega,k_x)$ was determined by employing the equations derived in chapters I and II and using constant-Q model.

To generate the synthetics we used the same procedure as in the previous paragraph.

The results are shown, for the silicon rubber, in Figures 3-22, 3-23. Different observations are made:

-All the synthetics have been generated with a slightly larger velocity than the center value of the one measured giving a theoretical elastic reflection coefficient of 0.0048 instead of 0.0040 as listed in Table III-1.

-For an angle of 7.5^0, which is the smallest value we can obtain with our set-up, the agreement between the simulated and the experimental signals is good. Nevertheless we see that the third and the fourth peaks of the signal are too high in the synthetic example but that the average amplitudes are well reconstructed by the simulated signal.

-For an angle of 10^0 the same observations may be made.

-The value of 15^0 angle is interesting for the experimental signal because it shows that the 180^0 phase shift is not finished: there is a small negative peak before the first big one. One can see that this is well simulated by the synthetic example. Again the amplitudes are well reconstructed

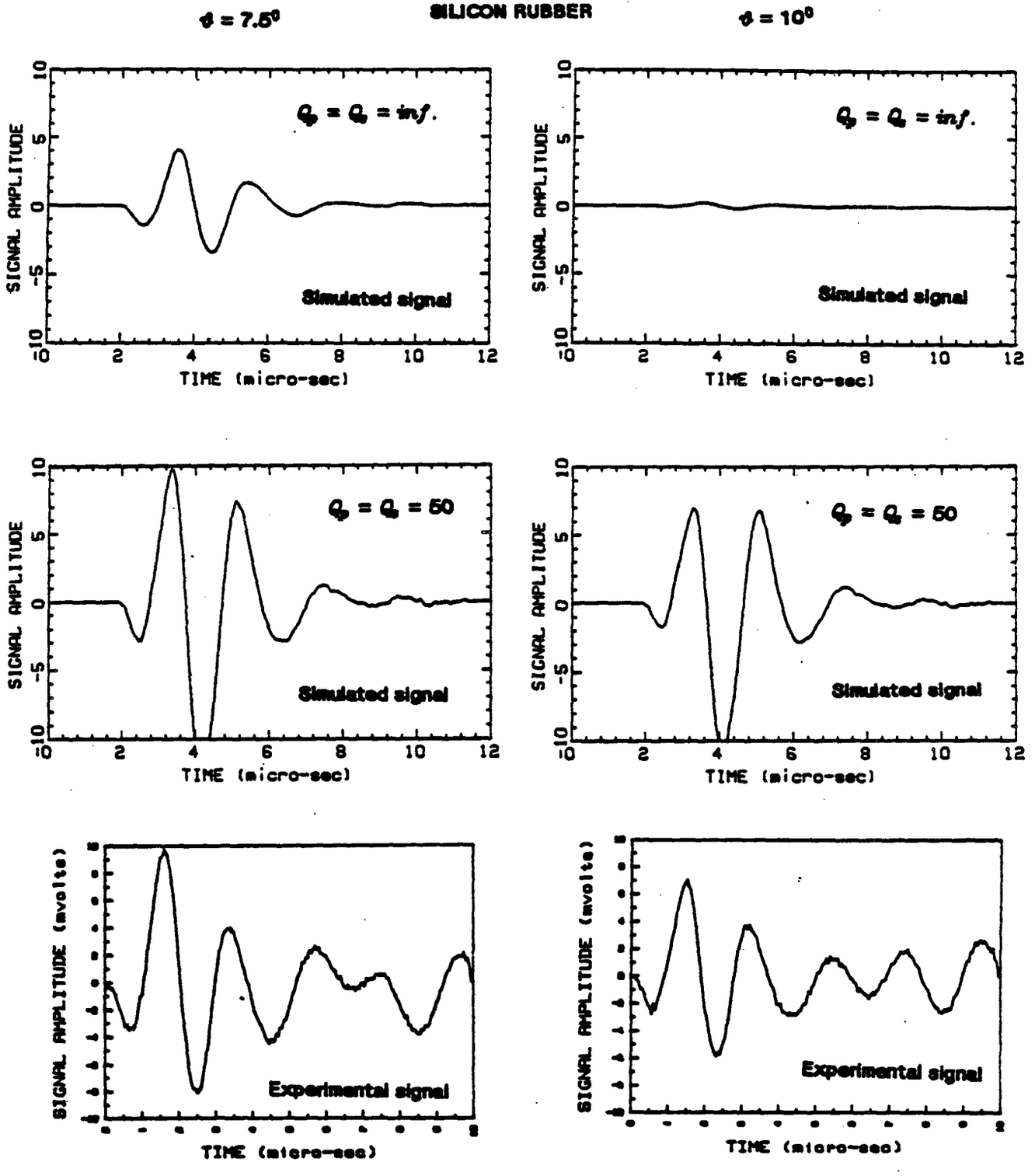

Fig.3-22 Comparison of simulated and experimental signals for different angles of incidence.The parameters of the second medium used for simulation are $\rho = 1.505 g/cc$, $V_p = 996 m/s$ and $V_s = 341 m/s$

No attenuation in the first medium

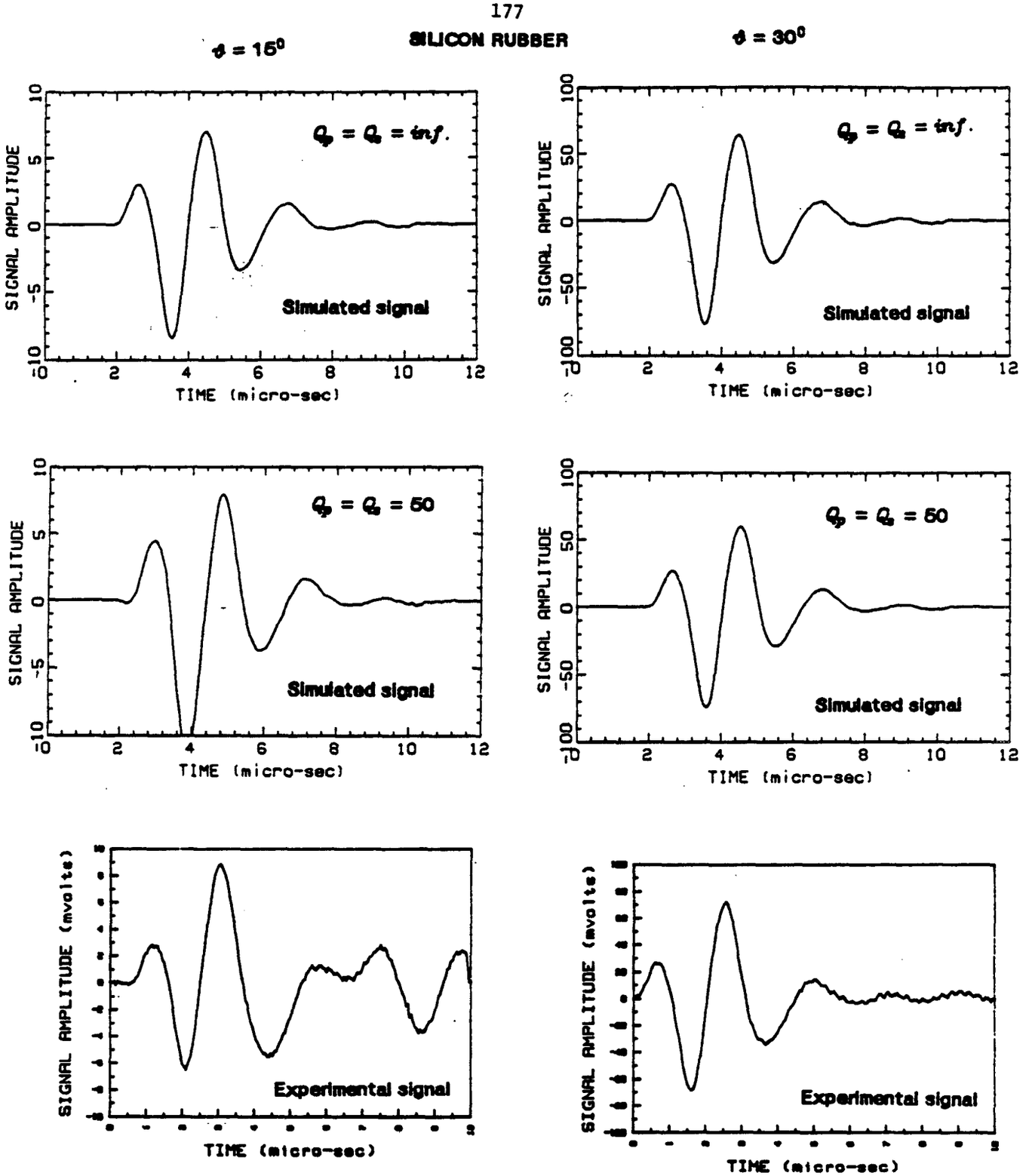

Fig.3-23 Comparison of simulated and experimental signals for different angles of incidence.The parameters of the second medium used for simulation are $\rho = 1.505 g/cc$, $V_p = 996 m/s$ and $V_s = 341 m/s$

No attenuation in the first medium

except for the observation on the amplitude of certain peaks.

-For the angle of 30^0 the effect of attenuation has nearly disappeared and the agreement is very good with both synthetics as well shown in the theoretical reflection coefficient curve (Figure 3-15).

This last point may give us a clue as to decide whether or not we are in the presence of an attenuation effect in seismic exploration: the first offsets should show an effect that the larger ones should not have.

VI-CONCLUSIONS

As previously stated, in this experiment it was impossible to use rock samples:

-Their acoustic impedance with respect to water is too large.

-The grain size and the surface roughness are too important with respect to the wave-lengths used in the laboratory.

On another hand it is very difficult to create an earth-like interface in terms of acoustic impedance contrast: as soon as we go to very small values the needed accuracy on the measurements of densities and velocities become very critical.

Nevertheless we have been able to show the following results:

-When there is an effect of Q-contrast on reflections it is exclusively an amplitude effect.

-This Q-contrast effect appears in laboratory observations when the elastic reflection coefficient is very small, at least < 0.1. In the earth we deal with reflection coefficient of 0.01; therefore the effect should be strong as soon as the quality factor is small enough ($\leq 60-70$).

-A significant attenuation is needed to see this effect. In the laboratory where elastic coefficients are still comparatively large (of the order of 0.05), we need a Q of 15 or less. In the earth where elastic coefficients are much smaller (on the order of 0.005), the quality factor Q can be greater and still create an important effect.

-The attenuation effect on reflections is angle dependent and dies out for angles greater than 20^0-30^0.

-The constant-Q model is a good model to use to simulate the effects we may encounter in reality.

REFERENCES

Borcherdt R.D, 1977, Reflection and refraction of typeII S-waves in elastic and anelastic medium. Bull.Seism.Soc.of Am., 67, 43-67.

Brennan B.J, Smylie D.E, 1981, Linear viscoelasticity and dispersion in seismic wave propagation, Rev.Geoph. and Space Phys., 19, 233-246.

Červeny V, Molotkov I.A, Pšenčik I, 1977, *Ray method in seismology*, Univ.Karlova, Praha, Tchecoslovaquia, 190-193.

Claerbout J, Kjartansson E, 1979, Powers of causal operators.Stanford Exploration Project, 16, 131-140.

Hartmann B, 1972, Ultrasonic hysteresis absorption in polymers, J.Ap.Phys., 43, 4304-4308

Hartmann B, 1974, Immersion apparatus for ultrasonic measurements in polymers, J.Ac.Soc.Am., 56, 1469-1482.

Kjartansson E, 1979, Attenuation of seismic waves in rocks, PhD Thesis, Stanford Univ., Calif.

Kjartansson E, 1979, Constant-Q, Wave propagation and attenuation, Jr Geoph.Res., 84, 3737-3748.

Kolsky H, 1956, The propagation of stress pulses in viscoelastic solids, Phys Mag., 1, 693-710.

Toksöz M.N, Johnston D.H, Timur A., 1979, Attenuation of seismic waves in dry and saturated rocks: I-Laboratory measurements, Geoph., 44, 681-690.

Winkler K, 1979, The effects of pore fluids and frictional sliding on seismic attenuation, PhD thesis, Stanford Univ., Calif.

ANNEX A

DEFINITIONS

AND

MEASUREMENTS OF Q

ANNEX A
DEFINITIONS AND MEASUREMENTS OF Q

1 - Definitions

Attenuation in a given medium is generally defined, for practical purposes, with respect to what is called the quality factor Q.

This term is not very clear since every author has derived his own definition! [O'Connell and Budiansky 1978]. All these definitions are not equivalent. However, for low attenuations, *i.e* quality factors Q of 10 or larger, there is no real discrepancy.

The different definitions depend on the way the author has studied the attenuation effect.

Using forced oscillations during loading, Q is defined by

$$Q = \frac{4\pi E_{av.}^{stored}}{\Delta W}$$

where

$E_{av.}^{stored}$ = Average stored energy during a cycle of loading.

ΔW = Energy dissipated per cycle of forced oscillations.

One can also define Q in the following way:

$$Q = \frac{2\pi E_{peak}^{stored}}{\Delta W}$$

where

E_{peak}^{stored} = Maximum value of the elastic energy stored during a cycle of loading.

Using traveling waves, one could define Q by

$$Q = \frac{2\pi T_{max}}{\Delta T_{max}}$$

where

T_{max} = Peak kinetic energy density at a given point.

ΔT_{max} = Drop in T_{max} over one spatial wavelength.

If studying resonating systems one can use the width of the resonance peak and define Q as the following :

$$Q = \frac{\omega}{\Delta\omega}$$

where

ω = Resonating frequency.

$\Delta\omega$ = Width of the resonance peak at one half the maximum power.

Or if looking at the decay of the resonance after switching off the driving force

$$Q = \frac{\omega}{2\varepsilon}$$

where

ω = Resonating frequency.

ε = Exponent of the decaying time exponential representing the signal.

Other parameters have been defined that are related to Q. A non exhaustive list is given here

α = Attenuation coefficient (in nepers/unit-length).

$$\alpha = \frac{\pi f}{QV}$$

α can be given also in decibels / unit length and then we have

$$\alpha_{dB/unit-length} = (20 \log_{10} e)\alpha_{neper/unit-length} = 8.686\alpha$$

Another useful parameter is:

γ = Characterizes the decay in amplitude of a single peak of a traveling plane wave

and

$$\gamma = \frac{\alpha x}{t} = \alpha V = \frac{\pi f}{Q}$$

Often also one speaks in terms of Logarithmic decrement.This is:

$$\delta = \log \frac{A_1}{A_2}$$

where A_1 and A_2 are successive peaks of a traveling plane wave.

We have also

$$\delta = \frac{\pi}{Q}$$

Very often one speaks of complex moduli, the given modulus being related to the type of wave one is looking at. If we define

$M = M_R + iM_I$ = Complex modulus

then we have

$$Q^{-1} = \frac{M_I}{M_R}$$

This is the most used formula for Q and it can be taken as a definition of Q.

Finally one can be interested in the phase lag between stress and strain.Then if we define

Φ = Phase angle between stress and strain and we have

$$\tan\Phi = \frac{1}{Q}$$

2 - Measurements

Q is measured by various techniques:

a- Pulse traveling technique

We look at a given pulse through an attenuating medium. The recorded signal is compared to the one obtained by doing the same thing through a reference sample for which there is " no attenuation". The comparison of the two power spectrum gives us the attenuation. (Toksoz and al 1979).

We have

$$\log\frac{A_1}{A_2} = (\gamma_2 - \gamma_1) + \log\frac{G_1}{G_2}$$

with

$$\gamma = \frac{\pi}{QV}$$

x = Sample thickness

G = Geometrical spreading

The slope of the straight line in the plot $\log \frac{A_1}{A_2}$ as a function of the frequency f gives us the value of $(\gamma_1 - \gamma_2)x$ from which we get the value of Q.

The problems inherent to this method are the following :

- $\log \frac{G_1}{G_2}$ is supposed to be non- frequency dependent : we need really the same geometry and a thick enough sample with respect to the wavelength of the pulse.

- The coupling between the transducers and the sample may be a problem.

b- Resonant bar methods

The rock is modeled as a simple resonating system. As already mentioned two ways of proceeding are possible

- using the width of the resonance peak; the accuracy of this measurement depends on the amplitude of the attenuation and on the order of the harmonics used (see ANNEX B).

- using the decaying exponential obtained by switching off the driving force at the resonance frequency. Again, the accuracy depends on the amplitude of the attenuation and on the order of the harmonic used.

c- Torsional pendulum

This method is similar to the last one. Instead of resonating a bar we apply a torque to a bar and look at the resonances.

d- Phase lag measurements

This method is very difficult, because it must be extremely accurate. J.Spencer (1981) has made work. It uses the formula already given:

$$\tan\Phi = \frac{1}{Q}$$

Φ = Phase lag between stress and strain

The main problem with this method is the high degree of accuracy needed on the measurements. It has the advantage of using very low frequencies similar to seismic ones.

ANNEX B

ACCURACY OF Q MEASUREMENTS IN THE LABORATORY

RESONANT BAR METHOD

ANNEX B
THE RESONANT PEAK METHOD : ITS ACCURACY FOR HIGH ATTENUATION

1 - INTRODUCTION

Single resonating systems are generally modeled by damped harmonic oscillators. This is a very good model for low attenuation and low harmonics.

For high attenuation and high harmonics, this method fails, because modeling the system as a damped harmonic oscillator does not take into account the interferences between the different normal modes of vibration.

Our approach is more general modeling the resonant bar as a linear viscoelastic medium, a medium responding linearly to an applied load and having a time-dependent relationship between stress and strain.

Our goal is to study the peak of resonance and its width as a function of $Q = \frac{M_R}{M_I}$, the attenuation and to compare the result obtained by this method to the one generally used in laboratory experiments (Winkler 1979).

2 - EXPERIMENT

The experiment is sketched in Figure A-1 . The bar is set on a support at its middle. It is driven constantly at one extremity by a sinusoidal force of amplitude q_0 and frequency ω_1. The origin of the x-axis is taken at the end where the driving force is applied. The length of the sample is L. The displacement at $x = \frac{L}{2}$ is 0 by construction of the apparatus: it is a node of displacement.

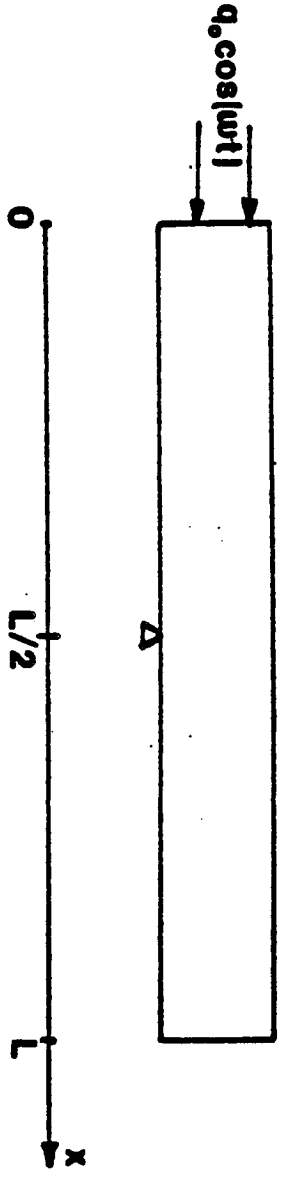

Fig.A-1 Schematic representation of the resonant bar experiment

2 - a. Equation of vibration

By applying the fundamental law of mechanics,we get

$$\rho \frac{\partial^2 U}{\partial t^2} = \frac{\partial \sigma(x,t)}{\partial x} + q_o \delta(x) \cos\omega_o t \qquad \text{(B-1)}$$

$\sigma(x,t)$ being the stress and $U(x,t)$ the displacement. As we have a linear viscoelastic medium we can write

$$\sigma(x,t) = m(t) * \varepsilon(x,t) = m(t) * \frac{\partial U(x,t)}{\partial x} \qquad \text{(B-2)}$$

with $m(t)$ = elastic modulus of the sample.

By combining equations (B-1) and (B-2), we obtain

$$\rho \frac{\partial^2 U}{\partial t^2} = m(t) * \frac{\partial^2 U}{\partial x^2} + q_o \delta(x) \cos\omega_o t \qquad \text{(B-3)}$$

In fact, this equation is not very practical and we are going to use a complex version of (B-3):

$$\rho \frac{\partial^2 V}{\partial t^2} = m(t) * \frac{\partial^2 V}{\partial x^2} + q_o \delta(x) e^{i\omega_o t} \qquad \text{(B-3')}$$

and $U(x,t)$ is given by

$$U(x,t) = Re[V(x,t)]$$

The time-part of (B-3') can be solved easily and gives us

$$V(x,t) = u(x) e^{i\omega_o t}$$

By Fourier transforming (B-3') we obtain :

$$M(\omega) \frac{d^2 u}{dx^2} \delta(\omega - \omega_o) + \rho\omega_o^2 u(x) \delta(\omega - \omega_o) + q_o \delta(x) \delta(\omega - \omega_o) = 0$$

or

$$M(\omega) \frac{d^2 u}{dx^2} + \rho\omega^2 u + q_o \delta(x) = 0 \qquad \text{(B-4)}$$

with

$M(\omega)$ = Fourier transform of the elastic modulus

ω= frequency at which the bar is driven.

If we know the solution of (B-4) , $U(x,t)$ is then given by

$$U(x,t) = Re[u(x)]\cos\omega t - Im[u(x)]\sin\omega t$$

And its maximum value is

$$|\ \max value\ U(x,t)\ | = |u(x)|$$

2 - b. Solution of equation (B-4)

We develop $u(x)$ on the normal modes. If $u_n(x)$ is a normal mode it is solution of

$$M_0\frac{d^2u_n}{dx^2} + \rho\omega^2 u_n = 0 \qquad \text{(B-5)}$$

with the boundary conditions

$$u_n(0) = u_{0n}$$

$$u_n(L) = -u_{0n}$$

and M_0 = elastic modulus of the sample without damping [$=M(\infty)$] .

From equation (B-5) and the boundary conditions we get

$$u_n(x) = u_{0n}\cos[\omega_n\sqrt{\frac{\rho}{M_0}}x]$$

with

$$\omega_n = \frac{(2n+1)\pi}{L}\sqrt{\frac{M_0}{\rho}}$$

We look for the solution $u(x)$ as a development along the normal modes,

$$u(x) = \sum_{n=0}^{\infty} a_n u_n(x) \qquad \text{(B-6)}$$

with

$$u_n(x) = \cos[\omega_n\sqrt{\frac{\rho}{M_0}}x]$$

By multiplying (B-4) by $u_n(x)$,integrating over x and plugging for $u(x)$ the development (B-

6),we obtain

$$M(\omega)\sum_{p=0}^{\infty}a_p\int\frac{d^2u_p}{dx^2}u_n\,dx+\rho\omega^2\sum_{p=0}^{\infty}a_p\int u_p u_n\,dx+q_0=0$$

By using the orthogonality of normal modes $\left[\int u_n u_p\,dx=\frac{L}{2}\delta_{np}\right]$ and by replacing $\frac{d^2u_p}{dx^2}$ by $-\rho\omega_p^2\frac{u_p}{M_0}$ we obtain

$$a_n\rho\frac{L}{2}\left[\omega^2-\frac{M(\omega)}{M_0}\omega_n^2\right]+q_0=0$$

This gives

$$a_n=\frac{2q_0M_0}{\rho L[M(\omega)\omega_n^2-M_0\omega^2]}=\frac{u_0}{M(\omega)\omega_n^2-M_0\omega^2}$$

And so

$$u(x)=u_0\sum_{n=0}^{\infty}\frac{u_n(x)}{M(\omega)\omega_n^2-M_0\omega^2} \qquad \text{(B-6b)}$$

3 - CALCULATION OF THE MODULUS OF $u(x)$ AND OF THE HALF-WIDTH OF THE RESONANT PEAK

Let us look at what happens at the end $x=L$ .There we have $u_n(x)=-1$ for every n, while in equation (B-6b), u_0 is a scaling factor that we make equal to 1 for simplicity. This gives

$$u_R(x)=-\sum_{n=0}^{\infty}\frac{M_R(\omega)\omega_n^2-M_0\omega^2}{[M_R(\omega)\omega_n^2-M_0\omega^2]^2+M_I^2\omega_n^4}$$

and

$$u_I(x)=\sum_{n=0}^{\infty}\frac{M_I(\omega)\omega_n^2}{[M_R(\omega)\omega_n^2-M_0\omega^2]^2+M_I^2\omega_n^4}$$

with the subscript R indicating the real part and the subscript I the imaginary part.

The experiment consists of driving the sample at different frequencies, so that one of the modes is more particularly excited.

To excite preferentially the mode n ,the frequency we must use is given by the formula

$$M_R(\omega) = M_0 \frac{\omega^2}{\omega_n^2}$$

At this frequency the denominator of $u(x)$ will be the smallest possible and so this mode is the main contribution to the peak amplitude.

If we excite the mode $(2p+1)$,the resonant frequency ω_0 is given by

$$M_R(\omega_0) = M_0 \frac{\omega_0^2}{\omega_p^2}$$

with

$$\omega_p^2 = (2p+1)^2\omega_p^2=0$$

3 - a. Modulus of $u(L)$

We have

$$M_R(\omega_0)\omega_n^2 - M_0\omega_0^2 = M_0\omega_0^2\left[\frac{(2n+1)^2}{(2p+1)^2} - 1\right] = \frac{4M_0\omega_0^2}{(2p+1)^2}(n-p)(n+p+1)$$

$$M_I(\omega_0)\omega_n^2 = M_I\omega_0^2\frac{(2n+1)^2}{(2p+1)^2} = \frac{M_0\omega_0^2}{Q}\left[\frac{2n+1}{2p+1}\right]$$

If we define Q by

$$Q = \frac{M_R(\omega_0)}{M_I(\omega_0)} = \frac{M_{R0}}{M_{I0}}$$

We can write

$$u_R(L) = -\sum_{n=0}^{\infty} A_n = -\sum_{\substack{n=0 \\ n\neq p}}^{\infty} A_n - A_p$$

$$u_I(L) = \sum_{n=0}^{\infty} B_n = -\sum_{\substack{n=0 \\ n\neq p}}^{\infty} B_n - B_p$$

with

$$A_n = \frac{M_R(\omega_0)\omega_n^2 - M_0\omega_0^2}{[M_R(\omega_0)\omega_n^2 - M_0\omega_0^2]^2 + M_I^2(\omega_0)\omega_n^4}$$

$$B_n = \frac{M_I(\omega_0)\omega_n^2}{[M_R(\omega_0)\omega_n^2 - M_0\omega_0^2]^2 + M_I^2(\omega_0)\omega_n^4}$$

and this whatever n.

We have by definition of ω_0 , $A_p = 0$.

A_n can be written

$$A_n = \frac{1}{M_R(\omega_0)\omega_n^2 - M_0\omega_0^2}\left[1 + \frac{M_I^2(\omega_0)\omega_n^4}{[M_R(\omega_0)\omega_n^2 - M_0\omega_0^2]^2}\right]^{-1} \qquad n \neq p$$

$$A_n \approx \frac{1}{M_R(\omega_0)\omega_n^2 - M_0\omega_0^2}\left[1 - \frac{M_I^2(\omega_0)\omega_n^4}{[M_R(\omega_0)\omega_n^2 - M_0\omega_0^2]^2}\right]$$

$$A_n \approx \frac{(2p+1)^2}{4M_0\omega_0^2(n-p)(n+p+1)}\left[1 - \frac{C}{Q^2}\right]$$

In this expression C is a constant with respect to n .

This implies

$$\sum_{\substack{n=0 \\ n \neq p}}^{\infty} A_n \approx \frac{1}{4M_0\omega_0^2} + C\frac{'}{Q^2}$$

(cf Appendix A)

And so

$$u_R^{\omega_0}(L) \approx \frac{-1}{4M_0\omega_0^2} + \frac{C}{Q^2}$$

We have also

$$B_p = \frac{1}{M_I(\omega_0)\omega_p^2} = \frac{Q}{M_0\omega_0^2}$$

As A_n,B_n can be written

$$B_n = \frac{M_I(\omega_0)\omega_n^2}{\left[M_R(\omega_0)\omega_n^2 - M_0\omega_0^2\right]^2}\left[1 + \frac{M_I^2(\omega_0)\omega_n^4}{[M_R(\omega_0)\omega_n^2 - M_0\omega_0^2]^2}\right]^{-1} \qquad n \neq p$$

$$B_n \approx \frac{M_I(\omega_0)\omega_n^2}{[M_R(\omega_0)\omega_n^2 - M_0\omega_0^2]^2}\left[1 - \frac{C}{Q^2}\right]$$

$$B_n \approx \frac{(2n+1)^2(2p+1)^2}{16QM_0\omega_0^2(n-p)^2(n+p+1)^2}\left[1 - \frac{C}{Q^2}\right]$$

This implies

$$\sum_{\substack{n=0\\ n\neq p}}^{\infty} B_n \approx \frac{(2p+1)^2}{16QM_0\omega_0^2}\left[\frac{\pi^2}{3}+\frac{1}{(2p+1)^2}\right]+\frac{C''}{Q^2}$$

(cf Appendix A)

Or

$$u_f^{\omega_0}(L) \approx \frac{Q}{M_0\omega_0^2}+\frac{(2p+1)^2}{16QM_0\omega_0^2}\left[\frac{\pi^2}{3}+\frac{1}{(2p+1)^2}\right]+\frac{C''}{Q^2}$$

So finally we get

$$|u|^2_{\omega_0}=u_f^2+u_R^2=\frac{Q^2}{M_0^2\omega_0^4}\left[1+\frac{(2p+1)^2}{16Q^2}\left[\frac{2\pi^2}{3}+\frac{3}{(2p+1)^2}\right]+\frac{K}{Q^2}\right]$$

The values obtained for the different harmonics are

First harmonic $$|u|^2_{\omega_0}=\frac{Q^2}{M_0^2\omega_0^4}\left[1+\frac{0.6}{Q^2}+....\right]$$

Third harmonic $$|u|^2_{\omega_0}=\frac{Q^2}{M_0^2\omega_0^4}\left[1+\frac{3.68}{Q^2}+....\right]$$

Fifth harmonic $$|u|^2_{\omega_0}=\frac{Q^2}{M_0^2\omega_0^4}\left[1+\frac{10.47}{Q^2}+....\right]$$

Seventh harmonic $$|u|^2_{\omega_0}=\frac{Q^2}{M_0^2\omega_0^4}\left[1+\frac{20.34}{Q^2}+....\right]$$

Already we see that higher the harmonic ,worst the accuracy on the peak displacement.

3 – b. Half–width frequencies

We define the half width frequencies as the frequencies ω_+ and ω_- (see also Figure A-2):

$$|u|^2_{\omega_\pm}=\frac{|u|^2_{\omega_0}}{2}$$

At a first order we know that (O'Connell and Budiansky 1978)

$$\omega^2_{\omega_\pm}=\omega_0^2\left[1+\frac{\varepsilon}{Q}\right]$$

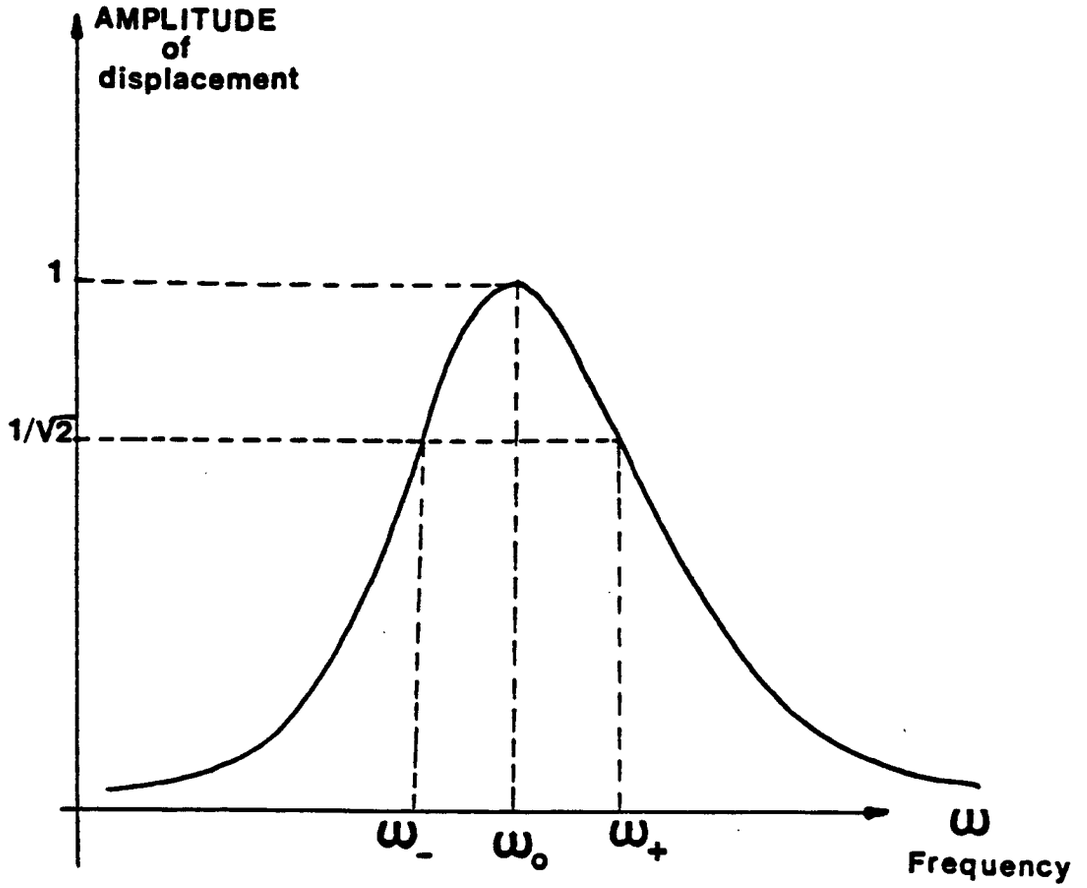

$$\text{HALF-WIDTH} = \Delta = \frac{\omega_o^2}{\omega_+^2 - \omega_-^2}$$

Fig.A-2 Resonant peak definitions

In this formula

$$\varepsilon = +1 \quad \text{for } \omega_+$$

$$\varepsilon = -1 \quad \text{for } \omega_-$$

As we are looking at secondary effect, we must look at the dependence of $\omega_\pm$ as a function of $(\frac{1}{Q})^k$. We write

$$\omega_\pm^2 = \omega_0^2[1 + \frac{\varepsilon}{Q} + \frac{\alpha_\pm}{Q^2} + \frac{\delta_\pm}{Q^3} + \ldots] \tag{B-7}$$

We must also consider the dispersion relations. If $M_R(\omega)$ and $M_I(\omega)$ are derivable functions of ω, we have

$$M_R(\omega_\pm) = M_{RO} + (\omega_\pm - \omega_0)\frac{dM_R}{d\omega}\Big|_{\omega=\omega_0} + \frac{(\omega_\pm - \omega_0)^2}{2}\frac{d^2M_R}{d\omega^2}\Big|_{\omega=\omega_0} + \frac{(\omega_\pm - \omega_0)^3}{6}\frac{d^3M_R}{d\omega^3}\Big|_{\omega=\omega_0} + \cdots$$

$$M_I(\omega_\pm) = M_{IO} + (\omega_\pm - \omega_0)\frac{dM_I}{d\omega}\Big|_{\omega=\omega_0} + \frac{(\omega_\pm - \omega_0)^2}{2}\frac{d^2M_I}{d\omega^2}\Big|_{\omega=\omega_0} + \frac{(\omega_\pm - \omega_0)^3}{6}\frac{d^3M_I}{d\omega^3}\Big|_{\omega=\omega_0} + \cdots$$

Equation (B-7) gives

$$\omega_\pm = \omega_0\left[1 + \frac{\varepsilon}{2Q} + \frac{1}{2Q^2}(\alpha_\pm - \frac{1}{4}) + \frac{1}{2Q^3}(\frac{\varepsilon}{8} - \frac{\alpha_\pm\varepsilon}{2} + \delta_\pm)\right]$$

So we can rewrite $M_R(\omega_\pm)$ and $M_I(\omega_\pm)$ in the following form

$$M_R(\omega_\pm) = M_{RO}\,[\,1 + \frac{\beta_1^\pm}{Q} + \frac{\beta_2^\pm}{Q^2} + \frac{\beta_3^\pm}{Q^3} + \cdots\,]$$

$$M_I(\omega_\pm) = M_{IO}\,[\,1 + \frac{\gamma_1^\pm}{Q} + \frac{\gamma_2^\pm}{Q^2} + \frac{\gamma_3^\pm}{Q^3} + \cdots\,]$$

with

$$\beta_1^\pm = \pm\frac{\omega_0}{2M_{RO}}\frac{dM_R}{d\omega}\Big|_{\omega=\omega_0}$$

$$\gamma_1^\pm = \frac{\omega_0}{2M_{IO}}\frac{dM_I}{d\omega}\Big|_{\omega=\omega_0}$$

$$\beta_2^\pm = \frac{\omega_0}{2M_{RO}}\left[(\alpha_\pm - \frac{1}{4})\frac{dM_R}{d\omega}\Big|_{\omega=\omega_0} + \frac{\omega_0}{4}\frac{d^2M_R}{d\omega^2}\Big|_{\omega=\omega_0}\right]$$

$$\gamma_2^\pm = \frac{\omega_0}{2M_{IO}}\left[(\alpha_\pm - \frac{1}{4})\frac{dM_I}{d\omega}\Big|_{\omega=\omega_0} + \frac{\omega_0}{4}\frac{d^2M_I}{d\omega^2}\Big|_{\omega=\omega_0}\right]$$

$$\beta_3^{\pm} = \pm\frac{\omega_o}{2M_{RO}}\left[\left(\frac{1}{8} - \frac{\alpha_\pm}{2} \pm \delta_\pm\right)\frac{dM_R}{d\omega}\Big|_{\omega=\omega_o}\right. \qquad \text{(B-8)}$$

$$\left. + \frac{\omega_o}{4}(2\alpha_\pm - \frac{1}{2})\,\frac{d^2M_R}{d\omega^2}\Big|_{\omega=\omega_o} + \frac{\omega_o^2}{24}\frac{d^3M_R}{d\omega^3}\Big|_{\omega=\omega_o}\right]$$

$$\gamma_3^{\pm} = \pm\frac{\omega_o}{2M_{IO}}\left[\left(\frac{1}{8} - \frac{\alpha_\pm}{2} \pm \delta_\pm\right)\frac{dM_I}{d\omega}\Big|_{\omega=\omega_o}\right.$$

$$\left. + \frac{\omega_o}{4}(2\alpha_\pm - \frac{1}{2})\,\frac{d^2M_I}{d\omega^2}\Big|_{\omega=\omega_o} + \frac{\omega_o^2}{24}\frac{d^3M_I}{d\omega^3}\Big|_{\omega=\omega_o}\right]$$

With all these relations, we are ready to develop $u_R^{\omega\pm}(L)$ and $u_I^{\omega\pm}(L)$.

In the following equations we simplify the notations by not writing the ± subscript, which are restored at the end of the calculus.

With these notations, we have

$$M_R(\omega)\omega_n^2 - M_0\omega^2 = M_0\omega_0^2\left\{\frac{4(n-p)(n+p+1)}{(2p+1)^2} + \frac{1}{Q}\left[\beta_1\left[\frac{2n+1}{2p+1}\right]^2 - \varepsilon\right] + \right.$$

$$\left.\frac{1}{Q^2}\left[\beta_2\left[\frac{2n+1}{2p+1}\right]^2 - \alpha\right] + \frac{1}{Q^3}\left[\beta_3\left[\frac{2n+1}{2p+1}\right]^2 - \delta\right]\right\}$$

$$M_I(\omega)\omega_n^2 = M_o\,\frac{\omega_o^2}{Q}\left[\frac{2n+1}{2p+1}\right]^2\left[1 + \frac{\gamma_1}{Q} + \frac{\gamma_2}{Q^2} + \frac{\gamma_3}{Q^3}\right]$$

As in the previous paragraph, we have

$$u_R(L) = -\sum_{\substack{n=0\\ n\neq p}}^{\infty} A_n - A_p$$

$$u_I(L) = \sum_{\substack{n=0\\ n\neq p}}^{\infty} B_n + B_p$$

We find

$$A_p = \frac{Q}{M_o\omega_o^2}\,\frac{\beta_1 - \varepsilon}{1 + (\beta_1 - \varepsilon)^2}\left[1 + \frac{1}{Q}\left[\frac{\beta_2 - \alpha}{\beta_1 - \varepsilon} - \frac{2\gamma_1 + 2(\beta_2 - \alpha)(\beta_1 - \varepsilon)}{(\beta_1 - \varepsilon)^2 + 1}\right] + \frac{d}{Q^2}\right]$$

$$A_n = \frac{(2p+1)^2}{4M_0\omega_0^2(n-p)(n+p+1)} + \frac{d_1}{Q}$$

And it implies

$$\sum_{\substack{n \neq p \\ n=0}}^{\infty} A_n = \frac{1}{4M_0\omega_0^2} + \frac{d_2}{Q}$$

(cf. Appendix A)

So

$$u_\beta^{\mu}(L) = -\frac{Q}{M_0\omega_0^2}\frac{\beta_1 - \varepsilon}{(1+(\beta_1-\varepsilon)^2)} - \frac{1}{M_0\omega_0^2}\left[\frac{1}{4} + \frac{\beta_1-\varepsilon}{(1+(\beta_1-\varepsilon)^2)}\left[\frac{\beta_2-\alpha}{\beta_1-\varepsilon} - \frac{2\gamma_1 + 2(\beta_2-\alpha)(\beta_1-\varepsilon)}{(1+(\beta_1-\varepsilon)^2)}\right]\right] - \frac{d_3}{Q}$$

$$B_P = \frac{Q}{M_0\omega_0^2}\frac{1}{(1+(\beta_1-\varepsilon)^2)}\left[1 + \frac{1}{Q}\left[\gamma_1 - \frac{2\gamma_1 + 2(\beta_2-\alpha)(\beta_1-\varepsilon)}{(1+(\beta_1-\varepsilon)^2)}\right] + \frac{f}{Q^2}\right]$$

$$B_n = \frac{f_1}{Q}$$

It implies

$$\sum_{\substack{n \neq p \\ n=0}}^{\infty} B_n = \frac{f_2}{Q}$$

So

$$u_f^{\mu}(L) = \frac{Q}{M_0\omega_0^2}\frac{1}{(1+(\beta_1-\varepsilon)^2)} + \frac{1}{M_0\omega_0^2}\frac{1}{(1+(\beta_1-\varepsilon)^2)}\left[\gamma_1 - \frac{2\gamma_1 + 2(\beta_2-\alpha)(\beta_1-\varepsilon)}{(1+(\beta_1-\varepsilon)^2)}\right] + \frac{f_3}{Q}$$

As

$$|u|_\omega^2 = u_f^2 + u_\beta^2 = \frac{|u|_{\omega_0}^2}{2}$$

By equating the constant terms, we get

$$\frac{1}{(1+(\beta_1-\varepsilon)^2)} = \frac{1}{2}$$

which implies

$$\beta_1 = 0 \qquad \text{(B-9)}$$

For the terms in $\frac{1}{Q}$, we get

$$-2\gamma_1 - \varepsilon + 2\varepsilon(\beta_2 - \alpha) = 0$$

$$\alpha = \beta_2 - \varepsilon\gamma_1 - \frac{1}{2}$$

which is equivalent to

$$\alpha_+ = \beta_2^+ - \gamma_1^+ - \frac{1}{2}$$

$$\alpha_- = \beta_2^- + \gamma_1^- - \frac{1}{2}$$

System (B-8) and Equation (B-9) show that

$$\beta_2^+ = \beta_2^- \qquad \gamma_1^+ = -\gamma_1^-$$

And then we have

$$\alpha_{+=}\alpha_{-=}\alpha = \frac{\omega_o^2}{8M_{RO}}\frac{d^2M_R}{d\omega^2}\Big|_{\omega=\omega_o} - \frac{\omega_o}{2M_{IO}}\frac{dM_I}{d\omega}\Big|_{\omega=\omega_o} \qquad \text{(B-10)}$$

To have the dependence of the peak width as a function of Q, we must go one step further and calculate the terms $d, d_1, \cdots$

To do that we use the two relations we have already derived:

$$\beta_1 = 0$$

$$\alpha = \beta_2 - \varepsilon\gamma_1 - \frac{1}{2}$$

This gives

$$A_p = -\frac{\varepsilon Q}{2M_0\omega_0^2}\left[1 - \frac{\gamma_1}{Q} - \frac{1}{Q^2}(\gamma_2 + \gamma_1^2 + \varepsilon\gamma_1 + \frac{1}{8})\right]$$

$$A_n = \frac{(2p+1)^2}{4M_0\omega_0^2(n-p)(n+p+1)}\left[1 + \frac{\varepsilon(2p+1)^2}{4Q(n-p)(n+p+1)}\right] \qquad n \neq p$$

$$\sum_{\substack{n\neq p \\ n=0}}^{\infty} A_n = \frac{1}{4M_0\omega_0^2}\left[1 + \frac{\varepsilon}{4Q}\left(\frac{\pi^2}{3}(2p+1)^2 - 3\right)\right]$$

(cf Appendix A)

$$u_R(L) = -\frac{\varepsilon Q}{2M_0\omega_0^2}\left[1 - \frac{1}{Q}(\gamma_1 + \frac{\varepsilon}{2}) + \frac{1}{Q^2}\left[\frac{1}{4} - \frac{\pi^2}{24}(2p+1)^2 - \varepsilon\gamma_1 - \gamma_1^2 - \gamma_2\right]\right]$$

And

$$B_p = \frac{Q}{2M_0\omega_0^2}\left[1+\frac{1}{Q}(\gamma_1+\frac{\varepsilon}{2})+\frac{1}{Q^2}\left[\varepsilon(\beta_3-\delta)-\gamma_1^2+\frac{1}{8}\right]\right]$$

$$B_n \approx \frac{(2n+1)^2(2p+1)^2}{16QM_0\omega_0^2(n-p)^2(n+p+1)^2}$$

This implies

$$\sum_{\substack{n=0\\ n\neq p}}^{\infty} B_n = \frac{(2p+1)^2}{16QM_0\omega_0^2}\left[\frac{\pi^2}{3}+\frac{1}{(2p+1)^2}\right]$$

Or

$$u_f(L) = \frac{Q}{2M_0\omega_0^2}\left[1+\frac{1}{Q}(\gamma_1+\frac{\varepsilon}{2})+\frac{1}{Q^2}\left[\frac{\pi^2}{24}(2p+1)^2+\frac{1}{4}-\gamma_1^2+\varepsilon(\beta_3-\delta)-\gamma_1^2+\frac{1}{8}\right]\right]$$

As $|u|^2 = u_R^2+u_I^2$ we obtain

$$|u|^2 = \frac{Q^2}{2M_0^2\omega_0^4}\left[2+\frac{2}{Q^2}\left[\frac{3}{4}-\gamma_2-\gamma_1^2\varepsilon(\beta_3-\delta)\right]\right]$$

And this must equal

$$\frac{|u|_{\omega_0}^2}{2} = \frac{Q^2}{2M_0^2\omega_0^4}\left[1+\frac{(2p+1)^2}{16Q^2}\left[2\frac{\pi^2}{3}+\frac{3}{(2p+1)^2}\right]\right]$$

We get

$$\beta_3-\delta = \varepsilon\left[\gamma_2+\gamma_1^2+(2p+1)^2\frac{\pi^2}{24}-\frac{9}{16}\right]$$

If we replace ε by its value, we get

$$\delta^+ = \beta_3^+-\left[\gamma_2^++\gamma_1^{+2}+(2p+1)^2\frac{\pi^2}{24}-\frac{9}{16}\right]$$

$$\delta^- = \beta_3^--\left[\gamma_2^-+\gamma_1^{-2}+(2p+1)^2\frac{\pi^2}{24}\frac{9}{16}\right]$$

Using system (B-8) we get

$$\beta_3^+=-\beta_3^-$$

$$\gamma_2^+=\gamma_2^-$$

$$\gamma_1^+ = -\gamma_1^-$$

And so finally we obtain

$$\delta^+ = -\delta^- = |\delta|$$

with

$$|\delta| = \left\{ \frac{\omega_o^2}{8M_{RO}} \left[(2\alpha - \frac{1}{2}) \frac{d^2 M_R}{d\omega^2}\Big|_{\omega=\omega_o} + \frac{\omega_o}{6} \frac{d^3 M_R}{d\omega^3}\Big|_{\omega=\omega_o} \right] - \frac{\omega_o}{2M_{IO}} \left[(\alpha - \frac{1}{4}) \frac{dM_I}{d\omega}\Big|_{\omega=\omega_o} + \frac{\omega_o}{4} \frac{d^2 M_I}{d\omega^2}\Big|_{\omega=\omega_o} \right] \right.$$

$$\left. - \frac{\omega_o^2}{4M_{IO}^2} \left(\frac{dM_I}{d\omega} \right)^2 \Big|_{\omega=\omega_o} + \frac{9}{16} - (2p+1)^2 \frac{\pi^2}{24} \right]$$

which can be written in the simplified form

$$|\delta| = \alpha + (2p+1)^2 \frac{\pi^2}{24}$$

In these equations α is given by equation (B-10).

The peak width being

$$\Delta = \frac{2\omega_\delta^2}{\omega_+^2 - \omega_-^2}$$

$$\Delta = \frac{Q}{1 + \frac{|\delta|}{Q^2}} = \frac{Q^3}{Q^2 + |\delta|}$$

The relation between the peak width and Q can be written

$$Q^3 - Q^2\Delta - \Delta|\delta| = 0 \qquad \text{(B-11)}$$

with

$$|\delta| = \alpha + (2p+1)^2 \frac{\pi^2}{24}$$

Experimentally, we found that even at low Q there is no real distorsion when we excite the first harmonic; we can assume the quantity " a " is a small number on the order of 1 . Then we can neglect " a " as the order of the harmonic "p" increases, and we can write Equation (B-11) in an approximate form for high harmonics (≥3):

$$Q^3 - Q^2\Delta - \Delta(2p+1)^2 \frac{\pi^2}{24} = 0$$

To see the effect of this correction factor, we can compare the Q given by this equation with the one usually taken, Δ . To see this effect we take a very low value for Δ , a very high attenuation. Using a Δ of 5, the results are shown in Table An-1.

4 - CONCLUSION

The resonant peak method of measuring attenuation is accurate when the first harmonic is used even when Q is low.For higher harmonics one should be careful and correct the raw value ,for low Q, by utilizing the formula derived in this chapter.The discrepancy between the two values will increase with increasing harmonics.

REFERENCES

O'Connell R.J.,Budiansky B.,1978,Measures of dissipation in viscoelastic media, Geoph.Res. Letters,5,5-8.

Winkler K.,1979,The effects of pore fluids and frictional sliding on seismic attenuation,PhD thesis ,Stanford Univ.,Stanford,Calif.

Table An-1

Half-Width $\Delta = 5$

Order of Harmonic	"Corrected" Value of Q
1	5.1
3	5.6
5	6.3
7	7.0
9	7.8
11	8.5
13	9.2

APPENDIX A : CALCULUS OF THE SUM OF SERIES INVOLVING INVERSE OF INTEGERS

$$1 - \sum_{\substack{n=0 \\ n\neq p}}^{\infty} \frac{1}{(n-p)(n+p+1)}$$

As

$$\frac{1}{(n-p)(n+p+1)} = \frac{1}{(2p+1)}\left[\frac{1}{n-p} - \frac{1}{n+p+1}\right]$$

And as

$$\sum_{\substack{n=0 \\ n\neq p}}^{\infty} = \sum_{n=0}^{n=p-1} + \sum_{n=p+1}^{\infty}$$

We get

$$\sum_{n=0}^{n=p-1}\left[\frac{1}{n-p} - \frac{1}{n+p+1}\right] = -\sum_{n=0}^{n=p-1}\left[\frac{1}{p-n} + \frac{1}{n+p+1}\right] = -\sum_{n=1}^{n=2p}\frac{1}{n}$$

And

$$\sum_{n=p+1}^{\infty}\left[\frac{1}{n-p} - \frac{1}{n+p+1}\right] = \sum_{n=1}^{\infty}\frac{1}{n} - \sum_{n=2p+2}^{\infty}\frac{1}{n} = \sum_{n=1}^{n=2p+1}\frac{1}{n}$$

So finally we get

$$\sum_{\substack{n=0 \\ n\neq p}}^{\infty} \frac{1}{(n-p)(n+p+1)} = \frac{1}{(2p+1)^2}$$

$$2 - \sum_{\substack{n=0 \\ n\neq p}}^{\infty} \frac{1}{(n-p)^2(n+p+1)^2}$$

As

$$\frac{1}{(n-p)^2(n+p+1)^2} = \frac{1}{(2p+1)^2}\left[-\frac{2}{(n-p)(n+p+1)} + \frac{1}{(n-p)^2} + \frac{1}{(n+p+1)^2}\right]$$

We have

$$\sum_{n=0}^{n=p-1}\frac{1}{(n-p)^2} = \sum_{n=1}^{n=p}\frac{1}{n^2}$$

$$\sum_{n=0}^{n=p-1} \frac{1}{(n+p+1)^2} = \sum_{n=p+1}^{n=2p} \frac{1}{n^2}$$

$$\sum_{n=p+1}^{\infty} \frac{1}{(n-p)^2} = \sum_{n=1}^{\infty} \frac{1}{n^2}$$

$$\sum_{n=p+1}^{\infty} \frac{1}{(n+p+1)^2} = \sum_{n=1}^{\infty} \frac{1}{n^2} - \sum_{n=1}^{n=2p+1} \frac{1}{n^2}$$

So

$$\sum_{\substack{n=0 \\ n\neq p}}^{\infty} \left[\frac{1}{(n-p)^2} + \frac{1}{(n+p+1)^2} \right] = 2 \sum_{n=1}^{\infty} \frac{1}{n^2} \frac{1}{(2p+1)^2}$$

As we know that

$$\sum_{n=1}^{\infty} \frac{1}{n^2} = \frac{\pi^2}{6}$$

We finally get

$$\sum_{\substack{n=0 \\ n\neq p}}^{\infty} \frac{1}{(n-p)^2(n+p+1)^2} = \frac{1}{(2p+1)^2} \left[\frac{\pi^2}{3} - \frac{3}{(2p+1)^2} \right]$$

$$3 - \sum_{\substack{n=0 \\ n\neq p}}^{\infty} \frac{(2n+1)^2}{(n-p)^2(n+p+1)^2}$$

We have

$$\frac{(2n+1)^2}{(n-p)^2(n+p+1)^2} = \frac{4}{(n-p)(n+p+1)} + \frac{(2p+1)^2}{(n-p)^2(n+p+1)^2}$$

So we get immediately

$$\sum_{\substack{n=0 \\ n\neq p}}^{\infty} \frac{(2n+1)^2}{(n-p)^2(n+p+1)^2} = \frac{\pi^2}{3} + \frac{1}{(2p+1)^2}$$

REFERENCES

REFERENCES

Achenbach J.D., 1973, *Wave propagation in elastic solids*, North-Holland/America Elsevier.

Aki K., Richards P.G., 1980, *Quantitative seismology: Theory and Methods - vol I-II.*, Freeman, San Francisco, Cal.

Azimi S.A., Kalinin V.V., Pivovarov B.L., 1968, Impulse and transient characteristics of media with linear and quadratic absorption, Phys. Solid Earth (Engl.Ed.), 1968, 88-93.

Balch A.H., Smolka F.R., 1970, Plane and spherical transient Voigt waves, Geoph., 35, 745-761.

Biot M.A., 1956a, Theory of propagation of elastic waves in a fluid saturated porous solid.I - Low frequency range, J.Ac.Soc.Am., 28, 168-178.

Biot M.A., 1956b, Theory of propagation of elastic waves in a fluid saturated porous solid.II - Higher frequency range, J.Ac.Soc.Am., 28, 179-191.

Bland D.R., 1960, *The theory of linear viscoelasticity*, Pergamon Press, N.Y.

Borcherdt R.D., 1971, Inhomogeneous body and surface plane waves in a generalized viscoelastic half-space, PhD thesis, Univ.Cal.Berkeley, Calif.

Borcherdt, R.D., 1973, Energy and plane waves in linear viscoelastic media, J.Geophys.Res., 78, 2442-2453

Borcherdt R.D, 1977, Reflection and refraction of type II S-waves in elastic and anelastic medium. Bull.Seism.Soc.of Am.67, 43-67.

Born W.T., 1941, The attenuation constant of earth materials, Geoph., 6, 132-148.

Born M., Wolf E., 1970, *Principles of optics*, Pergamon, N.Y.

Bracewell R., 1965, *The Fourier transform and its Applications*, Mc Graw Hill, N.Y.

Brennan B.J., Stacey F.D., 1977, Frequency dependence of elasticity of rock-test of seismic velocity dispersion, Nature, 268, 220-222.

Brennan B.J, Smylie D.E, 1981, Linear viscoelasticity and dispersion in seismic wave propagation.Rev.Geoph.and Space Phys., 19, 233-246.

Buchen P.W., 1971, Plane waves in linear viscoelatic media, Geoph.J.Roy.Astr.Soc., 23, 531-542.

Červeny V., Ravindra R., 1971, *Theory of seismic head waves*, Univ. of Toronto Press.

Červeny V, Molotkov I.A, Pšenčik I, 1977, *Ray method in seismology*, Univ.Karlova., Praha, Tchecoslovaquia, 190-193.

Christensen R.M., 1971, *Theory of viscoelasticity*, Academic Press, N.Y.

Claerbout J.F., 1976, *Fundamentals of Geophysical Data Processing*, Mc Graw Hill, N.Y.

Claerbout J, Kjartansson E, 1979, Powers of causal operators.Stanford Exploration Project 16, 131-140.

Clark G.B., Rupert G.B., 1966, Plane and spherical waves in a Voigt medium, J.Geoph.Res., 71 , 2047-2053.

Collins F., Lee C.C., 1956, Seismic wave attenuation characteristics from pulse experiments, Geoph., 21, 16-40.

Collins F., 1960, Plane compressional Voigt waves, Geoph., 25, 483-504.

Cooper H.F.Jr., Reiss E.L., 1966, Reflection of plane viscoelastic waves from plane boundaries, J.Ac.Soc.Am., 39, 1133-1138.

Cooper, M.F. Jr., 1967, Reflection and transmission of oblique plane waves at a plane interface between viscoelastic media, J.Acoust.Soc. of Amer., 42, 1064-1069.

Courant R, Hilbert D, 1953, *Methods of Mathematical Physics*, Interscience Publishers Inc., N.Y

Dana S.W., 1944, The partition of energy among seismic waves reflected and refracted at the earth's core, Bull.Seism.Soc.Am., 34, 189-197.

Domenico S.N., 1974, Effect of water saturation on seismic reflectivity of sand reservoirs encased in shale, Geoph., 39, 759-769.

Dutta N.C., Ode H., 1979, Attenuation and dispersion of compressional waves in fluid-filled rocks with partial gas saturation (White Model) - Part I: Biot Theory, Geoph., 44, 1777-1788.

Dzeban I.P., 1970, Apparatus and method for studying the elastic and absorptive properties of rocks and for ultrasonic modeling under conditions similar to those in rock beds (Translation), Izv.Earth Physics, 8, 90-95.

Eshelby J.D., 1957, The determination of the elastic field of an ellipsoidal inclusion and related problems, Proc.Roy.Soc., Ser.A, 241, 376-396.

Ewing W.M., Jardetzky W.S, Press F., 1957, *Elastic Waves in Layered Media*, McGraw-Hill Book Co, New York.

Flügge W., 1975, *Viscoelasticity*, Springer-Verlag, N.Y

Frasier C.W., 1980, A new time domain reflection seismogram, 12th annual O.T.C , no 3809.

Fung Y.C., 1965, *Foundations of solid mechanics*, Prentice-Hall.

Futterman W.I., 1962, Dispersive body waves, J.Geoph.Res., 67, 5279-5291.

Ganley D.C., 1981, A method for calculating synthetic seismograms which include the effects of absorption and dispersion, Geoph., 46, 1100-1107.

Gassmann F., 1951, Elastic waves through a pcking of spheres, Geoph., 16, 673-685.

Gladwin M.T., Stacey F.D., 1974, Anelastic degradation of acoustic pulses in rock, Phys. Earth Planet. Int., 8, 332-336.

Gordon R.B, Davis L.A., 1968, Velocity and attenuation of seismic waves in imperfectly elastic rock, J.Geoph.Res., 73, 3917-3935.

Grant F.S., West G.F., 1965, Interpretation theory in applied geophysics, Mc Graw Hill, N.Y.

Gregory A.R., 1976, Fluid saturation effects on dynamic elastic properties of sedimentary rocks, Geoph., 41, 895-921.

Gregory A.R., 1977, Aspects of rock physics from laboratory and log data that are important to seismic interpretation, Seismic Stratigraphy AAPG, 15-46.

Gross B., 1953, *Mathematical Structure of the theories of viscoelasticity*, Hermann, Paris

Hale D., 1981, An inverse Q filter, Stanford Explor.Project, Stanford Univ., Calif., 26, 231-243.

Hale D., 1981, Q an adaptive prediction error filters , Stanford Explor.Project, Stanford Univ., Calif., 28, 209-231.

Hartmann B, 1972, Ultrasonic hysteresis absorption in polymers, J.Ap.Phys., 43, 4304-4308

Hartmann B, 1974, Immersion apparatus for ultrasonic measurements in polymers, J.Ac.Soc.Am., 56, 1469-1482.

Heelan P.A-S.J., 1953, On the theory of head waves, Geoph., 18, 871-893.

Jaeger J.C., Cook N.G.W., 1976, *Fundamentals of rock Mechanics*, Halsted Press, N.Y.

Jaramillo E.E., Colvin J.D., 1970, Transient waves in a Voigt medium, J.Geoph.Res., 75, 5767-5773.

Johnston D.H., 1978, The attenuation of seismic waves in dry and saturated rocks, PhD thesis, M.I.T., Mass.

Johnston D.H., Toksöz N.M., Timur A., 1979, Attenuation of seismic waves in dry and saturated rocks: II-Mechanisms, Geoph., 44, 691-711.

Johnston D.H, Toksöz N.M., 1981, Seismic wave attenuation, Geoph.Repr.Series no2, S.E.G.

Kan T.K., Corrigan D., Huddleston P.D., 1981, Attenuation measurements from vertical seismic profiles, Preprint S.E.G Meeting.

Kanamori H., Anderson D.L., 1977, Importance of physical dispersion in surface wave and free oscillation problems: review, Rev.Geophys.Space Phys., 15, 105-112.

Kaye G.W.c., Laby T.H., 1973, *Tables of Physical and Chemical constants-14th ed.*, Long-

man, N.Y.

Kennett B.L.N, 1979, Theoretical reflection seismograms for elastic media, Geoph.Prosp., 27, 301-321.

Kjartansson E, 1979, Attenuation of seismic waves in rocks.PhD Thesis, Stanford Univ. Calif.

Kjartansson E, 1979, Constant-Q, Wave propagation and attenuation, Jr Geoph.Res., 84, 3737-3748.

Knopoff L., 1964, Q , Rev. Geoph. Space Phys., 2, 625-660.

Kogan S.Y., 1966, A brief review of seismic wave absorption theories II, Phys. Solid Earth (Eng.Ed.), 1966, 678-683.

Kolsky H, 1956, The propagation of stress pulses in viscoelastic solids.Phys Mag.1, 693-710.

Korringa J., Brown R.J., Thompson D.D., Runge R.J., 1979, Self-consistent imbedding and the ellipsoidal model for porous rocks, J.Geoph.Res., 84, 5591-5598.

Krebes E.S, Hron F, 1980, Ray-synthetic seismograms for SH waves in anelastic media Bull.Seis.Soc.Am., 70, 29-46

Krebes E.S, Hron F, 1980, Synthetic seismograms for SH waves in a layered anelastic medium by asymptotic ray theory Bull.Seis.Soc.Am., 70, 2005-2020

Kuster G.T., Toksöz N.M., 1974, Velocity and attenuation of seismic waves in two-phase media - I-Theoretical formulations, Geoph., 39, 587-606.

Kuster G.T., Toksöz N.M., 1974, Velocity and attenuation of seismic waves in two-phase media - II-Experimental results, Geoph., 39, 607-618.

Lamb G.L.Jr, 1962, the attenuation of waves in a dispersive medium, J.Geoph.Res., 67, 5273-5277.

Lindsay R.B., 1960, *Mechanical Radiation*, Mc Graw Hill, New-York.

Liu H.P., Anderson D.L., Kanamori H., 1976, Velocity dispersion due to anelasticity; implications for seismology and mantle composition, Geoph.J.Roy.Astron.Soc., 47, 41-58.

Lockett F.J., 1962, The reflection and refraction of waves at an interface between viscoelastic media, J. Mech. Phys. Solids, 10, 53-64.

Lomnitz C., 1957, Linear dissipation in solids, J.Appl.Phys., 28, 201-205.

Lomnitz C., 1962, Application of the logarithmic creep law to stress wave attenuation in the solid earth, J.Geoph.Res., 67, 365-368.

Lundquist G., 1977, Evidence for a frequency dependent Q (abstract), EOS Trans.AGU, 58, 1182.

Mason W.P., 1946, Measurement of the viscosity and shear elasticity of liquids by means of a torsionally vibrating crystal, Annual Meeting Am.Soc.Mech.Eng.

Mavko G.M., 1979, Frictional attenuation: an inherent amplitude dependence, J.Geoph.Res., 84, 4769-4776.

Mavko G.M., Nur A., 1979, Wave attenuation in partially saturated rocks, Geoph., 44, 161-178.

Mavko G.M., Kjartansson E., Winkler K., 1979, Seismic wave attenuation in rocks, Rev. of Geoph. and Space Phys., 17, 1155-1164.

Minster J.B., 1978a, Transient and impulse responses of a one-dimensional linearly attenuating medium - I.Analytical results, Geoph.J.Roy.Astron.Soc., 52, 479-501.

Minster J.B., 1978b, Transient and impulse responses of a one-dimensional linearly attenuating medium - II.A parametric study, Geoph.J.Roy.Astron.Soc., 52, 503-524.

Morse P.M., 1948, *Vibration and Sound*, Mc Graw Hill, N.Y.

Morse P.M., H. Feshbach, 1953, *Methods of Theoretical Physics*, McGraw-Hill Book Co, New York.

Murphy W.F.III, 1982, Effects of partial water saturation on attenuation in sandstones, in press J.Ac.Soc.Am.

Nafe J.E., Drake C.L., 1963, Physical properties of marine sediments, in The Sea, vol3, Interscience Publishers Inc., 794-814.

Newlands M., 1954, Lamb's problem with internal dissipation I, J.Ac.Soc.Am., 26, 434-448.

Nowick A.S., Berry B.S., 1972, *Anelastic relaxation in crystalline solids*, Academic Press, N.Y.

Nur A., Simmons G., 1969, The effect of saturation on velocity in low porosity rocks, Earth Plan.Sci.Lett., 7, 183-193.

Nur A., Murphy W.F III, 1981, Wave velocities and attenuation in porous media with fluids, Proc. of the 4th Int.Conf on Continuum Models of discrete systems, Stockholm, Sweden.

O'Connell R.J., Budiansky B., 1974, Seismic velocities in dry and saturated cracked solids, J.Geoph.Res., 79, 5412-5426.

O'Connell R.J., Budiansky B., 1974, Seismic velocities in dry and saturated cracked solids, J.Geoph.Res., 79, 5412-5426.

O'Connell R.J., Budiansky B., 1978, Measures of dissipation in viscoelastic media, Geoph.Res. Letters., 5, 5-8.

Palmer I.D, Traviolia M.L., 1981, Attenuation by squirt flow in undersaturated gas sands, Geoph., 45, 1780-1792.

Pandit B.I., Savage J.C., 1973, An experimental test of Lomnitz' theory of internal friction in rocks, J.Geoph.Res., 78, 6097-6099.

Pliant W.L.,1979, *Elastic waves in the earth*, Elsevier, The Netherlands.

Ricker N., 1953, The form and laws of propagation of seismic wavelets, Geoph., 18, 10-40.

Ricker N., 1977, *Transient waves in viscoelastic media*, Elsevier, Amsterdam.

Robinson J.C., 1979, A technique for the continuous representation of dispersion in seismic data, Geoph., 44, 1245-1251.

Savage J.C., 1965, Attenuation of elastic waves in granular mediums, J.Geoph.res., 70, 3935-3942.

Savage J.C., Hasegawa H.S., Evidence for a linear attenuation mechanism, Geoph., 32, 1003-1014.

Schoenberger M., Levin F.K., 1978, Apparent attenuation due to intrabed multiples II, Geoph., 43, 730-737.

Sheriff R.E., 1975, Factors affecting seismic amplitudes, Geoph.Pros., 23, 125-138.

Silva W, 1976, Body waves in a layered anelastic solid. Bull.Seis.Soc.Am., 66, 1539-1554.

Simmons G., Brace W.F., 1965, Comparison of static and dynamic measurements of compressibility of rocks, J.Geoph.Res., 70, 5649-5656.

Spencer J.W., 1981, Stress relaxations at low frequencies in fluid saturated rocks: Attenuation and modulus dispersion, J.Geoph.Res., 86, 1803-1812.

Stoll R.D., 1977, Acoustic waves in ocean sediments, Geoph., 42, 715-725.

Stoll R.D., Kan T.K., 1981, Reflection of acoustic waves at a water sediment interface, J.Ac.Soc.Am., 70, 149-156.

Strick E., 1967, The determination of Q, dynamic viscosty and creep curves from wave propagation measurements, Geoph.J.Roy.Astron.Soc., 13, 197-218.

Strick E., 1970, A predicted pedestal effect for pulse propagation in constant-Q solids, Geoph., 35, 387-403.

Strick E., 1971, An explanation of observed time discrepancies between continuous and conventional well ve;ocities surveys, Geoph, 36, 285-295.

Tittmann B.R., 1978, Internal friction measurements and their implications in seismic Q srtucture models of the earth's crust, in The Earth's crust, Geoph.Monog.Series, Vol.20 , Ed by J.Heacock, 197-213.

Toksöz M.N, Johnston D.H, Timur A., 1979, Attenuation of seismic waves in dry and saturated rocks: I-Laboratory measurements, Geoph., 44, 681-690.

Walsh J.B., 1966, Seismic wave attenuation in rock due to friction, J.Geoph.Res., 71, 2591-2599.

White J.E., 1965, *Seismic waves: Radiation, Transmission and attenuation*, Mc Graw Hill, N.Y.

White J.E., 1975, Computed seismic speeds and attenuation in rocks with partial gas satura-

tion , Geoph., 40, 224-232.

Widess M.B., 1973, How thin is a thin bed?, Geoph., 38, 1176-1180.

Winkler K, 1979, The effects of pore fluids and frictional sliding on seismic attenuation.PhD thesis, Stanford Univ.Calif.

Winkler.K, Nur.A, 1979, Pore fluids and seismic attenuation in rocks, Geoph.Res.Lett. , 6, 1-4.

Winkler.K, Nur.A, 1982, Seismic attenuation: Effects of pore fluids and frictional sliding,Geoph., 47, 1-15.

Winkler K., Nur A. and Gladwin M., 1979, Friction and seismic attenuation in rocks. Nature, 277, 525-531.

Zemanek J., Rudnick I., Attenuation and dispersion of elastic waves in a cylindrical bar, J.Ac.Soc.Am., 33, 1283-1288.

Zener C.M., 1948, *Elasticity and anelasticity of metals*, Univ. of Chicago Press.